Palmitoyl transferase Zdhhc21 is a candidate for the hair loss mutation *dep*

- a potential role in epidermal homeostasis

Angela Waishan Lee

Submitted for
the Degree of Doctor of Philosophy
At the
University of Edinburgh
2007

Declaration

I declare that:

this thesis is composed by myself;
this work is my own, except where otherwise stated;
any collaboration with other group is a result of my sole correspondence.

Angela W Lee

September 2007

Publication

Some of the data described in this thesis has been previously published.

Smyth,I.M., Wilming,L., Lee,A.W., Taylor,M.S., Gautier,P., Barlow,K., Wallis,J., Martin,S., Glithero,R., Phillimore,B. et al. (2006). Genomic anatomy of the Tyrp1 (*brown*) deletion complex. *Proc. Natl. Acad. Sci. U. S. A* 103, 3704-3709.

Acknowledgements

First of all, I would like to thank my supervisor Ian Jackson for being the most efficient and open-minded supervisor who is always there (as long as he is in Edinburgh!) for help and discussions, and always encourages me to learn from failures and to remain optimistic when things don't work.

I would especially like to thank Pleasantine Mill (Pleasie), for always sharing her knowledge and expertise in many areas, and for her generous help and directions on this project. Without her contribution, this project would not have progressed as far as it has.

Another person whose contribution is indispensable was Margaret, who maintains the mouse lines and made the rescue line. I genuinely feel blessed to have worked in such a supportive group, with Katrine, who is very knowledgeable and is always helpful; and Peter, whose protocol is guaranteed to work (!). I have enjoyed the company of Lisa, and sharing office with Sally, Fabien and Ada who have also helped me a lot, even though it was a short time. Thank you also to Brendan Doe (MRC Transgenic Unit) for re-deriving the Harwell allele.

I owe my thanks to many other people in the unit, from whom I have learned many important things from, this includes: Veronica, Kathy, Patricia, Judy, Paul Perry, Allyson, and those who have now left the MRC such as Martina Niksic, Louise Harewood, TomVA and especially Alan Hart who had helped me a lot at the start of my Ph.D. Thank you also for the kind and generous help from Craig Nicol who allowed my last day in the unit to be free of stress.
Special thanks to Dafni for helping me with the final bit of this thesis!

I feel very privileged to have worked in such dynamic environment where I was never short of practical help and advice, as well as some friendly faces! I have achieved a lot in my own respect over the past 4 yrs and it has been my best academic experience so far.

I would like to thank all the collaborators that were involved in this project, including Rebecca Porter, Masaki Fukata, Ian Smyth, and Yoichi Gondo. And those within the unit who have so generously provided help, reagents and advice, including Xinhua, Rachel Berry, Ellie, Andrea, Carlo and Kevin. Thank you also to Tilo for the antibody! I am sure there are people that I have forgotten but I would like to thank everyone.

Despite the distance, I need to thank my family in Hong Kong, especially my cousin Stephanie. Thanks also to all the friends that I have met in Edinburgh for the past 9 years especially BBN, Mabel, Craig, Bernard and Andrew. Last but not least, I would like to thank CT for everything over the past few years.

Most importantly, despite all human knowledge and all the contradicting views, I must acknowledge God, for His great ways, and for everything that allows me to appreciate the transcendent beauty of His work.

Abstract

Palmitoylation is a post-translational modification that involves the addition of the fatty acid palmitate onto specific cysteine residues. Recently, several members of a family of transmembrane proteins containing a zinc finger and a DHHC motif, have been shown to be palmitoyl transferases in yeast and mammalian cells.

The recessive hair loss mutant, *dep*, contains a spontaneous mutation (del-233F) at the C-terminal of Zdhhc21. Wild-type Zdhhc21 has been shown to enhance palmitoylation of several specific substrates in a transfected cell assay. Zdhhc21 localises to the cis-Golgi, whereas the mutant protein is mislocalised and is inactive in palmitoylation. We verified the candidacy of *Zdhhc21* by transgenic BAC rescue.

Dep is characterised by progressive hair loss, hyperplasia of the sebaceous glands, the interfollicular epidermis and the outer root sheath. *In-situ* hybridisation and immunohistochemistry show that both wild-type and *dep* mRNA and protein are present in the inner root sheath (IRS).

Phenotypic characterisation using molecular markers in cell culture and on skin sections reveals abnormalities that suggest a lack of correct hair shaft differentiation in *dep*. We speculate that *dep* may have a direct or indirect effect on 4 members of the Wnt family - essential regulators of hair shaft differentiation – because of their co-expression in the IRS and because *dep* exhibits a Wnt-deficient phenotype.

This hypothesis may provide an example of how local signalling centres may be established to allow for spatiotemporal gene expression. Furthermore, *dep* is the first mouse model that provides direct evidence of a function of the Dhhc family.

Table of contents

List of Figures

List of Tables

Appendix

Abbreviations

Ab	Antibody
ABE	Acyl-biotin exchange chemistry
AP staining	Alkaline phosphatase staining
BAC	Bacterial artificial chromosome
baf	*Brown associated fitness*
b-del	*brown* deletion
CESE	Conformation sensitive capillary electrophoresis
CmR	Chloramphenicol resistance
CMV	Cytomegalovirus
CRD	Cysteine-rich domain
DECAP	Deletion of Cap structure and poly(A)
dep	*depilated*
DP	Dermal papillae
Dvl2	Dishevelled 2
ECM	Extracellular matrix
eNOS	Endothelial nitric oxide synthase
ENU	N-ethyl-N-nitrosourea
ES cells	Embryonic stem cells
EPU	Epidermal proliferative unit
EUCOMM	European Conditional Mouse Mutagenesis Programme
H&E staining	Hematoxylin and eosin staining
HF	Hair follicle
HS	Hair shaft
ICSI	Intracytoplasmic sperm injection
IFE	Interfollicular epidermis
IRS	Inner root sheath
IVF	*In vitro* fertilization
K14	Keratin14
Lck	Lymphocyte-specific protein tyrosine kinase
Lef1	Lymphoid enhancer binding factor
LRC	Label-retaining cell
ncRNA	Non-coding RNA
NEM	N-ethylmaleimide
ORO	Oil Red O
ORS	Outer root sheath
PAT	Protein acyl-transferase
PMD cell	Post-mitotic differentiating cell
RNAi	RNA interference
SC	Stem cell
SG	Sebaceous gland
Shh	Sonic hedgehog
SLT	Specific loci test
TA cell	Transit-amplifying cell
Tyrp1	*Tyrosinase-related protein1*
Zdhhc21	Zinc finger, DHHC containing protein 21
zeoR	Zeocin resistance

Chapter 1 – INTRODUCTION

1.1. Use of Mouse Models to dissect gene functions

1.1.1. Reverse Genetics – Manipulation of Gene expression in Mouse

The most powerful and straightforward approach to study gene function, is by mutating a given gene and determine the phenotypic outcome in a model organism. The laboratory mouse (*Mus Musculus*) is considered one of the best species for such manipulation because unlike other model organisms such as flies and worms, they are closely related to human in evolutionary terms and thus share many of the physiological and developmental properties with humans. Therefore, it is reasonable to assume that the same gene in mouse is likely to provide similar function in humans, so the study of gene function in mice may allow us to predict the role of genes in human development and disease. Another reason why mouse is the most popular model in biomedical research is because of the abundant genomic resources that allows them to be genetically manipulated in a highly precise manner using gene knockout and transgenic technology (Peters et al., 2007; Rosenthal and Brown, 2007).

Generation of Transgenic Mice

DNA segments of a gene of interest may be introduced to a mouse by pronuclear microinjection so that the segment may incorporate randomly into the germline, and result in transgenic offspring with extra copies of the transgene (Hanahan et al., 2007). The transgene is most often engineered to express in a spatially specific manner by using tissue-specific promoter, this is usually applied to overexpression of a target gene. For example, the role of Wnt signaling in hair follicles has been studied by using the keratin 14 (K14) promoter to drive expression of genes of the Wnt pathway, such as Wnt3a, Dvl2 (Millar et al, 1999), Lef1 and Tcf3 (Merrill et al 2001) in the hair follicle outer root sheath (ORS) specifically.

The transgene may also be modified so that its expression may be inducible with certain drugs. Alternatively, to study the contribution of a candidate gene to a certain phenotype, a transgene cloned in a large DNA segment such as BAC may be injected into mutant embryos to speculate whether the expression of the transgene is able to rescue a given phenotype.

Gene Targeting

In gene targeting, the target gene is altered in its original genomic location by homologous recombination in embryonic stem (ES) cells. Mutant ES cells that have undergone the rare recombination event can be selected by drug (resistance or sensitivity), and injected into a blastocyst which is then implanted into a recipient mother to give chimeric offspring. If the mutant ES cells were incorporated into germ cells, the altered DNA will be passed on to subsequent offspring (Muller, 1999; Smithies et al., 1985). Currently, this manipulation of ES cells is used in several mutagenesis approaches which produce either 'knockouts' to inactivate a gene completely, or 'knockins' to replace a gene with a mutant version.

For example, using the mouse keratin 6 (MK6) knockout mouse that was generated by homologous recombination in ES cells, it was shown that although *MK6a*$^{-/-}$ mice have normal hair and skin, they show a delay in reepithelializaton from the HF. This indicates that even though MK6a may not play a major role in keratinocyte proliferation or migration, it has a role in the activation of HF keratinocytes after wounding (Wojcik et al., 2000).

Conditional Gene Targeting

Gene targeting is powerful in studying gene function by generating loss-of-function mutations. However, although the conventional approach is ideal in disrupting role of genes in embryogenesis, it has limited application in studying their functions in adulthood. For example, a protein may have an early role in embryogenesis, but also has other roles in development. In this case, a complete knockout in ES cells would not allow the study of the later phenotype.

Furthermore, given the complex temporal and spatial specificity of gene expression, and possible functional redundancy of proteins, the loss of a protein function may contribute to a human phenotype in a temporally and spatially specific manner. To induce gene activation / inactivation specifically, the Cre-loxP-induced site-specific recombineering recombination (Nagy, 2000) and tamoxifen-inducible systems (Hayashi and McMahon, 2002) may be employed in ES cell manipulation for conditional gene targeting.

Typically, conditional gene targeting involves crossing 2 genetic modified mice; one carries a Cre recombinase gene controlled by a tissue specific promotor, the other one carries the conditional (floxed) gene. Upon expression of Cre recombinase in the resulting offspring, the target DNA is removed at the loxP sites that are recognized by Cre, thereby inactivating the gene in a tissue-specific manner. The transgenic mouse strain carrying the tissue-specific Cre expression may be crossed with strains that carry other transgene targeted by loxP, and vice versa (O'Neal and Agah, 2007). A list of existing targeted gene mutations is maintained by the Jackson Laboratory[1].

As an example, the Cre/loxP technology has been used to generate a conditional mutation of β-catenin during embryogenesis and stem cell differentiation in adult skin (Huelsken et al., 2001). It was shown that β-catenin is required for placode formation, but it also essential for fate decisions of skin stem cells.

Over the past few years, several large-scale mutagenesis screens have been initiated on an international scale to study gene function. In collaboration with the Wellcome Trust Sanger Institute (WTSI), the European Conditional Mouse Mutagenesis programme[2] (EUCOMM) and the Knockout Mouse Project[3] (KOMP) aim to generate a collection of mouse mutants to include all genes encoded by the mouse genome (Friedel et al., 2007). This involves the construction of conditional gene targeting vectors and the production of targeted ES cell lines that will be available to the public when completed. Not only is this approach cost- and time-effective, it also enables high-throughput generation of knockout mutants in a standardized and systematic way.

The phenotype of the mutant lines derived from ES cells are initially assessed by the European Mouse Disease Clinic[4] (EUMODIC) which is build upon a comprehensive database of standardized phenotyping protocols called the European Mouse Phenotyping Resource of Standardised Screens[5] (EMPReSS) (Brown et al., 2005).

[1] The Jackson Lab: www.informatics.jax.org
[2] EUCOMM: www.eucomm.org
[3] KOMP: www.nih.gov/science/models/mouse/knock-out/
[4] EUMODIC: http://www.eumodic.org/
[5] EMPReSS: http://empress.har.mrc.ac.uk/

1.1.2. Forward Genetics – Identification of mutant alleles for certain phenotypes

While the reverse genetic approach or knockout technology is straightforward and essential, it is complemented by forward genetics, the first tools available to geneticists, where the observation of a phenotype is followed by the identification of the responsible genes, leading to discovery of many novel genes and their functions. Often, a mutagen such as radiation or other chemical substrates may be used to accelerate the mutagenesis process (Rinchik et al., 1990).

Spontaneous Mutations

Before the development of transgenic technology and gene targeting, many spontaneous mouse mutants have already been characterized and studied by geneticists. To date, the sequencing of the mouse and human genomes are completed and are frequently being updated and manually annotated for better quality of the finished genome sequence. The abundance in genomic data and availability of genetic markers has facilitated the identification of causative genes in spontaneous mutants.

Induced Mutations

Although spontaneous mutations are productive, they represent only a small number of all possible mutations, and they occur at an extremely low rate. To facilitate the study of gene function, new mutations may be induced by several methods such as radiation, chemical, and transposon insertion.

Early mutagenesis screens includes the specific locus test (SLT), which uses visible markers such as coat colour and ear morphology to recover chemical- and radiation-induced chromosomal deletions at defined genomic locations (Davis and Justice, 1998). The deletions lead to a loss of the genes within those regions, as well as the marker gene. One of the loci studied was the *brown* (*b*) locus, at which 30 deletions were initially recovered and will be described in **Chapter 2**. By complementation analysis against the panel of *b-del* chromosomes, several classical mutations have been mapped, including a hair loss mutant called *depilated* (*dep*). The identification of the responsible gene will be described in **Chapter 3**.

More recently, other mutagenesis strategies have been used that generate mutations in a more precise and unbiased manner. N-ethyl-N-nitrosourea (ENU) is a powerful alkylating mutagen that induces point mutations in mice, generating a range of effects including loss-of-function, gain-of-function and dominant-negative mutations (Justice et al., 1999). Unlike the gene targeting approach, ENU induces mutations in regulatory elements as well as known coding genes, and it does not require any knowledge or presumption of protein function. ENU mutagenesis screening is powerful both in isolating new alleles of a gene of interest and to confirm the functional identity of candidate gene (called gene-driven screens) (Coghill et al., 2002), and in identification of novel genes and pathways by screening for a certain phenotype (phenotype-driven screens) (Thaung et al., 2002). To date, several large-scale ENU mutagenesis programs exist worldwide, including the Baylor College of Medicine, MRC Mammalian Genetics Unit (Quwailid et al., 2004) and the Riken GSC Institute (Sakuraba et al., 2005).

Other induced mutagenesis alternatives include 'gene-trapping', which refers to the random insertion of a reporter that disrupts a gene locus in ES cells, followed by PCR-based gene identification techniques. The advantage of this approach is that the new allele can be tagged with a known marker that facilitates the identification of responsible gene in a phenotype. A list of characterized gene trap insertions in ES cells are available from the International Gene Trap Consortium (IGTC) (Nord et al., 2006).

DNA transposons can also be used to generate new mutants based on the principles of gene trapping, these include the reconstructed mariner element Sleeping Beauty (Dupuy et al., 2006) and piggyBac, a functional transposon from insects that also works in mammals (Cadinanos and Bradley, 2007). Due to the ability of transposons to mobilize within the genomes, they insert randomly into the genome and maintain the capacity to relocate and integrate at different genomic sites. Recently, an inducible version of the mouse codon-optimized piggyBac transposase was engineered by fusing with an oestrogen receptor ERT2, making it a highly active and regulatable transposase that is ideal for transposon-based mutagenesis for characterizing genes.

1.2. Using mice to study hair follicle and hair cycle

In addition to the aforementioned advantage of using mouse models, mouse is an excellent system for studying the hair cycle and hair follicle development for several reasons (Porter, 2003).

In mice, the hair cycle progresses as waves of synchronized growth among the follicles for the first 2 cycles following birth. After that, the cycle in different follicles becomes progressively unsynchronized. This makes it possible to discriminate certain stages from other stages and allows detailed characterization of each cycle stage within the first 2 cycles. In human, hair follicles mainly function independently of their neighbors, at least by the time when it is ethically possible to collect biopsies (Randall et al., 2003).

A complete murine hair cycle takes about 3 weeks, whereas in human, even the unpigmented, short vellus hairs take several months to complete a cycle. The pigmented, terminal hairs can take several years due to a prolonged anagen. The short hair cycle in mice allows us to access skin samples of specific time points easily during the first 2 cycles when follicles are synchronized (Porter, 2003).

One of the current challenges in mouse genetics is describing the phenotype of individual mutants. In order to recognize subtle abnormalities, each key stage of the mouse hair cycle have been systematically sub-divided and standardized based on morphologic differences, onset and progression of melanogenesis, and characterization with several other markers (Muller-Rover et al., 2001). The *dep* mutant was finely characterized by histology and use of hair-related markers, which will be presented in **Chapter 5**.

Originally, knowledge of hair follicles came from culture of specific cell type isolated from human follicles. Hair follicle cell types that have been cultured include the dermal papillae cells (Jahoda et al., 1984), ORS cells (Limat et al., 1993), connective tissue sheath cells (Reynolds et al., 1999). The major advantage is that primary cell culture allows individual cell types to be studied in detailed and to be manipulated *in vitro*. It also allows study of the interaction between individual cell types. The major disadvantage is that cycling hair follicles can only be maintained for a short length of time in primary culture, and that cells are not subjected to normal cellular interactions, physical constraints and their natural environment that supplies

nutrients and regulatory factors (Randall et al., 2003). The studies of spontaneous, transgenic and targeted mice thus represent a better model of hair follicle function and behavior in reality.

1.3. Thesis Outline.

In this thesis, the nature of the *dep* hair loss mutation is investigated. The identification of the candidate gene, *Zdhhc21*, will be described in **Chapter 3**, which includes the use of BAC transgenic rescue, ENU mutagenesis screen and RNA interference to verify the candidacy of *Zdhhc21*.

Zdhhc21 is one of the 23 mammalian proteins originally identified by its cysteine-rich zinc finger Dhhc-containing motif by protein sequence homology analysis. Subsequent functional assay have identified this class of proteins to be protein acyl-transferase (PAT). During the course of the project, the involvement of Zdhhc21 in palmitoylation has been verified in cell culture assay by several groups. However, no mammalian model is currently available to show a direct consequence of under-palmitoylation of a given substrate. The possibility that the *dep* phenotype is a result of a defective PAT function was investigated in **Chapter 4**. The identification of *Zdhhc21* mutation in *dep* may represent the first mammalian model of PAT activity.

Detailed phenotypic characterization of the mutant skin (presented in **Chapter 5**) reveals a defective hair shaft formation during the rapid growth phase. In combination with the detailed phenotypic characterization, and phenotypic comparison with existing mutants in the literature, we explored the possibility that the Wnt signaling pathway may affect the epidermal homeostasis in *dep* (**Chapter 6**).

Chapter 2 – Study of the *brown* deletion (*b-del*) interval and mapping of the *b-del* chromosomes

2.1. Introduction

2.1.1. The *brown* deletion complex

The mouse *brown* (*Tyrp1*) deletion complex is one of the most characterized regions of the mouse genome defined by a collection of 25 independent deletions of various sizes, spanning ~22Mb (~8.5cM) on mouse chromosome 4. Each deletion chromosome loses one copy of the coat colour gene, *tyrosinase- related protein 1* (*Tyrp1*), which encodes a melanocyte enzyme required to produce dark eumelanin, without which a homozygous mouse will have brown coat (Bennett et al., 1990).

The set of deletions was generated as part of the specific locus test (SLT) carried out at the Oak Ridge National Laboratory (ORNL, Tennessee) over the last 50 years (Davis and Justice, 1998; Rinchik et al., 1990). Wild-type mice treated with a potential mutagen (radiation or chemicals) were crossed with the Oak Ridge test stock (T stock), which is homozygous for 7 recessive mutations affecting visually recognizable traits, including the *brown* mutation (*b*) of *Tyrp1*. Five other loci also affect coat phenotype, they are: *nonagouti* [*a*, Chr.2], chinchilla at *albino* [c^{ch}, tyrosinase (Tyr), Chr.7], *dilute* [*d*, myosin Va (Myo5a), Chr.9], *pink-eyed dilution* [*p*, Chr.7] and *piebald*-spotting [*s*, endothelin receptor type B (Ednrb), Chr.14]; and one other locus that controls ear morphology, *short-ear* [*se*, bone morphogenetic protein 5 (Bmp-5), Chr.9], which is also visually detectable. These other 6 loci are also well-characterized.

After mutagen treatment, the efficacy of the treatment was assessed in the resulting F_1 progeny (Figure 2.1): a brown coat phenotype indicates a newly induced allele at the *Tyrp1* locus. A deletion will remove *Tyrp1*, along with varying amount of the genome flanking the locus. All the deletions generated must be hemizygous viable to be recovered. Homozygotes or 'compound heterozygotes' between individual *b-del* chromosomes confer a phenotype, most of which are prenatal lethal, indicating the presence of essential genes flanking the *Tyrp1* locus removed by the deletion.

Originally, genomic probes and sequences were not available, so the knowledge on the deletion chromosomes was limited. Nevertheless, the *b-del* complex had been utilized as a very powerful tool for mapping genes within the interval and investigating their functions. There were several ways of which informative data may be obtained: (1) By crossing overlapping deletions of different extent (at *Tyrp1*), it is possible to identify recessive phenotypes within the region and their candidate genes. (2) By complementation analysis of existing mutations against the *b-del* panel.

Using this approach, several phenotypic loci within the region were defined. At the proximal end was the spontaneous circling, head tossing and deaf mouse *whirler* (*wi*) (Fleming et al., 1994; Lane, 1963). Another interesting locus was the *baf* mutant (brown-associated fitness), which has been mapped very closely on either side of *Tyrp1* (section 2.1.4). Near the distal end of the *b-del* interval, was the spontaneous hair loss mutation, *depilated* (*dep*) (Green, 1970), which will be the focus of this thesis (Chapter 3 to 6). In addition, 3 lethal mutants were identified by Gene Rinchik using complementation analysis (Rinchik *et. al.*, 1994) (Figure 2.2).

Over a decade ago, our lab generated a genomic map which defines the endpoints of the *b-del* chromosomes using a set of 34 molecular markers scattered across the interval (Bell et al., 1995). Each deletion chromosome has either a C3H or 101 origin, and were crossed with the wild-derived inbred strain *Mus spretus* which allows us to define the deletion endpoints and the extent of each deletion using polymorphic markers (Bell et al., 1995; Rinchik et al., 1994; Simpson et al., 2000). This information had supplemented the preliminary molecular map and allows more precise isolation of the genes that lie within the interval.

2.1.2. The *brown* interval - Genomic Features

In collaboration with the UK Mouse Genome Sequencing Consortium and the Wellcome Trust Sanger Institute, the *brown* interval was sequenced and manually annotated using a 172-BAC contig encompassing the interval of about 21Mb. The *brown* deletion annotated sequence in the reference strain C57BL/6 is available from the Vertebrate Genome Annotation (VEGA)[6] browser (Ashurst et al., 2005; Loveland, 2005). Unlike other genome browsers which are

[6] Vertebrate Genome Annotation (VEGA) browser: http://vega.sanger.ac.uk

automated, data in the Vega browser is annotated by hand, which makes it more accurate at identifying splice variants, pseudogenes, non-coding transcripts and complex gene structures.

Intriguingly, the *brown* interval is unusually gene poor containing only 39 protein-coding genes that can be identified with confidence, in that they have human orthologues or encode known or predicted proteins (Smyth et al., 2006). This may explain why the large deletions are viable when heterozygous. There are 14 additional transcripts that are encoded by more than one exon and which contain a predicted open reading frame (ORF) of between 110 to 354 residues but lack homologues in other species. In addition, the interval harbors 74 recognizable pseudogenes and 28 spliced transcripts which do not contain any significant ORF nor homologues in other species (Smyth et al., 2006).

The overall gene density across this region is less than 2 genes/Mb, in contrast with the genome average of 10 genes/Mb. In addition, these genes are not evenly distributed across the region since there are 7 stretches of 1.0-2.5Mb regions that are completely absent of any protein-coding transcripts but however contain substantial number of non-coding segments that are highly conserved among mammalian species (presented on the ECR browser[7] Figure 2.3). If functional, these sequences may represent cis-regulatory elements, unknown protein-coding exons, non-coding RNA genes (ncRNAs) or unknown functional non-coding sequences (Smyth et al., 2006).

2.1.3. Identification of Deletion Phenotypes

The first part of this thesis involves refining the endpoints of these deletions and defining the location of essential genes deleted or disrupted by the breakpoints (Figure 2.4A).

Combinations of deletions within the interval have identified two early-acting embryonic lethal [*l(4)1Rn* and *l(4)3Rn*] and one neonatal lethal [*l(4)2Rn*] phenotypes. *l(4)1Rn* is mapped to a 2Mb region containing protein tyrosine phosphatase receptor type D (*Ptprd*), jumonji domain containing 2C (*Jmjd2c*) and an uncharacterized gene, which is the mouse orthologue of human *C9orf123* (Smyth et al., 2006). Homozygous deletion of the *l(4)1Rn* locus results in embryonic death, most likely around postimplantation stage (Rinchik, 1994). *Ptprd* has previously been

[7] Evolutionary Conserved Region (ECR) browser: http://ecrbrowser.dcode.org/

knocked out, and the *Ptprd*$^{-/-}$ is viable with a runting syndrome and mild neurological defects (Uetani et al., 2000). The *C9orf123* orthologue is only 111aa in length but contains 2 transmembrane domains that are conserved in humans, so it is likely to be a functional gene although nothing is known about it. Therefore, *Jmjd2c* and the *C9orf123* orthologue are both candidates for *l(4)1Rn.*

l(4)2Rn is mapped to a small region which contains only one gene: nuclear factor 1 B-type (*Nfib*). Deletion of the *l(4)2Rn* locus causes death in the late gestation/ neonatal period. *Nfib* has been knocked out, and the *Nfib*$^{-/-}$ mice die after birth but prior to weaning due to pulmonary hypoplasia (Grunder et al., 2002), which is similar to the phenotype observed in *l(4)2Rn.* It is therefore reasonable to conclude that *Nfib* underlies the lethal phenotype.

l(4)3Rn is mapped to a larger region containing 6 genes: Fras1 related extracellular matrix protein 1 (*Frem1*), the small nuclear RNA activating complex (*Snapc3*), basonuclin2 (*Bnc2*), the PC4- and SF2-interacting protein 1 (*Psip1*), also known as lens epithelium-derived growth factor (*Ledgf*) and two uncharacterized genes which are the mouse orthologues of human *C9orf52* and *C9orf93*. *Ledgf* is a chromatin-associated protein that has been implicated in transcriptional regulation, mRNA splicing, and cell survival *in vitro*. Recently, an embryonic stem cell clone with disrupted Ledgf was identified in a gene trap screen. The homozygous mice displays a range of phenotypes, and the majority of them died perinatally (Sutherland et al., 2006). Since lethality of *l(4)3Rn* occurs much earlier in pre-implantation stage, Ledgf is unlikely to be a candidate of *l(4)3Rn.*

Dep is a hair loss mutant (Figure 2.4C) that has been mapped to a very small region; its candidate genes will be discussed in **Chapter 3**.

The *Tyrp1*^{BW} allele contains an inversion with breakpoints at *Tyrp1*and basonuclin 2 (*Bnc2*), inverting about 5Mb of the chromosome (Javerzat and Jackson, 1998). RT-PCR shows that the *Tyrp1-Bnc2* fusion transcript expressed not only in melanocytes but also in kidney, liver, ovary and testis. It is speculated that the ectopic expression of fusion transcript results in melanocyte death and loss of hair pigmentation, which characterizes the phenotype.

2.1.4. Brown-Associated Fitness *(baf)* – small mouse with increased mortality

All of the *brown* deletions are prenatally lethal when homozygous; however, some of the crosses between individual b^{lethal} deletions were able to rescue the lethal phenotype, resulting in a runting syndrome evident during postnatal development (Rinchik, 1994). These mice are smaller in body size with increased mortality and usually die before weaning. Since this phenotype is recessive and lies very close to Tyrp1, all the viable mice also display a brown coat. Because of this, the locus is called *brown-associated fitness* (*baf*).

A large number of pairwise crosses between individual b^{lethal} deletions have been made in the ORNL, which is reported in Rinchik (1994). Later, it was found that some compound heterozygotes that deleted a minimal region around Tyrp1 were viable and normal (unpublished, Eleanor Simpson and Ian Jackson). Part of my project was to try to identify the *b*-region whose deficiency results in the reduced fitness observed in *baf*.

2.1.5. Regional ENU mutagenesis screen (Baylor College of Medicine)

Deletions spanning the *brown* interval have been used as the basis for a regional ENU mutagenesis screen for recessive phenotypes at the Baylor College of Medicine (Figure 2.5A). The basic idea is to use the *brown* deletions with known endpoints to isolate novel ENU-induced mutations that lie within the deleted region. The mutation is immediately localized to a specific chromosomal location, sidestepping the need to map a mutation.

About 550 chromosomes were tested over the largest proximal *brown* deletion (*b*-11R30M) and 360 were tested over the largest distal deletion (*b*-13R75M). As a result, more than 26 mutant phenotypes have been isolated, including 6 lethal, 10 neurological and 7 with craniofacial/ skeletal defects, one with hearing defect and another with eyes open at birth (Table 2.1, Figure 2.5B).

Table 2.1. ENU mutants isolated by regional ENU mutagenesis
The 2-generation recessive scheme has isolated a number of ENU mutants of various phenotypes, using the largest proximal and distal *brown* deletion chromosomes.

	Lethal	Neurological	Craniofacial/ Skeletal	Other
b-11R30M	1	9	5	2 (e.g. deafness)
b-13R75M	5	1	2	1

Collaboration has been established with the Wellcome Trust Sanger Institute to sequence all of the known and predicted exons in protein-coding and highly conserved non-coding elements within *brown* interval in the 26 mutant animals derived from the screen. Assuming that most mutant phenotypes are unigenic and are caused by an ENU mutation in a protein-coding gene, the sequencing approach would be time and cost effective in comparison to the complementation analysis. Currently, the sequences are being analyzed to flag mutations, and to distinguish any signal from noise.

Figure 2.1: The Specific Locus Test (SLT) carried out at Oak Ridge National Laboratory
Wild-type mice were exposed to radiation to induce mutations in germ cells, and then crossed with a special T stock which is homozygous for several recessive visible mutations. From this, new mutations at any of those 7 loci of the treated parent can be detected easily in the F1 progeny. In the case of the *brown* locus, a brown coat phenotype indicates a rearrangement across the *brown* locus.

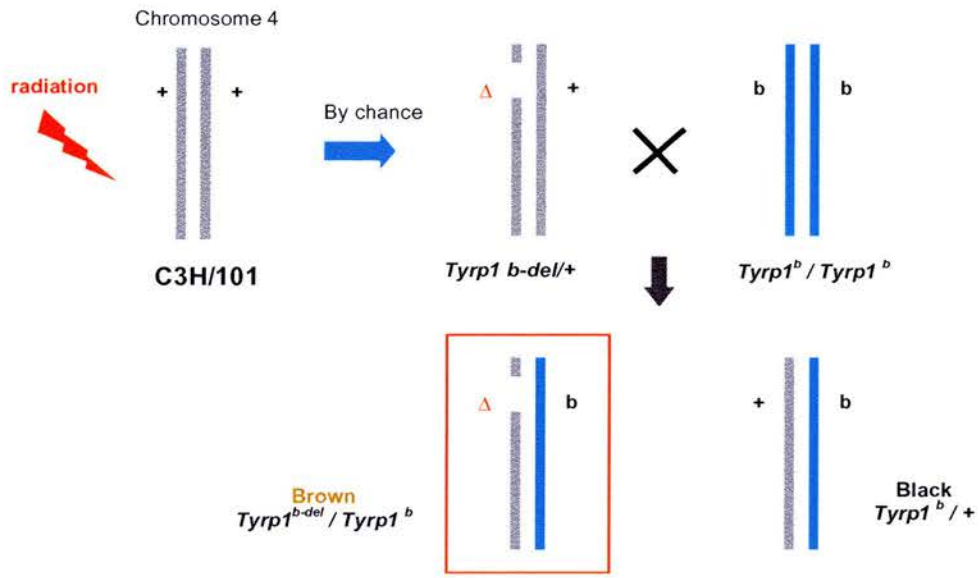

Figure 2.2. Complementation analysis of the *b-del* complex
(Diagram from Simpson et al, 2000)
The deletions represented by the black lines are lethal when homozygous, but when compound heterozygous, some of them exhibit the *baf* phenotype. The *b-del* deletion panel has been exploited this way in developing correlated physical and functional maps of the interval. For example, *l(4)2Rn* was mapped to between the distal endpoints of A and D based on the observation that deletions of type A complement *l(4)2Rn* but deletions of type D do not.

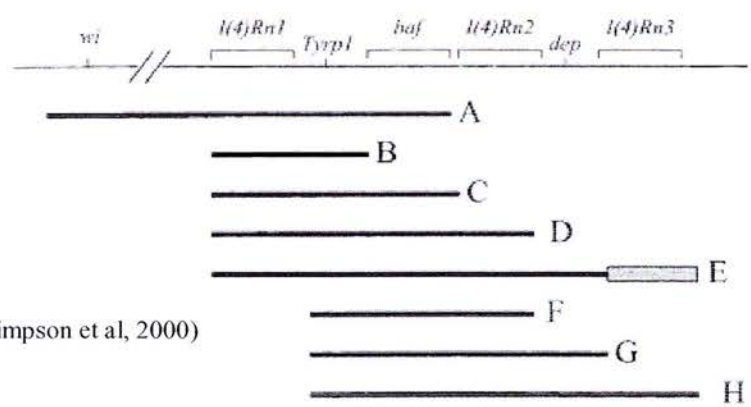

(Simpson et al, 2000)

Figure 2.3. Conservation across different species within the *b-del* interval
An overview of the *b-del* interval showing conservation across different species. The diagram was drawn in the ECR browser (Ovcharenko et al., 2005), which is a convenient tool for quick visualisation of multiple genome alignments. With the mouse genome being the reference sequence, the whole interval was aligned with corresponding regions in fugu, chicken, rat, dog and human. However, only human data is complete. The other species have some data missing. Individual peaks represent presence of <100bp long sequences that have over 75% identical with the mouse sequences. The blue are conserved seqs in coding exon, the pink are conserved seqs in introns, and the red are just any sequences that meet the criteria. The 7 gene deserts are highlighted with green lines, within which lies a considerable amount of conserved regions between human and mouse. The interval is very gene-poor especially the region of over 2Mb that is completely devoid of genes.
Blue bar – coding exon; yellow bar – UTR; pink bar – intron; red bar – intergenic element.

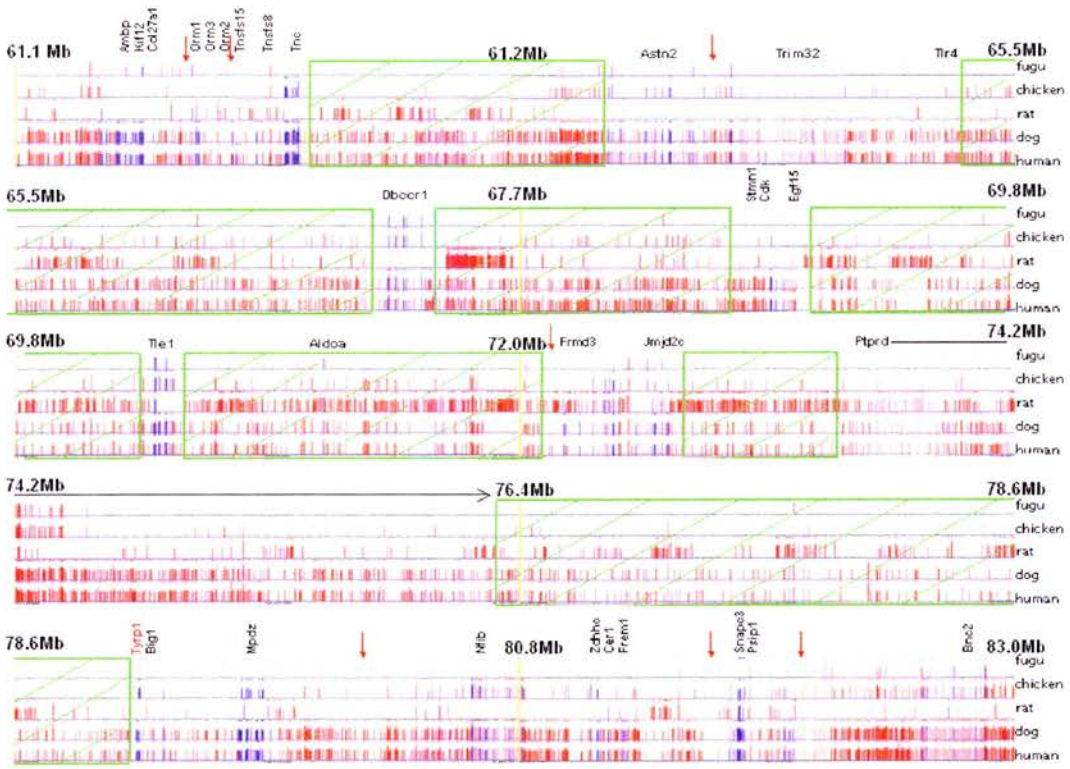

Figure 2.4: Mapping of mutants using complementation analysis against the *b-del* complex
[A] Several mutant loci (*l4Rn1*, *l4Rn1*, *l4Rn1*, *baf* and *dep*) were defined by complementation analysis against the *b-del* complex, and subsequent fine-mapping of the endpoints of informative *b-del* chromosomes (grey bars) using polymorphic markers. These markers distinguish between the C3H/101 and *M. spretus* backgrounds in the *b-del/ spretus* heterozygotes. The mapped loci contain (or overlap with) candidate genes that may underlie the phenotype. The largest proximal and distal deletions, *b*-11R30M and *b*-13R75M respectively (pink bars), were used for the regional ENU mutagenesis screen described in section 2.1.5. Fine mapping has also revealed that the further proximal and distal deletions of the *b-del* complex are *b*-11R30M and *b*-8Pub respectively. Only informative genes are shown.
[B] The *baf* mutant compared against wild-type control, showing that the *baf* mutant is obviously smaller in size in comparison with a wild type control littermate.
[C] Homozygote *dep* mutant showing the regional hair loss, although the phenotype is heterogenous in terms of region of hair loss.

[A]

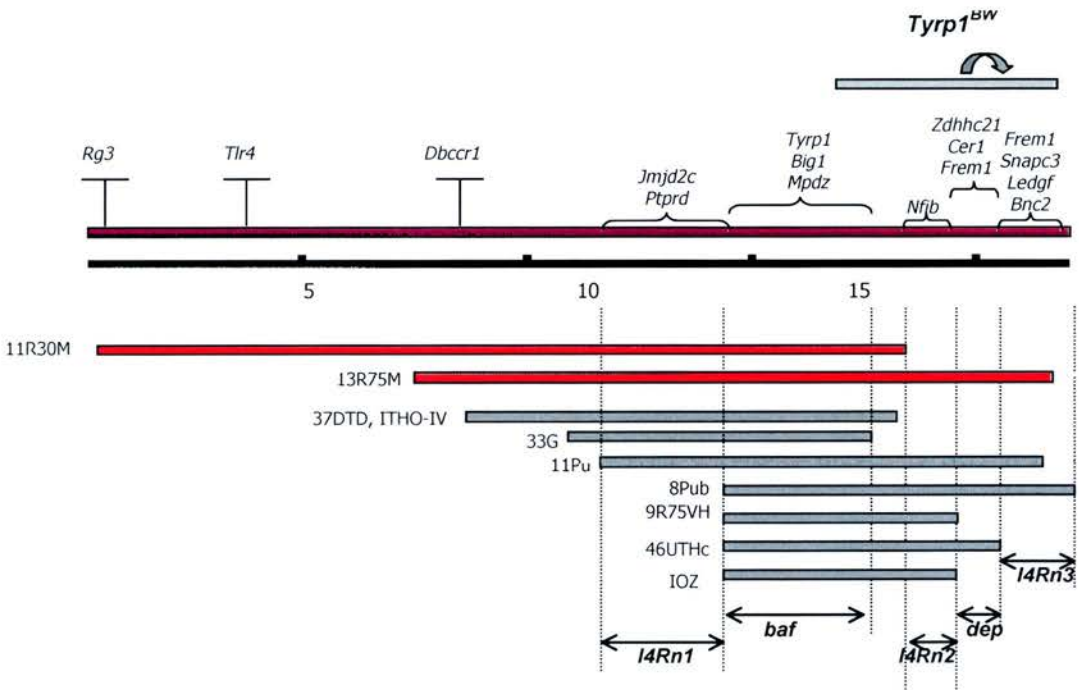

[B]

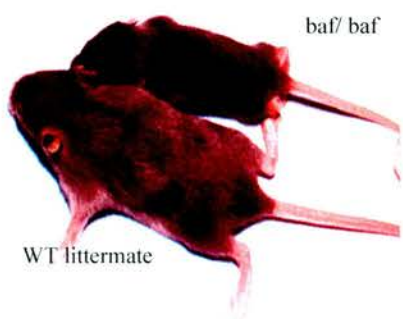

[C]

Figure 2.5: Regional ENU mutagenesis screen
[A] A simple two-generation scheme for isolating recessive phenotypes. Wild-type mice were treated with ENU before crossing with a brown mouse that carries homozygous brown mutation (*Tyrp1*$^{b\,b}$). The ENU-mutagenised chromosomes were then placed over 2 specific *brown* interval deletion by crossing with mouse carrying a known deletion. The resultant offspring are phenotypically screened for abnormalities.
[B] Three examples of ENU mutant generated by the regional ENU mutagenesis screen. Out of the 26 mutants, 7 of them have craniofacial or skeletal defects. Detailed phenotypic data may be available from Monica Justice.

[A]

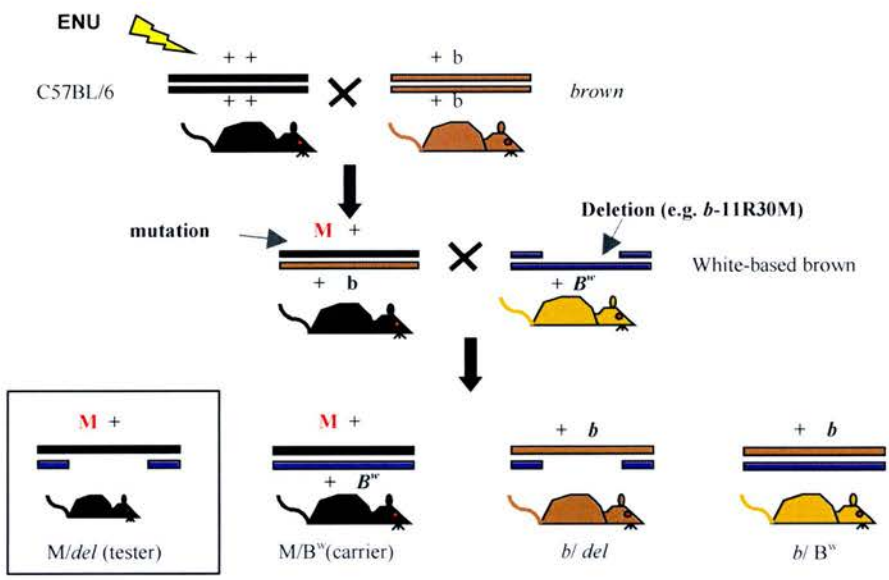

[B]

2.2. Results

Some of data presented in this section were published recently (Smyth et al., 2006). Here I describe my contribution to the work (details of my contribution are available in Appendix IA), which mainly involves refining deletion endpoints that define a mutation, so as to include or exclude certain genes of interest. In short, my major findings include:

- Out of 2 sub-groups of proximal and distal deletions, the furthest proximal and distal deletions were identified to be *b*-11R30M and *b*-8Pub respectively.
- The extent of the *b-del* interval was thus defined.
- The furthest proximal deletion chromosome, *b*-11R30M does not include *Rgs3*.
- The involvement of brown interval gene 1 (*Big1*) in *baf* was excluded.
- The involvement of multiple PDZ domain protein (*Mpdz*) in *baf* was excluded.
- The *dep* region was reduced to 160kb which includes zinc finger DHHC domain containing 21 (*Zdhhc21*), Cerberus 1 (*Cer1*) and only part of *Frem1*.

In addition, an RT-PCR expression profile of the *brown* interval was generated, which will serve as a useful resource for future studies of the interval.

2.2.1. Study of the *brown* interval and mapping of *b-del* deletions

(i) Gene Annotation of the b-del interval

To define the extent of the *b-del* interval, the endpoints of the furthest proximal deletion and the furthest distal deletion were refined by using polymorphic markers that define the endpoints. To date, the furthest proximal and distal deletions were confirmed to be $Tyrp1^{11R30M}$ and $Tyrp1^{8PuB}$ respectively, and the *brown* interval is approximately 22Mb in physical length (Table 2.2.).

The *b-del* chromosomes have a C3H/101 background, and is maintained by crossing with *Mus Spretus*. *Mus spretus* is a wild-derived inbred strain that is evolutionarily distant from *Mus musculus*, from which common inbred strains such as C3H and 101 are derived. Therefore any short sequence in the (C3H/101) x *Spretus* mice is likely to contain several single nucleotide polymorphisms (SNPs).

These SNPs can be detected by comparing amplified sequences from *Mus spretus* and the *Mus musculus*-derived inbred strains. Informative regions were then amplified from the *b-del* mutant in question and analysed using sequence analysis software. At individual SNPs, a double peak

would indicate that the C3H/101 chromosome is retained; whereas a single peak (of *Spretus* origin) would indicate that the C3H/101 chromosome is deleted at that point. An example is shown in Figure 2.6.

All deletion endpoints that define the loci being studied (i.e. *l(4)1Rn, l(4)2Rn, l(4)3Rn, dep* and *baf*) were refined by further markers. The data is summarized in Table 2.2. Mapping data of individual *b-del* chromosomes and sequences of primers are included in Appendix IA and IB. Sequences of primers used for mapping key chromosomal endpoints can be found in supplementary table 2 and 3 in Smyth et al (2006).

Table 2.2. Relative location of Oak Ridge deletion endpoints that defines the mutants

	Proximal endpoint of deletion mutant	**Distal endpoint of deletion mutant**
Furthest proximal: *b*-11R30M (Baylor's furthest proximal)	Just distal to (deletes) regulator of G-protein signaling 3 (*Rgs3*)	Lies about 300kb distal of multiple PDZ domain protein (*Mpdz*).
Furthest distal: *b*-8Pub	Cuts between *Ptprd* exon 9 and 10.	Loss at *Bnc2*-3'.
Baylor's furthest distal: *b*-13R75M	Lies within a gene desert between toll-like receptor 4 (*Tlr4*) and 'deleted in bladder cancer 1' (*Dbccr1*).	The R/L region* includes *Snap*, *Psip1* and 3 novel genes.
l(4)1Rn	Proximal end of *b*-11Pu: cuts *Jmjd2c* (exon 18 to 3')	Proximal end of *b*-8Pub [as above]
l(4)2Rn	Distal end of *b*-11R30M [as above]	Distal end of *b*-9R75VH: cuts *Nfib* (5' to exon4)
l(4)3Rn	Distal end of *b*-46UTHc: cuts *Frem1*.	Distal end of *b*-8Pub [as above]
dep (depilated)	Distal end of *b*-IOZ: does not disrupt *Zdhhc21*.	Distal end of *b*-46UTHc [as above]
Baf (brown-associated fitness)	Proximal end of *b*-46UTHc and *b*-IOZ: lies within gene desert between *Ptprd* and *Tyrp1*	Distal end of *b*-37DTD, *b*-ITHO-IV, *b*-33G which loses, cuts and retains *Big1* respectively.
$Tyrp1^{B/w}$ (white-based brown)	*Tyrp1* intron1, 105bp from exon2 splice acceptor site.	15kb upstream of *Bnc2*, distal of deletion complex.

* 'R/L region': the distance between the two markers that are 'retained' and 'loss' at that point respectively.
^ Please refer to Appendix IA for the markers that define the endpoints, and Appendix IB for primer sequences.

(ii) Generation of an RT-PCR expression profile for the brown interval

Gene expression patterns across the whole interval were characterized by RT-PCR for the 39 known genes and 14 putative coding transcripts within the interval. RNA was extracted from BALB/c for the following tissues: brain, ES cells, eye, heart, kidney, liver, lungs, ovary, spleen, testis, E9.5, E12.5 and E16.5 embryos. Most genes are widely expressed; some have alternative

splice forms (Table 2.3). This provides resources for gene identification in mutant mouse strains within the b-del interval. RT-PCR showing multiple bands were repeated and cloned for sequencing to confirm the expression of gene. They were also checked in VEGA for alternative splice sites that may have resulted the multiple band appearance.

The RNA expression profile may serve as a useful resource for studying the Baylor mutants isolated from the regional ENU screen once their mutations are identified.

2.2.2. Mapping the distal *baf* locus

More than half of the pairwise crosses between individual b^{lethal} deletions results in the *baf* phenotype, and less than half of them are prenatally lethal (Rinchik, 1994). In addition, there were a few combinations that result in phenotypically normal mice. These combinations delete a minimal region around *Tyrp1*, and include the following: $Tyrp1^{IOZ/37DTD}$, $Tyrp1^{46UTHc/33G}$, $Tyrp1^{46UTHc/37DTD}$, and $Tyrp1^{46UTHc/ITHO\text{-}IV}$ (E.M. Rinchik, unpublished) (represented in Figure 2.8.).

Combining the pairwise complementation crosses and our mapping data, *baf* has been mapped to 2 positions, one of which is *Ptprd* (the proximal *baf*) based on the observation that minimum proximal *baf* deletions delete the 5' end of *Ptprd*. On the other hand, combinations that do not delete *Ptprd* but delete distal DNA still exhibit a *baf*-like phenotype. Therefore, a second *baf* locus distal to *Tyrp1* must exist.

My involvement of this project was to investigate this second locus. To map the distal *baf*, the endpoints of the *baf*-associated deletions were further refined using additional polymorphic markers (C3H/101x *Spretus*). The orthologue of human *C9Orf150*, which we termed the brown interval gene (*Big1* hereafter), is an uncharacterized gene that lies 70kb distal of *Tyrp1*. Using polymorphic markers, the involvement of *Big1* is ruled out based on evidence that *Big1* is deleted in 2 non-*baf* deletions (i.e. *b*-33G and *b*-37DTD in Figure 2.7B).

Mpdz involvement is also considered less likely based on a previous finding that *Mpdz* is retained in two distal *baf*-associated deletions including *b*-173G and *b*-47DthWb (Simpson et al., 1999b). When both deletions were crossed to deletions that contain intact *Ptprd* (e.g. *b*-

46UTHc) respectively, the offspring still have the *baf* phenotype (Rinchik, 1994). The *b*-173G deletion retains exon2 of *Big1* (see Appendix 1, 'Big1-ex2'), which is 320kb from the 3' of *Mpdz*. The *b*-47DthWb deletion is retained at a marker that is 152kb from the 3' of *Mpdz* (Appendix 1, '395J04-10k'). This indicates that an intact *Mpdz* is unable to rescue *baf*, and so *Mpdz* is unlikely to underlie *baf*.

Therefore, we conclude that the distal *baf* must be between *Mpdz* and *Big1*. A summary of the final mapping of *baf* is presented in Figure 2.8. Details of the mapping of *baf*-associated or complementing deletions and sequences of the marker primers can be found in Appendix IB, and the major primers are published as supplementary data (Smyth et al., 2006).

To date, the distal *baf* locus is further refined to a 179Kb region (between markers 395J04[8] and s79.48[9]) that is about 2.7Mb distal of *Ptprd1*; and 73Kb proximal to Mpdz. When blasted against the human and dog genomes in the ECR browser (Ovcharenko et al., 2005), this region was found to harbor several highly conserved elements with stringency of at least 500bp and about 80% identity (e.g. 87% of 412bp, 93% of 155bp with human).

[8] 395J04 primers: 5'GGGTTGTGGGTTCTCAGTG-3'(F) and 5'CTAGCTAGCGTTTCGTGCAG-3'(R)
[9] s79.48 primers: 5' GTGAGTGTGTGGGGGACTTT -3'(F) and 5' TCCCTGCTCCTATTGCATCT -3'(R)

Table 2.3. Expression Pattern of brown interval genes and transcripts

Gene/ tissue	Size	Brain	ES cells	Eye	Heart	Kidney	Liver	Lung	Ovary	Skin	Spleen	Testis	E9.5	E12.5	E12.5 head	E12.5 body	E16.5	E16.5 head	E16.5 body
Ambp	249	+	+	+	+	+	+	+	+	+	+	+	+	+	+	+	+	+	+
Kif12	169	-	+	-	-	+	+	-	-	-	+	-	-	+	-	+	+	-	+
Col27a1	275	+	+	+	+	+	+	+	+	+	+	+	F	+	+	+	+	+	+
Orm1	223	-	-	+	+	+	+	+	F	+	+	-	F	-	-	-	+	+	+
Orm3	222	-	?	-	-	-	+	-	-	-	-	-	-	-	-	-	F	F	F
Orm2	216	-	-	-	F	-	+	-	+	+	-	+	+	-			+		
Akna	182	F	+	+	+	+	+	+	+	+	+	+	+	+	+	+	+	+	F
Whrn	198	+	+	+	+	+	+	+	+	+	+	+	F	+	+	+	+	+	+
Atp6	168	+	+	+	+	+	+	+	+	+	+	+	+	+	+	+	+	+	+
C9Orf91	205	+	+	+	+	+	+	+	+	+	+	+	+	+	+	+	+	+	+
Tnfsf15	207	-	F	-	F	+	+	+	+	?	-	-	-	F	F	F	F	F	F
Tnfsf8	250	-	-	+	+	+	+	+	-	F	+	-	+	-	-	-	+	+	-
Tnc	416/260	-	+	F	F	F	-	-	+	+	-	-	-	+			+		
Pappa	173	+	+	+	+	+	-	+	+	+	+	+	+	+			+		
Astn2	344	+	-	+	+	+	+	+	+	F	+	+	F	+	+	+	+	+	+
Trim32	140													+			+		
Tlr4	499	+	-	+	+	+	+	+	+	+	+	F	+	-			+		
Dbccr	277	+	-	+	?	?	?	+	-	-	-	+	-	+	+	+	+	+	+
Cdk5rap2	172	+	+	+	+	+	+	+	+	+	+	+	+	+	+	+	+	+	+
Egf15	262	+	F	+	+	+	+	+	+	+	+	+	F	+	+	+	+	+	+
Tle1	242	+	+	+	+	+	+	+	+	+	+	+	+	+			+		
Rasef	198	-	+	+	F	+	+	+	+	+	+	+	+	+	+	+	+	+	+
Frmd3	207	+	+	+	+	+	+	+	+	+	+	+	+	+	+	+	+	+	+
Jmjd2c	284	+	+	+	+	+	+	+	+	+	+	+	+	+	+	+	+	+	+
NM025849	271	+	+	+	+	+	+	+	+	+	+	+	+	+	+	+	+	+	+
Ptprd	257	+	+	+	+	+	+	F	+	+	-	+	F	+			+		
Tyrp1	285	+	-	+	-	-	-	-	-	+	+	-	-	+			+		
Big1	178	+	-	F	F	+	+	+	+	-	-	-	-	-			+		
Mpdz	518/224	+	+	+	+	+	+	+	+	+	+	+	+	+			+		
Nfib	244	+	-	F	F	+	+	-	+	+	-	F	-	+			+		
Zdhhc21	239	+	+	+	+	+	+	+	+	+	+	+	+	+	+	+	+	+	+
Cer1	420	-	-	-	-	-	-	-	-	-	-	-	-	-			-		
Frem1	235	+	F	+	+	+	+	+	+	+	+	+	+	+	+	+	+	+	+
C9Orf52	332	+	+	+	+	+	+	+	+	+	+	+	+	+	+	+	+	+	+
Snapc3	295	+	+	+	+	+	+	+	+	+	+	+	+	+	+	+	+	+	+
Ledgf	503	-	+	-	+	+	+	-	+	-	-	+	+	+			+		
C90Orf93	230	+	+	+	+	+	+	+	+	+	+	+	+	+	+	+	+	+	+
Bnc2	238	+	+	+	+	+	+	+	+	+	+	+	+	+	+	+	+	+	+
Transcripts > 1 exon, contains ORF.																			
ts58.76	267	?	?	?	?	?	?	?	?	?	?	?	?	?	?	?	?	?	?
ts58.98	298	-	-	-	-	-	-	-	-	-	-	+	-	-	-	-	-	-	-
ts67.0	233	-	-	-	-	-	-	-	-	-	-	-	-	-	-	-	-	-	-
*ts68.6	263	-	+	-	-	-	-	-	-	-	-	-	-	-	-	-	-	-	-
*ts68.8	246	+	+	+	+	+	+	+	+	+	+	+	+	+	+	+	+	+	+
ts76.8	148	?	?	?	?	?	?	?	?	?	?	?	?	?	?	?	?	?	?
Gapdh control	269	+	+	+	+	+	+	+	+	+	+	+	+	+	+	+	+	+	+

KEY:
'+' expressed;
'-' not expressed;
'F' faint band (but may be expressed);
'?' RT-PCR result was inconclusive, may represent multiple bands that are yet to be verified.
Blank – not completed.
* 'ts68.6' and 'ts68.8' are specific RT primers for amplifying the 10-fold repeat transcript (Smyth et. al., 2006).

Figure 2.6: Deletion Mapping
At the nucleotide base where C3H/101 (base A) and *spretus* (base T) are polymorphic, the double peak in Deletion A (base T/A) shows that both C3H/101 and *spretus* DNA are present at this genomic location, meaning that the chromosome is not deleted at this point. Whereas Deletion B only has a single peak (base T), showing that the C3H/101-derived chromosome is deleted at this point, and that the observed sequence is derived from *spretus*.

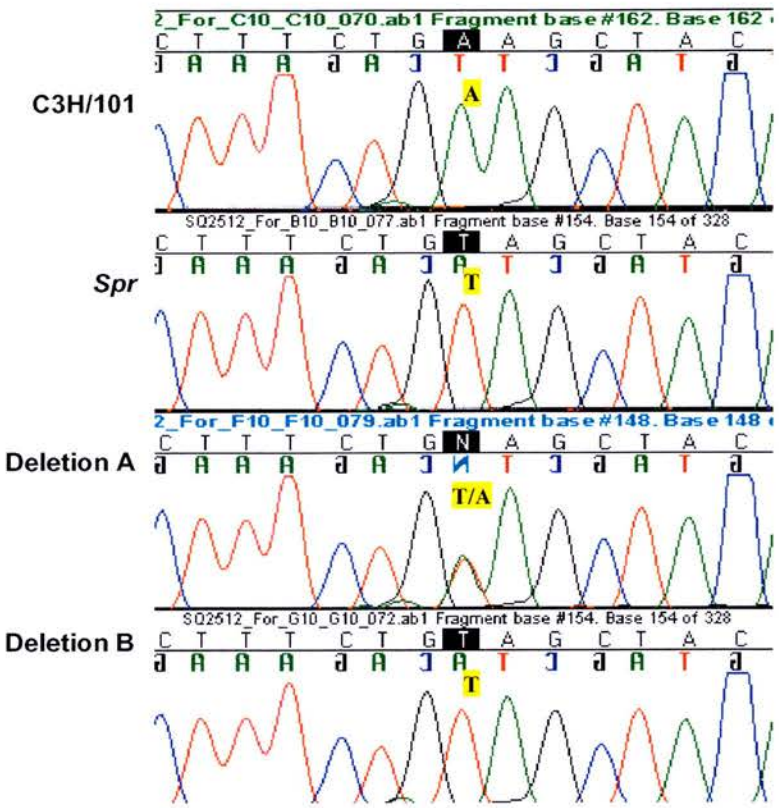

Figure 2.7: The involvement of *Big1* is ruled out in *baf*

[A] The relative location of *Tyrp1*, *Big1* and *Mpdz* (VEGA browser). The distal *baf* region was mapped within this region (Each bar line represents a 20-kb interval).

[B] Sequence traces showing that *Big1* is not related to *baf*. The three *b-del* mutants *b*-ITHO-IV, *b*-37DTD and *b*-33G that carry a *spretus* chromosome are all normal (non-*baf*). However, each one of them deletes, disrupts or retains *Big1* respectively, showing that the presence or the loss of *Big1* does not alter the *baf* phenotype and must therefore be unrelated to *baf*.

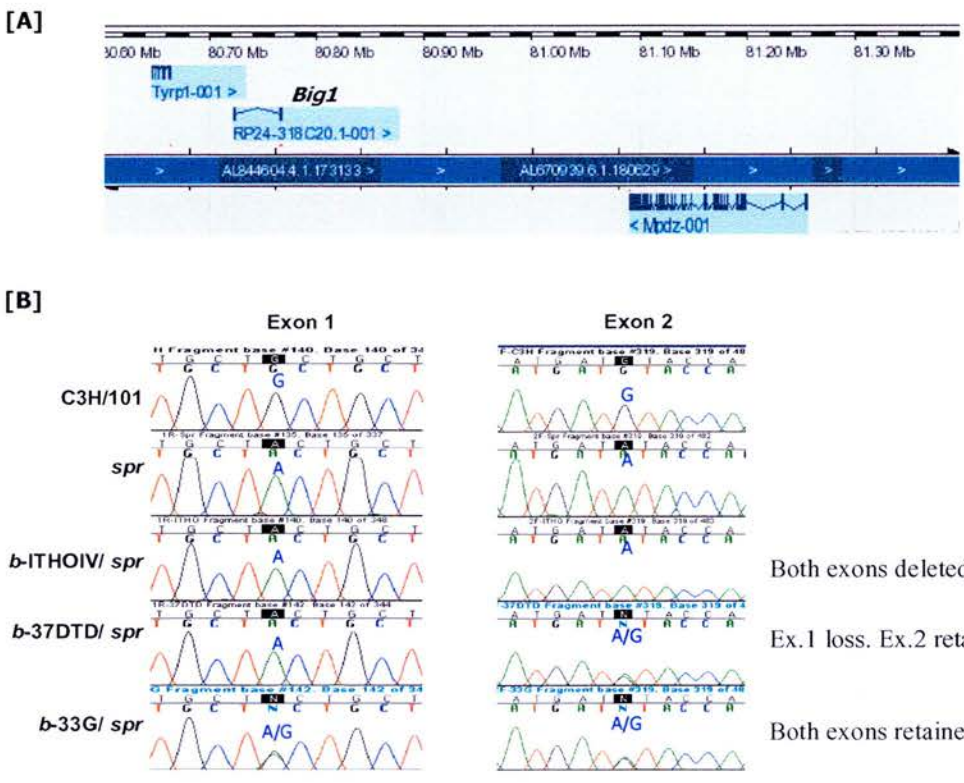

Figure 2.8. Final mapping of *baf* to two positions on either side of *Tyrp1*
The proximal *baf* locus is defined by a non-*baf* deletion *b*-46UTHc and a *baf* deletion *b*-9R75VH. The 179-kb distal *baf* locus is defined by the furthest distal non-*baf* deletion *b*-ITHO-IV and the furthest proximal *baf* deletion *b*-173G. Green bars represent the distance between the two markers that are 'retained' and 'loss' at that point respectively. The vertical black line indicates the 179-kb region of highly conserved elements where the distal *baf* is now mapped. Fine map of the deletion endpoints are available in Appendix 1A.

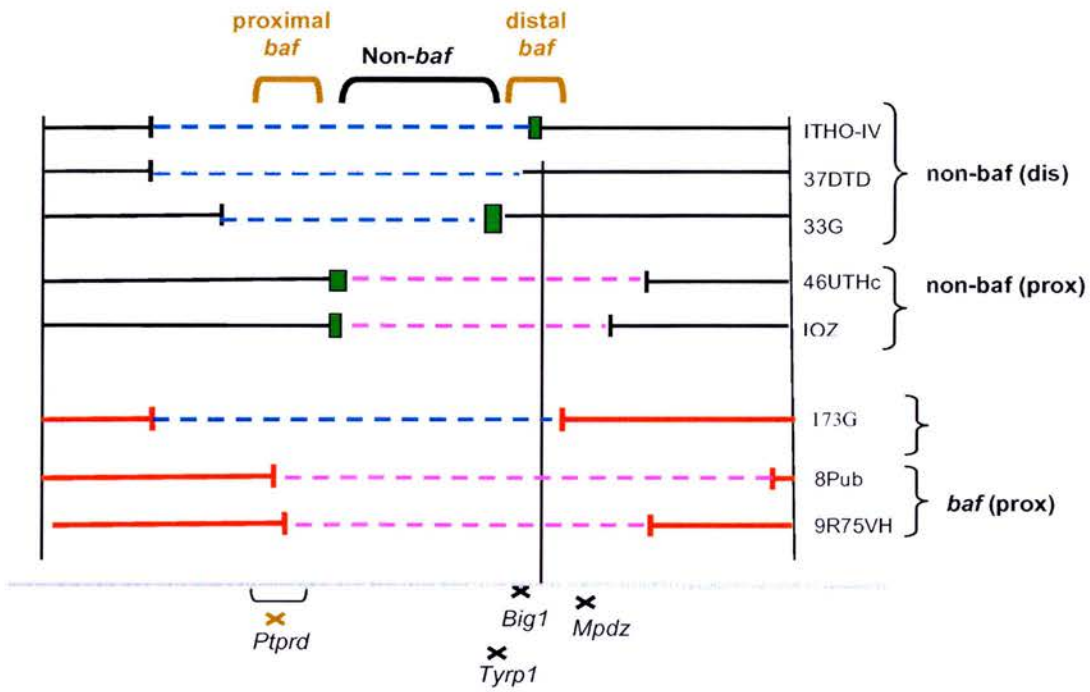

2.3. Discussion

2.3.1. Mapping of baf

In this study, the *baf* deletion was finely mapped by refining the deletion breakpoints of the *b-del* chromosomes using sequence polymorphisms. As a result, 2 loci were identified.

The proximal locus is likely to be *Ptprd* because some of the non-complementing (*baf*) deletions lose part of the coding *Ptprd* and results in the *baf* phenotype. This is supported by previous literature that *Ptprd* $^{-/-}$ mice have neurological defects that is consistent with those observed in many of the *baf* deletions (Uetani et al., 2000). Therefore, the disruption of *Ptprd* is likely to underlie *baf*. However, in some cases, even though the coding region of *Ptprd* is intact in the *b-del* chromosomes; they do not complement *baf*. Therefore, we conclude that a second locus must exist within the mapped region.

Initially, *Big1* and *Mpdz* have both been considered candidates of the distal *baf* region, however, the involvement of both genes was ruled based on: (1) *Big1* is deleted in two complementing (non-*baf*) deletions; and (2) *Mpdz* is retained in two non-complementing (*baf*-associated) deletions. This is consistent with previous findings in our lab that *Big1* does not rescue *baf* phenotype completely although it seems to rescue the male hypogonadism to a limited extent but with varied phenotypes (Andrew Childs, unpublished data).

Using further markers, the distal region is now reduced to a 179kb region, which contains several highly conserved elements. These elements do not encode known or predicted genes. Therefore, it is conceivable that they may represent potential regulators of *Ptprd*, separated from its target gene by *Tyrp1* (and *Big1*). This is consistent with the fact that, although the effects of the *baf* mutation are heterogeneous, individual *baf* mutants of the proximal and distal *b*-deletions can not be distinguished from each other. So the proximal and distal loci may be in the same expression pathway, thus have similar effect as deleting *Ptprd* itself.

Nevertheless, we do not rule out the possibility that the distal deletion may delete regulatory elements for other genes, such as *Mpdz*, or a distant gene on the chromosome (Kleinjan and van Heyningen, 2005). But given the above data, this possibility seems less likely. To assess

whether the 179-kb segment contains elements that underlies *baf*, the region could be deleted with a simple deletion to observe the consequence of it.

2.3.2. Expression Patterns of genes across the b-del *interval*

The RT-PCR results (Table 2.3) indicate the presence of transcripts in the selected tissues; however, it is not informative for determining the level and specific location of expression. In addition, there are alternative ways of looking at expression patterns that are readily available in the following databases:

-NCBI (Jax/ Unigene) cDNA
-EMAGE database http://genex.hgu.mrc.ac.uk/Emage/database/emageIntro.html (mouse)
-SAGE data http://5sage.gi.k.u-tokyo.ac.jp (human line)
-Microarray http://www.mged.org/index.html
-MPSS (massively parallel signature sequencing) http://mpss.licr.org/ & http://sgb.lynxgen.com
-EURExpressII http://www.eurexpress.org/ee/intro.html (mouse embryos RNA *in-situ*)

Chapter 3 – Molecular analysis of *dep*

3.1. Introduction

3.1.1. Mapping of *dep* interval

The original background on which the *dep* mutation arose was an offspring of a cross between a mouse that was T/tufted(tf) and a mouse that was C57BL/10 (Green, 1970). The T/tf line was a stock used for study of the T-complex on mouse chromosome 17, and is heterozygous for Brachyury (on one chromosome 17) and tufted (on the other chromosome 17). According to the information supplied by the Jax® database[10], *dep* was subsequently crossed to various strains including CBA/Ca, Sec/1 and C3H, before it was crossed to C57BL/6 for 85 generations. Since the re-derivation of the strain at the MRC, *dep* has been maintained by homozygote crosses until recently, *dep* was crossed once to C57BL/6, and subsequently maintained by heterozygote crosses for the purpose of obtaining age-matched controlled littermates for homozygotes.

Over the past 50 years, a panel of 30 chromosomal deletions within the 22Mb *brown* (*b*, *Tyrp1*) interval has been generated at the Oak Ridge Laboratories as part of the specific loci test (SLT) (Davis and Justice, 1998). *Dep* was initially mapped to the *b-del* interval by a 3-point cross for studying the linkage of *dep* with *brown* (*Tyrp1*) and pintail (Pt) on chromosome 4 (Mayer et al., 1976). The recombination frequency for the *brown-dep* was estimated to be 1.93, meaning that the chance of the two loci being segregated is low, and thus the 2 loci are likely to be closely linked.

In combination with the sequence data generated from BAC contig, the *brown* deletion endpoints have been utilized to define the *dep* interval, which has been mapped to a very small region at the distal end of mouse chromosome 4.

This is defined by complementation analysis of *dep* against the *b-del* deletion panel. Out of the 30 deletion chromosomes, $b\text{-}del^{IOZ}$ is the furthest distal deletion that when crossed to *dep*, the offspring exhibit the hair loss phenotype. $b\text{-}del^{46UTHc}$ is the furthest proximal deletion that yield

[10] Breeding history of *dep* available from: http://jaxmice.jax.org/strain/003020_3.html

offspring with normal appearance when crossed with *dep* (Rinchik, 1994). This indicates that the mutation of *dep* most likely lies within the genomic difference of these 2 deletions, defined by the distal breakpoints of both *b-del*^{1OZ} and *b-del*^{46UTHc} (Figure 3.1A). The endpoints of these deletions were further refined by polymorphic markers, and from this the region has been reduced to about 160kb which contains 3 genes that lie at the distal end of the *b-del* complex; *Zdhhc21*, *Frem1* and *Cerberus1* (See Table 2.2. and Figure 2.4.).

Nevertheless, there may also be a possibility that a regulatory element of a distant gene is deleted or disrupted in *dep*. However, our subsequent data shows that *Zdhhc21* is most likely to be affected in *dep*.

3.1.2. Zdhhc21 is the most probable candidate for *dep*

Despite its expression in developing hair follicles, previous literature has shown that *Frem1* is associated with 2 ENU-induced alleles and the classical mutation *head blebs* (*heb*) which is characterized by the formation of embryonic subepidermal blisters, leading to subsequent eyelid and limb defects after birth (Smyth et al., 2004). Furthermore, complementation analysis between a *Frem1* mutant (*bfd*) and *dep* gives normal mice (unpublished data, Monica Justice), suggesting that *Frem1* involvement in *dep* is unlikely. In addition, no *Frem1* mutations were found in DNA of *dep* mice. *Cer1* has also been knocked out previously but the null mutants do not exhibit *dep* phenotype (Shawlot et al., 2000; Simpson et al., 1999a). All known exons of both genes have been sequenced in *dep* but no mutations were found. Having ruled out the involvement of the other 2 genes, *Zdhhc21* remains most likely candidate for *dep*.

3.1.3. Functional domains of Zdhhc21

The mouse Zdhhc21 (zinc finger, DHHC containing protein 21) encodes a 31.2kDa protein of 265a.a. that has 4 predicted membrane-spanning domains and a cysteine-rich domain (CRD) containing a conserved DHHC (Asp-His-His-Cys) motif. The entire protein is encoded by 7 exons, each of which encodes part of a functional motif predicted in Ensembl (Figure 3.1C). The orthologous gene is located on 9p22.3 in human; and 23 DHHC members have been identified in human and mouse genome.

The DHHC-type zinc finger domain (Znf_dhhc), was first isolated in the Drosophila putative transcription factor DHZ1 (Mesilaty-Gross et al., 1999). The Znf_dhhc domain is highly conserved among all other DHHC-family proteins, however, the rest of the sequences share little or no homology beyond this consensus domain (Mitchell et al., 2006). However, it is predicted that mutation within the Znf_dhhc domain in different family members may disrupt similar cellular function even though the resulting phenotypes may be diverse. The function of the Dhhc family as a palmitoyl acyl transferase (PAT) will be discussed in Chapter 4.

3.1.4. Zdhhc21 (del-233F) mutation in *dep*

On sequencing the 7 exons in *Zdhhc21*, a 3-bp deletion was identified[11] in *dep* by comparing to the wild-type sequence (Figure 3.1B). The mutation deletes one single phenylalanine amino acid at residue 233 (del-233F). The phe233 residue lies in the C-terminal tail, downstream of the 4 transmembrane (TM) domains but does not lie within any functional domains predicted in Ensembl (Figure 3.1C). Nevertheless, the C-terminal may encode a function that has not yet been recognized. Bioinformatics predictions using online structural prediction algorithm[12] predicts the functional Dhhc motif and the C-terminal of the protein to be intracellular on the basis of in-out structure (represented in Figure 3.1C).

[11] *dep* mutation: the Zdhhc21-del233F was identified previously by Ian Smyth.
[12] Transmembrane topology was predicted by TMHMM (http://www.cbs.dtu.dk/services/TMHMM-2.0/)

Figure 3.1: The *dep* mutation

[A] Mapping of the *dep* interval against the *b-del* complex. When *dep* is crossed with the deletion of *b*-IOZ (bars indicates extent of deletion), the offspring exhibit the hairloss phenotype, but when crossed with *b*-46UTHc, the *dep* phenotype disappears, indicating that the *dep* mutation must lie within the genomic difference of the distal breakpoints of the 2 deletions.

[B] Sequence trace showing a 3-bp deletion in *Zdhhc21* found in *dep*. The deletion of the 3 nucleotides: TCT lie in exon 7 of Zdhhc21, which has not been predicted to encode any functional domain. The deletion is not in-frame but as a result deletes one single amino acid residue at a.a.233, Phenylalanine (F).

[C] The location of *dep* mutation in *Zdhhc21*. The *dep* mutation is at the C terminal of the Zdhhc21, which is not within any of the predicted functional domain. The seven exons are indicated by alternating pink and purple bars. The red dotted line indicates the proposed transmembrane topology of Zdhhc21 as predicted by TMHMM. 'IN' and 'OUT' denotes intracullar and extracellular space respectively.

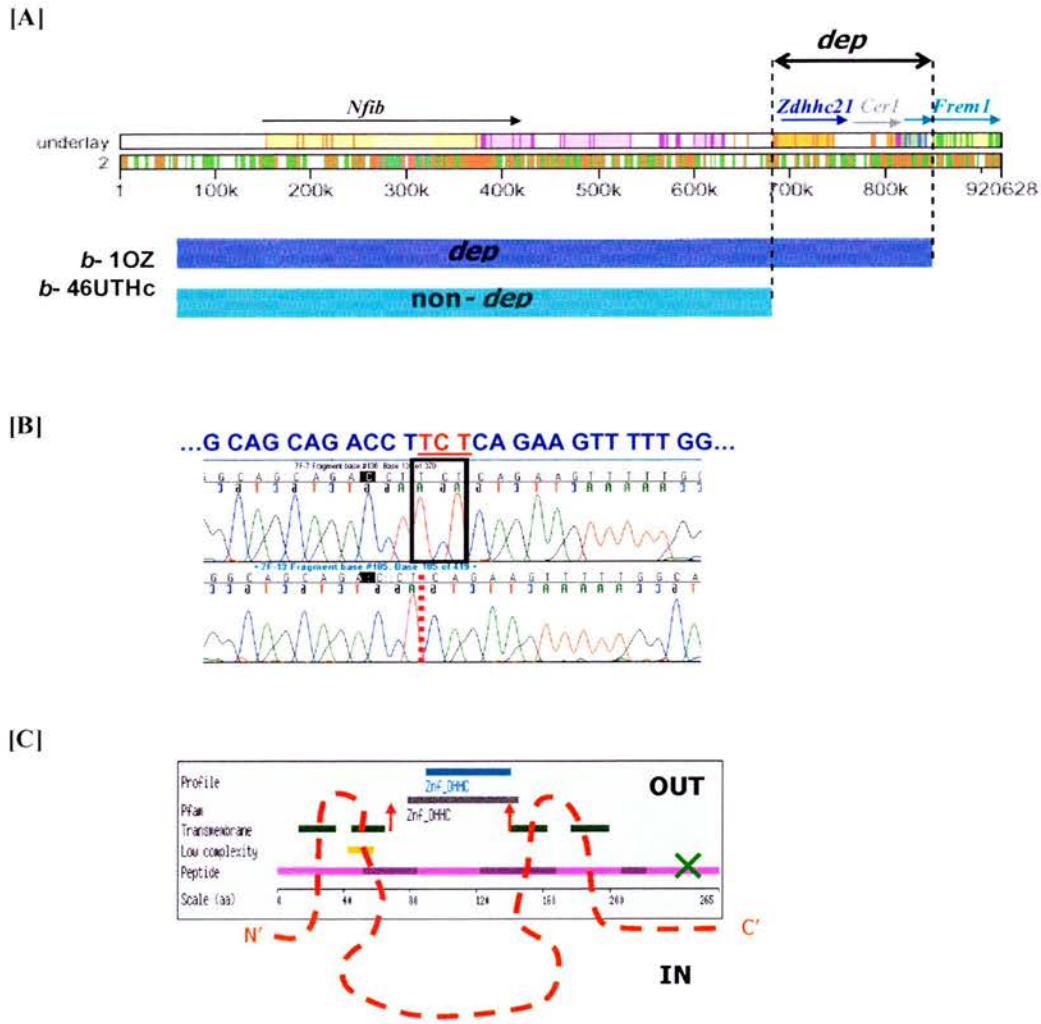

3.1.5. Molecular study of Zdhhc21 candidacy for *dep*

To verify the involvement of *Zdhhc21* in *dep*, 3 main approaches were used to answer firstly, whether wild-type Zdhhc21 has an effect on *dep* phenotype; secondly, whether other *Zdhhc21* mutants resemble the *dep* phenotype; and thirdly, the effects of knocking down *Zdhhc21* expression with RNAi.

To address the first approach, we used a BAC transgenic rescue experiment to ask whether a normal copy of *Zdhhc21* is able to rescue *dep*. So far, one rescued line has been generated that shows the rescued phenotype robustly. The second approach is to screen the candidate gene in an archive of DNA samples from individual ENU-mutagenised mice. One missense mutation has been isolated so far (L91F). A new screen on the Riken ENU-archive is also under way and may isolate some new alleles. The third approach to study Zdhhc21 function was by mean of an siRNA knockout experiment using pDECAP vector (Shinagawa and Ishii, 2003) to examine the effect of knocking down *Zdhhc21* expression in transgenic mice. Despite some potentially interesting findings, this approach lacks consistency and a robust marker for assessing RNAi transgene expression is required.

(i) BAC transgenic rescue experiment for dep

Utilisation of BAC to rescue a phenotype of interest

Bacterial artificial chromosomes (BACs) are DNA vectors that are capable of holding large DNA inserts of up to 300kb. They are essential tools for mapping the genomes of most organisms. Recently, BAC inserts have been used to generate transgenic mice in high-throughput mutagenesis programme (e.g. EUCOMM). The advantage of BAC transgenesis is its convenience of propagation and DNA preparation, and the ease of modifying genomic DNA by recombineering (Sparwasser and Eberl, 2007).

Recently, highly efficient phage-based *E.coli* homologous recombination systems have been widely used to enable large fragments of DNA such as BACs to be modified and subcloned by the use of recombination functions that are encoded by phages, without the need for restriction enzymes or DNA ligase (Copeland et al., 2001; Warming et al., 2005). Also because of its

ability to incorporate large genomic regions, BAC transgenesis allows potential regulatory regions to be included with the targeted gene.

Rescue of *dep* phenotype using BAC containing Zdhhc21

Given the evidence that suggests *Zdhhc21* to be the candidate of *dep*, the introduction of wild-type *Zdhhc2*1 expression may reverse the mutant effects *in vivo*. To test this hypothesis, a BAC transgenic rescue experiment was carried out by introducing a normal copy of *Zdhhc21* into mutant embryos to see if it is able to rescue the *dep* phenotype. To date, one transgenic line has been successfully generated by an unmodified RP23-76J17 BAC construct. This indicates that the BAC has been properly incorporated into the genome and that the transgene was successfully expressed. Most importantly, it confirms that Zdhhc21 is indeed the causative protein of *dep*.

(ii) Gene-driven Approach for isolating Zdhhc21 allelic series

To isolate an allelic series of *Zdhhc21*, a gene-based screen of two *Zdhhc21* exons was carried out on an archive of ~5300 DNA samples from individual F1 ENU-mutagenised mice [BALB/c (ENU) X C3H]. The archive was generated by a dominant genome-wide mutagenesis screen at the MRC Mammalian Genetics Unit at Harwell (Figure 3.2). Individual exons of the target gene may be chosen for high-throughout genotyping in the archive. Each of these DNA samples is paralleled with a frozen sperm sample that can be used to reconstitute stocks by a number of assisted reproductive technologies including artificial insemination, IVF and intracytoplasmic sperm injection (ICSI) (Justice et al., 1999). Live births resulted from the backcross may subsequently be used for functional analysis and for comparison with *dep*.

The gene-driven approach is reported to be very powerful in generating a variety of alleles with potentially different phenotypic outcomes resulted from different mutations of the same gene (Quwailid et al., 2004). The target gene is selected and screened for ENU-induced point mutations in an archive of genomic DNA samples paralleled by frozen genetic material such as sperm, embryos and ES cells. Once an allele is identified, the mutant line can then be recovered in live animals for detailed phenotypic analysis.

ENU is an efficient mutagen which induces point mutations at random throughout the genome at a rate of 1.5- 1.6 mutations per locus per 1000 mutagenised offspring (about 1 in 600) depending on dose and mouse strain (Justice et al., 1999). Quwailid and colleagues (2004)

reported a mutation rate of 1 in 1.01 Mbp of which 1 in 1.82 Mbp were potentially functional. In addition, approximately 64% of ENU mutations are reported to cause nonsynonymous mutation. Using this approach, series of alleles of candidate genes can be isolated, which will greatly facilitate the investigation of gene function (Justice et al., 1999).

(iii) Knocking out Zdhhc21 *using siRNA technology (pDECAP-*Zdhhc21*)*

To study the gene function of Zdhhc21 *in vivo*, the most direct way is to knock out gene expression in ES cells and determine the functional consequence in mouse. However, a possibly easier alterative such as RNA interference (RNAi) may be used to silent gene expression specifically. RNAi aims to introduce double-stranded DNA (dsDNA) into the cell, where it induces degradation of complementary mRNA and thereby suppresses gene expression (Hannon, 2002).

To achieve this, the pDECAP [Deletion of Cap structure and poly(A)] vector was used in attempt to knock down *Zdhhc21* expression in C57BL/6 by RNAi mechanism. Using the pDECAP expression vector, Shinagawa and Ishii reported a successful knockout of the transcriptional corepressor *Ski* (Sloan-Kettering viral oncogene homolog) in the transgenic mice embryos by expressing long dsRNA for *Ski* from the pDECAP vector. The transgenic embryos exhibited phenotypes that were similar to those of the *Ski*-deficient embryos, including defects of neural tube closure and eye formation (Shinagawa and Ishii, 2003).

The pDECAP vector expresses mRNA from the cytomegalovirus (CMV) promoter that lacks 7-methylguanosine (m^7G) cap structure at its 5' end and a poly(A) tail at its 3' end that normally facilitates dsRNA export to the cytoplasm, where interferon synthesis may be induced. The interferon response would otherwise lead to a block in translation and sequence-nonspecific mRNA degradation, and should therefore be avoided.

Figure 3.2. Gene-driven approach for isolating ENU allelic series for a given gene
The Harwell archive consists of ~5300 DNA samples from individual F1 ENU-mutagenised mice, paralleled with frozen sperm samples. The mice were all phenotypically screened and potentially carry a dominant mutation. The archive can be screened for a particular gene using high throughput method, to isolate an allelic series of that gene. The corresponding sperm samples may then be used to generate mutant backcross progeny, for functional analysis and comparison of phenotype with the original mutant of interest.

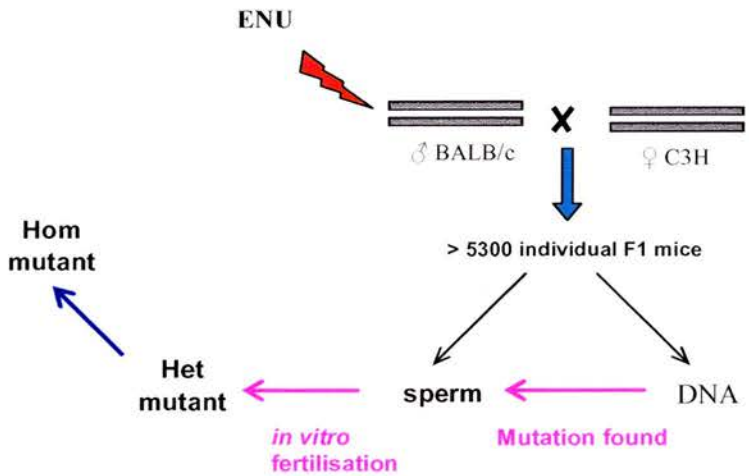

3.2. Results

3.2.1. Genotyping the mutation

Based on the 3-bp difference between wild-type and mutant *Zdhhc21*, the del-233F mutation can be rapidly genotyped on the ABI310. PCR products of exon 7, where the mutation resides, were amplified using 5'FAM fluorescence-tagged primers and loaded onto the ABI310 (Materials and Methods). The genotype of wild-type, heterozygote and homozygote can be robustly read out by the size reading of individual peaks. Heterozygotes appear as double peak that are 3-bp apart (Figure 3.3).

3.2.2. The F233 residue is conserved across mammals

The potential effects of the del-233F on Zdhhc21 function was assessed by comparing amino acid conservation at this position in paralogs and orthologs within and across species.

The *Zdhhc21* transcripts of different species were aligned in Clustal W (EMBL-EBI) and the del233F mutation is conserved across mammalian species including *Rattus norvegicus* (rat), *Bos Taurus* (bovine), *Canis familiaris* (dog), *Pan troglodytes* (chimpanzee), and *Homo Sapiens* (human). However, the residue is not conserved to *Fugu rubripes* (Fugu) (Figure 3.4). The alignment suggests that the 233F residue is likely to be important and the deletion of it is likely to have a molecular consequence.

Although the Dhhc21 protein is conserved across mammalian species, the del-233F is not conserved across other Dhhc family members (data not shown). However the residue lies 3 a.a. upstream of a 3-residue 'VFG' motif which is conserved among several members of the DHHC family, including Dhhc-2, 3, 4, 7, 15 and Dhhc21. *In vitro* assays currently suggest that this 'VFG' motif may be important for a function in post-translational lipid modification (Fukata, personal communication, Chapter 4).

The deletion of the 3 base pairs results in a single residue deletion in *dep*, as a result, subsequent codons are in frame, and the mutant protein is likely to express normally in *dep*.

3.2.3. Testing expression of *Zdhhc21* using RT-PCR

RT-PCR shows that the *Zdhhc21* transcript is present in C57BL/6 embryos at E9.5, E12.5 and E16.5, and a range of tissues including brain, eye, spleen, kidney, liver, lungs, ovary and testis (Figure 3.5). RT-PCR on *dep* skin RNA (1-week) shows that *Zdhhc21* is expressed in *dep*; the expression of mutant transcript is confirmed by the cDNA sequences. Based on the presence of the mutant transcript, the mutant protein is likely to be expressed (as proved by Western blotting in Figure 4.2. and 4.4.). Therefore, we would expect the mutant protein to be defective.

Figure 3.3: Rapid genotyping of del-233F on ABI310
The heterozygous genotype is represented by the double peak, which has size reading of '245' and '248' respectively. *Dep* has a single peak of size reading '245', which is 3-bp less than the wild-type peak that reads '248'.

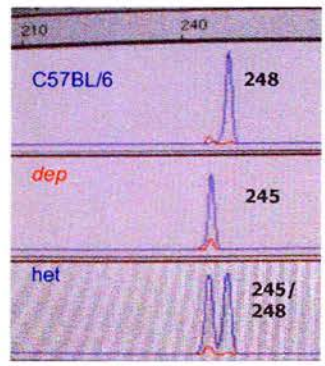

Figure 3.4: The 233F phenylalanine residue is conserved across mammalian species
The del-233F residue is conserved across mammalian species including rat, dog, human, chimpanzee and bovine, but not fugu. Asterisk (*) denotes position at which all aligned sequences share the same residue; colon (:) and dot (.) indicate strong and weak conservation respectively.

```
                  220        230        240        250        260
[dep]             IEKMSNCCEEISRPRKPWQQT-SEVFGTRWKILWFIPFRQRQPLRVPYHFANHV
Mus musculus      IEKMSNCCEEISRPRKPWQQTFSEVFGTRWKILWFIPFRQRQPLRVPYHFANHV
Rattus norvegicus IEKMSNCCEEISRPRKPWQQTFSEVFGTRWKILWFIPFRQRQPLRVPYHFANHV
Canis familiaris  IEKMSNCCEEISRPRKPWQQTFSEVFGTRWKILWFIPFRQRQPLRVPYHFANHV
Homo sapiens      IEKMSNCCEDISRPRKPWQQTFSEVFGTRWKILWFIPFRQRQPLRVPYHFANHV
Pan troglodytes   IEKMSNCCEDISRPRKPWQQTFSEVFGTRWKILWFIPFRQRQPLRVPYHFANHV
Bos taurus        IEKMSNCCEEISRPRKPWQQTFSEVFGTRWKILWFIPFRRRQPLRVPYHFANHV
Fugu rubripes     IEKMAHFSNEMFTSKRSWQFALAEVCGTRWKLLWFLPLRSRQPLQ---------
                  ****:: .::: .::.** : :** *****:***:*:* ****:
```

Figure 3.5: RT-PCR of *Zdhhc21* across tissues
Zdhh21 transcript is present in wide range of tissues including ES cells, testis, brain, eye, ovary, spleen, kidney, liver, lungs and various stages of embryos. For each RNA sample, RT-PCR of GAPDH was run in parallel as a control (data not shown).

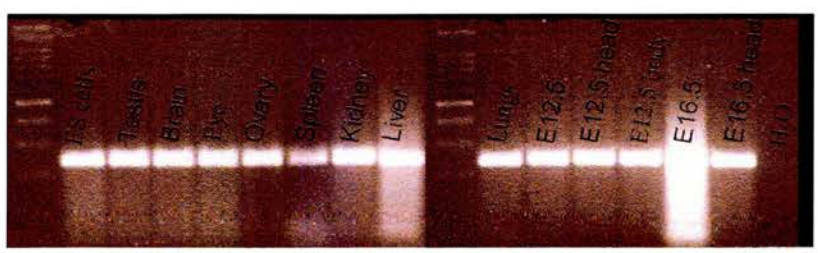

3.2.4. Investigating Zdhhc21 candidacy for *dep*

(i) Transgenic BAC rescue

Dep phenotype is rescued by *Zdhhc21*

Using an unmodified BAC, a rescue line of *dep*, *dep/dep*-Tg(RP23-76J17)1Jkn, was successfully generated. A BAC containing an intact copy of *Zdhhc21* (Figure 3.6A) was microinjected directly into 85 homozygous *dep* embryos, 36 of which were transferred into a pseudo-pregnant CD1 recipient[13] (Figure 3.6B); from there 5 were born, of which 4 had the *dep* phenotype and 1 a wild-type phenotype. This animal was identified as transgenic by PCR using 3 markers that are specific to the BAC construct, including the chloramphenicol resistance (CmR) marker specific to the carrier vector, and the proximal and distal end of the genome-specific region amplified with the T7 and SP6 primers flanking the BAC region respectively (Figure 3.6B, 3.7). Alternatively, the transgene can be genotyped robustly by electrophoresis analysis described in Section 3.2.1.

Genotyping with the transgenic markers expectedly corresponds to the rescued phenotype. The *dep/dep*-Tg(RP23-76J17)1Jkn mouse has a smooth and shiny dorsal hair coat that is comparable to wild-type, whereas the hair coat of non-rescued littermates remains greasy and disorderly (Figure 3.8). Later the non-transgenic mutant littermates lose their hair, whilst the transgenic mouse retains its hair.

The transgenic founder was backcrossed to a homozygote female, and to date, 10 out of 17 pups also exhibit the rescued phenotype (Figure 3.9). The wild-type copy of *Zdhhc21* supplied by the transgene can be reflected by the peaks that resemble the *dep*/+ genotype (Figure 3.10). Skin sections of the *dep/dep*-Tg(RP23-76J17)1Jkn rescue mice show normal histological appearance comparable to wild-type, confirming that the *dep* phenotype is adequately rescued (Figure 3.11).

In the same litter as the transgenic founder, another mouse was also found positive for the 3 transgenic markers but its *dep* phenotype was not rescued. It is possible that even though the transgene germline transmission was successful, the transgene was not expressed. Alternatively, this animal may be a mosaic in which only some populations of cells contain the

[13] The microinjection and embryo transfer were carried out by Margaret Keighren.

transgene which were insufficient to rescue the phenotype. This possibility was investigated by backcrossing the transgenic non-rescued mouse to a *dep* homozygote. If it is a mosaic, a proportion of the offspring would be expected to show a rescued phenotype given that the transgene is successfully passed on and expressed.

However, none of the 10 post-weaning offspring from the backcross is rescued, indicating that it is unlikely that the lack of rescued phenotype is due to mosaicism. Alternative, the animal might be a mosaic and that the transgene has incorporated into the genome, but was not expressed. The expression of the transgene is yet to be tested in these animals.

Deletion of *Cer1* by BAC recombineering

The BAC clone that was selected for transgenic rescue of the *dep* phenotype, RP23-76J17, is 202Mb in length and contains an intact copy of *Cer1* that lies ~40kb upstream to *Zdhhc21* (Figure 3.6A). This clone was selected because it contains minimal amount of known coding DNA other than the target gene. Nevertheless, to circumvent any effect of the *Cer1* gene, the BAC clone was modified to ensure that it only contains an intact copy of *Zdhhc21*, and that any rescued phenotype is the sole result of the expression of candidate transgene.

The deletion of *Cer1* is targeted by means of a double homologous recombination system in *E.coli* strain EL250 (For details, see Figure 7.1 in Materials and Methods), which involves 2 steps: First, the targeted region of *Cer1* was replaced with a zeocin resistance gene (ZeoR) flanked by 2 FRT sites. Secondly, the *zeoR* gene and one of the FRT sites were removed by treatment with the FLP recombinase. As a result, about 2kb of the Cer1-coding region distal to Zdhhc21 was deleted, and was replaced with 85bp of foreign DNA. The resulting construct was checked for rearrangement by restriction digestion, and the transgene was sequenced for possible mutation.

The Δ*Cer1* BAC construct was injected into heterozygous embryos and subsequently backcrossed to *dep* (see below section). Altogether, 25 animals were born and 2 were typed positive for the transgenic markers. However, neither the founder nor their transgenic offspring exhibit a rescued phenotype. With the first line, the transgene was not intact as evident by a lack of wild-type sequence across the del233F mutation.

With the second line, the transgene was intact but was not expressed based on RT-PCR data using *Zdhhc21*-specific primers and sequencing data as described below.

Generation of the *ΔCer1*-BAC transgenic line

As efficiency of transgenesis into some background is poor, the modified BAC construct was microinjected into heterozygous embryos from a cross between *dep* and an F1 superovulated female, which is a standard established line for microinjection. The embryos were then transferred into a pseudo-pregnant recipient to give a heterozygous litter (*dep*/+), which was genotyped for a transgenic founder. The transgenic founder (*dep*/+ [Tg]) was further crossed to a *dep* homozygote to yield a litter that may contain a transgenic carrier that is homozygote (*dep*/*dep* [Tg]). If the transgene is correctly passed on and expressed, the phenotype should be rescued in this animal (Figure 3.12).

This method is complicated because of the difficulty in distinguishing Zdhhc21 expression from the C57/CBA hybrid, *dep* and the BAC background (C57BL/6J). As a result, we were unable to distinguish between homozygote and heterozygotes robustly by amplifying across the del233F mutation or using polymorphic markers within the region. Therefore, markers outside the BAC genomic regions were designed.

A program called 'SPUTNIK' (see Materials and Methods) was used to develop markers of pentanucleotide repeats (simple sequence repeats, SSRs) that can be visualised on the ABI310 based on fragment size difference (Figure 3.13). The proximal and distal sputnik markers are 0.2Mb and 0.5Mb from the *dep* mutation respectively, and so if they both match, the result should be reliable unless there were 2 or more occurrences of recombination within such limited genomic distance, which is highly unlikely (Figure 3.6B – showing relative location of sputnik markers).

At the proximal sputnik marker, the transgenic animal has 2 peaks that resembles that of F1-CBA/C57 but different from the *dep*/C57 heterozygote, showing that the transgenic animal has a CBA background. This is confirmed by the distal sputnik marker at which the transgenic animal has a single peak, and is of same size to CBA and *dep*. Therefore, CBA and *dep* share the same polymorphisms, but C57BL/6 is different at both sputnik markers. It means that if the

transgenic founder has a CBA (instead of C57BL/6) background, these markers would not be able to distinguish homozygotes from heterozygotes (Figure 3.13).

To overcome this problem, the transgenic founder with CBA background (*dep*/CBA[Tg]) was crossed to a C57BL/6 mouse to switch the background onto C57BL/6 (*dep*/C57[Tg]). The subsequent cross to *dep* homozygote can then be effectively genotyped by the sputnik markers that distinguish homozygote (*dep*/*dep* [Tg]) from heterozygote (*dep*/C57[Tg]) (Figure 3.12). However, this strategy is extremely tedious and time-consuming, so alternatively, polymorphic markers between CBA and *dep* may be designed to distinguish between heterozygotes and homozygotes.

Figure 3.6: The BAC transgenesis rescue experiment
[A] The BAC clone RP23-76J17 harbours intact genomic sequence of *Zdhhc21* and *Cer1*. It contains an intact copy of *Zdhhc21* and about 40kb upstream of it which may contain regulatory elements for *Zdhhc21*. Each bar line represents a 20-kb interval.
[B] Summary of the BAC rescue experiment. The purified BAC construct is microinjected into *dep* embryos and transferred onto pseudo-pregnant female to produce a transgenic founder, which can be genotyped by the CmR marker, and the proximal and distal end of the genomic BAC region with T7 and SP6 that are flanking the BAC region. The position of the 2 sputnik markers were indicated [see Section 3.2.4.(i) and Figure 3.13.].

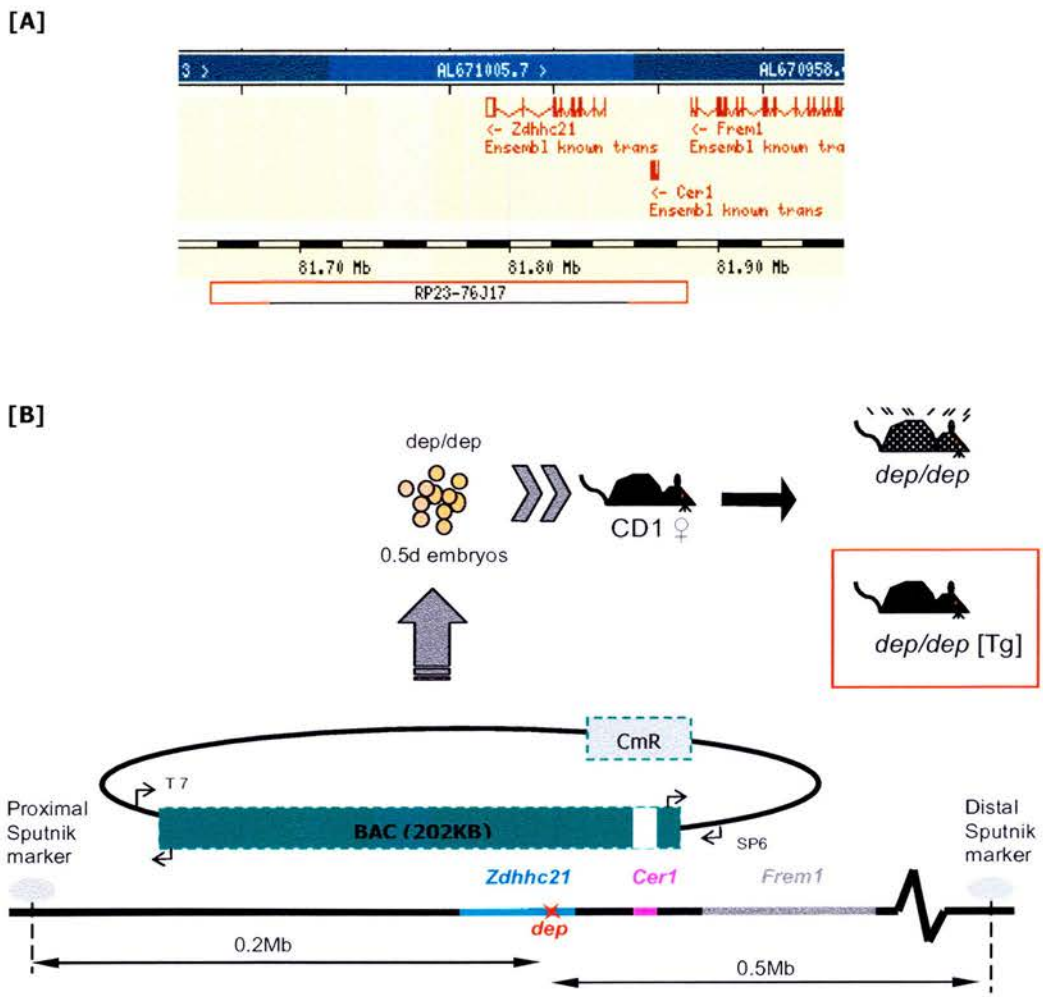

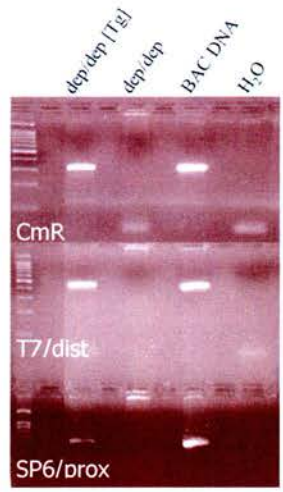

Figure 3.7: Genotyping for the BAC transgene
Three transgenic markers were used for genotyping the successful incorporation of transgene into the genome. The relative positions of the marker are represented in Figure 3.6B.

Figure 3.8: The *dep* phenotype is rescued
[A] By 3 week of age, a significant difference can be observed in the rescued homozygote by the smooth and shiny dorsal hair coat, comparing to the non-rescued littermate, which exhibits the typical matted and disorderly pattern and sparse hair around the eyes. [B] The difference remains apparent at week 6.

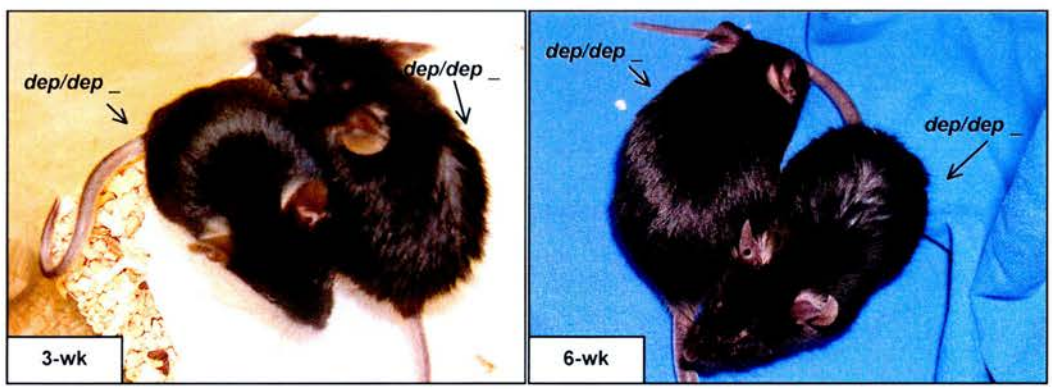

Figure 3.9: Offspring of the transgenic founder
Backcross litter between the original transgenic founder (*dep*/*dep*-Tg(RP23-76J17)1Jkn) and *dep* homozygote, in which 2 out of 4 are rescued. Altogether, the original rescued founder has generated 10 out of 17 rescued mouse, showing that the transgene is robustly incorporated into genome and successfully passed on to the next generation.

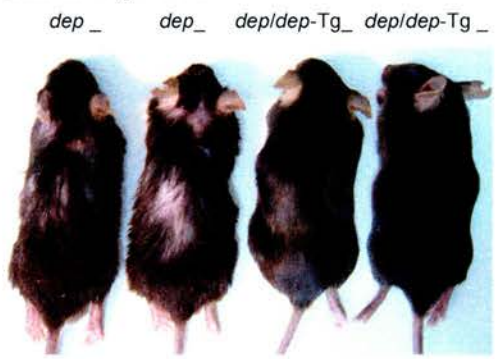

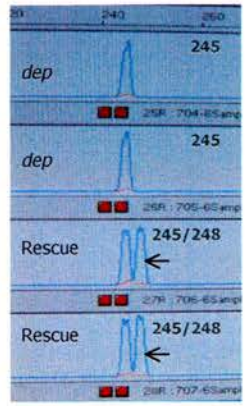

Figure 3.10: Alternative genotyping for the transgene
The presence of a wild-type Zdhhc21 copy may be tested robustly on the ABI310 as described in Section 3.2.1. The presence of the wild-type peak, labeled '248', would indicate the presence of a wild-type copy of Zdhhc21 in the genome.

Figure 3.11: H&E sections of rescue and non-rescue littermate
At the same age, the rescue and non-rescue mice are in mismatched hair stage. The anagen follicle in the non-rescued mouse (arrow) appears to be abnormally small.

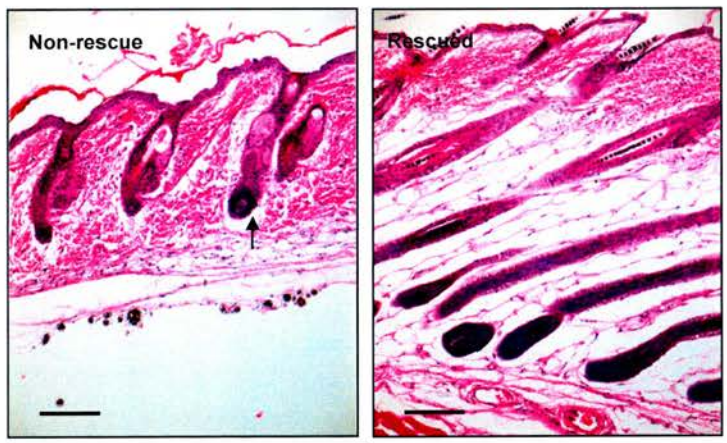

Figure 3.12: Alternative breeding scheme for generating BAC transgenic rescue animal
The BAC construct was microinjected into heterozygous embryos which were then transferred into a pseudo-pregnant recipient to give a heterozygous litter (*dep*/+). The transgenic founder (*dep*/+ [Tg]) was further crossed to a *dep* homozygote to yield a litter that may contain a transgenic carrier that is homozygote (*dep*/*dep* [Tg]). If the transgene is correctly passed on and expressed, the phenotype should be rescued in this animal (red box). The transgene may be genotyped by markers of CmR and the proximal and distal BAC ends. Homozygotes and heterozygotes are distinguished by using markers flanking the BAC region to avoid the effect of the BAC transgene (Figure 3.6B).

CBA and *dep* share the same polymorphism at both BAC-flanking markers, whereas C57 is polymorphic. Since the heterozgoous transgenic animal will have 50% chance of inheriting either CBA or C57 background, they were genotyped before backcrossing to *dep*. Animal with a CBA background were transferred onto a C57 background before backcrossing to *dep* (blue box). Tg, transgenic.

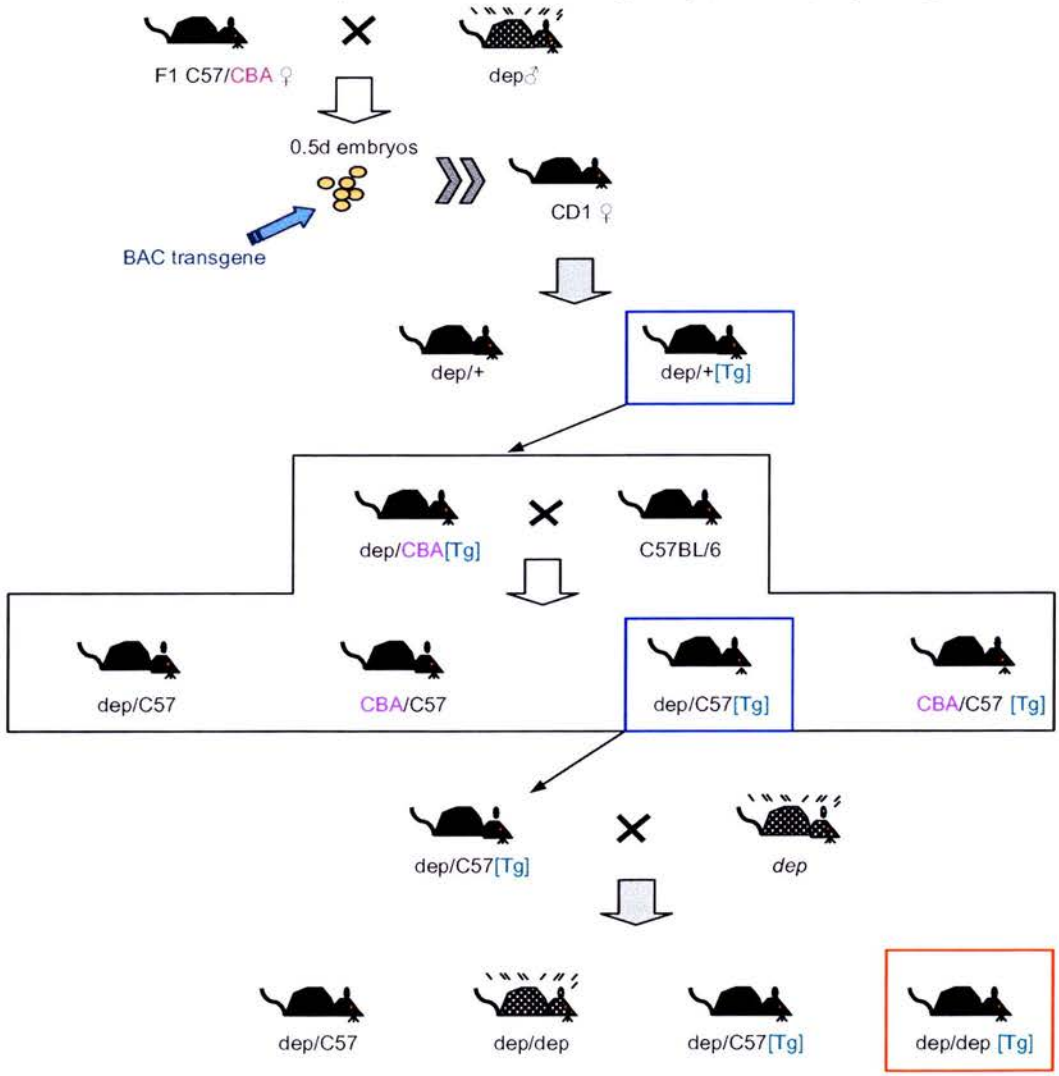

CmR + BAC ends	-ve	-ve	+ve	+ve
Markers flanking BAC region			heterozygous	homozygous

Figure 3.13: Markers flanking genomic BAC region
At the proximal marker, *dep*/+[Tg] has 2 peaks similar to that of CBA/C57 but is different from *dep*/C57, showing that the mouse has a CBA background. At the distal marker, *dep*/+[Tg] has a single peak, which is the same size of that of CBA and *dep*. Therefore, CBA and *dep* share the same polymorphism at both markers, and that this animal has a CBA background. For distinguishing homozygotes from heterozygotes, the animal must have a C57 background.

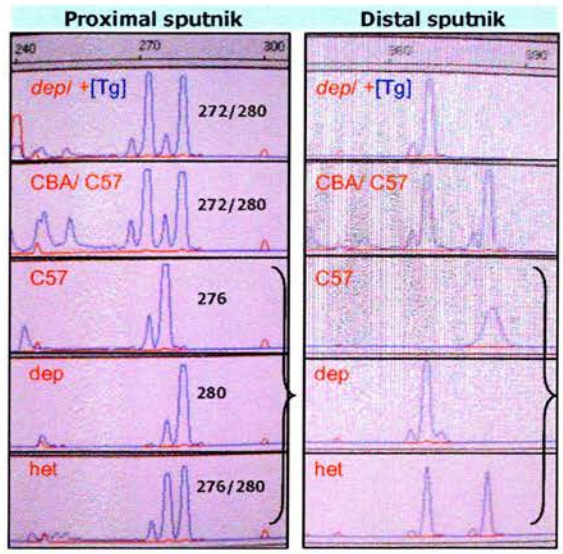

(ii) Isolating new Zdhhc21 mutations from Harwell ENU archive

One *Zdhhc21* allele (L91F) is isolated

The MRC Mammalian Genetics Unit has an archive of DNA samples from mutagenised mice, matched with frozen sperm from the same animals. I screened the DNA from this archive for new mutations in *Zdhhc21*. Altogether, about 5300 samples from the Harwell ENU-archive were successfully screened in exon 3 and exon 4 of *Zdhhc21* by heteroduplex analysis, which involves the denaturation of dsDNA and subsequent formation of heteroduplex, followed by detection of loops and bubbles in heteroduplex regions where the two DNAs differ.

Exon 3 encodes part of the Znf_Dhhc domain which is highly conserved across species; whereas exon 4 encodes part of the same domain and part of the third transmembrane domain. When a shift was detected by the fluorescent signal on the ABI3100 machine, the 4 DNA samples within the pooled sample were individually amplified by PCR and repeated by CESE (Section 8.6.1. in Materials and Method). Any samples still showing the shifted peak were then sequenced using both 5' and 3' primers to identify the mutation[14].

In total, about 1.33Mb coding sequence was screened[15] and one ENU mutation was isolated[16]. It is a C->T substitution at base 479 (Figure 3.14A), which convert a leucine (CTC) residue into Phenylalanine (TTC) at residue 91 where the Znf_dhhc domain lies (479C->T Leu91Phe). Both amino acids are neutral, the L91F mutation results in the R-group '-CH2' of leucine being replaced by a benzene ring in phenylalanine. This could have a phenotypic effect if the size of the group is important even though both groups are neutral.

The L91F allele is conserved across species

The L91F residue is conserved across multiple species (Figure 3.15) including *Rattus norvegicus* (rat), *Bos Taurus* (bovine), *Canis familiaris* (dog) and *Homo Sapiens* (human) and also to *Takifugu rubripes* (pufferfish), *Gallus gallus* (chicken) and *Tetraodon nigroviridis* (Tetraodon). But despite the shared zinc finger cysteine-rich DHHC domain, the residue is not

[14] After the initial screen on AB3100, 21 (exon 3) and 14 (exon 4) PCR samples were re-run on AB310, but none of them showed a shift; this may be due to discrepancies in the operating temperature (32°c on ABI3100 and 60°c on ABI310). To confirm, all samples that showed a shift on the ABI3100 were sequenced (6x4 for ex3 and 3x4 for ex4).
[15] About 1.33Mb coding sequence was screened: [(exon3: 112bp) + (exon4: 139bp) * 5300 samples] = 1.33Mb
[16] Etiology plate 21 well A2.

conserved among other Dhhc family members. Nevertheless, the L91F mutation may be important because it lies immediately next to one of the 2 CXXC motifs upstream to the consensus core of the Dhhc finger (Figure 3.15).

The isolated mutation disrupts a restriction site in *Zdhhc21*

The 479C->T mutation disrupts a *Sac*I restriction site, which normally cut the screened PCR product once at GAGCT^C and divide this 257bp fragment into about 174bp and 83bp with 3' overhang. The mutant fragment remains uncut. This method allows rapid genotyping to distinguish between wild-type, heterozygote and homozygote mice for the Harwell allele (Figure 3.14B).

Re-derivation of L91F allele by ICSI and IVF

The frozen sperm from the BALB/c ENU-treated male was obtained from MRC Mammalian Genetics Unit, Harwell. Several attempts using *in vitro* fertilization had failed due to low sperm density and poor quality possibly as a result of sperm samples not being properly cryo-protected, stored or transported. After several attempts, the allele was re-derived by Brendan Doe (MRC Transgenic Unit) using a revised ICSI protocol.

The resultant litters were found to segregate according to Mendelian frequencies confirmed by PCR and restrictive digestion genotyping. Since the sperm and egg are both haploid, half of the offspring typically carries the mutant allele and the other half were wild-type.

The L91F mutation complements *dep*

The heterozygote L91F carrier was crossed to a *dep* to answer whether the two mutations are allelic to the observed phenotype. The compound heterozygote between the Harwell allele and *dep* (*Zdhhc21*$^{L91F/\,dep}$) does not exhibit a phenotype, indicating that the L91F copy of the gene must be either fully functional, or at least has a sufficient function to complement the *dep* allele.

To purify the L91F mutation from other ENU mutations in the genome, the allele was backcrossed to C57BL/6 three times to ensure that the resultant mouse carries minimal amount of other ENU mutations. A homozygote of the L91F allele was generated (*Zdhhc21*$^{L91F/\,L91F}$) by a het x het cross, which has a brown hair coat (Figure 3.16A). However, the brown color coat is due to the linked *Tyrp1* mutation that is 2Mb from *Zdhhc21*. This mutation originated from the BALB/c mouse that carries mutation at *Tyr* and *Tyrp1*. The *Tyrp1* mutation disrupts a *Taq*I site

and was readily confirmed by restriction digestion (Figure 3.16B). Furthermore, skin sections of *Zdhhc21*$^{L91F/\,L91F}$ from different time points confirms that the L91F homozygote is normal (Figure3.16C).

Collaboration with RIKEN Genomic Science Centre in Japan

Despite the negative result from the Harwell-ENU archive screen, a collaboration has been set up with Dr. Yoichi Gondo from the Riken Genomic Science Centre in Japan. The Riken ENU archive consists of 10,000 samples and uses multiplex PCR for high-throughput genotyping. The PCR conditions of Exon 1, 2, 3, 4 and 7 were optimised, and the 5'FAM-tagged primers were sent to the Riken group.

Comparing the amount of DNA that will be tested in total by the end of the screen (6.38Mb), it will be 5 times as much of the Harwell screen. Since one single mutation in the Harwell ENU archive was isolated, it is estimated that at least 5 ENU mutations will be isolated from the Riken-GSC ENU archive. Currently, exon 2 and exon 4 of *Zdhhc21* has been screened in part of the archive (together represents about ~1.7Mb coding genome), from which several ENU mutations have been isolated. This includes 2 mutations from the coding region, P79P and L138V. Although L138V is a non-synonymous change, it probably has little effect based on the mild nature of the amino acid change.

Figure 3.14: Isolation of a new Zdhhc21 allele from the Harwell ENU archive
[A] The Harwell ENU DNA archive was screened by high-throughput genotyping from which a shift in the peak was identified. Peaks that contain genuine mutation tend to appear as a subtle but detectable shoulder, instead of an extra/ separate peak. Subsequent sequencing reveals the 479C->T substitution. [B] The C -> T mutation disrupts a *Sac*I restrictive site.

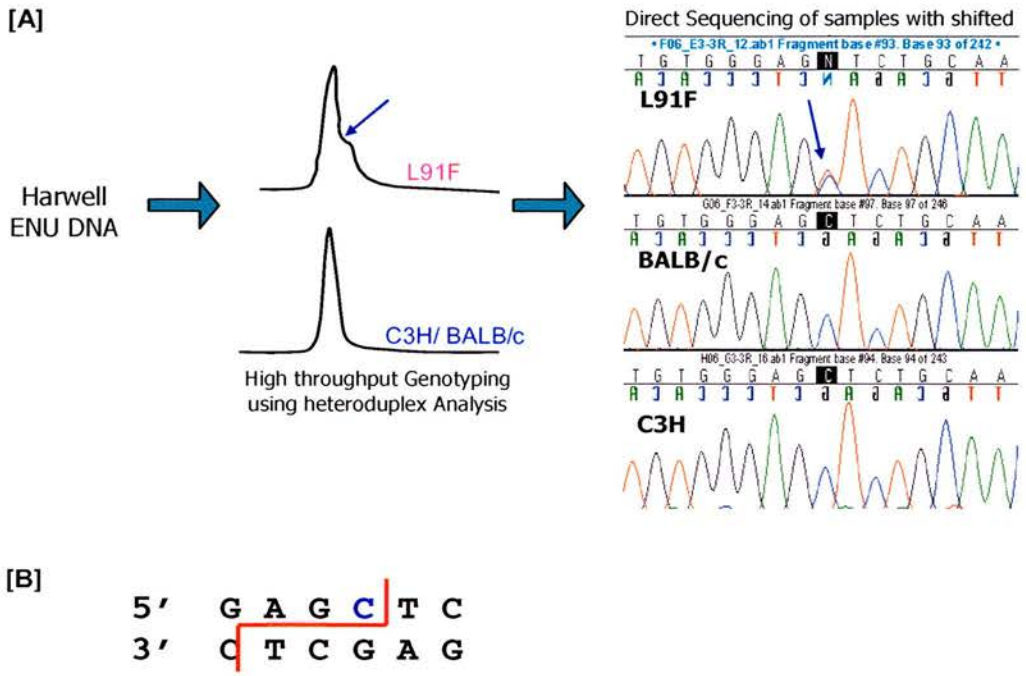

Figure 3.15: The L91F allele is conserved across species
The L91F mutation lies immediately upstream to the cysteine-rich DHHC consensus core (highlighted in green), which is also conserved across all DHHC members (data not shown).

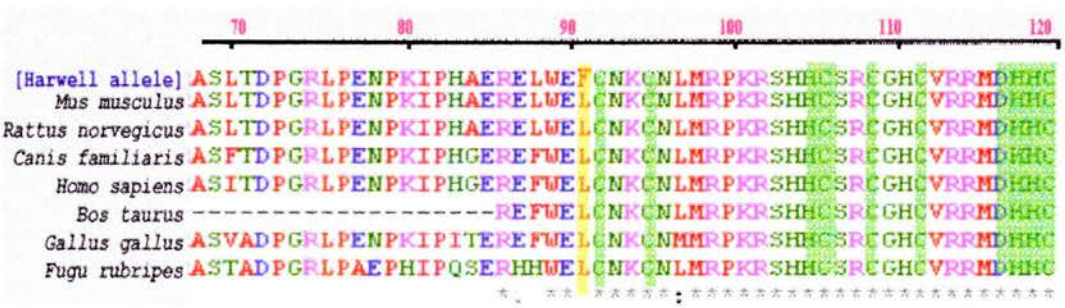

Figure 3.16: The re-derived Harwell homozygote has no phenotype
[A] Comparison between 7.5wk wild-type and L91F homozygote littermates. The homozygote has no visible hair loss phenotype. The coat colour is brown due to a linked *Tyrp1* mutation carried by the BALB/c strain that disrupts a *Taq1* site. [B] PCR products of *Tyrp1* amplified from DNA of a het x het litter are digested with *Taq*I. The *Taq*I site of L91F homozygote is disrupted and therefore remains uncut (224bp), whereas wild-type fragments are completely cut (103bp and 121bp). [C] H& E sections from 2-wk animals confirm that L91F mutants have normal histology.

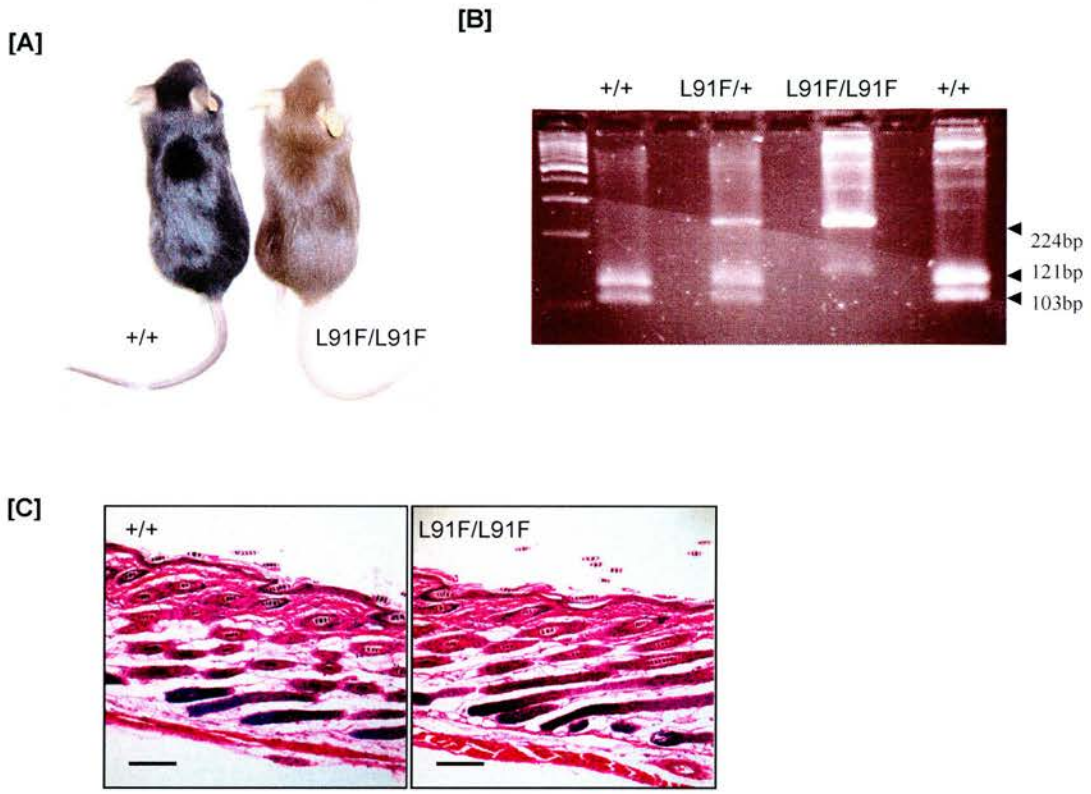

(iii) Knocking out Zdhhc21 by siRNA using pDECAP vector

The construction of pDECAP-*Zdhhc21* expression vector involves the incorporation of the target cDNA into the vector (456bp), and another copy in the opposite orientation (Figure 3.17). It is aimed that the transgenic mice will express a 456bp hairpin dsRNA from this vector and induce degradation of *Zdhhc21* RNA[17]. Using the pDECAP-Zdhhc21 fragment, several transgenic lines have been generated. The transgenic founders were typed by PCR amplification of the insert in both directions. The transgenic founder is then crossed to C57BL/6 and half of the litter was expected to carry the intact transgene.

Abnormally folded skin in the abdomen of E17.5 embryos

In another transgenic experiment with the DECAP-Zdhhc21 construct, a litter of fifteen E17.5 embryos was collected. Some embryos were positive for the forward insert, and some were positive for the reverse insert. No unusual phenotype were observed in the litter, however, 3 of the embryos appear to have highly wrinkled skin on the ventral side of the abdomen (Figure 3.18). This may be due to the mere positioning of the embryo in the placenta, where the wrinkled embryos might be forced into gesture that may result in the observed folds.

Unfortunately, it was proved difficult to correlate this observation with the genotyping data because all 3 embryos exhibiting the wrinkly appearance are only positive for the reverse insert. On the other hand, the embryos that are positive for both inserts are normal. However, the expression of the transgene was not tested, so it is not sure whether the *Zdhhc21* dsRNA was successfully transcribed in these animals or whether it is able to silence *Zdhhc21* expression. Furthermore, the genotyping data is not consistent, so this finding remains essentially inconclusive.

pDECAP-Zdhhc21 generates a hair loss phenotype

In one of the transgenic lines, 3 out of 6 pups were typed positive for both inserts of the hairpin (Figure 3.19A), this includes 1 female and 2 males. Interestingly, the transgenic female exhibits a hair loss phenotype at about 12-week (Figure 3.19B), however, the other 2 transgenic males appear normal. Intercross between the hair loss female and one of the transgenic males was set up to increase the transgene dosage. If Zdhhc21 expression was successfully knocked down, a

[17] The pDECAP-Zdhhc21 vector was designed by Peter Budd and Ian Smyth.

quarter of the litter would be expected to exhibit the hair loss phenotype. However, none of the offspring shows a hair loss phenotype even though they all carry both inserts of the hairpin transgene. This suggests that the transgene had passed on successfully, but it was unsuccessful in knocking down Zdhhc21 expression.

The phenotype of the hair loss female persists until it was culled. Like *dep*, the pDECAP-Zdhhc21 transgenic female loses hair on the dorsal hair coat, as well as on the face. However, there are subtle differences in the texture, distribution of hairless patches and the onset of hair loss. In addition, the *dep* mutant typically exhibits depigmentation of the ventral hair coat, which is not observed in the pDECAP transgenic female. Therefore, it is speculated that the hair loss phenotype seen in the DECAP-Zdhhc21 female, may be due to factors other than the transgene.

Figure 3.17: Structure of the 2-kb *Bgl*2-*Bam*H1 pDECAP-Zdhhc21 fragment
The vector contains the CMV promoter, Ribozyme and MAZ site. The gene-specific targeting sequence was cloned between the ribozyme cassette and the MAZ site as an inverted repeat separated by a 12-bp spacer containing a *Kpn*1 cut site.

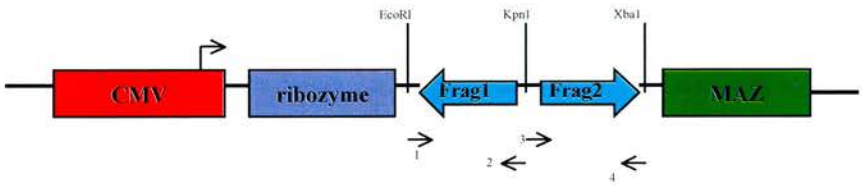

(1)DECAPFrag1f AWH001: AAGAATTCAAACATCAGTGCATAGCAAG
EcoRI

(2)DECAPFrag1r AWH002: AATCTAGAAAGGTACCATGGGTCTTCGGATTCATTTG
XbaI KpnI

(3)DECAPFrag2f AWH003: AAGGTACCACATGGATGGGTCTTCGGATTCATT
KpnI

(4)DECAPFrag2r AWH004: AATCTAGAAAACATCAGTGCATAGCAAG
XbaI

Figure 3.18: E17.5 embryos from oocytes injected with pDECAP-Zdhhc21
Pictures of E17.5 embryos from a litter derived from oocytes injected with pDECAP-Zdhhc21. Highly wrinkled skin can be seen in pictures (b) and (d), whereas (b) and (d) are normal. The vibrissae follicles (e) are normal in all embryos observed (x2 objective).

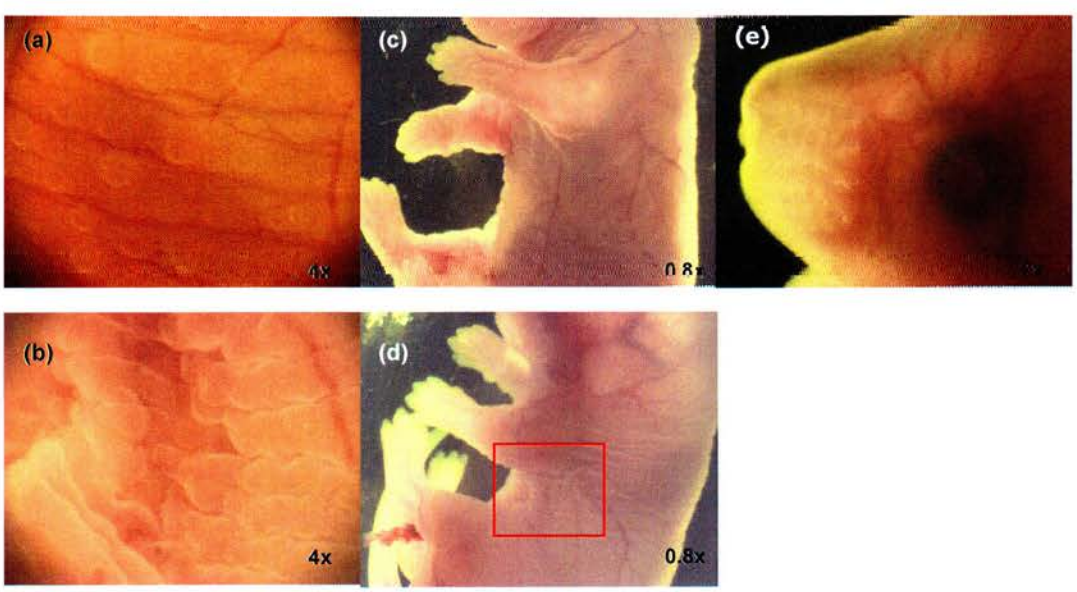

Figure 3.19: pDECAP-Zdhhc21 generates a hair loss phenotype
[A] Genotyping for the forward and reverse insert of the pDECAP-Zdhhc21 construct (upper and lower panel respectively). Animal '1', '4' and '6' and positive for both inserts, whereas animal '2' and '3' are only positive for the forward insert. [B] The transgenic female that is positive for both inserts (Animal '1' of [A]) exhibit a hair loss phenotype that is comparable to that of *dep*.

[A]

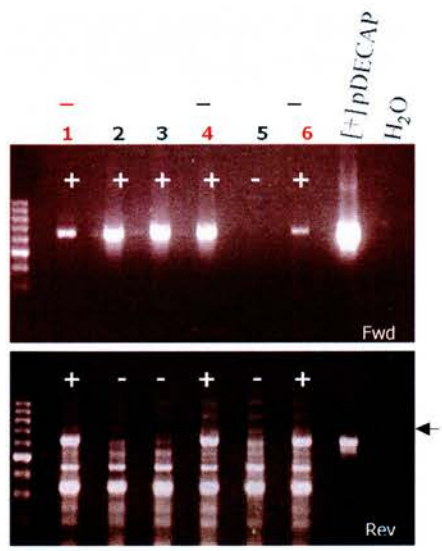

[B]

3.3. Discussion

3.3.1. Transgenic rescue experiment using BAC

The generation of a rescued line by BAC transgenesis confirms that *Zdhhc21* is likely to be the candidate gene for *dep*. However, the BAC construct used in the successful rescue experiment was unmodified and thus contains *Cer1*. Therefore, it may be argued that the rescued phenotype is due to *Cer1* expression. However, this is unlikely to be the case because coding region of *Cer1* is intact in *dep*, and *Cer1* null mutants have no phenotype. Based on the same arguments, an additional copy of *Cer1* is thus unlikely to have any effect on *dep* phenotype.

To date, no rescue line has been generated from the modified ΔCer1 BAC constructs. Although 2 transgenic founders were generated using this construct, in the first case, the transgene is not intact, and with the second line, the transgene is intact but not expressed (shown by RT-PCR). Since the BAC recombineering strategy involves transferring vectors into a different bacterial strains and inducing recombinations between vectors, the construct might be rearranged during the process and result in a disruption in the transgene.

With transgenic rescue experiments, the chromosomal integration site may often silence the transgene. This may explain why some of our transgenic lines contain intact transgene that is not expressed. However, this happens much less often with BACs, whose longer length seems to protect them from silencing.

There may also be a possibility that a transgenic animal contains an intact transgene that is expressed, but the phenotype is not rescued. In this case, it may be possible that deleting *Cer1* (which is only 20Kb upstream to Zdhhc21) may disrupt a regulatory element of *Zdhhc21*, which may render the BAC unable to rescue *dep*.

3.3.2. ENU-mutagenesis approach

Quwailid *et. al.* (2004) reports successful recovery of sperm from ENU mutants. However, with our isolated allele, several attempts of IVF and ICSI had failed due to low sperm density and poor quality possibly as a result of sperm samples not being properly cryo-protected, stored or

transported (Brendan Doe, personal communications). Nevertheless, the mutant line was recovered by ICSI at the end.

One criticism of the ENU mutagenesis approach is that the outcome of the screen is not targeted, and the rate of success is not guaranteed. On screening 1.33Mb coding DNA, only one missense mutation was found and even though comparative sequence analysis suggest that it may have a functional importance, the re-derived animal does not exhibit a phenotype. Out of the 1.7Mb DNA screened so far, 2 coding mutations were found, but only one of which is non-synonymous.

The efficiency of ENU mutagenesis was predicted to be 1 mutation/locus per 600 mice. And since the mouse genome is currently estimated to have 24,000 coding genes, each mutagenised mouse will have approximately 40 functional ENU mutations. The coding part of the genome is currently estimated to be ~37.5Mb in size, so there should be approximately one change every 1.875Mb (37.5Mb/ 40mutations). This agrees well with Quwailid's reported functional mutation rate of 1 in 1.82 Mb.

Given the currently reported genome size of 2,500Mb and the reported ENU mutation rate of 1 in 1.01Mb, we would expect about 2500 mutations per mouse, most of which would be non-functional, and about 37 will hit a coding region. Furthermore, about 20 (1/1.875 x 40) of them will be functional.

3.3.3. The pDECAP vector for siRNA knock down

The siRNA experiment using pDECAP vector technique was attempted by several groups in the MRC Human Genetics Unit but there has been no success. In some cases, although both copies of inserts are present in the transgenic animal, the animal always failed to exhibit the founder mutant phenotype. This may be due to the dsRNA not being generated as expected for directing the degradation of the target protein. The low rate of success may also be due to inefficiency of the dsRNA to knockdown the target expression in a transgenic animal.

Since *Zdhhc21* is believed to have a role in hair follicle development, the pDECAP construct may be tested in keratinocyte culture, since the efficiency of knocking down Zdhhc21

expression may be more readily detected in cell culture. If pDECAP-*Zdhhc21* successfully knock down Zdhhc21 expression in cell line, it may be tested *in vivo* with better confidence.

Apart from the low success rate, there is also a lack of robust genotyping for the transgene due to difficulties in amplifying across the hairpin structure. This may be improved by digesting the vector at the hinge of the hairpin before PCR amplification. Over all, the genotyping results have not been consistent and robust enough to conclude the presence of the transgene at the genomic level.

In our experiment, transgenic mice were crossed with C57BL/6, and the heterozygote progeny were genotyped for brother-sister mating. The subsequent progeny would have a quarter chance of inheriting 2 copies of the transgene that may increase the chance of knocking down Zdhhc21 expression.

Chapter 4 – Functional Studies of Dhhc21

4.1. Introduction

4.1.1. DHHC proteins are palmitoyl-acyl transferases (PATs)

Assuming that *Zdhhc21* is the causative gene for *dep*, the most interesting question would be how a loss of protein function gives rise to the *dep* phenotype. Over the past few years, several DHHC proteins have been found to promote palmitoylation in yeast and mammalian cells, suggesting that Zdhhc21 is likely to be a palmitoyl-acyl transferase (PAT) and that a loss in its activity may result in the *dep* phenotype *in vivo*. Functional studies of Zdhhc21 could contribute to the evidence that the del-233F mutation underlies the *dep* phenotype.

4.1.2. What is palmitoylation?

Palmitoylation (or S-palmitoylation, protein S-acylation) is a posttranslational lipid modification, which involves the addition of the fatty acid palmitate onto specific cysteine residues through thioesterification (Smotrys and Linder, 2004). The PATs share a common feature in that they all contain a cysteine-rich domain (CRD) with a characteristic Asp-His-His-Cys (DHHC) motif, which is required for PAT activity.

Post-translational lipid modifications such as myristoylation, prenylation and palmitoylation generally serve to tether proteins to the cytoplasmic surfaces of cellular membranes. But unlike the other 2 modifications, palmitoylation is reversible and thus allows for membrane tethering to be regulated. Palmitoylated proteins are often key proteins in membrane trafficking (Hayashi et al., 2005), cell signalling, synaptic transmission (Fukata et al., 2004; Yanai et al., 2006), and are affected in the progression of diseases such as cancer (Acconcia et al., 2005).

4.1.3. Palmitoyl transferase and identification of substrates

Although the genes encoding PATs can be easily identified by the shared CRD-DHHC domain consensus sequence, identification of specific substrates are problematic. This is due to the lack of consensuses for predicting palmitoylation from sequence using bioinformatic tools.

The finding that DHHC proteins are PAT was first discovered in *Saccharomyces cerevisiae* by forward genetic screens. The two identified yeasts PATs are Erf2/Erf4, which palmitoylates prenylated Ras2 (Lobo et al., 2002); and Akr1, the PAT for the yeast casein kinase 2 (Roth et al., 2002). Deletion of Erf2/4 or Akr1p prevents palmitoylation of Ras2 or Yck2 respectively, indicating that they confer PAT activity for the yeast proteins. Since Erf2 and Akr1p share a conserved CRD-DHHC domain, based on these findings, it was first predicted that DHHC members might be a PAT family.

Based on the CRD-DHHC domain consensus sequence, it was predicted that there are 7 yeast DHHC proteins and 23 DHHC proteins in mouse and human genome (Linder and Deschenes, 2004; Smotrys and Linder, 2004). The first mammalian DHHC protein that was associated with a palmitoylated substrate, was the Golgi-specific DHHC zinc finger protein (GODZ, or DHHC3), which is shown to enhance palmitoyl transfer to the $GABA_A$ receptor $\gamma 2$ subunit in heterologous cells. This mechanism is proposed to be important for regulated trafficking of these receptors in the secretory pathway (Keller et al., 2004).

In another study, a subset of 4 mammalian DHHC proteins was found to enhance palmitoylation of the neuronal scaffold protein PSD-95 at cysteine residues 3 and 5 in cultured cells. These 4 proteins, Dhhc2, 3, 7 and 15, are closely related within the Dhhc family (Figure 4.1), which reflects a correlation between structure and enzyme specificity for PSD95 palmitoylation. It has also been shown that individual DHHC clones are specific for its substrates, suggesting the possibility that other limbs of the tree are specific for palmitoylating another class of proteins (Fukata et al., 2004).

Other DHHC proteins that have demonstrated a PAT function includes the yeast protein Erf2/Erf4, Pfa3p, Swf1p, and the human proteins DHHC9/ GCP16 and HIP14. H-Ras and N-Ras are palmitoylated by Erf2 in complex with Erf4 in yeast, and are also palmitoylated by the human PAT complex DHHC9/ GCP16 in a substrate specific manner (Swarthout et al., 2005). In another study, the yeast DHHC-CRD proteins Pfa3p and Swf1p were found to palmitoylate Vac8p in vitro and in vivo, and play a role in vacuole fusion (Smotrys et al., 2005). The Huntingtin-interacting protein (HIP14, or DHHC17) palmitoylates a number of specific neuronal substrates including SNAP25 and PSD95, thus regulates their trafficking and synaptic functions (Huang et al., 2004).

Very recently, several mutations in human ZDHHC9, PAT of NRAS and HRAS, were found to cause X-linked mental retardation associated with Marfanoid Habitus (Raymond et al., 2007). In another case, a balanced reciprocal translocation between chromosomes X and 15 that causes a breakpoint in ZDHHC15, was found in a patient with severe nonsyndromic mental retardation (Mansouri et al., 2005). Furthermore, a SNP variant of ZDHHC8 was found to associate with risk of schizophrenia, and that Zdhhc8-knockout mice have decreased exploratory activity in a new environment, and decreased sensitivity to the locomotor stimulatory effects of a psychomimetric drug (Mukai et al., 2004). These findings suggest that other PATs may be good candidates for causing other mental syndromes. However, in neither cases of DHHC8 or DHHC15 a palmitoylated substrate has been suggested.

Endothelial Nitric Oxide Synthase (eNOS) is a substrate of Zdhhc21.

The palmitoylation of the endothelial NO synthase (eNOS) is enhanced by a set of DHHC proteins including Dhhc21. However, only the inhibition of Dhhc21 by siRNA reduces eNOS palmitoylation, suggesting a regulatory role of Dhhc21 in governing eNOS function (Fernandez-Hernando et al., 2006). It was also shown that palmitoylation-deficient mutants of eNOS release less nitric oxide in endothelial cell culture. However, although eNOS-deficient mice have vasoconstriction due to reduced nitric oxide release, they have no reported skin or hair phenotype (Shesely et al., 1996), suggesting that the *dep* phenotype is unlikely to be eNOS mediated, and therefore Zdhhc21 must have another target for palmitoylation that is specific to the observed hair loss phenotype.

4.1.4. Identification of palmitoyl substrates for individual DHHC proteins.

Traditionally, palmitoyl proteins were identified through *in vivo* [^{3}H]palmitate labeling, which is limited by the long exposure time and its requirement for known protein substrate. Recently, a new proteomic methodology called the acyl-biotin exchange chemistry method (ABE, or Biotin switch) for purifying and identifying palmitoyl proteins was used to characterize the palmitoyl proteome of yeast (Roth et al., 2006). From the screen, over 30 new palmitoyl proteins were identified, including SNARE proteins, amino acid permeases (AAP), and participants in cellular signaling and membrane trafficking (Roth et al., 2006).

The ABE protocol developed by Drisdel and Green (Drisdel and Green, 2004) involves 3 major chemical steps. First, any free thiols that are not palmitoylated can be blocked by N-ethylmaleimide (NEM), which forms a stable covalent linkage with the free thiols; secondly, thioester linkages of palmitoylated cysteine thiols are cleaved by hydroxylamide. And finally, these cysteinyl thiols are exposed to a thiol-specific biotinylation reagent. The biotinylated proteins were affinity purified by streptavidin agarose and subjected to Western blotting.

The samples are then compared with proteins that were not treated with hydroxylamide to ensure that the bands observed are due to palmitoylation alone because some proteins become non-specially labeled with biotin independent of the hydroxylamine treatment or some proteins may adhere to the streptavidin resin nonspecifically, leading to misinterpretation of the data (Linder and Deschenes, 2007).

The ABE protocol is not only more sensitive and time-efficient, another advantage is that it does not require the use of radioactivity, but instead uses palmitate as a specific pull-down. This provides the potential to isolate substrates of the DHHC protein in question, and the potential to identify novel substrates by mass spectrometry sequence analysis.

Using the ABE protocol, PSD-95 palmitoylation by DHHC-15 and DHHC-3 in HEK cells was specifically detected (Masaki Fukata, personal communication). This alternative protocol may be used to assess PAT activity of the Dhhc21 protein and identify potential substrates that give rise to the hair loss phenotype. It does not require any knowledge or presumptions on the substrates, and so it will allow us to identify other substrates of Zdhhc21 that may not be hair-loss related e.g. eNOS and Lck.

4.1.5. Functions of Palmitoylation

Like other lipid-modification, palmitoylation is involved in membrane association. However, it is better described as a secondary signal as other primary signals (e.g. myristoylation) must bring the protein to the membrane to allow access to the membrane-bound PAT enzymes. Protein-protein interactions, or prenylation/ myristoylation provide a weak or transient membrane interaction, whereas palmitoylation gives a more stable anchor to the membrane. Nevertheless, palmitoylation also occurs on proteins that are already in tight association with

the membrane such as transmembrane proteins (e.g. AMPA), suggesting that the palmitoylation is more than just a membrane tether.

(i) Protein trafficking

Palmitoylation may regulate membrane retention and protein sorting by modification of specific cysteine sites. Indeed, palmitoylation of different cysteine sites of the same proteins often have distinct effect of trafficking (Greaves and Chamberlain, 2007).

The ligand-gated cation channel, α-amino-3-hydroxy-5-methyl-4-isoxazolepropionic acid (AMPA) receptor have 4 subunits (GluR1-4), each of which is palmitoylated on 2 specific cysteine residues in their transmembrane domain (TMD) and in their C-terminal region. Palmitoylation of the TMD site is enhance by GODZ (Dhhc3) and leads to an accumulation of the receptor in the Golgi and a reduction of plasma membrane expression. This is consistent with previous findings that the overexpression of several PAT-Dhhc members (such as Dhhc15 and Dhhc21) also have similar effect on the trafficking of their substrate (PSD-95 and eNOS) (Fukata et al., 2004; Huang et al., 2004; Keller et al., 2004). Whereas palmitoylation at the C-terminal site causes the protein to retain in the cytosol via interaction with the cytoskeletal protein 4.1N (Hayashi et al., 2005). The differential fate of specific site palmitoylation may underlie the important role of palmitoylation in receptor trafficking and synaptic plasticity.

(ii) Protection from ubiquitination

Palmitoylation has also been reported to play a role in prevention of ubiquitination of the palmitoylated protein. In yeast, palmitoylation of Tlg1 by the Dhhc protein Swf1, ensures that it is retained on the trans-golgi/ endosome membranes. When Swf1 is mutated or inactivated, Tlg1 is unpalmitoylated and recognized by the ubiquitin ligase Tlu1, resulting in targeting to the vacuole for degradation (Valdez-Taubas and Pelham, 2005). On the other hand, cysteine mutants of Tlg1 have similar distribution to wild-type when ubiquitin ligases were inactivated, implying that palmitoylation is not required for membrane targeting of Tlg1, but to prevent ubiquitination specifically (Greaves and Chamberlain, 2007; Valdez-Taubas and Pelham, 2005).

Figure 4.1. Dhhc family members show specificity for palmitoylation substrates
The Dhhc members that enhance PSD95 palmitoylation (P-PATs) include 4 closely related members in the Dhhc family. This may reflect a correlation between structure and enzyme specificity for PSD-95 palmitoylation. Other branches of the phylogenetic tree may be specific for targeting other substrates.

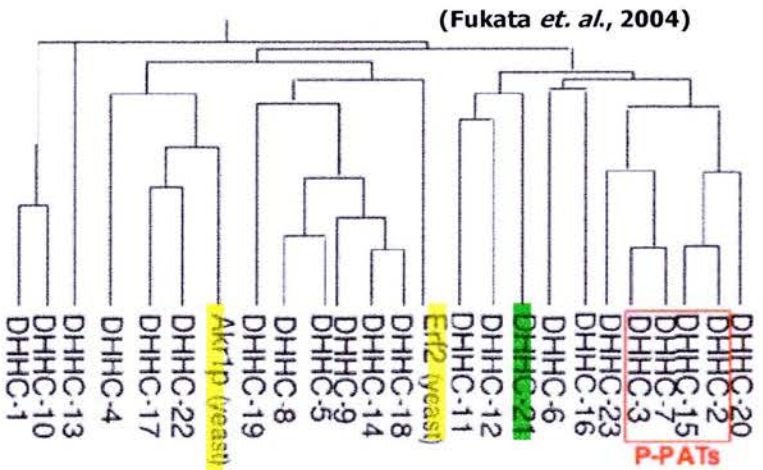

4.2. Results

4.2.1. Palmitoylation assay – *dep* mutation is inactive for palmitoylation *in vitro*

(Collaboration with Masaki Fukata)

Considering the previous literature suggesting that DHHC members are palmitoyl transferases, it is likely that Zdhhc21 is responsible for palmitoylating a set of substrates *in vivo*, and that the proteins that are under-palmitoylated as a result, may have a defective function that gives rise to the *dep* hair loss phenotype. Nevertheless, the first question is, whether the *dep* mutation affects palmitoylation at a molecular level.

To answer this, I set up a collaboration with the author of the PSD95 paper, Masaki Fukata from the National Institute of Longevity Sciences in Japan (moved to National Institute for Physiological Sciences from 01.06.07). To examine whether *dep* has palmitoyl transferase activity, 2 substrates were used based on their recent findings, including eNOS and the lymphocyte-specific protein tyrosine kinase (Lck). eNOS has been proposed to be a specific target of Zdhhc21 (Fernandez-Hernando et al., 2006). Lck was found to be robustly palmitoylated by DHHC-21 among the 23 DHHC members (Yuko Fukata and Masaki Fukata, unpublished data).

Lck knockout mice exhibit a marked thymic atrophy, with a dramatic reduction in the double-positive ($CD4^+CD8^+$) thymocyte population, and a complete absence of the mature, single-positive thymocyte population (Molina et al., 1992), indicating that a defective Lck is likely to have an effect on thymocyte development. However, apart from the phenotypes described in Chapter 5, *dep* does not show any thymus-related phenotype under unchallenged conditions in the laboratory.

To test the PAT activity of the mutant protein, Dhhc21 constructs of wild-type, *dep* and another mutant construct C120S (a mutation in the conserved Dhhc motif, DHHS, Fukata) were individually transfected into HEK293 cells together with eNOS and Lck respectively. The palmitoylation of eNOS and Lck were assessed by metabolic labelling with [^{3}H]palmitate. The experiments showed that the wild-type DHHC21 protein increased incorporation of [^{3}H]palmitate into eNOS, whereas the *dep* and C120S mutant proteins have no effect on eNOS palmitoylation, indicating that they are inactive for palmitoylating eNOS. The same pattern

applies to Lck being the substrate, suggesting that both mutations are likely to abolish PAT activity completely (Figure 4.2; the experiment was carried out by Ryouhei Tsutsumi and Masaki Fukata as a collaboration).

In a separate experiment, Fukata and colleagues found that the short region of the C-terminal cytoplasmic region of DHHC-15 is required for the enzyme activity, and that mutations of VFG (273-275aa) in DHHC-15 impairs the enzyme activity (Masaki Fukata, personal communications). The VFG motif corresponds to 236-238 a.a. in DHHC-21, and is conserved among all P-PATs and also to DHHC-4, 7 and 21. The VFG motif is only 3 bp upstream of the *dep* del233F mutation, suggesting that the mutation may affect Dhhc21 function at the VFG motif.

This data is potentially exciting, because if the *dep* hair loss phenotype were due to the mutant protein being inactive for palmitoylation, the *in vitro* result would be the first direct evidence that the enzymatic activity of DHHC family is involved in a mammalian mutant condition.

4.2.2. Acyl-biotin exchange chemistry (ABE) – an alternative to [^{3}H]palmitate labeling

Generation of DHHC-21 mutant constructs by site-targeted mutagenesis

To assess the functional significance of individual mutations, I made a set of Dhhc21 mutant constructs for overexpression of the corresponding mutant proteins in cultured cells. The *dep* mutation was subcloned by replacing wild-type cDNA from the original construct with a *dep* cDNA carrying the single amino acid deletion.

A construct containing the missense mutation isolated from the MRC Harwell ENU archive, was also generated by site-targeted mutagenesis using the wild-type construct provided by Masaki Fukata as a template. This is to assess whether the L91F mutant retains its PAT activity in culture, since the re-derived animal does not exhibit any phenotype. In addition, 2 other mutant constructs were made on the cysteine residues within the cysteine-rich DHHC domain (Figure 4.3). The integrity of mutant constructs was tested by sequencing.

Auto-palmitoylation – dep and some other mutants are defective in auto-palmitoylation

Using the biotin switch protocol, it was shown that there is a difference between wild-type and *dep* activity in auto-palmitoylation. The set of constructs generated by site-targeted mutagenesis were transfected into HEK293 cells and subjected to ABE chemistry, streptavidin pull-down and Western blotting. The result shows that the wild-type Dhhc21 and the Harwell L91F mutant are pulled down in greater quantity, in comparison to *dep* and the other 2 mutants C95S and C106S (Figure 4.4), indicating that the wild-type and L91F mutant are active for auto-palmitoylation, whereas *dep* and the other 2 mutants are unable to self palmitoylate. As the Harwell L91F mutant appears to retain its cellular function as a PAT of its own, this data is consistent with the fact that the re-derived animal of the Harwell L91F mutation does not exhibit a phenotype.

4.2.3. Cellular nature of Zdhhc21 – *dep* is mislocalised in the ER

Having established the fact that *dep* has a cellular defect in palmitoylation, the expression of individual constructs were visualized in cultured cells to investigate any obvious phenotype that is associated with the dysfunction since a mislocalisation may contribute to the mutant's inability to palmitoylate its substrate. The set of constructs used for the auto-palmitoylation assay was over-expressed in NIH3T3 cells, and visualised by immunohistochemistry with antibody that targets the HA tag of the Dhhc21 constructs, together with cellular markers such as the cis-Golgi marker Gm130.

It was found that the wild-type Dhhc21 protein localizes to a highly specific ribbon-like structure in the cytoplasm, which co-localises with the cis-Golgi marker Gm130, whereas the *dep* mutant is completely delocalised and dispersed in the cytoplasm, and does not co-localise with Gm130 (Figure 4.5). The localization of the Harwell L91F mutant resembles that of wild-type, which is consistent with the fact that the re-derived animals do not exhibit a phenotype and that the mutant L91F protein retains its auto-palmitoylation activity. The C95S and C106S mutants are both mislocalised, although the C95S mutant appears to partially retain the structure as a globe of protein in the cytoplasm where the Gm130 localises. In the future we may initially test the cellular localisation of an isolated ENU mutant before considering to re-derive the mutant line by *in vitro* fertilization.

The wild-type and *dep* constructs were further transfected into keratinocyte culture by Ian Smyth, who also showed that the wild-type protein colocalises with the cis-Golgi marker (Figure 4.6A), but not the trans-Golgi marker (data not shown). And instead of the cis-Golgi, the *dep* mutant protein seems to co-localise with the endoplasmic reticulum marker PDI (protein disulfide isomerase) (Figure 4.6B).

Taken together the above findings, it looks as though the wild-type Dhhc21 protein localizes to the cis-Golgi, but the *dep* mutant fails to associate with the cis-Golgi and gets trapped in the ER (Figure 4.7).

4.2.4. Zdhhc21 involvement in *dep* and in eNOS function

Given that eNOS is a reported substrate of Zdhhc21, and that a *Zdhhc21* mutation demonstrates a loss of PAT activity in *dep*, the following 2 parallel questions may be asked:

Do eNOS knockout mice have a hair phenotype?

Although eNOS knockout mice have no reported hair loss phenotype, the mutant skin had never been carefully examined. Recently, a regulatory role in melanogenesis has been suggested for the NOS isoforms including eNOS and neuronal NOS (nNOS) and inducible NOS (iNOS) (Sowden et al., 2005). Since *dep* exhibits a hair loss phenotype, this piece of evidence may be relevant to the contribution of unpalmitoylated eNOS in melanogenesis in epidermis and HF keratinocytes. Normally, eNOS is highly expressed in melanocytes in the epidermal basal layer. Although eNOS is not expressed in melanogenically active melanocytes of anagen hair bulb, it shows a preferential restriction to melanocyte dendrites in undifferentiated melanocytes in the ORS and melanocytes that have survived HF regression. This may reflect a role for locally produced NO in the maturation and transport of melanosomes along the cell dendrites (Sowden et al., 2005).

To test the possibility that eNOS deficiency is associated with the hair loss phenotype, we could look at the skin of eNOS knockout mice, which are available from Dr. Rob van T'Hoff (University of Edinburgh). These mice have superficially normal hair. More detailed histological analysis might show hair-related defects but this has not yet been done.

Do dep mice show an eNOS-related phenotype?

(Collaboration with Dr. Tom van Agtmael)

On the other hand, eNOS may still be a substrate for Dhhc21 *in vivo* even though it may be unrelated to the hair loss phenotype. Based on the eNOS substrate specificity for Zdhhc21 in cellular assay demonstrated by Fernandez-Hernando and colleagues (2006), it is speculated that the eNOS substrates in *dep* may be under-palmitoylated and have a functional defect in releasing nitric oxide, which may lead to vasoconstriction as a result. To test this hypothesis, a collaboration has been set up with Dr.Tom van Agtmael (University of Edinburgh) to investigate eNOS activity by asking whether the aorta of *dep* and wild-type differ in the degree of vasodilation under treatment with acetylcholine (Ach) which activates eNOS to release nitric oxide. To date, preliminary data shows a significant difference between wild-type and *dep* in Ach response, and that the difference is due to a reduction in eNOS function (data not shown).

So far, it is established that eNOS is a specific substrate of Dhhc21 in cell culture assay. Since eNOS knockout mice do not resemble the *dep* hair loss phenotype, eNOS can not be a mediator of *dep*. Therefore, we conclude that there must be another substrate that contributes to the *dep* phenotype.

Figure 4.2. Assessing PAT activity of *dep* (Masaki Fukata)
(Experiment carried by Masaki Fukata and colleagues as a collaboration)
Individual Dhhc21 clones of wild-type, *dep* and C120S (mutation of the Dhhc motif) were individually transfected together with eNOS and Lck into HEK293 cells. After metabolic labelling with [^{3}H]palmitate, proteins were separated by SDS-PAGE and subjected to fluorography (upper panel). Arrows indicated the position of eNOS and Lck respectively. Increased incorporation of [^{3}H]palmitate into eNOS and Lck is clearly observed when co-transfected with the wild-type Dhhc21 construct, indicating an enhancement of eNOS and Lck palmitoylation by DHHC21. The *dep* mutation and the mutation of the Dhhc motif (del-233F and C120S) clearly blocked eNOS and Lck palmitoylation. Immunoblots against Lck and the eNOS tag protein Myc (middle panel), and the HA tag protein for the DHHC21 clones (lower panel) are shown as controls. The mobility of palmitoylated Lck is shifted by wild-type Dhhc21 (indicated by an asterisk).

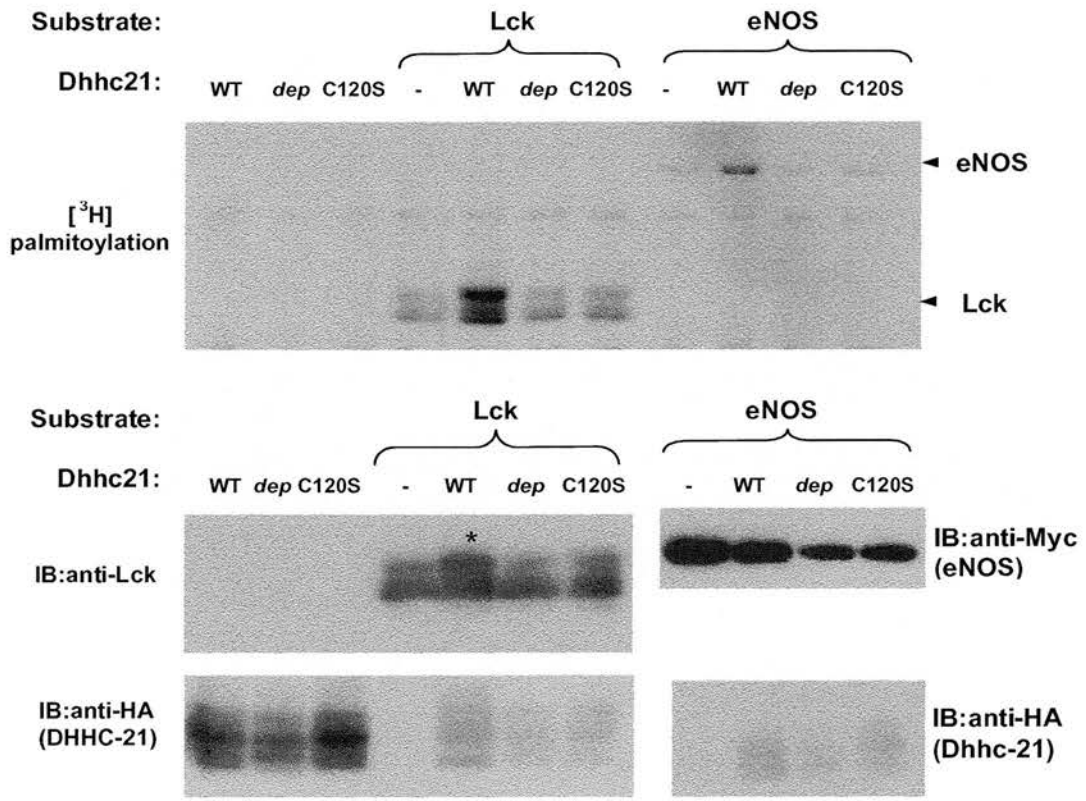

Figure 4.3. Relative location of mutations targeted by cloning or mutagenesis
The *dep* mutation lies at the C terminal of DHHC21; all other mutant constructs used in this project lie within the cysteine-rich DHHC consensus core. The L91F construct was generated because of an isolated ENU mutation from the MRC Harwell ENU archive.

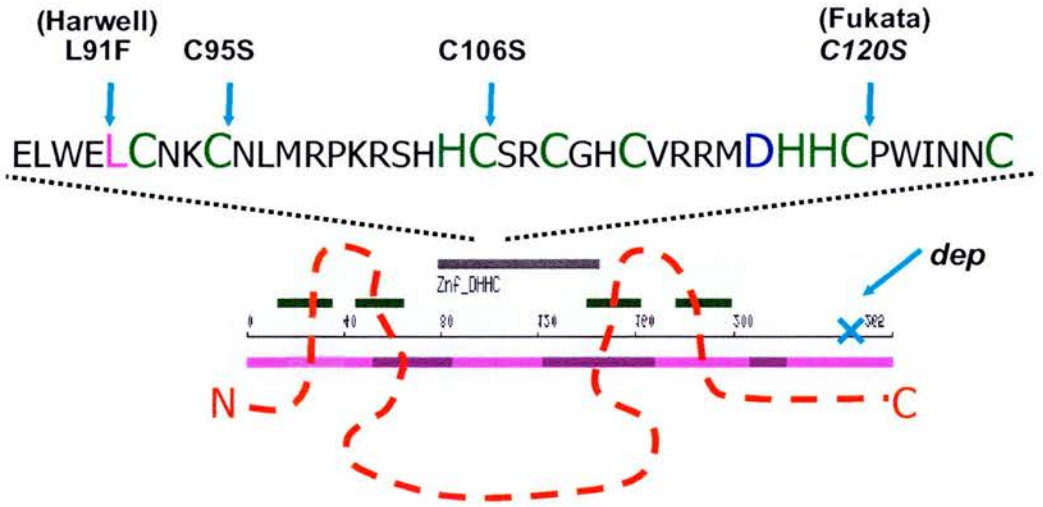

Figure 4.4. Auto-palmitoylation of Dhhc21 proteins using the ABE protocol
Individual Dhhc21 constructs were transfected into NIH3T3 cells and were left to grow overnight. The lysates were then subjected to ABE chemistry, and subsequently pulled down by streptavidin agarose beads and resolved by SDS-PAGE. The result shows that the wild-type and L91F proteins were pulled down at a greater quantity than *dep*, C106S and C95S (right panel), comparing to the portions that are not pulled down (left panel). This indicates that wild-type and L91F proteins are active for auto-palmitoylation, whereas the other mutants are unable to autopalmitoylate.

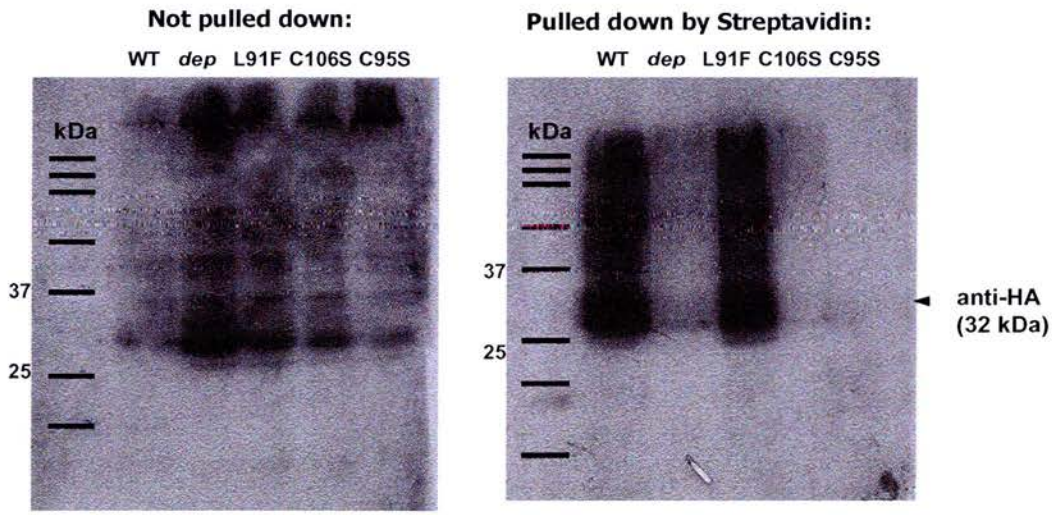

Figure 4.5. Cellular localisation of the Dhhc21 constructs
HA-tagged Dhhc21 cDNAs (wild-type, *dep*, L91F, C106S and C95S) were over-expressed in NIH3T3 cells, and were stained by anti-HA antibody (red); the degree of co-localisation with the cis-Golgi marker Gm130 (green) was assessed. Wild-type and L91F (Harwell) Dhhc21 localises to a specific tubular, ribbon-like structure in the cytoplasm, which co-localises with Gm130, whereas the *dep* mutant is completely delocalised and dispersed in the cytoplasm, and does not co-localise with Gm130. The C95S and C106S mutants are also mislocalised.

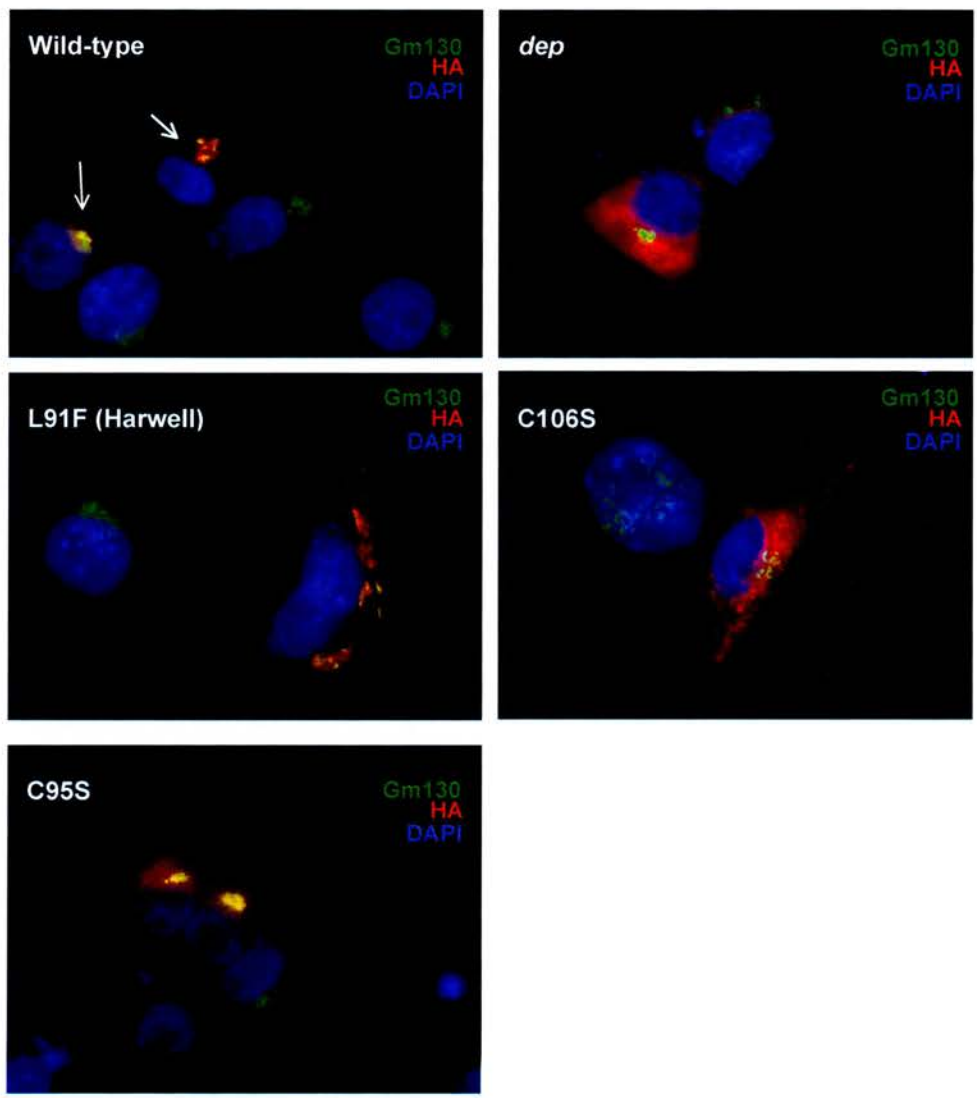

Figure 4.6. Wild-type and *dep* Dhhc21 over-expressed in keratinocyte culture
(experiment carried by Ian Smyth as a collaboration).
[A] Wild-type Dhhc21 protein co-localises specifically with Gm130, a marker of the cis-Golgi network, but not with the trans-golgi marker Tgn38 (data not shown).
[B] Instead of the cis-golgi, *dep* mutant protein seems to localise to the ER, as shown by its co-localisation with the ER marker PDI. Wild-type Dhhc21 does not co-localise with PDI.

[A]

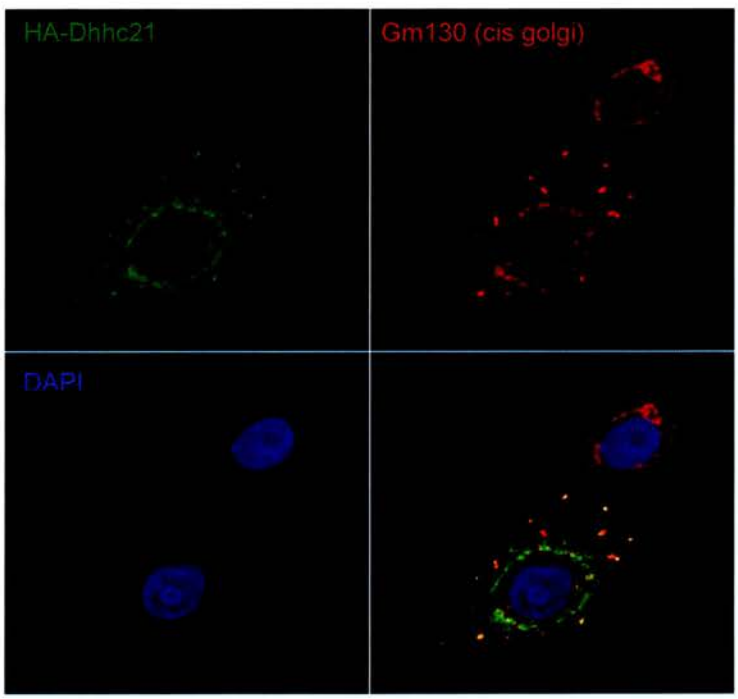

[B]

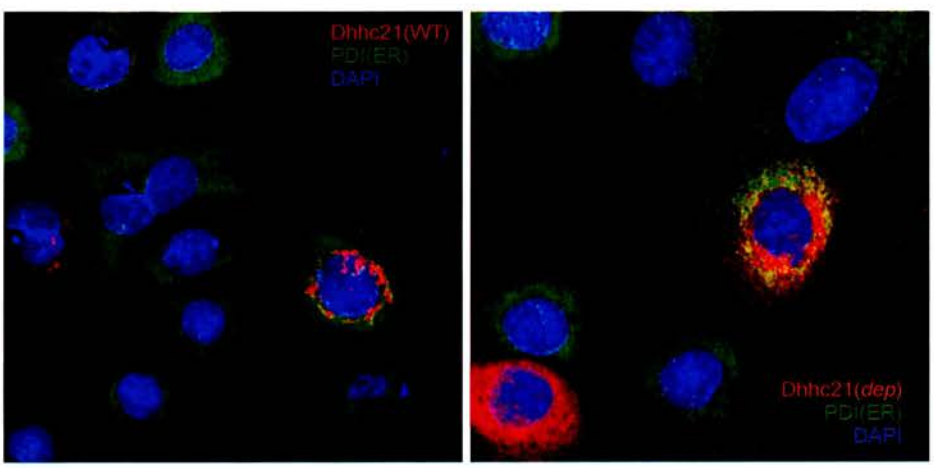

Figure 4.7. Cellular localisation of wild-type and *dep* proteins
Based on immunocytochemistry, wild-type Dhhc21 seems to localise to the cis-Golgi network, whereas the *dep* mutant is trapped in the ER. It is speculated that the del-233F mutation at the C-terminal may affect protein folding, leading to the trapping of protein in the ER.

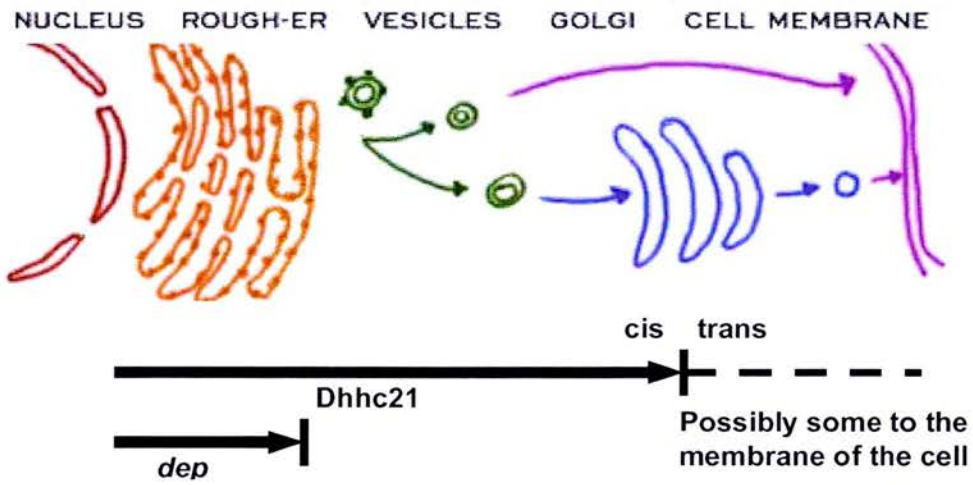

4.3. Discussion

4.3.1. *Dep* mutation may lead to protein trapping in the ER

Based on the immunocytochemistry assay on cellular localization, it is observed that the wild-type Dhhc21 protein localizes to the cis-Golgi. This is consistent with previous literature which shows that other Dhhc members also localise to the cis-Golgi (Fernandez-Hernando et al., 2006; Fukata et al., 2004). According to the predicted transmembrane topology, the Dhhc functional motif is intracellular and is therefore facing the cytosol (Figure 3.1C), so palmitoylation is likely to take place in the intracellular space. The *dep* mutant protein, on the other hand, is unable to target specifically to the cis-Golgi and appears to be trapped in the ER. If the C-terminal is in the ER lumen then it seems that the mutation may hinder protein folding which may subsequently lead to trapping of the mutant protein in the ER (represented in Figure 4.7).

This is the case with the most common mutation of cystic fibrosis (del508F CFTR), which is also a single deletion of Phenylalanine. Previous literatures had shown that correct localisation of the CF mutant is restored by growing the cells at a lower incubation temperature (Denning et al., 1992). Based on this finding, it may be reasonable to anticipate that the mislocalisation of *dep* protein may also be rescued by overexpressing the mutant at a lower temperature.

In combination with the palmitoylation assay, this experiment may answer whether the lack of PAT activity of *dep* is due to the mislocalisation, or an inactivity of PAT, which may result in the unpalmitoylated protein not being unable to localise specifically. In the case of the cysteine mutations (C106S, C95S and C120S), the lack of PAT activity may be due to both a mislocalisation and the PAT being inactive.

If the mislocalisation of *dep* is rescued at a lower incubation temperature, the same lysate may be used for palmitoylation to assess if the PAT activity is also rescued. If the PAT activity is then rescued, it suggests that the loss of palmitoylation is due to mislocalisation of the mutant protein, and that the site of palmitoylation is likely to be the cis-Golgi.

However, if palmitoylation is not rescued despite correct localisation, it may suggest that the PAT activity *of dep* is abolished and that its mislocalisation is independent of the loss of PAT activity. It may also suggest that the cis-Golgi is not necessarily the site of palmitoylation.

Zdhhc21 may target several palmitoyl proteins unrelated to hair loss

Previous data shows that Zdhhc21 is able to enhance palmitoylation of a range of substrates in cell culture, including PSD95, eNOS and Lck (Fernandez-Hernando et al., 2006; Fukata et al., 2004). In the case of eNOS, even though the five Dhhc proteins seem to share a functional redundancy in eNOS palmitoylation, the inhibition of Zdhhc21 alone in endothelial cell culture reduces eNOS palmitoylation, indicating that Zdhhc21 may be indispensable for this function.

Although the effects of lack of eNOS palmitoylation in *dep* is yet to be determined, it suggests the possibility that Zdhhc21 may have a regulatory role in governing palmitoylation of a range of substrates. The *dep* mutation may potentially affects substrates other than the one specific for the hair loss phenotype. This is supported by the RT-PCR data which shows that *Zdhhc21* is widely expressed across a range of tissues (Figure 3.5, chapter 3).

The *dep* mutants are often smaller in body size at an early stage (up to 4 weeks of age, Chapter 5), which may be caused by the lack of palmitoylation of a substrate other than the hair-loss-related substrate. Furthermore, the *dep* mutation may potentially give rise to other phenotypes may be repressed under controlled, unchallenged laboratory environment.

4.3.2. The role of auto-palmitoylation

While the lack of PAT activity in *dep* may be due to mislocalisation of *dep*-Dhhc21, it is not clear whether the mutant protein is functional. Our ABE assay has shown that the *dep* mutant, and the cysteine-targeted mutants (C106S and C95S) are inactive for auto-palmitoylation. This implies that the PAT activity of *dep* is abolished by the mutation, but it is also possible that mislocalisation affects the protein conformation required for auto-palmitoylation.

The function of auto-palmitoylation is not clear. It is a very rapid process that occurs before palmitate transfer to a substrate (Swarthout et al., 2005), and has been suggested that it serves as a covalent acyl-enzyme intermediate required for the PAT reaction (Mitchell et al., 2006). So it is conceivable that the loss of auto-palmitoylation function prevents the PAT activity on the targeted substrates.

Chapter 5 – Phenotypic and Molecular characterization of *dep*

5.1. Introduction

5.1.1. The skin

The skin is the largest organ in the body and serves a wide range of functions such as physical protection, temperature regulation and social signaling. It is composed of an epithelial and a mesenchymal compartment joined together by the basement membrane (BM). The epithelium includes the interfollicular epidermis (IFE) and the hair follicles (HF), and the mesenchyme includes the dermal papillae (DP), dermis and the subcutis. The IFE is composed of multiple layers of keratinocytes at successive stages of differentiation, from undifferentiated, proliferative keratinocytes attached to the BM in the basal layer, to terminally differentiated, cornified cells in the suprabasal layers as they migrate up the IFE layers (Fuchs and Raghavan, 2002).

The epidermis primarily consists of differentiating keratinocytes which makes up 95% of the skin layer, but other functional cell types can also be found in the epidermis, including melanocytes, Langerhans cells and Merkel cells and melanocytes. Langerhan cells play a role in the immune defense of the body, and Merkel cells are involved in sensory reception.

Melanocytes are derived from neural crest progenitors (melanoblasts). They are the skin pigment cells that are located between keratinocytes in the epidermal basal layer and are also present in the hair follicles. Melanocytes synthesize melanin and deposits into cytoplasmic organelles (melanosomes) that are transferred to the keratinocytes via their dendrites. Melanin functions to provide protection against UV irradiation, photo-carcinogensis and photoaging. Individual melanocytes are able to associate with multiple keratinocytes via their multiple long dendritic projections.

The basement membrane is a complex layer of tissue that is composed of a series of elaborately interconnecting extracellular matrix (ECM) proteins including collagen IV, laminin and fibronectin. The main role of the BM is to separate the epidermis and the dermis and act as a diffusion barrier for nutrients and growth factors between them. Another role of the BM is to

ensure that the proliferating keratinocytes are attached to the basal layer through an anchoring complex composed of the hemidesmosomes and anchoring filaments.

The dermis is a thick skin layer located beneath the epidermis that provides support to the skin. The layer predominantly consists of fibroblasts that form a supporting matrix made of collagen and elastin, which gives the skin its strength and flexibility. The dermis also harbors an extensive vascular network which supplies the skin with nutrients and oxygen. The dermis also contains other cell types such as endothelial cells and mast cells, and plays a part in immune defense.

The subcutis is a layer of tissue beneath the dermis and is composed of protein fibres and adipose tissue. The adipocytes store energy as triglycerides and release the energy as free fatty acids and glycerol during starvation. They are also important in temperature insulation and provide a cushioning function against injury. Although the subcutis layer is not part of the skin, it contains skin structures such as the sweat glands and sensory receptors.

5.1.2. Stems cells of the skin

Throughout the entire life of a mammal, the epidermis is maintained by constant replenishment from stem cells, which possess full self-renewal/ proliferative capacity and produce progeny that undergo terminal differentiation along the lineages of the interfollicular epidermis (IFE), hair follicles (HF) and the sebaceous glands (SG) (Watt et al., 2006). Several stem cells populations exist in the HF, but the best characterized is the bulge stem cells which resides in a permanent portion of the HF. In addition to the bulge cells, there are also stem cells in the IFE, the SG, and a separate stem cell population for the hair lineages in the hair matrix (Figure 5.1A). However, it is also possible that the SG is maintained by the bulge stem cells. Although these populations are interconvertible, they respond to constituents of the microenvironment such as the ECM, growth factors and availability of nutrients, which determine the differentiation pathways selected by stem cell progeny (Niemann and Watt, 2002).

Another property of stem cells is that they divide very infrequently. For sufficient keratinocytes to maintain epidermal homeostasis, the stem cell progeny may first divide a finite number of times before they become terminally differentiated. These cells are known as transit-amplifying

(TA) cells. Terminal differentiation of the IFE and SG lineages gives rise to one final fate, which are the cornified cells and terminally differentiated sebocytes (which degrade into sebum) respectively. However, the HF is more complex, comprising 8 different differentiated lineages.

(i) The hair follicle

Under normal conditions, an anagen hair follicle (HF) consists of several parts, including the bulge, dermal papillae (DP), the hair matrix, which give rise to the hair shaft lineages, and the sebaceous gland (SG) (Figure 5.1A and 5.3).

The bulge is a thickened region of the outer root sheath (ORS) that lies close to the attachment site of the arrector pili muscle. It contains a reservoir of quiescent multipotent stem cells that are capable of maintaining the epidermis and regenerate new hair growth.

At the proximal tip of the HF lies the dermal papillae (DP), which is a specialized population of mesenchymal cells that provides growth stimulus during morphogenesis and at the start of each hair cycle via signaling through epithelial-mesenchymal interactions. In addition, the size of the DP is directly proportional to the size of the resulting follicle (Porter, 2003).

At anagen, the DP becomes encapsulated by the hair matrix (HM), which consists of HF progenitors that rapidly proliferate, and subsequently differentiate into 7 specialized lineages of keratinocytes, forming the hair shaft (HS) and the inner root sheath (IRS). The HS consists of 3 lineages, including the medulla, cortex and the hair cuticle. The IRS is also made of 3 lineages, including the outmost Henle's layer (consists of a thin layer of flattened cells), the middle Huxley's layer (consists of several layers of cuboidal cells) and the innermost cuticle layer (made of tiny cuboidal cells). Like epidermal differentiation, HF differentiation results in different lineages of keratinocytes, each of which has differential expression of molecular markers (Figure 5.1B). Therefore, the type of keratin each layer expresses defines its unique lineage and allows most layers to be identified.

At the onset of anagen, the matrix progenitors gradually become terminally differentiated and more cornified as the whole structure moves distally. The cuticle layers of the HS and IRS then separate from each other as the HS starts emerging from the skin. The IRS thus forms a channel

of the HS as it moves. There is then a structural transition in the HF, during which all the cell layers become highly compressed.

The matrix expresses numerous regulatory factors and signaling molecules during anagen, some of which are expressed uniformly throughout the matrix (e.g. Ptc1), whereas others have restricted expression pattern (e.g. Shh and Lef1). The prevalent hypothesis is that the matrix contains equivalent multipotent cells which acquire their terminal differentiated state as they leave the matrix according to their position (Niemann and Watt, 2002; Porter, 2003). This is supported by previous studies in which markers specific to IRS and HS lineage determination (e.g. GATA3) were detected in different layers immediately above the hair bulb (Kobielak et al., 2003). On the contrary, other studies suggest that the HS and IRS lineages each have specific progenitors, for example, ectopic expression of the Bmp inhibitor, Noggin, in the matrix results in a defect in HS differentiation in Msx2-Noggin transgenic mice (Kulessa et al., 2000).

Recently, it was shown by Legue and Nicolas, that the matrix is divided into several sectors, which give rise to individual HF compartments (Legue and Nicolas, 2005). The study employed clonal analysis of HF morphogenesis based on temporal induction of β-galactosidase labeling by OHT in the CMV Cre ER^t x Rosa26 reporter mice to trace matrix progenitor cells. It was found that the matrix cells are highly organized within the structure, and is divided into SC, progenitor and post-mitotic layers in the radial dimension; and in the proximodistal dimension, it is divided into 3 sectors of precursors for the IRS, the HS cuticle and medulla, which corresponds to the order of the concentric cell layers in the HF, from the most peripheral IRS, to the innermost medulla core. These precursors are capable of self-renewal and producing transient progenitors, but the proliferative activity of distinct cell lineages is different.

On the other hand, the outer root sheath is a continuation of the IFE, and is of a different lineage from the HS and IRS. In contrast with the HS and IRS progenitors which occupy specific niche, the ORS is produced by progenitors dispersed throughout the ORS that display local division and apoptosis (Legue and Nicolas, 2005). The companion layer is a single layer of small flattened cells internal to the ORS that is thought to be derived from the IRS lineage (Niemann and Watt, 2002), although it has been a constant subject of debate (Gu and Coulombe, 2007).

The sebaceous glands (SG) lie above the bulge. Terminally differentiated sebocytes secrete and supplement the HF with lipid-rich sebum and nutrients from the SG duct into the hair canal that empties out to the skin surface.

(ii) Epidermal differentiation

The epidermis is composed of layers of keratinocytes that are in different differentiated states. To maintain homeostasis, the basal keratinocytes continually undergo terminal differentiation while old cells are shed from the skin surface. The basal layer consists of 3 cell subtypes: stem cell (SC), transit-amplifying (TA) cells and post-mitotic differentiating (PMD) cells (Jensen et al., 1999). The epidermal SCs have complete self-renewal capacity and high proliferative potential. At the induction of IFE differentiation, selected progeny of SC become TA cells, which go through finite number of cell divisions before committing to terminal differentiation. PMD cells are the committed cells in the basal layer that are eventually detached from the BM and migrate upwards through the suprabasal layers which consists the spinous, the granular and the cornified layers, in the order of their differentiated state (Figure 5.2).

According to the above model, IFE homeostasis is maintained by 2 progenitor populations: SCs and TA cells. Recently, this model is being challenged by a new finding that epidermal SCs alone are able to maintain normal epidermis. Using inducible genetic labeling, it was shown that under normal circumstances, individually labeled SCs were able to undergo both symmetric (horizontal) and asymmetric (vertical) divisions at a rate that ensure IFE homeostasis (Clayton et al., 2007).

Epidermal differentiation requires dermal-epidermal interaction via growth factors such as the epidermal growth factors (EGFs), transforming growth factors (TGFs), and ECM proteins. And so the programme of epidermal differentiation is a highly ordered and controlled process. Keratinocytes at different differentiated state express specific growth factors and structural proteins in a temporal and cell-specific manner. For example, as the PMD cells exit the cell cycle and begin to detach from the basal layer, they switch from the expression of K14 and K5 to K1 and K10. The spinous cells are the most proximal suprabasal layer that express K1 and K10, this reflect their cytoskeleton of K1/K10 filament bundles connected to the adhesion junctions (called desosomes) that hold the basal and suprabasal layers together as well as their neighboring keratinocytes (Edmondson et al., 2003). However, under wound healing or other

hyperproliferative situations, K6, K16 and K17 are also expressed in the suprabasal layers (Fuchs, 2007).

(iii) Sebocyte differentiation

SGs are holocrine glands that are composed of round-shaped termination (acini) attached to a common excretory duct connected to the hair canal. Sebocyte differentiation starts at the periphery of the gland. The basal cells lining the SGs contain stem cells and highly proliferative sebocytes that eventually differentiates and mature, as they migrate toward the central excretory duct. As sebocytes disintegrate, they release the lipid-rich sebum made of triglycerides, wax esters, squalene and the decomposed sebocytes into the hair canal for lubrication, waterproofing and protection against bacterial infections (Fuchs, 2007).

SGs are also found in non-hair region such as the lips, eyelids, mammalian anal glands, perputial glands. The structure consisting of the hair shaft, hair follicle and SG is often known as a pilosebaceous unit.

5.1.3. The normal hair cycle

Throughout the entire life of most mammals, hair follicles go through cycles of rapid growth phase (anagen), apoptotic-driven regression (catagen), and relative quiescence (telogen) during which the hair follicles are constantly being renewed and regenerated (Figure 5.3). Each of the hair stage in mouse is well-characterized and documented; anagen has been subdivided morphologically into 6 and catagen into 8 different stages (Muller-Rover et al., 2001). The major events of a hair cycle are summarized below:

At the start of a hair cycle, progeny of bulge stem cells (transit-amplifying cells) migrate downwards to the mesenchymal compartment and rapidly proliferate to generate a new hair matrix of IRS and HS progenitors. In response to mesenchymal cues from the connective tissue sheath and the DP, the TA matrix cells change migration direction and terminally differentiate into IRS or HS in a upward distal direction (Paus and Cotsarelis, 1999).

In mid-anagen, while the 7 lineages of HS, IRS and the companion layer keratinocyte are being generated as an upward growth, the ORS grows downwards into the connective tissue of the

dermis. The counter-current movement of these migrating cell layers is facilitated by the slippage plane formed by the companion layer, which only form desomosome adhesion junction with the IRS keratinocytes (Porter, 2003).

At catagen, the follicles undergo an apoptotic-driven regression when the lower part of the follicle stops proliferating and enter apoptosis. The matrix cells are called TA cells because they only survive through the anagen phase of a hair cycle. The hair bulb then shrinks in size, pulling away from the mesenchymal cluster of DP cells which it previously enveloped. The whole follicle then shortens and retracts upwards, drawing the DP closer to the bulge. The proximity of the DP and the bulge is thought to be important for epithelial-mesenchymal signaling in subsequent hair cycles. However, in mouse whiskers, the DP never reaches the bulge before a new anagen (Oshima et al., 2001), supporting the notion that bulge SCs migrate to the hair bulb where they become activated to proliferate.

While the hair shaft may be shed and part of the hair follicle structure degenerates, throughout each hair cycle, the HF maintains several permanent non-cycling parts including the bulge SCs, the SG, the connection with the arrector pili muscle and the DP which is in close association with the HF. The hair shaft, including the 7 lineages of keratinocytes and the matrix progenitors are the cycling portion of the hair follicle.

At telogen, the hair follicles are in a quiescent state, during which the club hair may be shed. After a period of mitotic quiescence, signal from the DP initiates proliferation of bulge stem cells for a new hair growth. In mouse, the first telogen usually lasts for 1 or 2 days, whereas the second anagen may last more than 2 weeks (Muller-Rover et al., 2001).

5.1.4. Hair-related abnormalities

Of all the mouse mutants (spontaneous, targeted or randomly induced) with abnormal hair phenotypes, the major characterisations may be divided into 6 categories (Nakamura et al., 2001; Porter, 2003): (1) reduction in number of hair follicles, (2) abnormalities in HF morphogenesis, (3) abnormalities of hair follicle cycling, (4) hair follicle or hair shaft structure defects, (5) immunological disorders and (6) abnormal SG development. (Nakamura et al, 2001).

This categorisation also reflects human hair growth disorders. For example, androgenetic alopecia is partially due to the progressive shortening of successive anagen cycles, coupled with a reversion of the androgenic-sensitive terminal hairs (thick, pigmented hair that penetrates into the subcutis) of the scalp to vellus hairs (thin, unpigmented hair). Alopecia areata results when anagen terminates prematurely.

In contrast, hirsutism occurs when abnormally enlarged vellus HFs become terminal HFs inappropriately, a process that usually occurs in puberty when several regions of hair follicles in the body, e.g. male facial region, convert from vellus to terminal hair follicles in response to androgen.

In most of the conditions in both mice and human, the HFs are not actually lost. So by understanding the mechanism of the conditions, it may be possible to reverse the effects of these disorders as we gain better understanding of the regulation of hair cycle and hair growth.

5.2. Background knowledge on dep

Depilated (*dep*) is an autosomal recessive mutation that is characterised by the loss of hair shortly after birth. It arose spontaneously on a brachyury (T) tf background at the Jackson Laboratories in 1966 (Green, 1970). Homozygotes are viable and fertile. Mutant mice can be identified by an unusually thin and short hair coat as early as 1 week of age when hairs first emerge from follicles. By 3 weeks some mice are nearly hairless, whereas others retain a rather substantial coat. Adult hairs are greasy, matted and slightly depigmented in comparison to wild-type.

The *dep* mutant is currently available as "B6C3Fe a/a-*dep*/J" at the Jackson Laboratory. It was reported that many hair follicles are misshapen and disorientated with 20% of the hairs showing an irregular arrangement of septa in the hair shaft. In addition, clumps of pigment are also observed and are thought to be remains of degenerating follicles. However, the skin stage of when this observation is taken was not specified.

A similar description of *dep* has also been entered in Skinbase[18], the mutant mouse skin and hair pathology database, including histological sections that illustrates the reported pigment clumping phenotype of *dep*.

The site of action of the dep locus was analyzed by the technique of dermal-epidermal recombination grafting (Mayer et al., 1976). In this study, dermal-epidermal recombination was made between embryonic skin of *dep* and normal mice transplanted onto histocompatible mice. It was found that the grafts that contained mutant epidermis as one of the components (i.e. '*dep* epidermis-wild type dermis' and '*dep* epidermis-*dep* dermis') produced hairs with a morphology similar to hairs found in *dep* mice; whereas grafts of the combination 'normal epidermis-dep dermis' produced hairs that are comparable to wild-type. This indicates that the *dep* phenotype is of an epidermal origin.

[18] Skinbase website: http://www.pathbase.net/~skinbase/mutant_images.php?mutant=*Dep*ilated_(*dep*)_Chr4_38.8cM European mutant mouse pathology database (Pathbase), University of Cambridge, World Wide Web (http://www.pathbase.net)

Figure 5.1. Schematic representation of the hair follicle
[A] Stem cell locations in mammalian epidermis (Watt et al, 2006). Apart from the bulge region (blue), epidermal stem cells are also thought to be present in the basal layer of the IFE (green) and the SG (red). The cells highlighted in yellow present transit-amplifying cells. Terminally differentiated cells are not shown. [B] The hair bulb showing 8 distinct lineages of keratinocytes of the hair follicle. The diagram also includes the specific pattern of expression of several markers that allow individual lineages to be distinguished.
Abbreviations: DP, dermal papilla; HF, hair follicle; IFE, interfollicular epidermis; SG, sebaceous gland; ORS, outer root sheath; Cp, companion cell layer; IRS, inner root sheath; He, Henle's layer; Hu, Huxley's layer; Ci, cuticle of IRS; Ch, cuticle of hair shaft; Co,cortex of hair shaft and Me, medulla.

[A] (Watt et al., 2006)

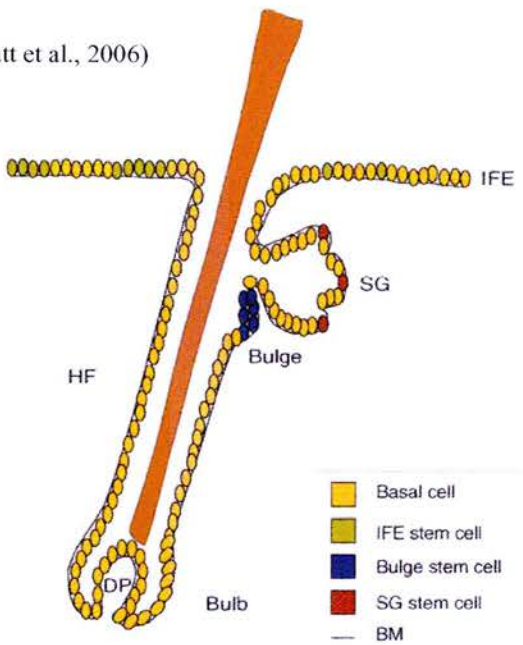

[B] (Kobielak et al., 2003)

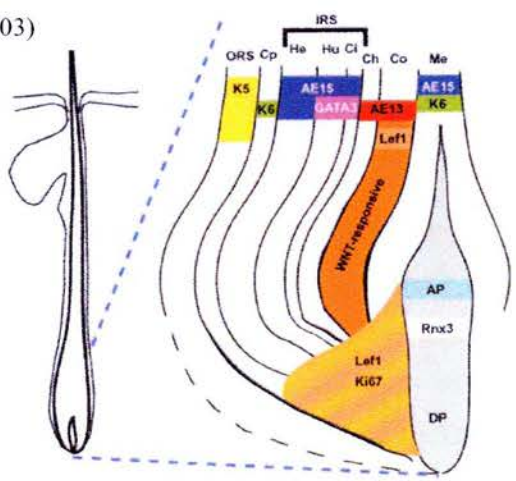

Figure 5.2 Differentiation of epidermal keratinocytes
(Diagram from Edmondson *et al*, 2003).
The basal cell layer consists of three types of cells namely IFE stem cells (SC), transit amplifying (TA) cells and post- mitotic differentiating (PMD) cells. Epidermal differentiation begins when selected daughters of SC becomes TA cells, which go through finite number of cell divisions and finally become PMD cells that are committed to the process of terminal differentiation. The PMD cells detach from the BM and move to the suprabasal layer where they continue to differentiate as they migrate upward through successive layers of basal layer, spinous layer, granular layer, and finally becomes the cornified layer of anucleated cells, which is eventually shed (Edmondson et al, 2003).

BM, basement membrane; Circular green arrow, represents self-renewal ability; green arrow, progression of keratinocytes. The boxed region represents a single epidermal proliferative unit (EPU).

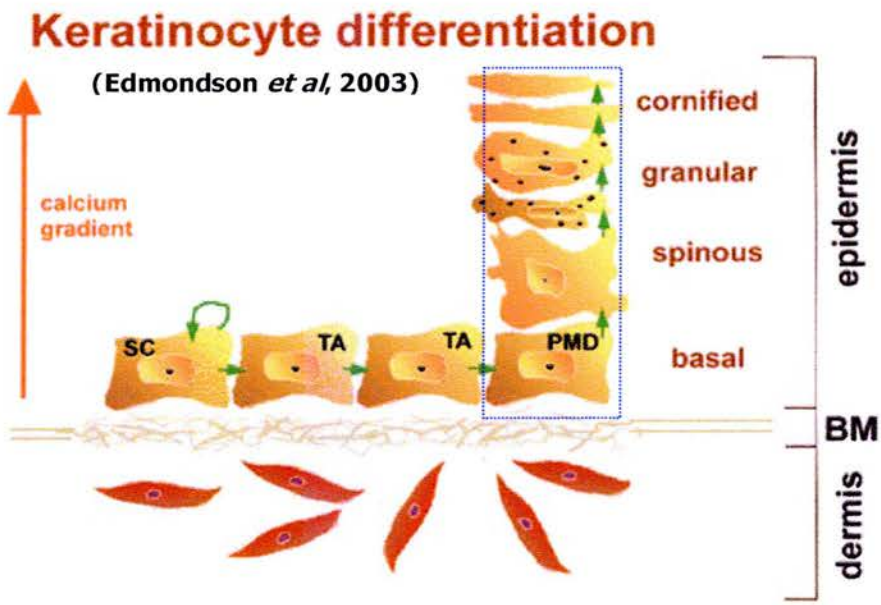

Figure 5.3: The hair growth cycle
(Diagram from Fuchs *et al.*, 2001)
At anagen, a mature hair follicle consists of the bulge, which lies under the sebaceous gland. At the base of the follicle, is the hair bulb which consists of the dermal papillae, surrounded by the matrix, which proliferates and differentiate into the 7 lineages of keratinocytes, that form the hair shaft (HS) and the inner root sheath (IRS). The outer root sheath (ORS) is of a different lineage, and is a continuation of the interfollicular epidermis (IFE).

Throughout the entire life of most mammals, hair follicles go through periods of anagen, catagen, and telogen during which hairs are constantly being renewed and regenerated. At anagen, the matrix cells at the hair bulb goes through rapid proliferation to generate an upward growth of a hair fibre. At catagen, the follicles undergo an apoptotic-driven regression when the lower part of the follicle stops growing and is reabsorbed, drawing the DP closer to the bulge which maybe for the purpose of epithelial-mesenchymal signaling, and maybe essential in converting stem cells into matrix cells. And at telogen the follicles are at rest, waiting for the next wave of signals to act on. During this stage, the hair maybe actively shed.

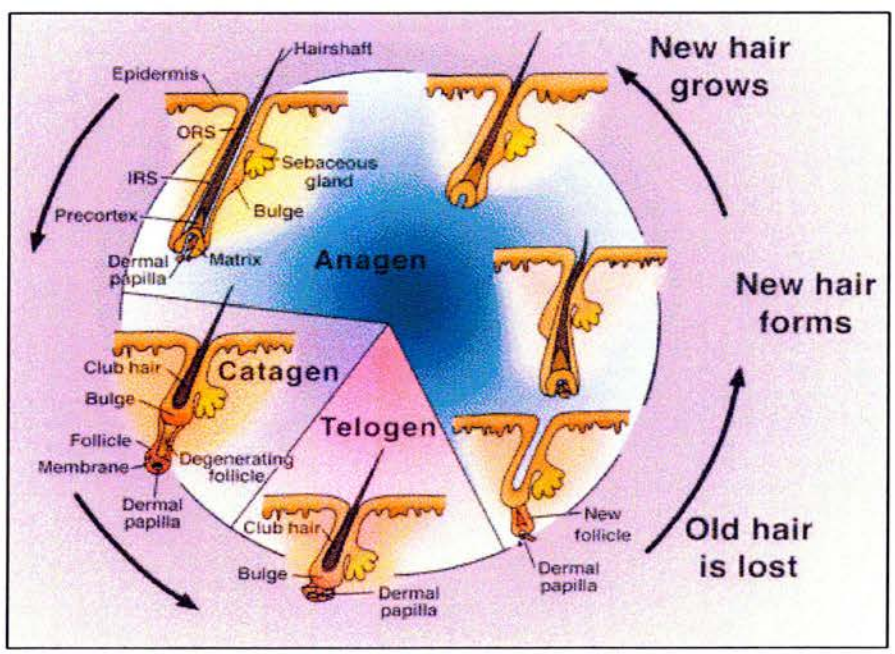

5.3. Results

5.3.1. Characterization of *dep* phenotype.

(i) Visible phenotype of dep

Our observations were consistent with some of the documented descriptions of *dep*. In general, *dep* seems to lose their hair shortly after birth, when hairs first emerge from hair follicles, but others lose hair later (Figure 5.4A). The hair loss phenotype is heterogenous and is variable in terms of the onset of phenotype, degree and region of hair loss.

Adult hairs of *dep* are greasy, matted and sparse throughout the body in comparison to wild-type (Figure 5.4C). The hairs of adult mice are typically depigmented especially on the ventral side of the body. The orange-brown colour indicates a lack of eumelanin, and this phenotype becomes more prominent as the mutants become older (Figure 5.4D). The lack of eumelanin can be observed by eye as early as P5 (Figure 5.5A), just after the eruption of hairs from the follicles, at which stage, the hair distribution is sparse and disorderly (Figure 5.5B). The development of skin tumors or lesions has never been observed in *dep*. Heterozygotes have no phenotype, indicating it is likely that *dep* is a loss of function or partial loss of function mutation.

Apart from the hair loss phenotype, it is often observed that *dep* mutants are smaller in body size during the first few weeks of birth (Figure 5.4B). However, this difference becomes insignificant and gradually disappears as the mice get older.

(ii) Histological analysis of dep

Crosses between *dep* heterozygotes were set up and skin samples were collected at weekly interval of up to 12 weeks. Earclips from all mice were collected for genotyping on weaning so that a set of wild-type, heterozygote and homozygote was collected for each timepoint. Comparison between *dep* and a control littermate is necessary due to the complicated breeding background of *dep* and the possible discrepancy in morphology as a result of strain difference. This also ensures that the animals are age-matched at every stage.

Some sections were sent to Dr. Rebecca Porter (Department of Dermatology, University of Cardiff) who analysed the samples by comparing H&E sections between wild-type and *dep*, and by measuring the length of 8week *dep* mutant (without littermate control). In summary, she concluded that *dep* has enlarged sebaceous glands, dilated infundibulum at telogen and a delayed 2nd catagen. It was also observed that the *dep* HFs have unusually long epithelial strands and possibly disintegrating HFs.

Subsequent analysis by myself verifies all findings except that, instead of a delayed 2nd catagen, *dep* follicles seem to enter the 3rd anagen at 7-weeks, after it had gone through the 2nd catagen at week 5/6 (Figure 5.6B), same as wild-type. The findings are detailed below. In general, the *dep* anagen HFs also appear smaller in size. Despite the discrepancy, there is definitely a mismatch in hair cycling events between wild-type and *dep*. In addition to the hyperplastic sebaceous glands, the epidermis and outer root sheath of *dep* are also shown to be hyperproliferative using specific markers. The thickness of the skin layer generally varies throughout the hair cycle, but in some cases there are discrepancies between wild-type and *dep*.

Dilated infundibulum

The first catagen occurs at the same time in wild-type and *dep*, but when regression is completed at week 3, the telogen follicles of *dep* have a dilated infundibulum [Figure 5.6A(iv)], which is the upper segment of the HFs between the epidermis and the entry of the SGs.

Abnormal histological morphology

Despite the abnormal appearance of the telogen follicles, the mutant follicles start cycling again at week 4 and enter anagen, as do wild-type. In wild-type, the hair bulbs, melanin, matrix cells can be clearly observed at this stage, indicating that the matrix progenitors are actively proliferating and differentiating [Figure 5.6A(ii)]. However, even though *dep* is also in anagen, the morphology of the HFs at this stage is generally abnormal and malformed [Figure 5.6A(v)]. The follicles appear stunted and under-developed, which resemble the appearance of embryonic hair follicles. Furthermore, the mutant follicles are not as deeply invaginated into the subcutaneous layer.

Sebaceous hyperplasia of *dep* follicles

The morphogenesis of *dep* follicles appears normal in general, however, the sebaceous glands are enlarged especially at anagen [Figure 5.6A(v)] whereas in wild-type, the SGs are not as

often seen because they are relatively small. The IFE of *dep* also appears thicker comparing to wild-type [Figure 5.6A(v)].

Mismatch in hair cycle events

The *dep* follicles go through the first hair cycle normally, and enter the second hair cycle at about 3.5week. Both wild-type and *dep* follicles start to regress at about 6 week of age (Figure 5.6B). However, while wild-type HFs are still in telogen at 7week [Figure 5.6A(iii)], *dep* follicles are already in the (3^{rd}) anagen [Figure 5.6A(vi)] with apparent hyperplastic phenotype. This persists until 9-wk, at which point the regression appears to have occurred with shortened follicles. At 10 and 12 weeks, both wild-type and *dep* follicles are in telogen. The hair cycling events of wild-type and *dep* follicles are summarized in Table 5.1.

Apart from the above observations, however, *dep* generally has a complete morphology with intact HF components.

Table 5.1: Epidermal Stages at weekly time points observed in histological sections.

WEEK	C57BL/6	*Dep*
1	Morphogenesis	Almost Normal morphogenesis
2	Morphogenesis -> Catagen	Morphogenesis
3	Telogen	Telogen
4	Anagen	Anagen
5	Late Anagen	Early Catagen (anagen)
6	Catagen/ Telogen	Catagen/ telogen
7	Telogen	Anagen
8	Telogen	Anagen

Note: Anagen (growth phase), catagen (destruction), telogen (rest stage).

The onset of *dep* phenotype

Consistent with the visible differences that can be readily identified by eye (Figure 5.5), histological sections show the onset of *dep* phenotype is between P4 and P5. The hair follicles between P4 wild-type and *dep* are similar (Figure 5.7), indicating that HF development is normal at this stage. However, *dep* follicles at P5 shows an obvious thickening of the epidermis; the sebaceous hyperplasia phenotype becomes noticeable by P7.

Discrepancy from previous findings

It was previously reported in 'Skinbase' that *dep* exhibits various degree of follicular dystrophy based on histological sections, including melanosome clumping within the HFs. A similar observation was made by Rebecca Porter when looking at a sample of *dep* skin (from *dep* x *dep*

(ii) Expression of custom-made Zdhhc21 antibody.

The above conclusion was based on a comparison between patterns of RNA *in-situ* and protein immunohistochemistry in separate experiments. To confirm the exact location of Zdhhc21 expression, it requires counter staining with a marker of known pattern of expression. Therefore, an antibody targeting Zdhhc21 was designed and made to allow better localization and more relevant comparison with other markers.

Two peptides targeting the N- and C- terminals were designed from the 265 a.a. Zdhhc21 peptide by Eurogentec (Double X purified program) based on hydrophilicity, surface probability, antigenic index and the alpha helix predictions of the targeted peptide.

```
 73- 87: GRLPENPKIPHAERE+C
219-232: CEEISRPRKPWQQT

MGLRIHFVVD PHGWCCMGLI VFVWLYNIVI IPKIVLFPHY EEGHIPGILI IIFYGISIFC 60
LVALVRASLT DPGRLPENPK IPHAERELWE LCNKCNLMRP KRSHHCSRCG HCVRRMDHHC 120
PWINNCVGED NHWLFLQLCF YTELLTCYAL MFSFCHYYYF LPLKKRNLDL FVVRHELAIM 180
RLAAFMGITM LVGITGLFYT QLIGIITDTT SIEKMSNCCE EISRPRKPWQ QTFSEVFGTR 240
WKILWFIPFR QRQPLRVPYH FANHV                                       265
```

A first bleed of the immunisation against the antigen was tested on western blot against lysate of cells transfected with wild-type HA-*Zdhhc21* construct, two bands of size not expected of Zdhhc21 (~31kDa) were seen with the bleed immunised against the N terminal peptide, no bands were observed with the C-terminal peptide.

The purified antibody (against N + C terminal peptides) was tested against the same cell lysate transfected with HA-Zdhhc21on western blot, but has not yet been successful. Immunofluorescence of these cells transfected with HA-*Zdhhc21* construct shows that the N-terminal antibody (N-dhhc21 hereafter) co-localises with the cis-Golgi marker Gm130 in a very small proportion of cells (data not shown). Ideally, the N-dhhc21 antibody may be tested against cells transfected with HA-*dep* to show a mislocalisation of the protein.

Using the purified antibody, immunohistology was performed on skin sections. The IHC pattern of N-dhhc21 localises to a specific region in the HFs of both wild-type and *dep*. Although N-dhhc21 does not co-localise with GATA-3 (Figure 5.10), it is in a similar region as observed with RNA probes. This emphasizes the needs of designing a Zdhhc21 antibody which allows counter-staining and a more accurate localization of the protein.

The N-terminal antibody localises to the Henle's layer of IRS

To determine the exact location of N-dhhc21 expression, several markers have been used (see Figure 5.1B for reference). N-dhhc21 co-localises partially with AE15 in 4-wk wild-type follicles (Figure 5.11A), but does not overlap with GATA3 staining (Figure 5.10). AE15 stains all 3 layers of the IRS, whereas GATA3 only stains the inner 2 layers of the IRS: Huxley's layer and the cuticle layer. This indicates that N-dhhc21 colocalises with the Henle's layer. If the raised antibody is specific, it means that Zdhhc21 is expressed in the outermost layer of the IRS, which is the Henle's layer. It was also observed that, at 4wk, N-Dhhc21 expression overlaps almost completely with AE15 in *dep* follicles, suggesting that the inner two layers of the IRS, and/ or the medulla may be absent in *dep* at that stage (Figure 5.11B). We show that GATA3 is expressed in *dep* skin (Figure 5.9), suggesting that only the medulla (but not any part of IRS) is absent in *dep*.

At 5-wk, however, the other regions of AE15 staining appear again in *dep*, and is identical to wild-type (Figure 5.11C and D).

Specificity of the N-Dhhc21 custom-made antibody

The expression pattern observed with the N-antibody maybe due to other antibodies in the source other than the one specifically targets the Zdhhc21 antigen. To test whether the expression pattern is specific, saturating amount (1mg/ml) of the immunogen peptides was added together with the purified N-terminal antibody to compete binding with the antigen on the skin sections. Under normal conditions, the N-dhhc21 antibody stains about half of the follicles in 5-wk wild-type skin, especially in the dermis. When the N-Dhhc21 specific immunogen peptide is applied in addition to the antibody, none of the follicles were positive, indicating that the immunogen completely blocks N-Dhhc21 binding specifically (Figure 5.12a). Therefore, the staining pattern is likely to be due to antigen-specific antibody, but not any non-specific antibodies that might have accidentally developed through immunization.

In addition, staining with pre-immune serum and secondary antibody alone (Alexa 594 anti-rabbit IgG), show that the specific pattern observed with the N-Zdhhc21 antibody was not

caused by non-specific protein interactions with cellular proteins/ lipids/ carbohydrates, or non-specificity of the secondary antibody respectively (Figure 5.12b[19]).

5.3.3. Matrix proliferation and HF morphogenesis are normal in *dep*

Endogenous alkaline phosphatase (AP) staining can be used as a marker for the dermal papillae (DP) and the dermal sheath, which is the outmost layer of the follicle. AP activity is observed in the DP and dermal sheath, indicating that the HF morphogenesis in *dep* is likely to be normal (Figure 5.13).

The hyperplasia phenotype observed in *dep* may be due to an increase in cell proliferation in response to an upregulation of certain signaling events. To determine whether the underlying cause of the basal layer hyperplasia is due to an increase in cell proliferation, we used Ki67, a standard proliferation marker that stains cells in all phases except G0 (Figure 5.14), and Phosphohistone 3 (Ph3), a proliferative marker specific to M-phase (Figure 5.15). Neither marker shows a significant difference in the number of positive cells. This indicates that the matrix proliferation in *dep* is likely to be normal, and that the hyperplasia phenotype is not due to an increase in proliferation.

The extent of cell death was also looked at using Caspase3a, a specific cell death marker, and was also normal, indicating that the observed phenotype is not due to apoptosis (data not shown).

5.3.4. Aberrant differentiation in *dep* epidermis

Epidermal progenitor compartment is expanded

Immunohistochemistry using keratin 5 (K5), marker of the ORS, bulge and the basal layer, highlights the much thicker IFE and basal layer in *dep* (Figure 5.16). Although the SGs are not usually visible using the K5 marker, K5 staining reveals the appearance of SGs due to the significant expansion of the organ.

Keratin5 is a marker of the epidermal progenitor compartment which marks basal keratinocytes at an early differentiation state, the expansion of K5 signal directly indicates the expansion of

[19] Control experiments from Figure 5.12b images provided by Margaret Keighren and Pleasantine Mill.

the compartment. This indicates that the hyperplasia phenotype in *dep* is due to an actual expansion of the progenitor compartment as a result of a disturbed programme of epidermal differentiation, rather than an increase in proliferation.

Increased number of undifferentiated cells in dep basal layer

Nuclear staining of the epidermis using DAPI shows an increased number of nucleated cells in *dep* epidermis that have not undergone terminal differentiation (Figure 5.17). In wild-type, the cells flatten as they differentiate up the suprabasal layer, whereas in *dep*, the suprabasal cells are often vertically elongated.

Usually, an epidermal proliferative unit (EPU) consists of a stack of cells including the basal post-mitotic cell and their suprabasal differentiating progeny, and finally the cornified cells (Allen and Potten, 1974; Kaur, 2006). In wild-type IFE, individual EPUs intersperse throughout the basal layer. Whereas in *dep*, individual EPUs can not always be distinguished due to an increased number of cells.

Expansion of the suprabasal layer of dep epidermis

The expansion of K5 staining in *dep* (Figure 5.16) suggests an expansion of the basal layer (i.e. epidermal progenitor compartment). To further address this finding, a basal/ progenitor marker P63 was used to determine whether the K5+ compartment contains an increase in proliferative cells.

P63 (also known as p51 or KET), was originally identified as a member of the p53 tumor suppressor family. It is highly expressed in the basal or progenitor layers of many epithelial tissues and is involved in initiating epithelial stratification during development and maintaining proliferative potential of basal keratinocytes in mature epidermis (Blanpain and Fuchs, 2007; Koster et al., 2004). When P63 expression is knockdown in the epidermis, the mice fail to develop stratified epithelia as well as epithelial appendages and limbs (Koster et al., 2007). Although P63 expression is required in the highly proliferative basal cell layers, its downregulation is required in the differentiating layers to ensure correct terminal differentiation.

In *dep*, there is an increase in P63+ cells in the basal layer which may be a result of an overall increase of nucleated cells in the epidermis. Normally, proliferative keratinocytes are only found in the basal layer, so P63 is expected to express in proliferating transit-amplifying (TA) cells, which count for the majority of the basal cell layer. However, double staining of K5 and P63 reveals that the progenitor cell layer is expanded beyond its normal one-cell layer thickness in *dep* (Figure 5.18).

The P63 signal in layers beyond the first basal layer typically appears weaker than those in the first basal layer. This suggests that, even though K5 expression is sustained, the progenitor cells gradually lose their P63 status and perhaps their proliferative ability as they migrate away from the basal layer and become more terminally differentiated (Figure 5.18, white arrows).

The increased frequency of P63+ cells in the basal layer suggest that *dep* epidermis has an increase in cell proliferation and that epidermal stratification may be delayed. This aspect of phenotype resembles closely to the $Ptc1^{mes/mes}$ (mesenchymal dysplasia) mutant that has epidermal hyperplasia and an expansion of the epidermal stem cell compartment (Nieuwenhuis et al., 2007).

Since K5 staining in *dep* covers the entire thickness of the epidermis (excluding the cornified layer), it is necessary to use a suprabasal marker to determine the region of expansion. Normally, keratinocytes switch off K5/K14 expression as they detach from the BM into the suprabasal layer where they express K10 instead. However, double labeling with K10 and P63 shows that the expression pattern of K10 overlaps with that of K5, and that the suprabasal layer is thickened in *dep* (Figure 5.19). In *dep* epidermis, K10 is absent from the basal layer (first epidermal layer), but express suprabasally in up to 5 or 6 cell layers. Some of these suprabasal layers contained large and round keratinocytes with prominent nuclei (Figure 5.19, green arrow), instead of the flattened shape usually seen in terminally differentiated cells. Although P63+ cells are seen in the K10+ suprabasal layer of *dep* skin, they are also found in wild-type epidermis, but at a lower frequency. The expression pattern of K5, K10 and P63 in wild-type and *dep* epidermis is represented in Figure 5.20.

The sustained K5 expression is not coupled with sustained progenitor properties, as evident by the observation that P63+ cells never get beyond the second/ third cell layers. But instead, the

sustained K5 expression seems to be associated with a delay in terminal differentiation. It is not clear whether the downregulation of K5 is required for correct terminal differentiation, or whether these are 2 independent consequences as a result of a disruption in epidermal homeostasis.

Taken together, the elevated P63+ cells and the expansion of the suprabasal layer indicate an aberrant differentiation. The causes or consequences of the sustained K5 expression is unknown, however, it seems to couple with mislocalisation of undifferentiated *dep* keratinocytes. Although the number of P63+ cells is significantly increased in *dep* epidermis, Ki67 and Ph3 staining (Figure 5.15) suggest that it is unlikely to be due to an increase in proliferation rate.

Analysis of differentiation markers of each layer including involucrin (granular and upper spinous layer), profilaggrin (differentiating granular layer), filaggrin (keratinocytes in transition from nucleated granular to anucleated cornified layer), and loricrin (cornified envelope) may be necessary to determine whether a specific layer of the suprabasal compartment of the epidermis is expanded.

Another observation is that, even though P63+ cells lining the SGs are clearly visible in *dep* but not in wild-type due to their small size, the P63+ cells are more sparsely distributed in SG-lining basal cells of *dep* when compared to the epidermis. It seems that there is not an increase in the number of sebocyte progenitors. The sebocytes within the SG cavity are not positive for P63, so they are likely to be differentiated lipid-secreting sebocytes as expected. Immunostaining using markers of the SGs such as the adipogenic transcription factor PPARγ (an early differentiation marker which govern genes involved in lipid synthesis), and ORO (a terminally differentiation marker) may be used to determine the status of these sebocytes.

5.3.5.The hyperplasia phenotype is not due to upregulation of Shh signaling.

At anagen, Shh signaling is required to maintain a balance between cell proliferation and differentiation in the epidermis. It promotes proliferation of hair progenitor cells in the distal matrix cells. It controls spatially and temporally expansion and differentiation of HF progenitor cells to prevent ectopic proliferation of the matrix.

During epidermal morphogenesis, a series of epithelial-mesenchymal signals are turned on to instruct the undifferentiated epithelium and mesoderm to placodes and dermal condensate (Fuchs and Raghavan, 2002). Loss of Shh expression in knockout skin grafts results in absence of hair shaft due to aberrant differentiation (St-Jacques et al., 1998). Whereas Shh overexpression leads to formation of basal cell carcinomas in transgenic mice (Oro et al., 1997).

During development, Shh is expressed in the placode, while the Shh targets, Ptc1 and Gli1 are expressed in the dermal condensate. In postnatal skin, Shh is normally restricted to a small group of cells in the anterior or posterior hair matrix. Ptc1 is expressed in the epithelial portion of the hair bulb and the DP of postnatal skin. The expression of Gli1 partially overlap with Ptc1 in the hair bulb.

The expression level and pattern of *Shh*, and its responsive genes, *Ptc1* and *Gli1* are compared in wild-type and *dep* hair follicles by RNA *in-situ* on postnatal skin (Figure 5.21), but no significant difference were found. Therefore, we conclude that the *dep* mutation does not result in direct or indirect upregulation of Shh target genes in the skin.

5.3.6. Sebaceous hyperplasia

Tail epidermal in-situ assay

In comparison with the epidermis of the dorsal skin, tail epidermis contains fewer numbers of follicles and the follicles are arranged as triplets. The tail follicles have more complex tertiary structure with a pigmented scale pattern. Although the tail follicles do not cycle in synchrony with the backskin, the follicle triplets do coordinate with each other even though the central follicles typically remain in anagen for longer than the flanking two.

The recent development of whole-mount labeling techniques in mouse epidermis has facilitated examination of follicles in large areas of the epidermis without the need to prepare conventional histological sections (Braun et al., 2003). So far, two-dimensional images from skin sections reveal cross-sections of the HFs, allowing us to study expression pattern against various antibodies in different compartments. However, it is often difficult to assess co-localisation of two markers, and the access to the overall structure is restricted. In contrast, whole-mount

labeling and confocal microscopy allow us to analyze the 3D topography of the follicles. Tail epidermis is commonly used because compared to the dorsal skin sample, it has easier access, and the epidermis can be spilt from the dermis more readily.

Tails from wild-type and *dep* mice were collected. After incubation in 5mM EDTA at 37°c for 4 hrs, the epidermis was separated from the dermis to expose the follicles underneath the epidermal layer. An initial *in-situ* assay was then carried out by Ian Smyth as a collaboration.

Normally, wild-type tail follicles are arranged as triplets, with a pair of well-defined SGs per follicle. When examined for K14 and K15 expression in *dep*, the SGs show various abnormalities including an evident hyperplasia, malformed and extra glands (Figure 5.22). Despite the differences observed with confocal microscope, the tail of the mutant does not show any visible phenotype in any mice collected and the tail does not exhibit hair loss.

Sebum staining using the lipophilic dye Oil Red O (ORO) also shows the sebaceous hyperplasia appearance and also an accumulation of lipid in the infundibulum (Figure 5.23), which may explain the greasiness of the *dep* hair coat. The limitation of using this type of lipid staining is that it is an assay of sebum production (i.e. not *in-situ*), therefore the region that is positive for ORO does not necessary represent the site of production/ secretion. Therefore, the samples must be handled gently to prevent any artifacts created by physical movement.

Comparison with glands with SG-like morphology

Although *dep* exhibits a prominent SG hyperplasia phenotype, rather than being a cause of the hair loss phenotype, it may be a consequence of an imbalance of various cell types in skin homeostasis secondary to the hair loss phenotype.

To get some idea of a causal link of the SG phenotype, glands that have SG-like morphology were collected from adult mice to see if they are also affected in *dep*. They included the meibomian gland, preputial gland (male), anal gland and ceruminous gland.

Histological sections were compared for the preputial glands (Figure 5.24), and no difference were found in terms of gland size, number of sebocytes and sebocyte size. The other glands were sent to Rebecca Porter and she reported no difference (data not shown). This shows that the *dep* mutation is unlikely to affect sebocyte proliferation in other tissues, and that the SG

phenotype is specific to hair follicles. So, the SG hyperplasia phenotype is likely to be a consequence secondary of a skin/hair phenotype.

5.3.7. HS differentiation is delayed in *dep*

Apart from the phenotypes already described, H&E sections reveal an abnormality in hair shaft development in *dep* mice. In wild-type mice, at anagen, strands of hairs can be seen in the epidermis and emerging from the HFs through to the skin layer. However, these hair shafts are not seen in *dep* HFs. Occasionally, differentiating hair shafts may be observed in *dep* at that stage, but are different from that of wild-type (Figure 5.6ii and v). It may be that the *dep* HFs lack correct hair shaft differentiation, rather than losing hair by an active shedding.

Immunohistochemistry on skin sections using hair shaft-specific markers shows that this is the case. The staining pattern of AE13, marker of the acidic hair keratin filaments in the cortex and cuticle of the hair shaft, appears to be different between wild-type and *dep* (Figure 5.25). The AE13 staining in wild-type appears as a oval-shaped hoop, within which lies the medulla, the innermost core of the hair shaft. However, this non-staining space is missing in *dep* HFs; the AE13-staining structure on the 2 sides seem to 'collapse' onto each other, indicating that the medulla may be absent in *dep* in early anagen.

AE15 is an antibody against trichohyalin granules, which are normally present in all 3 layers of the IRS and the medulla. At early anagen (4 weeks), AE15 signal can be clearly seen in the IRS and medulla in wild-type HFs as two clearly separated compartments. However, in *dep*, the AE15 signal only appears as one region (Figure 5.26A, also Figure 5.11A and B), indicating that the medulla is absent. Combining with the AE13 staining data (Figure 5.25), it suggests that the AE15 region represents the IRS and that the medulla is absent, indicating a lack of hair keratin-specific protein of the medulla being made at this stage of anagen.

At late anagen (5 weeks), however, the expression pattern of AE15 in *dep* becomes normal again (Figure 5.26B, also Figure 5.11C and D). It is possible the *dep* HFs require longer time to reach a threshold for hair-specific keratin production, during which the full extent of hair growth is attained for a functional hair to be made.

Figure 5.4. Gross phenotype of *dep*

[A] Hair loss phenotype of *dep*. An example of an early hair loss phenotype showing *dep* being almost completely bald at week 4. At this stage, *dep* has a normal body size comparable to wild-type. [B] Reduced body size. The mutant mice are often observed to have a reduced body size during the first few weeks after birth, but the difference becomes insignificant as they grow older. [C] Greasy hair coat appearance. Comparison between wild-type and *dep* reveals the typical greasy phenotype and disorderly pattern of the dorsal hair coat of *dep*. It also appears to be sparse and matted which is typical of the phenotype. [D] Depigmentation of *dep* hair. At later stage, the hair of *dep* mutants are typically depigmented, especially on the ventral side. Patches of hair loss region can also be observed at this stage. The described phenotypes appear at various different stages and do not correlate to the age shown.

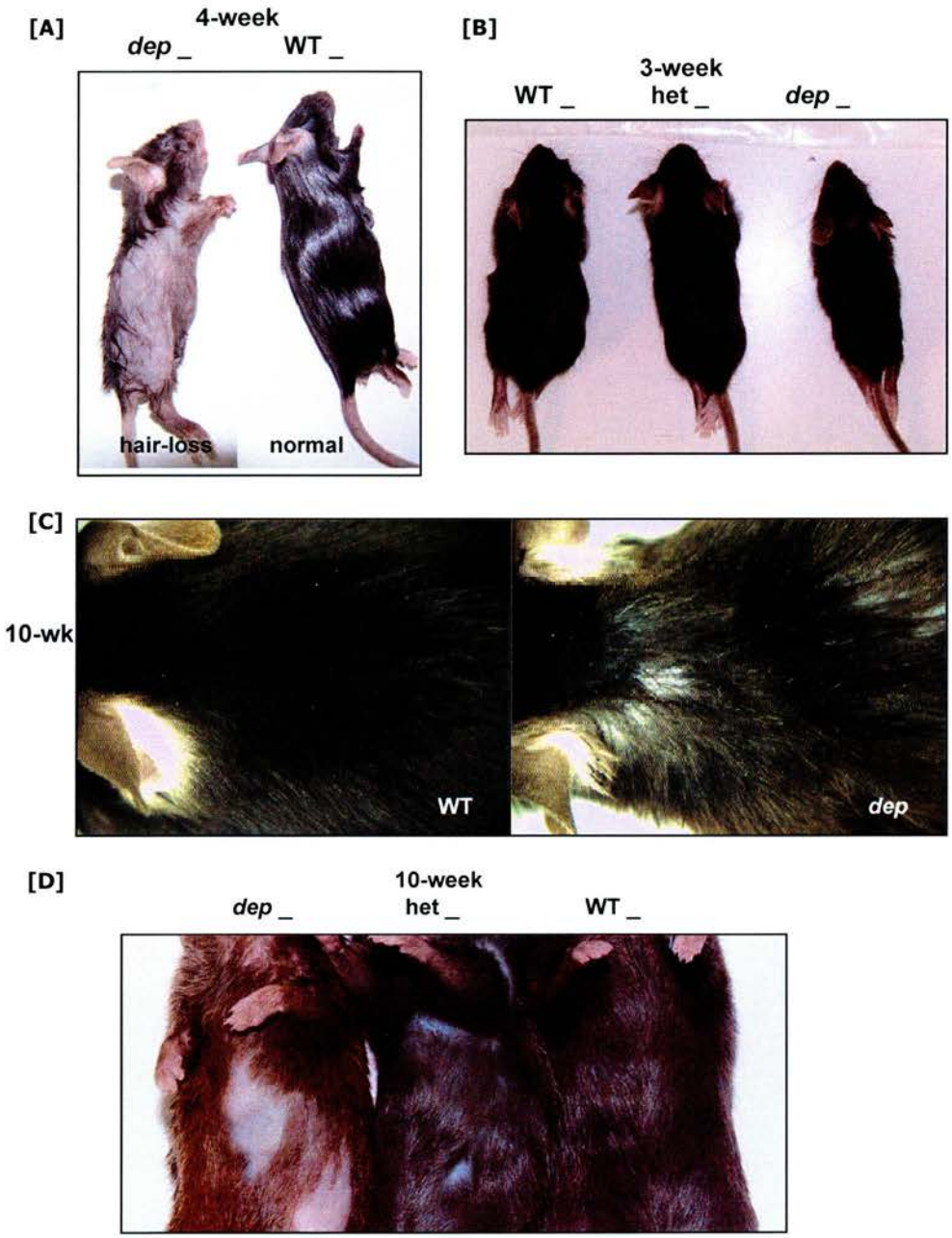

Figure 5.5. Mutants can be identified at P5
[A] Lack of pigment in *dep*. Dorsal skin samples collected from P5 mice showing a lack of pigment in *dep* in comparison to wild-type and heterozygote. [B] Sparse and disorderly pattern. The same samples under the microscope (x10) reveals the sparse and disorderly pattern of *dep*. Scale bar, 100_m.

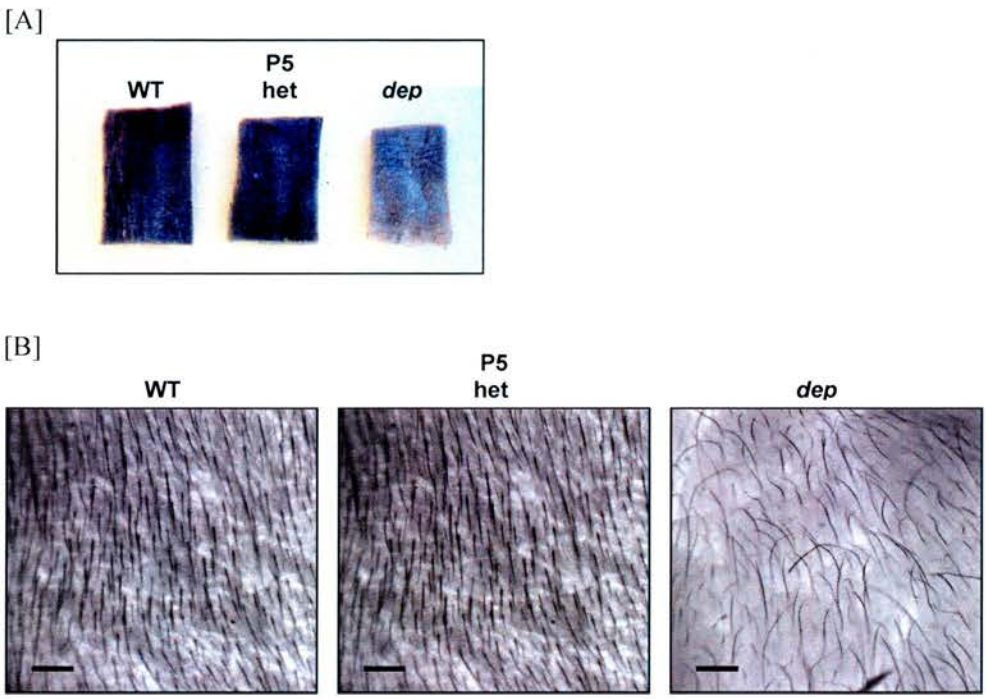

Figure 5.6. H&E staining reveals the major histological phenotypes of *dep*

[A] At 3-wk, both wild-type [i] and *dep* [iv] have undergone catagen, and are now in telogen, when the follicles are at rest, but the infundibulum of *dep* is dilated [iv]. But after a week, *dep* HFs start to cycle again and are in anagen [v], when the melanosomes can be observed in the hair bulb of wild-type HFs [ii]. Even though *dep* is also in anagen, the HFs resemble embryonic follicles in size and appearance, indicating that the HFs are malformed at this stage. Furthermore, the *dep* HFs are not as deeply invaginated into the subcutaneous layer. There is also a hyperplasia of sebaceous gland (SG) and the interfollicular epidermis (IFE). The *dep* HFs go through the first hair cycle normally, and then into the second anagen again at about 3.5-wk. But at 7-wk, the WT follicles [iii] are at the end of its second hair cycle in telogen and have regressed into the upper dermis but the mutant follicles [vi] are in anagen, indicating a cycling difference between WT and *dep* HFs. The magnification of each picture is indicated, highlighting the variability in thickness throughout a hair cycle. The follicles pictured are from similar mid-dorsal regions. (a) epidermis (b) dermis (c) subcutaneous layer.

[B] At 6-wk, both WT and *dep* undergo telogen, indicating that the anagen observed at 7wk is a premature 3rd anagen rather than a prolonged 2nd anagen. Scale bar, 50_m.

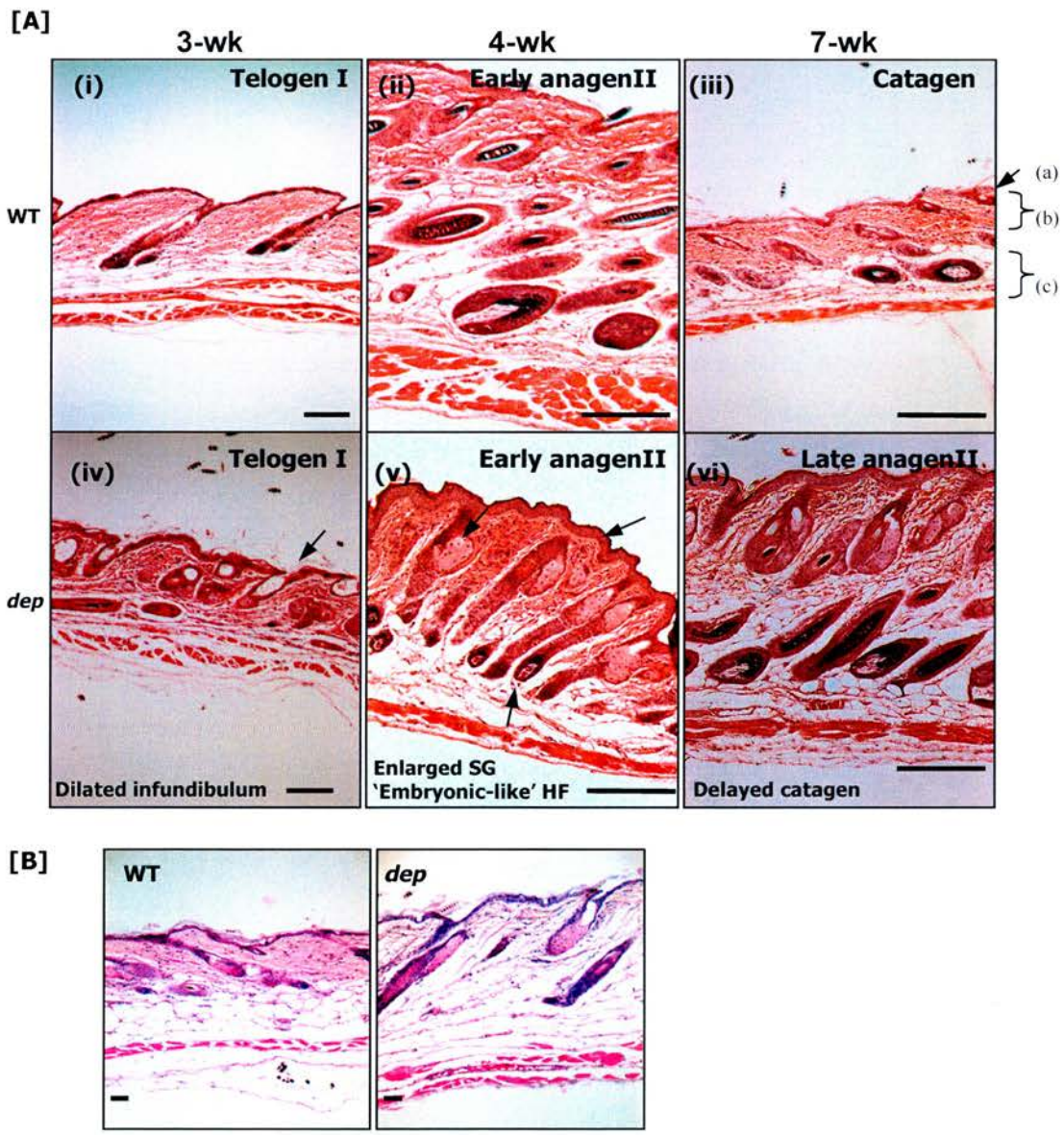

Figure 5.7. The onset of histological phenotype appears as early as P5
At P4, the thickness of the epidermis and the size of sebaceous glands are similar between wild-type and *dep*. At P5, an obvious thickening of the epidermis can be observed. At P6 and P7, the difference becomes less pronounced, although the increase in size of the sebaceous glands can be seen in P7. Scale Bar, 100_m.

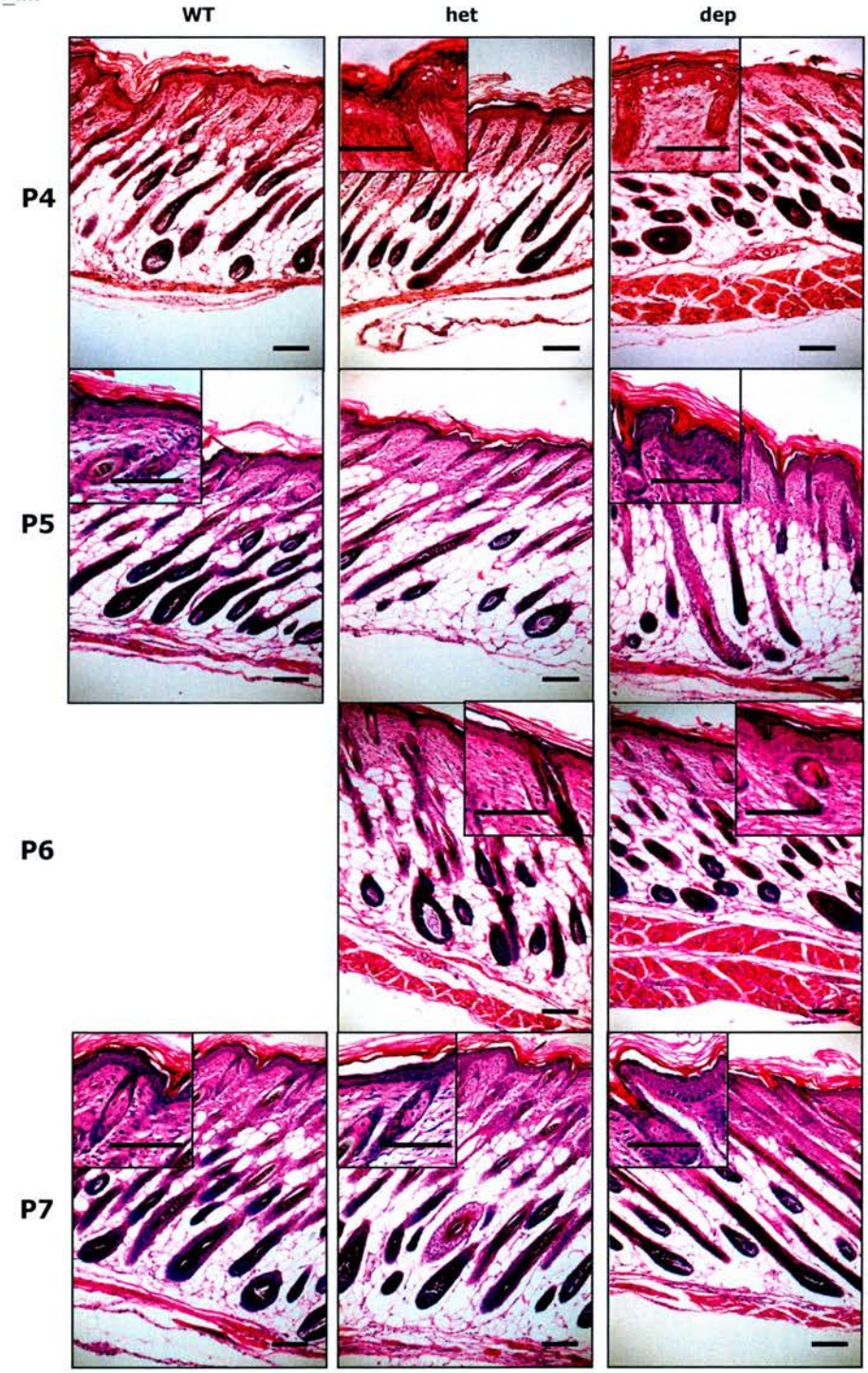

Figure 5.8. The degree of pigmentation in medulla varies in *dep*
Sample of plucked hairs from a 9-wk *dep* dorsal region. The medullary septae are pigmented to various degree within a sample of *dep* hair. Nevertheless, the septal patterns are normal, in contrast with previously record. Scale bar, 50_m.

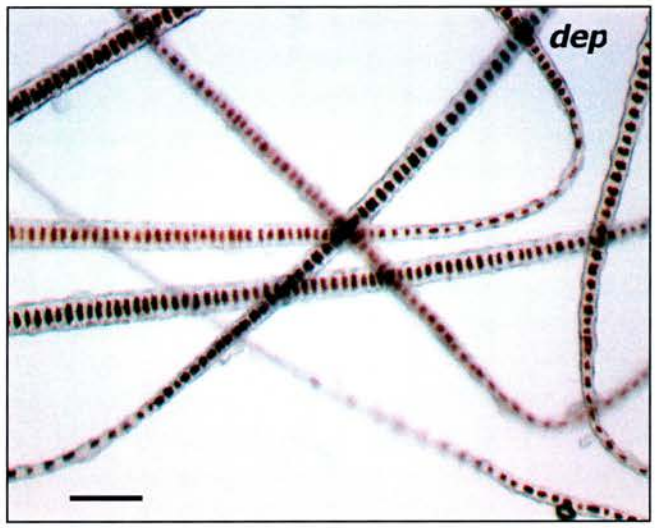

Figure 5.9. Transcript of Zdhhc21 is present in the inner root sheath
RNA *in-situ* hybridisation on E17.5 embryo shows that Zdhhc21 is expressed in hair follicles. Skin sections in anagen shows that both wild-type and *dep* transcripts are localised to a very specific region in the hair bulb. The signal is evident when the follicles are in anagen. Using a marker of the IRS, GATA-3, it shows that the site of expression seems to be at the inner root sheath. The GATA3 signal and the BM purple stain of the *Zdhhc21* transcript seem colocalised. The *dep* follicles are clearly smaller comparing to wild-type at the same magnification, and the GATA3 signal is biased towards the differentiating end of the follicles, whereas in wild-type, the signal is all around the hair bulb.
Scale bar, 100μm.
Zdhhc21 (Region of *Zdhhc21* transcript expression)
GATA3 (inner root sheath progenitor), α-K5 (Basal layer, Outer root sheath and Bulge).

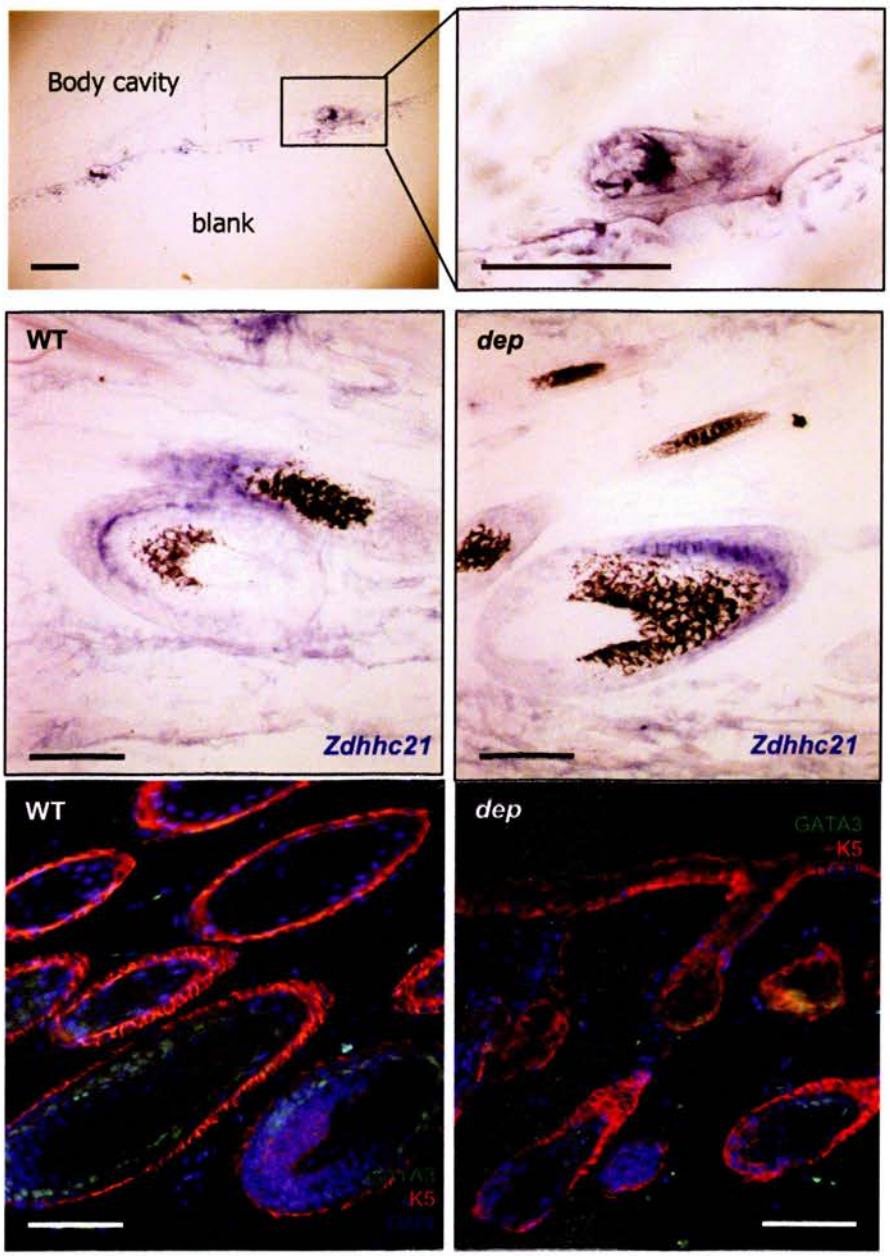

Figure 5.10. The N-Dhhc21 antibody does not co-localise with GATA3
The N-dhhc21 Ab does not colocalise with GATA3, which targets the sheath cuticle and Huxley's layer of the IRS, in either wild-type and *dep* follicles at 5week, or any other stage of anagen (data not shown). The N-dhhc21 Ab appears to target the layer that lies immediately outside of the GATA3-staining region. Scale bar, 100μm.
α-GATA3 (sheath cuticle and Huxley's layer of IRS)
α-N-Dhhc21

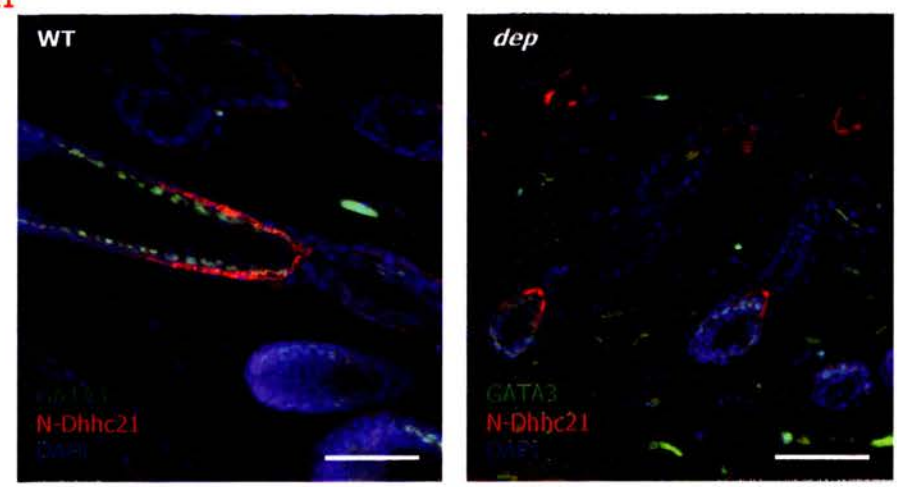

Figure 5.11. The N-Dhhc21 antibody targets the outermost layer of the inner root sheath
At early anagen, the N-Dhhc21 Ab colocalises partially with AE15 [A], which normally stains all 3 layers of the IRS and the medulla. However, in *dep* the N-Dhhc21 pattern overlaps almost completely with AE15 [B], suggesting that the inner two layers of the IRS, and/ or the medulla may be absent in *dep* at this stage. At 5wk, the AE15 and N-Dhhc21 costaining pattern becomes normal in *dep* [D], in comparison to wild-type [C]. Scale bar, 100μm.α-AE15 (IRS + HS medulla) α-N-Dhhc21

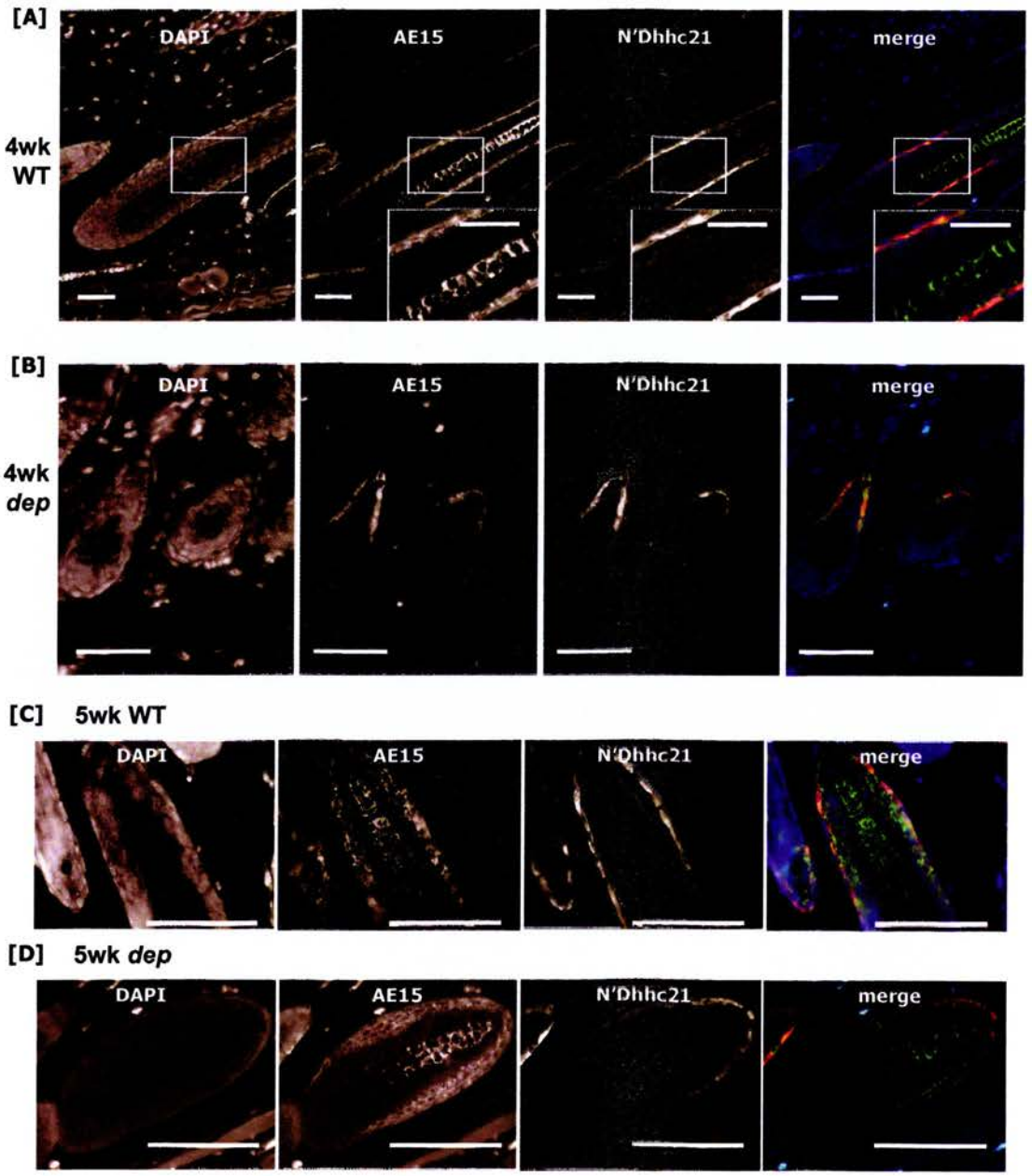

Figure 5.12. Specificity of N-Dhhc21 antibody.
[A] Antigen blocking of the N-Dhhc21 antibody with specific immunogen peptide. α-N-Dhhc21 Scale bar, 100μm. [B] Staining with pre-immune serum (pre-bleed) and secondary antibodies as negative control. α-N-Dhhc21. GATA3. Scale bar, 50μm.

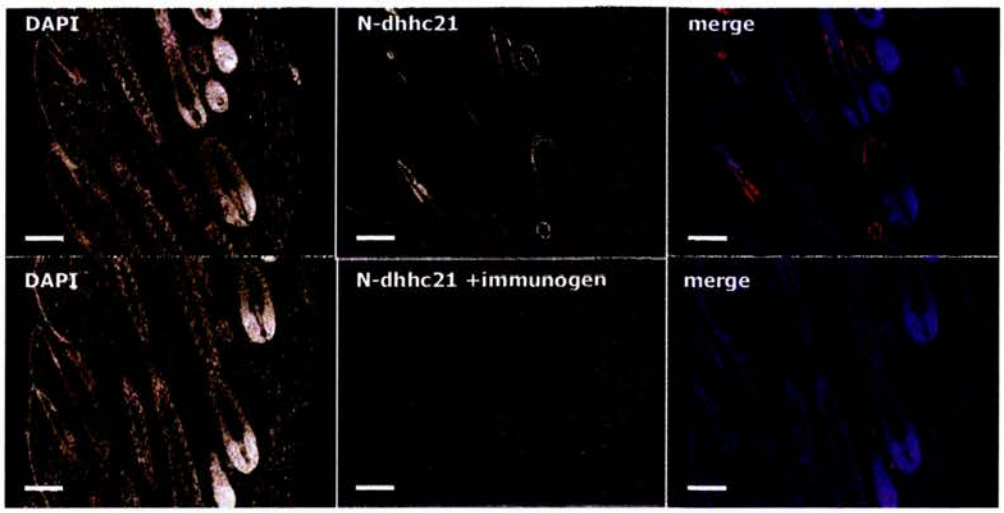

[B]

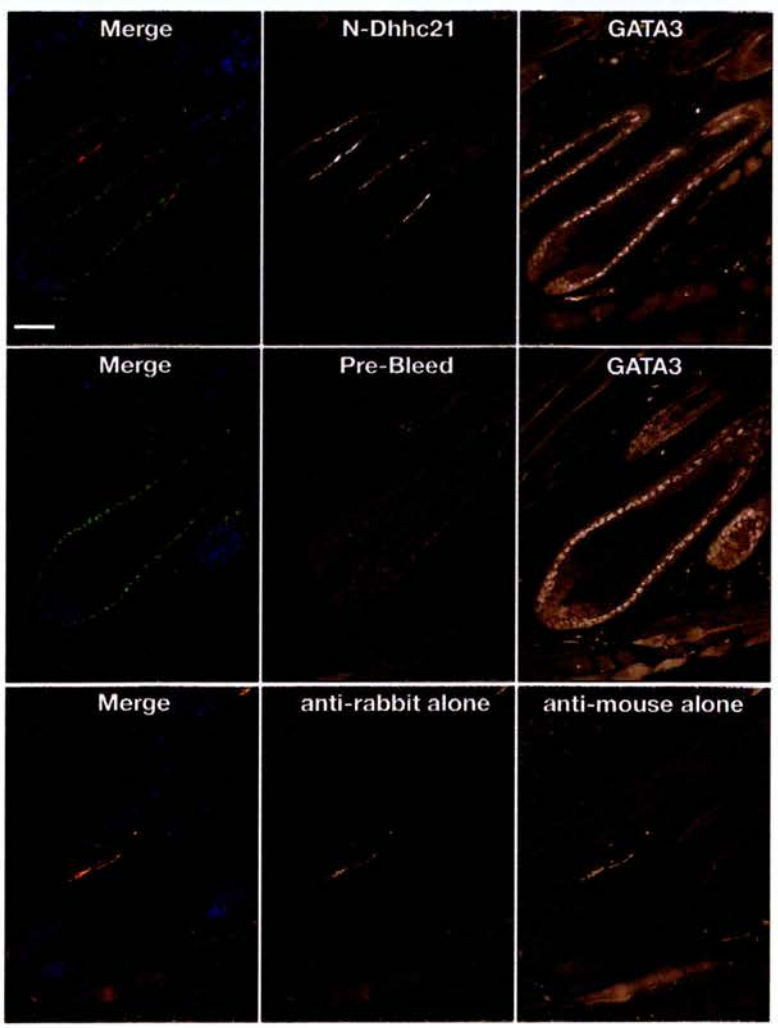

Figure 5.13. Morphogenesis of *dep* follicles is normal
AP staining on 2-wk dorsal HFs shows that *dep* has a normal pattern of alkaline phosphatase activity in the DP and dermal sheath, despite the reduction in follicle size. This indicates that the HF morphogenesis is normal. The black pigment of the melanosomes can be observed from these pictures. Scale bar, 100_m.
AP (dermal papillae, dermal sheath)

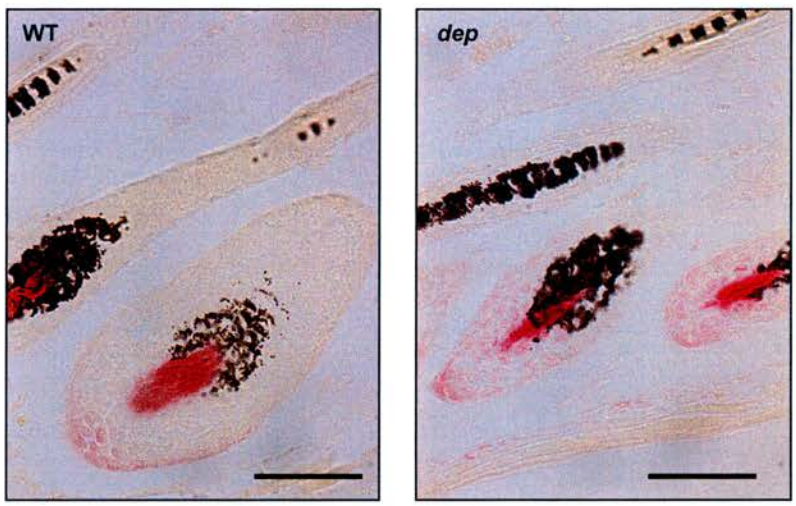

Figure 5.15. The number of mitotic cells in *dep* follicles at anagen is normal
At early anagen, when the *dep* phenotype is most prominent, the number of Ph3+ cell between wild-type and *dep* appear similar. Scale bar, 100_m.
_-Phosphohistone3 (cells in M phase)

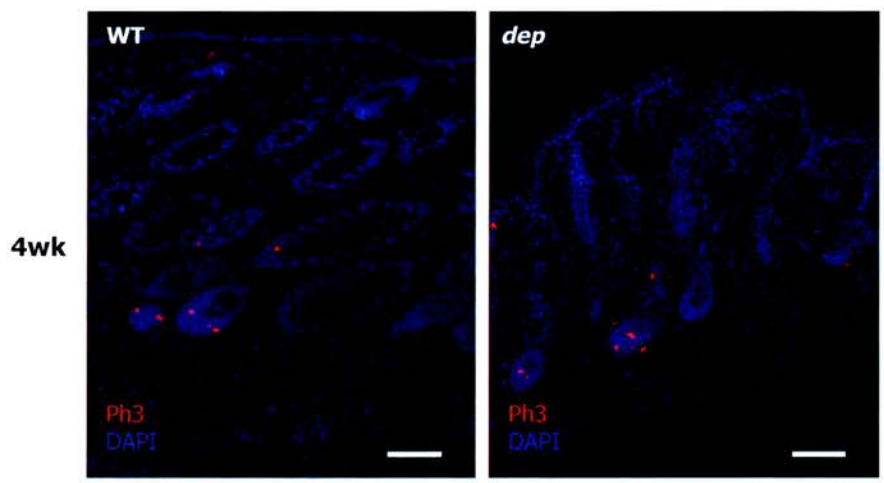

Figure 5.14. The number of proliferating cells remain normal in *dep* follicles
[A] The distribution of Ki67+ cells highlights the malformed follicles at the hair bulb of *dep* at early anagen. The Ki67+ cells appear to be all around the hair bulb. [B] At 5-wk, the distribution of Ki67+ cells becomes normal. [C] The number of Ki67+ cells at the infundibulum between wild-type and *dep* is similar, even though the *dep* sebaceous glands are enlarged. Scale bar, 100_m.
_-Ki67 (proliferating cells) _-MK6

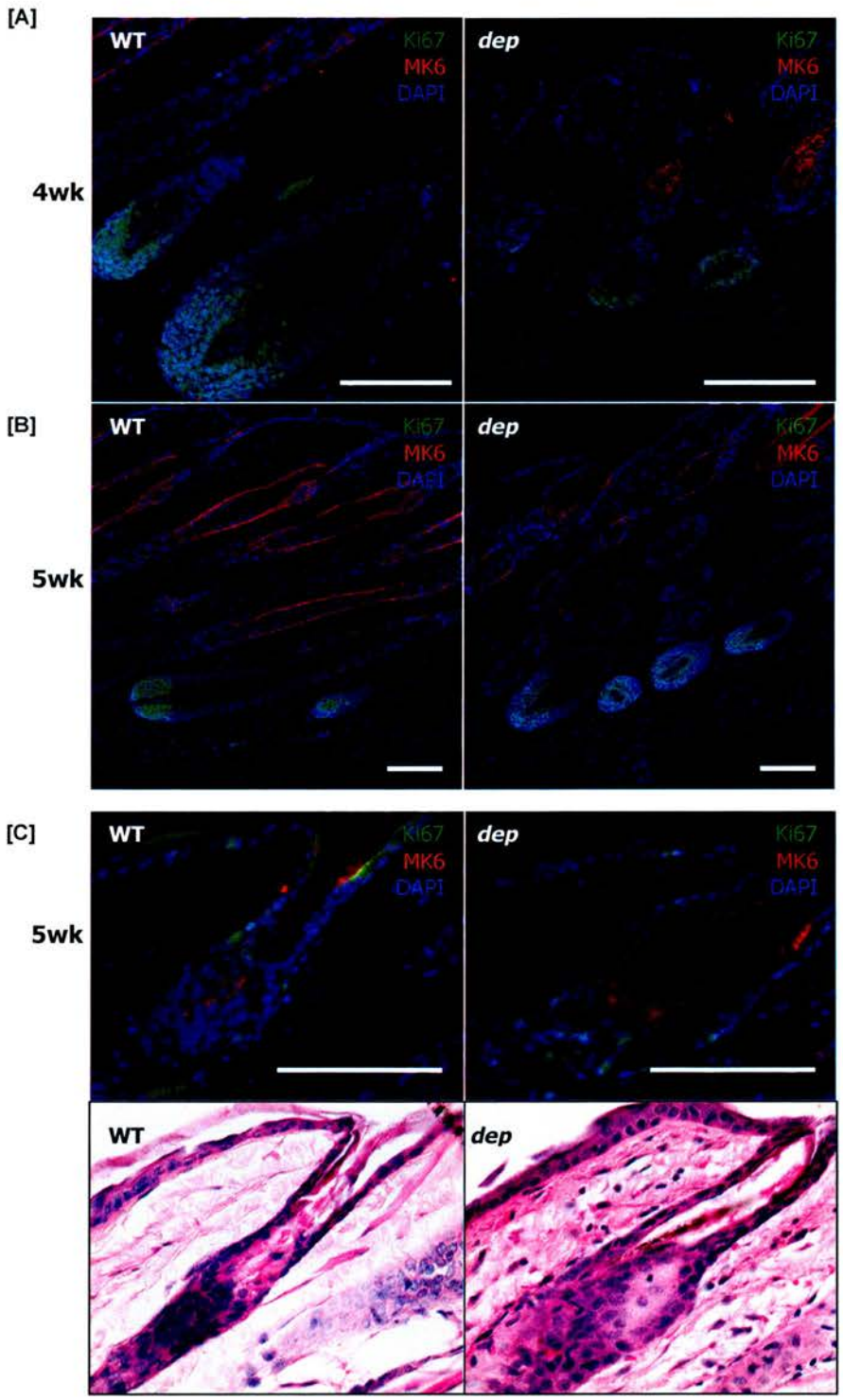

Figure 5.16. Expansion of the epidermal progenitor compartment of *dep*
Immunohistochemistry on 4-wk dorsal skin sections using _-K5 highlights the significantly thicker epidermis, the outer root sheath, and the basal layer. The SG hyperplasia appearance is also marked. The expansion of the K5 signal indicates the expansion of the epidermal progenitor compartment of *dep*. Scale bar, 100_m.
_-K5 (Basal layer, Outer root sheath and Bulge)

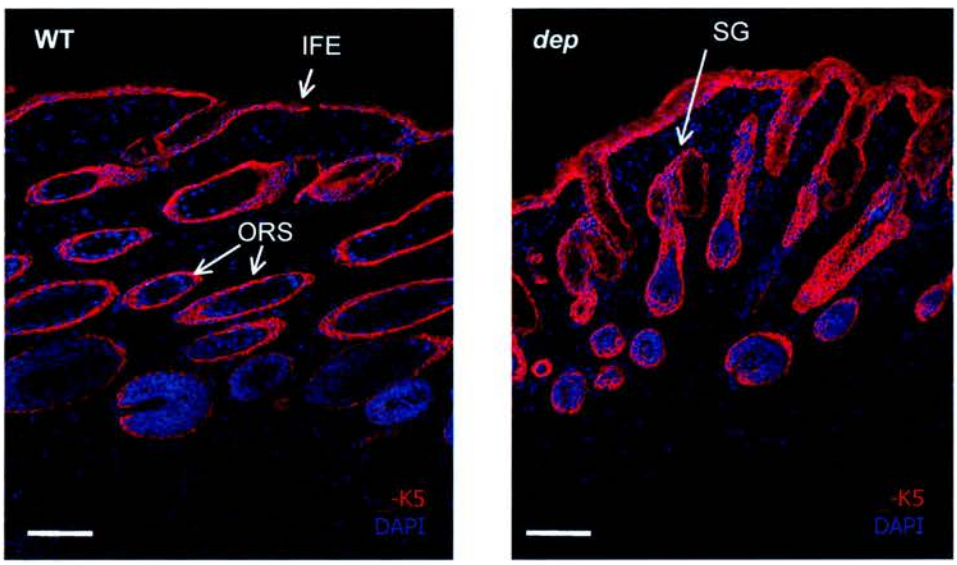

Figure 5.17. Epidermal proliferative units (EPU) in *dep* epidermis are indefinable
[A] DAPI staining, and [B], counterstained with _-cat, show an overall increase in cells in the *dep* epidermis, as well as in the mesenchymal compartment. [C] Individual EPUs can be easily identified in wild-type; whereas in *dep*, there is an increase number of sparsely distributed cells of ambiguous status based on the shape of cells.
Red: cells that belongs to an identifiable EPU; yellow: basal cells; green: cells that can be not identified as basal cell or part of an EPU. Scale Bar, 20_m.

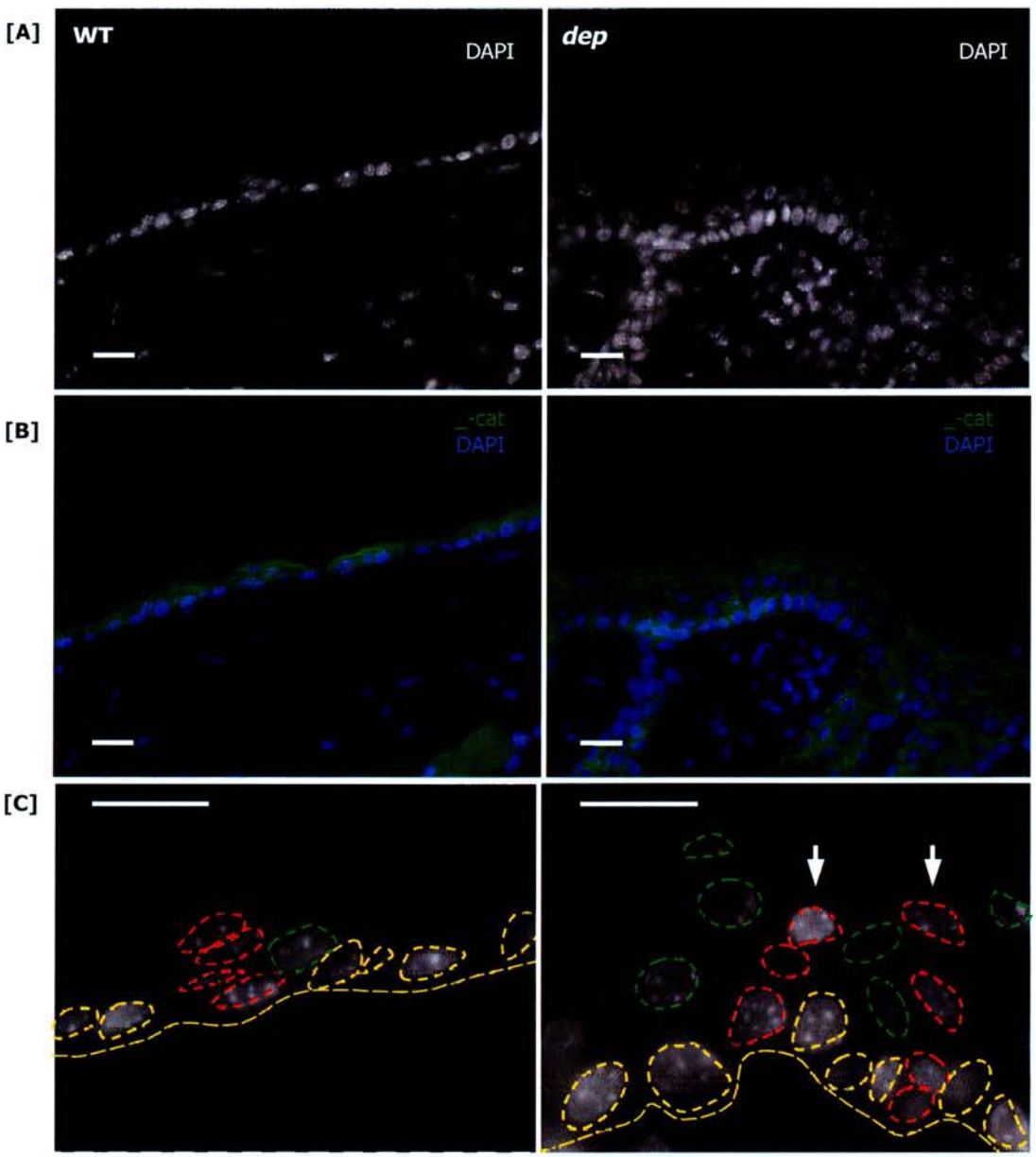

Figure 5.18. The staining of K5 is expanded with an elevated number of P63+ cells
K5 and P63 double staining in 4-week dorsal skin (A and B), and tail epidermis (C). [A]Usually, K5 is expressed in the basal layer of the epidermis, which consists of one single layer of cells consisting of epidermal stem cells, transit amplifying cells, and post-mitotic basal cells, which migrate out of the basal as they differentiate. The P63+ cells represent the later two populations. In *dep*, however, K5 is expressed further up the skin layer, possibly in the suprabasal layer including the spinous and granular layer. The expression of P63 also persists beyond the first cell layer. There is an increase in the overall number and density of cells in the epidermis. [C] Tail epidermis of WT and *dep* highlighting the increase in cell density and the vertically elongated shape of basal cells. Scale Bar for [A], 100_m; [B] and [C], 10 _m.

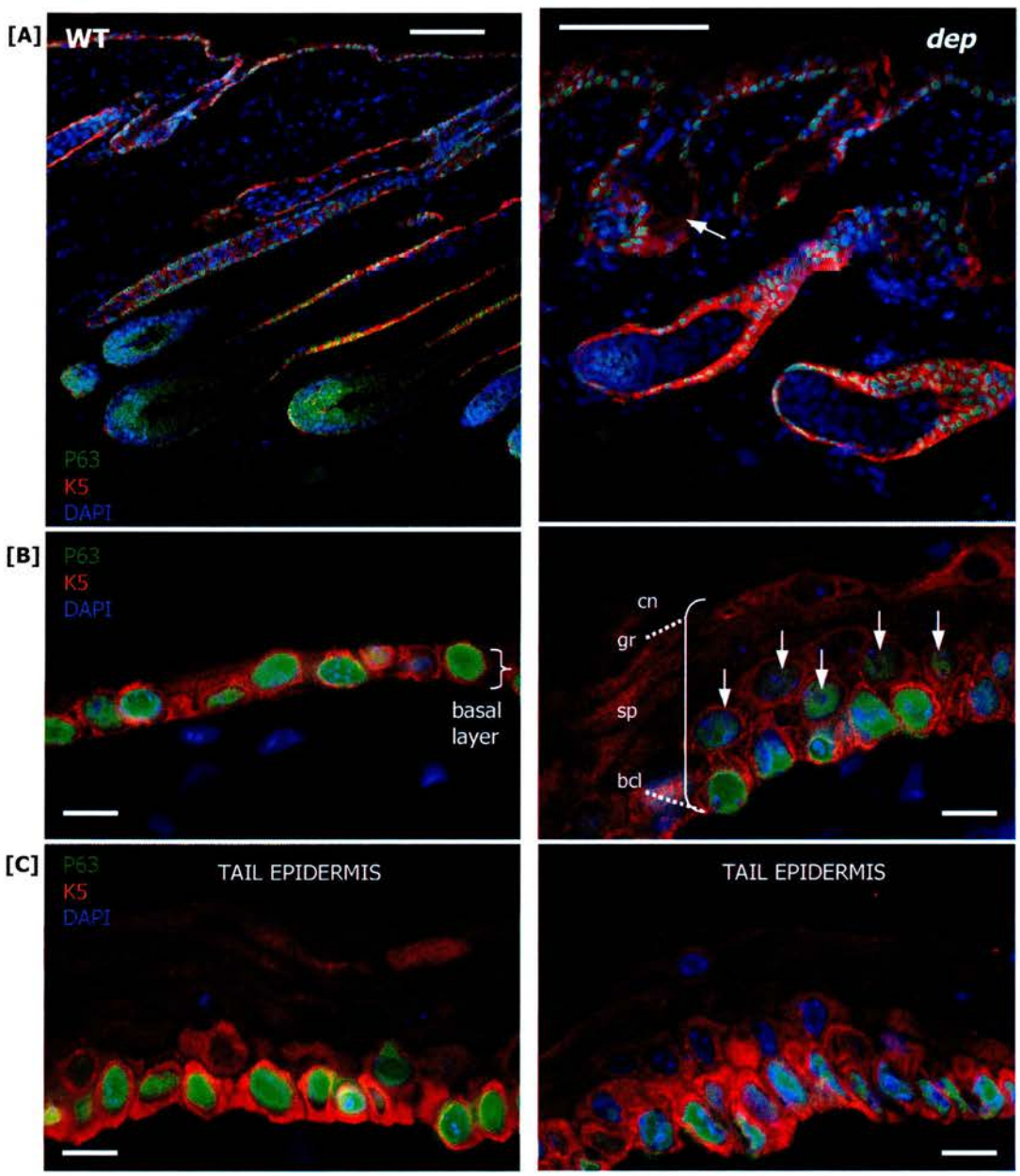

Figure 5.19. The suprabasal compartment of *dep* is expanded
K10 and P63 double staining in 4-week dorsal skin, showing that the suprabasal layer is thickened in *dep*. *cn*, cornified layer; *gr*, granular layer; *sp*, spinous layer; *bcl*, basal cell layer. Scale Bar = 10_m.

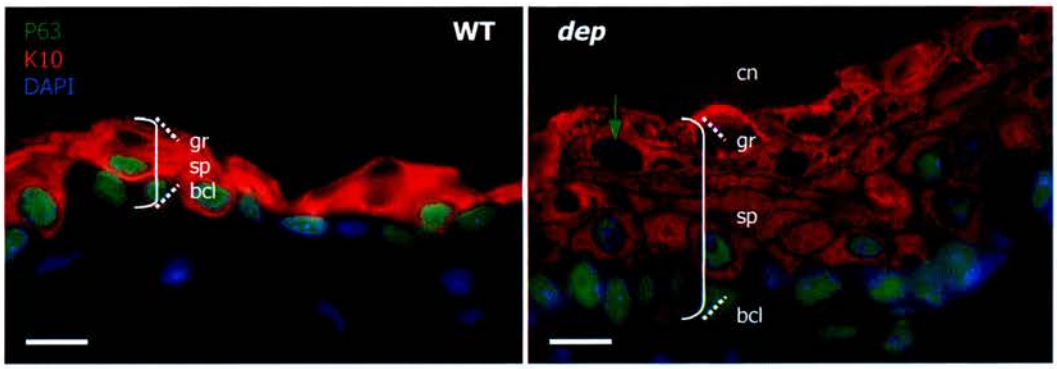

Figure 5.20. Schematic representation of K5 and K10 expression in *dep* epidermis
A simple representation of K5 and K10 staining of the basal and suprabasal layers in wild-type and *dep* epidermis. Although K5 staining is expanded in *dep*, K10 staining shows that the expanded region is likely to represent the suprabasal layer. There is an increase in the overall number of keratinocytes, which is reflected by the increased number of P63 cells, which persists through to the suprabasal layer. However, P63-positive cells are rarely seen in the third layer from the basement membrane. In wild-type, cells become more flattened and gradually become anucleated as they migrate upwards and become more differentiated. In *dep*, however, circular nucleated cells are often seen in the suprabasal layer, suggesting that terminal differentiation may be delayed.

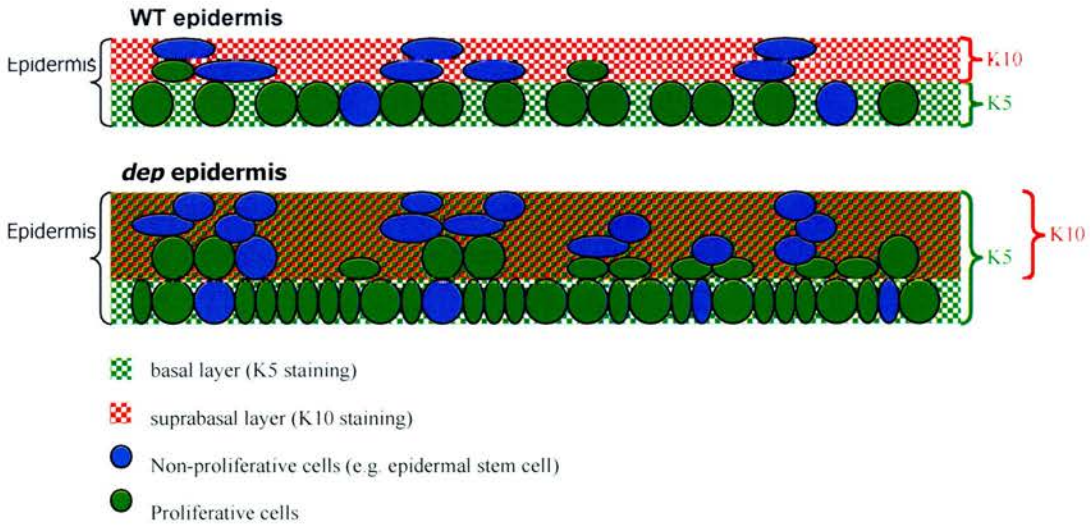

Figure 5.21. Expression of *Shh*, *Gli1* and *Ptc1* in 7-wk wild-type and *dep* skin
The expression pattern of *Shh* and the Shh-responsive genes, *Ptc1* and *Gli1* is similar between wild-type and *dep*, suggesting that the hyperplastic phenotype is unlikely be due to Shh upregulation. Scale bar, 100_m.

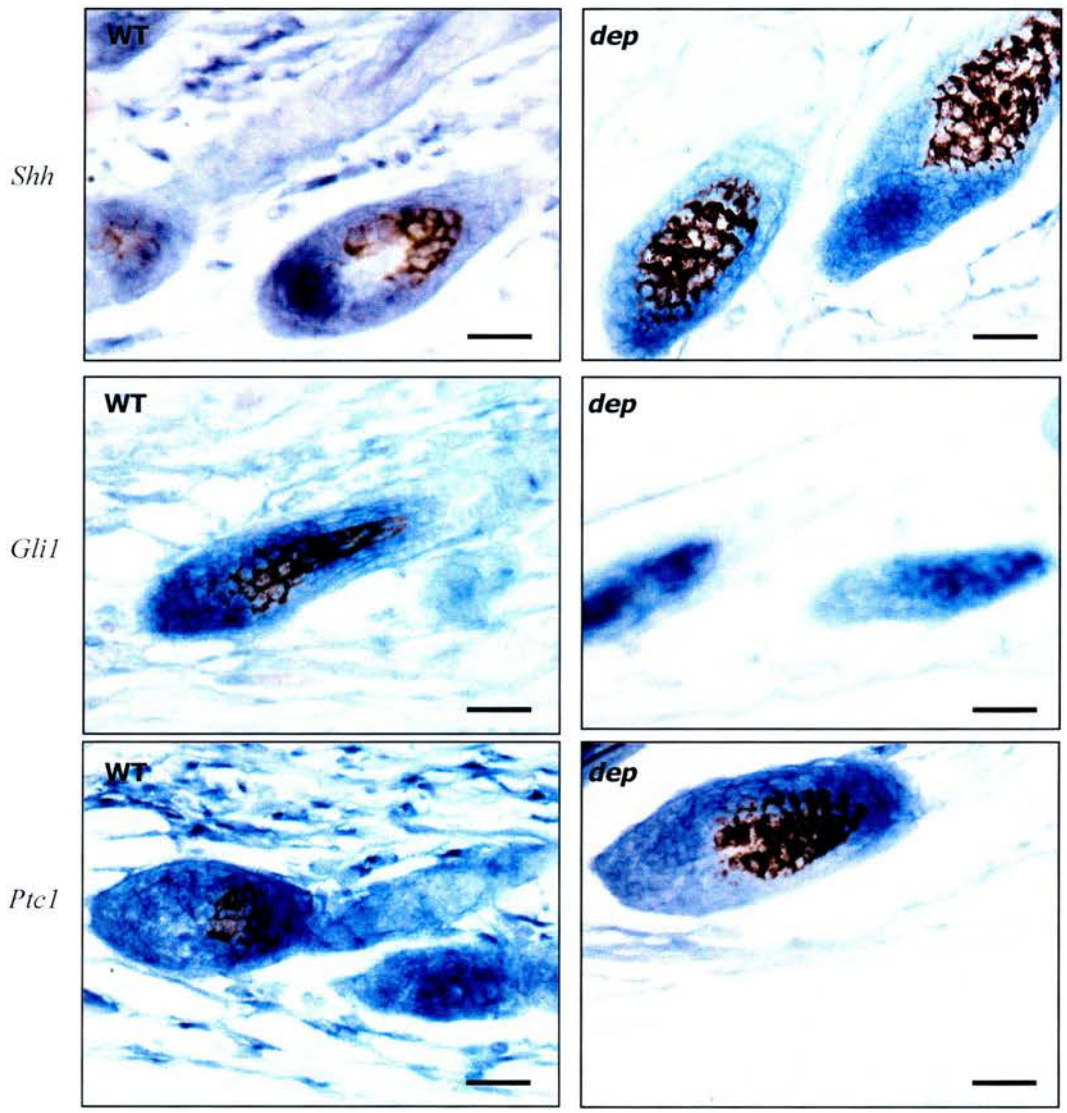

Figure 5.22. Tail epidermal *in-situ* analysis of *dep* (Ian Smyth)
Wild-type tail epidermis consists of triplets of HFs, each of which has a pair of SGs. Whereas the SGs of *dep* follicles are often hyperplastic and malformed. At some places there are also extra glands and some follicles are bent. An unusually large number of melanocytes were also reported.
_-K14 (basal layer of epidermis), _-K15 (bulge).

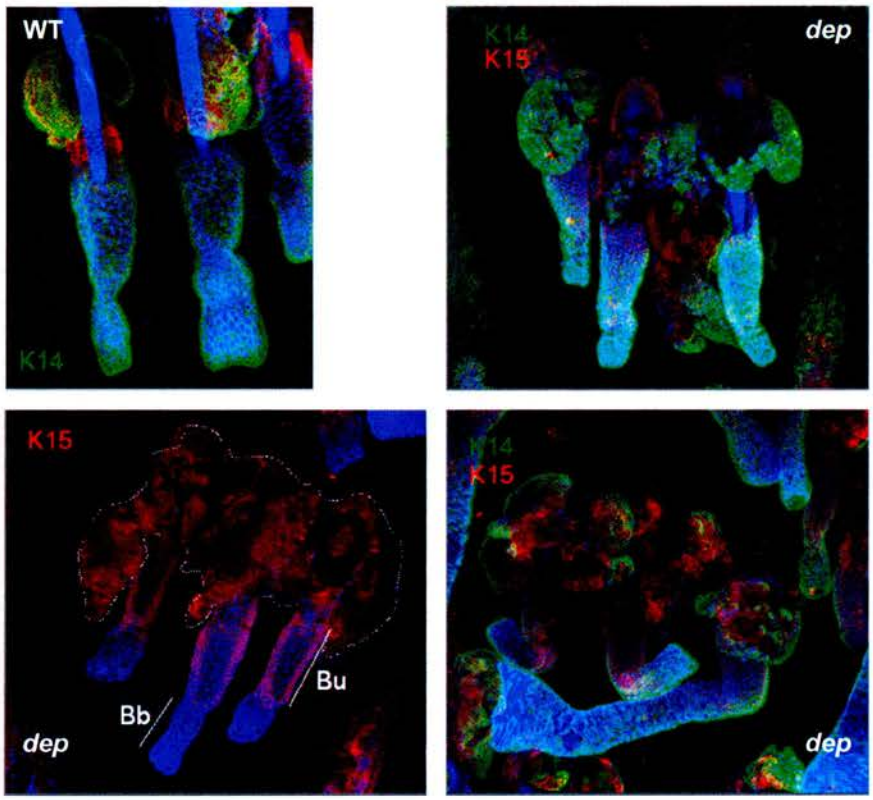

Figure 5.23. Lipid accumulation in *dep* infundibulum (Ian Smyth)
Staining of sebum using Oil Red O (ORO) reveals the sebaceous hyperplasia phenotype and an accumulation of lipid in the infundibulum (arrow), which may explain the greasiness of *dep* hair coat.
ORO (sebum/ lipid staining)

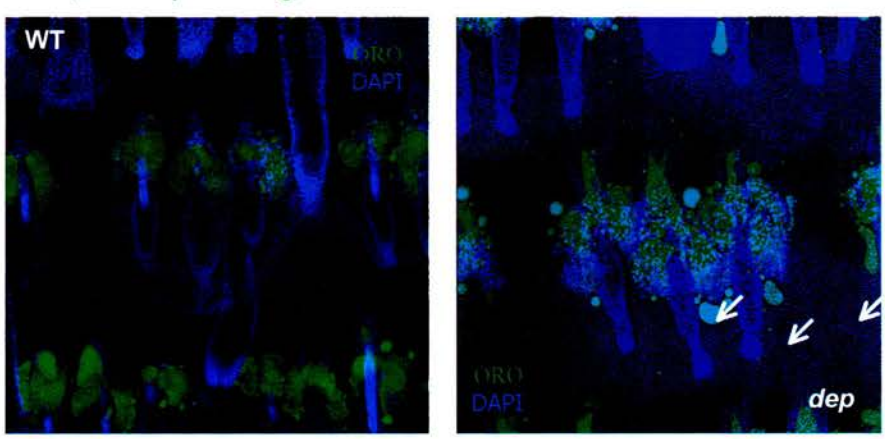

Figure 5.24. Comparison of perputial glands between wild-type and *dep*
Despite the obvious sebaceous hyperplasia in the *dep* hair follicles, there is no difference in size and number of sebocytes between wild-type and *dep* perputial glands. Boxed area in panels [A-C] are shown at higher magnification in panels [D-F]. Furthermore, no difference is observed in other glands that have similar morphology to the SGs, including the anal glands, mebomian glands, ceruminous glands (data not shown). Scale bar, 50μm.

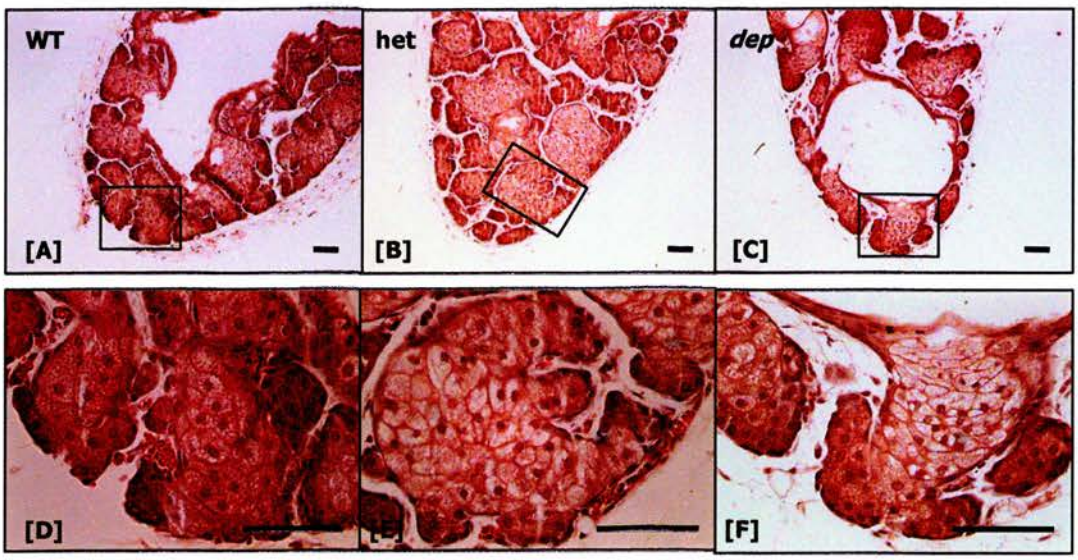

Figure 5.25. Hair-keratin deficiency in *dep* at onset of anagenThe hair-specific keratin marker AE13 directs against the hard, acidic keratins in the hair shafts, including the cortex and cuticle layers. In wild-type HFs, the AE13 signal appears as hoops within which is the medulla, whereas in *dep*, the signal only appears at the tip of the hair follicles in 4-wk dorsal skin samples. At week5, most follicles restore normal AE13 staining (data not shown). Scale bar, 50μm.
α-AE13 (cortex and cuticle layers of hair shaft) MK6

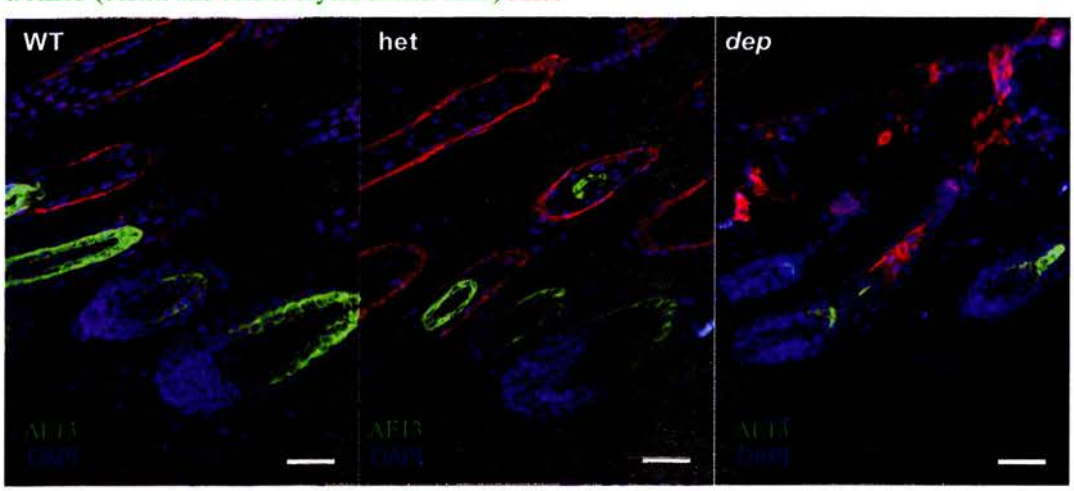

Figure 5.26. Aberrant HF differentiation in *dep* at onset of anagen[A] The hair-specific keratin marker AE15 is normally expressed in the IRS and the medulla of the hair shaft, as shown in 4-wk dorsal HFs of wild-type and heterozygote. Whereas in *dep*, AE15 is only positive in the IRS but not in the medulla, indicating that there is a lack of hair shaft-specific protein being made at this stage of anagen. [B] However, at 5-week, AE15 staining pattern becomes normal again in *dep*. Scale bar, 50_m.
_-AE15 (IRS + HS medulla)

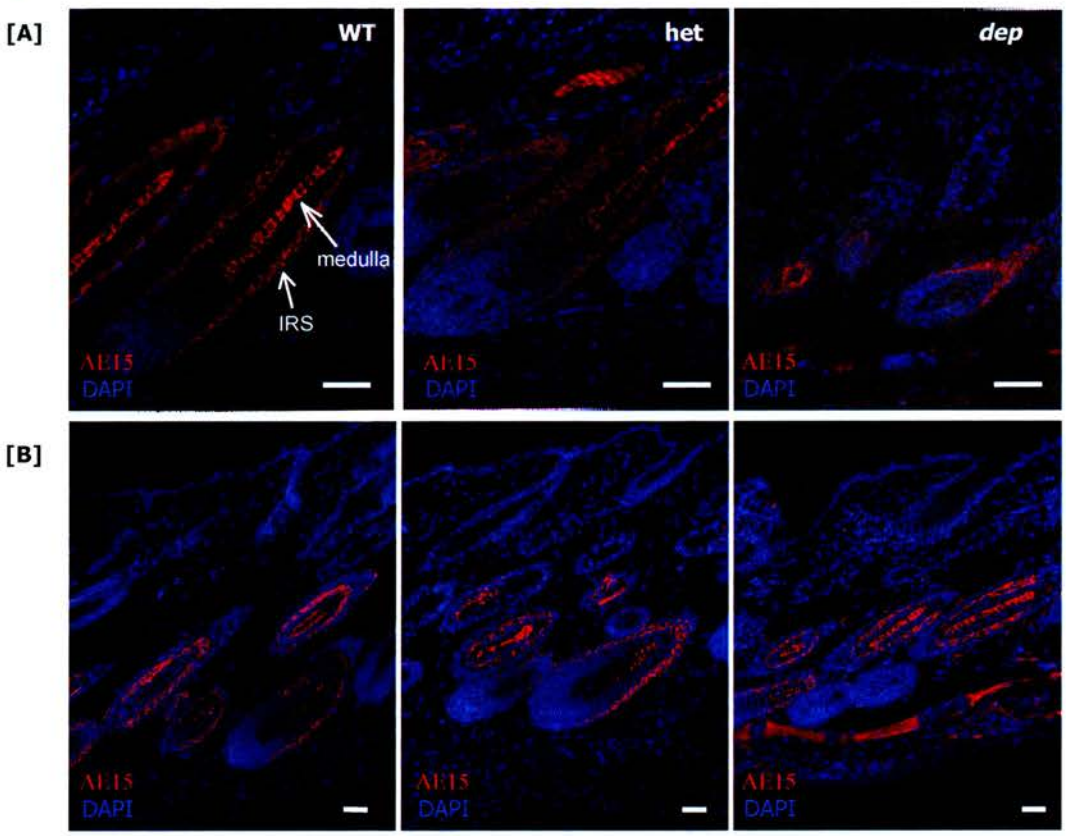

Figure 5.27. Conditional knockout of Smad4 exhibits phenotype similar to *dep*
(Picture from Qiao et al., 2006) At P10, almost no hair shafts are visible in Smad4$^{-/-}$ hair follicles. At P17, SGs are hyperplastic which look similar to *dep*.

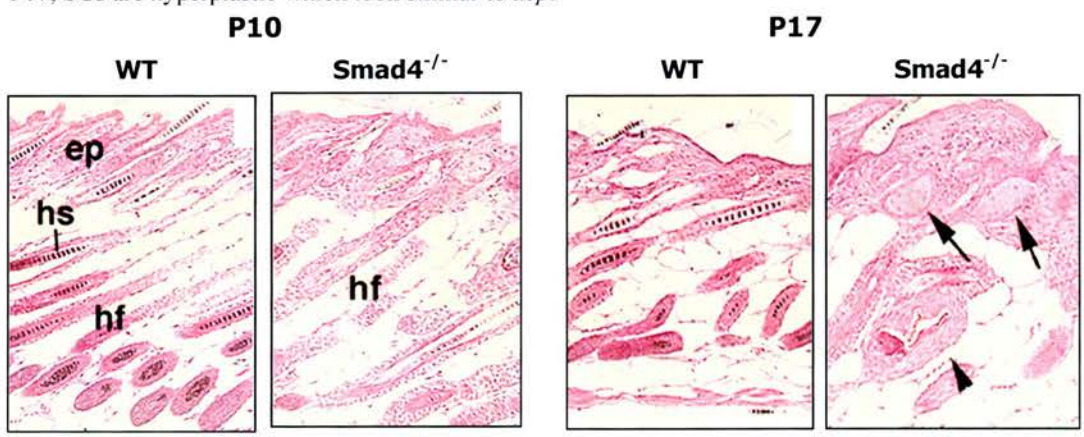

5.4. Discussion

5.4.1. Comparison of *dep* phenotype with existing mutants

The *dep* phenotype is mainly characterised by a progressive hair loss, SG hyperplasia, epidermal and outer root sheath hyperplasia, and small follicles of the hair bulb. Although previous literature has not reported a mutant or transgenic mouse that has similar phenotypes, the histological appearance of the Smad4 conditional knockout mouse, in which *Smad4* was removed by activating the *MMTV-Cre* promotor expressed in the epidermis and hair follicles (Qiao et al., 2006), exhibits a similar but more severe phenotype than *dep* (Figure 5.27).

The absence of Smad4 in the epidermis blocked HF differentiation and cycling, leading to a progressive hair loss. The mutant follicles also have a reduced expression of Lef1, and hyperproliferation of the outer root sheath, epidermis and basal keratinocytes. In particular, the absence of pigmented septae in hair shafts resembles closely to that of *dep*.

Lef1 is a transcription regulator for hair-specific keratin genes, that mediates the Wnt signalling pathway by associating with its co-activator beta-catenin. Since there is a reduced level of Lef1 in the Smad4 epidermal knockout mouse, it may be possible the *dep* phenotype may involve the Wnt signalling pathway, based on the fact that HS progenitors in the matrix require expression of Lef1 to become responsive to Wnt signalling. If Wnt is unable to signal, it affects the differentiation of matrix cells along the HS lineage, which may result in a secondary phenotype such as SG and epidermal hyperplasia.

5.4.2. Sebaceous gland (SG) hyperplasia is likely to be a secondary phenotype.

Initially, the increase greasiness observed in *dep* was considered to be a possible cause of hair loss. Indeed, it is possible that excess sebum combined with dead cell flakes may clog hair follicles and inhibit normal hair cycle. As a result, dry and brittle hair may result due to clogging of the HFs which prevents sebum from traveling downwards to the hair canal for nourishment and lubrication, and upwards for waterproofing and protection against antigens.

However, our data shows that other glands with SG morphology do not exhibit hyperplasia as observed in the hair follicles, indicating that the SG phenotype is unlikely to be primary for the *dep* phenotype, but rather, it is more likely to be a consequence due to a disturbed differentiation programme secondary to the hair loss phenotype, given the observation of hyperplasia in the ORS and the epidermis as well as the SGs.

Excessive sebum production is commonly associated with acne and inflammation. However, this is not observed in the *dep* mutants. It may be possible that the dilated infundibulum allows sebum to be released to the skin surface, or that the lack of penetrating hair shafts prevents blocking of the infundibulum.

5.4.3. The complex hair cycling events

The most complicated aspect of the *dep* phenotype, is perhaps its mismatch in cycling with wild-type. On one hand, even though *dep* displays a striking phenotype at the start of anagen, the hair shaft structure and Wnt signaling response (Figure 6.2E and 6.3B, Chapter 6) resumes by 4.5-wk to 5-wk, and the HFs start to regress at 6-wk, same at wild-type. This perhaps demonstrates a potential ability of the epidermis to restore normal function at the absence of correct temporal signaling, possibly by accumulating signal until it reaches a certain threshold. In this sense, normal HS differentiation is delayed, which is consistent with the epidermal situation, where we see P63+ cells beyond the basal epidermal layer, suggesting a delay in epidermal differentiation.

On the other hand, even though the normal HS differentiation is resumed, the various peripheral compartments remain hyperplastic. In addition, while the wild-type follicles are normally in telogen for more than 2 weeks before the third anagen, *dep* enters the third anagen prematurely at 7-wk despite the delay in HS differentiation. Since the hair cycles in mice are only synchronized for the first 2 weeks, we are unable to trace the pace of subsequent cycles. However, give the above observation, we wonder if *dep* HFs generally cycle more frequently than wild-type do. This hypothesis is consistent with the finding that the guard and awl hairs in *dep* are slightly shorter - possibly due to a reduced in anagen length.

Although the required threshold is reached for correct HS differentiation, its delay might have caused a mismatch in other cycling events, which may result in an overall imbalance in epidermal homeostasis. Therefore, it is possible that the loss of the signal required, is partially redundant for cycling progression, but not for maintaining epidermal homeostasis. This demonstrates the importance of precise temporal and spatial coordination to allow precise timing of events in successive hair cycles.

Mice that are completely bald are only observed within the first 2 hair cycles (i.e. up to 12 weeks), whereas adult mice usually have some hairs although a sparse hair phenotype. This may be explained by the fact that cycling events of individual HFs are only synchronized within the first 2 cycles, after which they cycle independently of each other. A murine hair cycle usually takes about 3 months; so it is unlikely that the hairs are lost all at once.

It may be possible that the infundibulum is required to dilate briefly for the emergence of hair shaft during anagen. In *dep*, the dilation of the infundibulum continues to telogen as well as in anagen HFs. The dilated infundibulum due to a mismatch in cycling events, and as a result promotes a premature anagen.

One of the fundamental questions in studying hair cycle, is why does hair cycle? It has been suggested that hair cycling is evolved as a mechanism for physical adaptation to change in environments, and transformation of HF keratinocytes. Most importantly, hair cycle confers protection against malignant degeneration by ridding the organism of uncontrolled growth in the rapidly dividing skin tissue (Stenn and Paus, 2001).

Many signaling molecules involved in the hair cycle are also involved in tumor progression. One of the interesting questions about *dep* is, even though *dep* exhibits hyperplasia in various epidermal compartments, tumors have not been observed in the mutant, at least not under unchallenged lab conditions.

Chapter 6 – Potential involvement of Wnt signaling in *dep*

6.1. Introduction

Throughout the entire life of most mammals, the cycling portion of the HF is constantly regenerated at the start of each hair cycle (anagen). This growth requires the multi-potential stem cells (SC) that reside at the lowest non-cycling permanent portion of the HFs. This region is named the 'bulge' because of new growth that adds extra layers to the SCs, and because of its appearance possibly as a result of the new hair shaft pushing the old one to the side. Bulge SCs divide less frequently than other keratinocytes, but are activated to generate new HF at the onset of each anagen. However, only a small number of bulge SCs is activated at anagen, and most SCs remain quiescent for a long time.

The relationship between the bulge and the hair matrix is a frequent topic for debate. More commonly known is the 'bulge activation hypothesis' (Fuchs et al., 2001; Niemann and Watt, 2002), which states that there is only one population of HF stem cells, which is the bulge, and that the bulge SCs are activated to divide at the end of HF regression when it comes to close proximity with the dermal papillae. The progenitors then migrate along the ORS to the base of the HF to form the matrix.

An alternative to this hypothesis, is that SCs themselves might exit the bulge and migrate to the base of developing HF. This hypothesis is based on the observations that vibrissal bulge never comes to close proximity with the DP during HF regression, but yet the hair bulb region contains clonogenic keratinocytes that respond to morphogenetic signals (Oshima et al., 2001). This hypothesis maintains that the bulge is the only population of HF stem cells.

A contradictory model has been proposed by Panteleyev and colleagues (Panteleyev et al., 2001), which states that there are two location of HF stem cells, namely the bulge and the matrix. While the HS and IRS lineages are derived from the matrix progenitors, only the ORS is derived from the bulge. This model proposes that SCs from the bulge migrate to matrix during anagen, and survive through the apoptosis-driven catagen. The matrix SCs then respond directly to the DP to replenish the HS and IRS at the onset of the next cycle. On the other hand, the matrix cells may replenish the bulge under certain circumstances. This model differs from

the one-HF stem cell model, in the location of epithelial-mesenchymal signalling (DP->bulge vs DP->matrix), and the origin of the cycling portion of the HF.

In support of this model, a lineage marking study has shown that, on average, the matrix contains up to 4 active long-lived progenitors which are capable of differentiating into multiple follicular lineages in the hair matrix (Kopan et al., 2002; Niemann and Watt, 2002).

The epidermal lineage network also contains stem cell populations in the IFE and SG and it is proposed that these populations of SCs are interconvertible. At any one time, this network is maintained at a precise homeostasis; any disruption to any of the pathways may result in an overall imbalance, which is likely to affect other compartments as well as the resulting lineages of the pathway in question. Many signalling pathways are involved in maintaining the epidermal homeostasis, some of which are discussed below.

Under normal conditions, SCs in the bulge are in a quiescent and undifferentiated state. However, when placed in culture or in response to tissue damage, they are capable of long-term cell-renewal (Watt et al., 2006). It is important that SCs maintain their quiescence and only divide when required to prevent premature exhaustion of the SC pool under epidermal stress. On the other hand, SCs must be capable of cycling to supply and replenish the functions of terminally differentiated cells in tissues.

6.1.1. Maintenance of SC quiescence

The quiescent status of the SCs is largely maintained by factors that are expressed within the SCs. The first protein that was associated with this function was the ß1-integrin that was reported to express in human epidermal stem cells at a higher level than that in the TA cells. Reduced ß1-integrin expression in SCs triggers exit from the SC compartment (Jones and Watt, 1993), demonstrating that ß1-integrin is required for maintaining SC quiescence in the epidermis.

Using a K15 promoter to target mouse bulge SCs (Liu et al., 2003), a lineage tracing and microarray profiling approach was carried out for identification of factors that maintain SC quiescence. The factors identified by this approach include the Wnt-inhibitory protein Dkk3

(Dickkopf3) and other signaling proteins that are upregulated in the HFs such as the BMP and TGFB pathways. The SC identity of the isolated cells was verified by their ability to reconstitute all HF lineage and maintain an intact HF (Morris et al., 2004).

More recently, a new strategy was used in the Watt group that allows the generation of cDNA libraries from individual SC and TA cells isolated by FACS (fluorescent activated cell sorting) (Jensen and Watt, 2006). Using this approach, Lrig1 (Lig1/leucine-rich repeats and Ig-like domains), a negative regulator of EGFR receptors, was demonstrated to be a major determinant of SC quiescence in human IFE SCs.

Although the LEF1/TCF family proteins can act as functional bipartite transcriptional activator upon association with ß-catenin (directing cells along the hair lineage), T cell-specific transcription factor (Tcf3) was among the proteins identified in SCs by the global gene profiling approach with previous knowledge that Tcf forms a complex with β-catenin which is important in activating Wnt-responsive genes in progenitor proliferation. Tcf3 alone represses transcriptional regulators of IFE, SG and HF differentiation, and when Tcf3 is sustained transgenically, terminal differentiation of all 3 lineages are repressed (Nguyen et al., 2006), demonstrating the role of Tcf3 in maintaining the progenitor, non-differentiated state of epidermal cells. On the other hand, a reduction of Tcf3 expression and upregulation of Lef1, in combination with Wnt activity are required for placode formation (Fuchs, 2007).

6.1.2. Genes that regulate exit from the stem cell compartment.

Apart from the factors that regulate stem cell quiescence, the bulge SCs also express a range of factors that regulate exit from the SC compartment to allow the epidermis to be repaired and replenished.

One of the factors that promotes exit from the SC niche is the proto-oncogene c-Myc, which stimulates epidermal SC differentiation in cultured human keratinocytes when transiently activated in c-MycER mice, and causes depletion of the SC compartment (Arnold and Watt, 2001; Bull et al., 2005). The activation of c-Myc drives SCs to the TA compartment and stimulates differentiation into IFE and SG at the expense of HF lineages (Arnold and Watt,

2001; Takeda et al., 2006). On the other hand, conditional ablation of c-myc results in alopecia as a result of long-term failure to sustain HF SCs (Arnold and Watt, 2001; Fuchs, 2007).

The Rho GTPase, Rac1, regulates the exit of the SC compartment by negatively regulating Myc (Benitah et al., 2005) through PAK2 phosphorylation. When Rac1 is deleted in the K14CreER/floxed Rac1 adult mice, SCs are stimulated and undergo terminal differentiation prematurely, leading to failure in maintaining IFE, HF and SGs. It is therefore concluded that Rac1 and Myc represent a global SC regulatory axis (Benitah et al., 2005).

In addition, Myc acts by negatively regulating genes that mediate keratinocyte adhesion, such as integrins and actin cytoskeleton components (Frye et al., 2003). Whereas Rac1 enhances integrin levels (Benitah et al., 2005), confirming their critical regulatory role in cell adhesion and cytoskeleton in controling exit from the SC niche.

Another factor that was identified by the global gene expression profiling approach was the Lim-homeodomain transcriptional factor Lhx2, in the absence of which mutant animals display defects in patterning and cell fate determination during brain development (Rhee et al., 2006). It was demonstrated that LHX2-deficient bulge SCs are unable to retain Brdu label and use SCs more rapidly. The involvement of Lhx2 is positioned downstream of signals necessary to specify HF SCs (e.g. Wnt and Shh), but upstream from signals required to drive activated SCs to terminally differentiate (e.g. Bmp) (Rhee et al., 2006), showing its role in maintaining the growth and undifferentated properties of HF progenitors.

Other factors that control the exit from SC compartments include Cdc42 (cell division cycle 42), which controls progenitor differentiation through β-catenin stabilisaton (Wu et al., 2006), and Bmp signaling (Kobielak et al., 2007). When Bmpr1a was conditionally ablated by K14-Cre in epidermis, HF stem cells are activated to proliferate to form tumor-like branches that express high level of Lef1 and β-catenin. Whereas sustained expression of Bmpr1a in SCs of transgenic mice results in premature HF differentiation.

6.1.3. Signals required in HF maturation and lineage differentiation.

Involvement of canonical Wnt signaling in HF development and hair cycling

Wnts encode secreted glycoproteins that stimulate receptor-mediated pathways and initiate numerous cellular and transcriptional responses. Wnt signaling has diverse functions; Wnt is an important mediator of key cell-cell signaling events in virtually every aspect of embryogenesis, and is required for the control of homeostatic self-renewal in a number of adult tissues. Perturbations in Wnt signaling is implicated in several hereditary diseases, developmental disorders, degenerative diseases, and cancer in human (Clevers, 2006; Logan and Nusse, 2004).

The canonical Wnt pathway involves stabilization of the cytoplasmic pool of the key mediator β-catenin. Wnt proteins act by binding to receptors of the Frizzled (FRZ) and LRP families on the cell surface, which relay signals to β-catenin through the inhibition of the degradation machinery by members of the Dishevelled (Dvl) family. β-catenin is then translocated to the nucleus and interacts with the T cell–specific transcription factor (TCF) and lymphoid enhancer–binding factor (LEF) families of high-mobility-group (HMG)–box transcription factors to promote and regulate expression of targeted genes.

Without Wnt signaling stimulation, the scaffolding protein Axin assembles a protein complex that contains glycogen synthase kinase 3b (GSK3b) and the adenomatous polyposis coli protein (APC), forming the "β-catenin destruction complex", which targets β-catenin to be degraded by the proteosome pathway. Wnt signaling can also initiate an independent 'non-canonical' signaling pathway involved in planar cell polarity (PCP), that may lead to protein kinase C (PKC) and Jun kinase (JNK) activation, resulting in calcium release, which induces cytoskeletal rearrangement and convergent extension movements during embryo development (Dasgupta et al, 2005).

Canonical Wnt signaling is essential for the induction of HF formation, HF maturation and lineage differentiation. Multiple Wnt genes are expressed in the epithelium prior to the 'first dermal signal' from mesenchyme to epithelium that causes induction of the hair follicle placode (Andl et al., 2002; Reddy et al., 2001). Once the placode is formed and the dermal cells are condensed to form the DP precursors, these regions express nuclear β-catenin in response to Wnt (DasGupta and Fuchs, 1999; Merrill et al., 2001). Furthermore, the embryonic placode and DP exhibit Wnt reporter activity, which demonstrates Wnt involvement in HF initiation. On the

other hand, ectopic expression of the Wnt inhibitor Dickkopf-1 (Dkk1) results in impaired HF formation (Huelsken et al., 2001). In addition, the formation of *de novo* HFs after wounding is controlled by Wnts (Ito et al., 2007).

In postnatal skin, hair shaft differentiation of the matrix is largely dependent on Wnt/ β-catenin signaling, which targets hair shaft-specific keratin genes (Ha/Hb) through the Lef1/β-catenin complex (Merrill et al., 2001). Ablation of β-catenin with K14-Cre causes failure in placode formation at embryogenesis, blocks HF differentiation and cells adopt an epidermal fate instead (Huelsken et al., 2001). Postnatal transgenic mice expressing a stabilized β-catenin controlled by K14 undergo *de novo* hair morphogenesis and develop tumors composed of the hair lineages (Gat et al., 1998). Furthermore, activity of Wnt reporter genes were detected in hair shaft precursor cells during anagen, and in the bulge at anagen onset (DasGupta and Fuchs, 1999).

To investigate how different levels of β-catenin activation affect stem cell differentiation, Watt and colleagues (Silva-Vargas et al., 2005) developed the K14ΔNβ-cateninER transgenic mice, that can be stimulated with the oestrogen analogue 4-hydroxytamoxifen (4OHT) at desired levels. It was found that high-level activation triggers ectopic HF differentiation from cells in the IFE, whereas low level of β-catenin activation results in conversion of HFs into cysts of IFE (Watt et al., 2006), indicating that a precise level of β-catenin activation is required for specific niche.

Furthermore, Wnt3 and its putative effector Dishevelled 2 (Dvl2) are normally expressed in HS progenitors; overexpression of Wnt3 or Dvl2 in transgenic mice result in a similar short-hair phenotype due to altered differentiation of HS progenitors, and cycling hair loss resulting from HS structural defects and associated with an abnormal profile of protein expression in the HS. This indicates that Wnt3 has a function in hair growth (Millar et al., 1999).

Involvement of other regulatory proteins in HF development and hair cycling

Other regulatory proteins that control the transcription of hair shaft keratin genes include Hoxc13 (Peterson et al., 2005) and Foxn1 (Mecklenburg et al., 2001). Mice overexpressing Hoxc13 in the epidermis develop severe hair growth defects and alopecias (Peterson et al., 2005). Recently, Foxq1 was proposed to be a downstream target of Hoxc13 (Potter et al., 2006) and together they control medulla differentiation through a common regulatory pathway.

The progenitors of the HS and IRS have a common origin in the HF matrix (Niemann and Watt, 2002). GATA3 and Lef1/Wnts are essential for matrix stem cell determination between HS and IRS lineages. In particular, GATA3 is expressed at the onset of IRS differentiation and epidermal stratification and acts by recruiting HDACs to repress target gene expression, without which IRS progenitors do not differentiate (Kaufman et al., 2003). And although the HS cortex progenitors differentiate, the overall hair structure is aberrant, giving rise to a HS phenotype secondary to the loss of IRS.

Notch signalling is essential for the regulation of multiple stages of HF differentiation and homeostasis (Okuyama et al., 2007) and its precise expression is required for correct differentiation. Activated Notch is normally cleaved by γ-secretase to generate a nuclear intracellular cofactor (NICD) for the transcription repressor RBP-J. Sustained expression of active Notch1in the IRS progenitors delays differentiation, leading to abnormal hair formation and anagen-associated alopecia in transgenic mice. Whereas conditional knockout of γ-secretase using Msx2-Cre results in a failure of IRS cells to maintain their fates, and result in a complete conversion of HFs to epidermal cysts (Pan et al., 2004).

While the Wnt signal is essential for placode formation, the inhibition of BMP (bone morphogenetic protein) signal is required at the epidermis/ hair placode switch. In particular, different modes of BMP inhibition are specific to the formation of different types of follicles (Fuchs, 2007). On the other hand, BMP receptor signalling is required for correct IRS and HS differentiation in postnatal HFs. In the absence of BMP receptor 1A (Bmpr1A) activation, GATA3 is down-regulated and Lef1 is up-regulated. However, despite the accumulation of Lef1, the Bmpr1A-null follicles are unable to activate Lef1/ß-catenin-regulated keratin genes, due to a lack of stabilized ß-catenin (Kobielak et al., 2003).

Transgenic mice that express the BMP inhibitor Noggin under the Msx promotor, which drives expression in proliferating matrix cells and differentiating HS precursors, have impaired HS differentiation and reduced expression of the HS keratin-associated transcription factors including Foxn1 and Hoxc13 (Kulessa et al., 2000). Recently it was reported that the transcriptional interactions between ectodysplasin receptor (Edar) and BMP signalling are central to generation of the primary HF pattern (Mou et al., 2006).

The proxisome-proliferator-activated-receptor- γ (PPAR-γ) is expressed in differentiated sebocytes and is required for sebocyte differentiation (Di-Poi et al., 2004). Overexpression of c-myc in suprabasal in epidermis and HF of transgenic mice results in SG hyperplasia, suggesting that it has a role in SG homeostasis (Bull et al., 2005). And recently, a population of cells have been identified by their expression of the transcriptional repressor Blimp1, which regulates SG homeostasis and plays a role in governing bulge SC activity. The loss of Blimp1 (using K14-Cre) results in elevated c-myc expression and SG hyperplasia (Horsley et al., 2006).

6.2. Hypothesis of the dep hair loss phenotype

The phenotype of *dep* described in Chapter 5 leads us to think that the hair loss phenotype of *dep* may be due to a lack of correct hair shaft differentiation. Based on the strikingly similar phenotype between *dep* and the Smad4 conditional knockout in the epidermis (Qiao et al., 2006), we speculate that *dep* may have an effect on the concentrated level of Wnt signals in growing HFs.

Wnt signalling is known to have an important role in the differentiation of matrix cells along the hair shaft lineage (Merrill et al., 2001). It is possible that the hair shaft differentiation pathway is affected in *dep* due to a disruption in the Wnt signaling pathway (Figure 6.1A). Blocking of the Wnt signaling pathway does not only affect terminal differentiation of hair shaft progenitors, but is likely to perturb epidermal homeostasis and affect other compartments other than the resulting lineages in question. This disruption may push proliferation and differentiation towards other lineages such as the sebocytes, the IFE, and keratinocytes of the ORS, as reflected by the hyperplasia phenotype.

(i) Wnt pathway as target for Zdhhc21

Based on the hypothesis, we might consider the possibility of Wnts themselves being the substrate target of Zdhhc21. Since both wild-type and *dep* proteins are expressed in the Henle's layer of the IRS, which consists of 3 distinct cell lineages surrounding the matrix cells, it is likely that the substrate of Zdhhc21 that is affected also reside in the same keratinocytes in the IRS. Out of the Wnt family, 4 members are expressed in the IRS, some of which are specific to the IRS, others are expressed in other compartment, such as Wnt5a, which is expressed in the matrix as well as the IRS (Reddy et al., 2001).

Following this notion, the palmitoylation of Wnt3a is reported to be required for bioactivity and for obtaining the threshold concentration for initiating a signal (Willert et al., 2003). Therefore, it is conceivable that that *dep* may have an effect on one of these Wnt proteins due to its inactivity as a PAT.

However, such possibility is less likely based on the topological prediction of Dhhc21 and the cellular location of its known targets (discussed in Section 6.4.4.2). Nevertheless, the mutation may have an indirect effect on Wnt signalling via a Wnt-related substrate in the IRS that may cause a loss of canonical Wnt signalling in the nearby matrix cells. As a result, there will be a lack of TCF/Lef1 differentiation of matrix cells that bind to and drive the promoter of hair-specific keratins to form a functional hair shaft that can break through the skin to form a nice even coat, leading to a hair loss phenotype.

(ii) Depigmentation in *dep* may be a result of a lack of HS progenitor cells

The lack of differentiating hair shaft keratinocytes may subsequently lead to an abnormal or uneven transfer of melanin in the HFs because the melanosomes are not adequately transported or incorporated into the keratinocytes, causing the depigmented hair coat observed in *dep*.

(iii) Hyperplasia phenotype may be caused by ongoing signaling of Shh and Ihh

The hyperplasia phenotype of the IFE, HF and SG may be caused by an ongoing Shh/ Ihh signaling which is likely to be normal (as judged by the comparable *Shh*, *Gli1* and *Ptc1* expression between wild-type and *dep*) but may cause progenitor cells to enter the other lineages when Wnt signaling is compromised.

The response to Wnt signalling in *dep* epidermis may be tested by looking at the expression of Wnt downstream effectors, such as β-catenin and Lef1, since a reduced or ectopic expression of these proteins may be indicative of a defect in the Wnt producing or responding pathways.

6.3. Results

6.3.1. Wnt response is reduced in *dep* hair follicles

To test whether the *dep* mutation has an effect on Wnt signaling, we looked at the expression pattern of the transcriptional response to Wnt in the epidermis.

Immunostaining of Lef1 shows a specific pattern in the wild-type matrix, where HS progenitors reside, as well as the cortex of the HS. However, in *dep*, although Lef1appears positive in the matrix, the stained cells do not exhibit an apparent nuclear signal, and there are no Lef1+ cells further up the hair shaft (Figure 6.2). It may first appear that the morphological difference between wild-type and *dep* follicles may account for the difference in the Lef1-staining pattern, i.e. lack of Lef1-expressing cells rather than a lack of signal. However, the structural difference is likely to be a consequence of a disruption in Wnt signaling in the HF progenitors of the *dep* matrix, which is reflected by the aberrant Lef1 expression pattern.

The β-catenin antibody (clone 15B8) shows a robust Wnt response in wild-type HFs, as judged by the presence of nuclear β-catenin in the matrix and the HS cortex, the outcome of Wnt signal. However in *dep*, even though there is apparent β-catenin signal, it appears more diffused and possibly cytoplasmic in the matrix (Figure 6.3), indicating that there may be an absence of Wnt signaling at this stage that prevents translocation of β-catenin into the nucleus to interact with transcription factors and regulate transcription of HS specific keratin genes. Without the presence of Wnt signals, excess β-catenin that is not utilized or stabilized may accumulate at cell-cell adherens junctions, as seen in Figure 6.3.

While most of the hair follicles display clear nuclear β-catenin signal in wild-type HS cortex, we also observe that only some of the follicles have β-catenin positive cells in the dermal papillae, whereas the intensity of signal in the HS cortex varies between follicles. This observation may reflect the coordinated reciprocal signaling between the DP and the epidermis (DasGupta and Fuchs, 1999; Maretto et al., 2003).

To conclude, nuclear staining of β-catenin and Lef1 is only observed in wild-type but not in *dep*. The expression pattern in wild-type is consistent with previous findings which shows that Wnt responsive cells reside in the HS precortex region and cuticle (DasGupta and Fuchs, 1999; Millar et al., 1999).

Figure 6.1. Lack of Wnt palmitoylation may cause *dep* phenotypes
[A] Diagram showing the lineage relationship within the epidermis. It is believed that there is a population of multipotent stem cells which reside in the bulge, and the stem cells for the IFE, HF and SG cells are interconvertible (double arrows). Many signalling pathways are involved in maintaining the homeostasis of the network. Wnt signaling is important in the initiation of hair follicle formation in embryos, and also the differentiation of matrix cells along the HS lineage. For this to happen, a very concentrated level of Wnts is required to initiate the pathway. It is therefore speculated that the HS differentiation pathway (yellow arrow) maybe affected due to an unpalmitoylated Wnt protein, as a result pushes proliferation and differentiation towards other lineages, including the sebocytes, ORS and the epidermis.

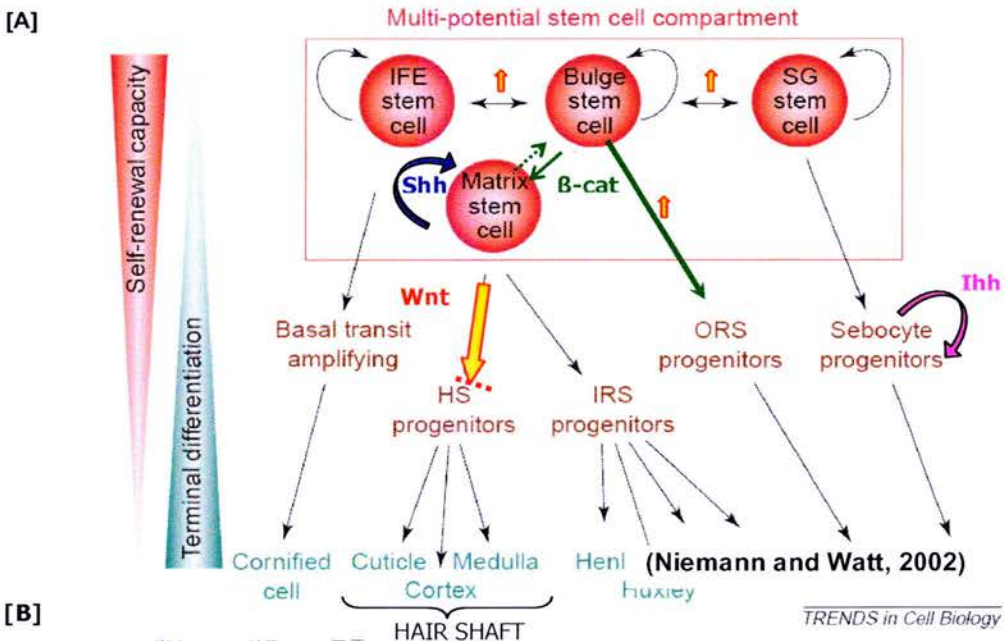

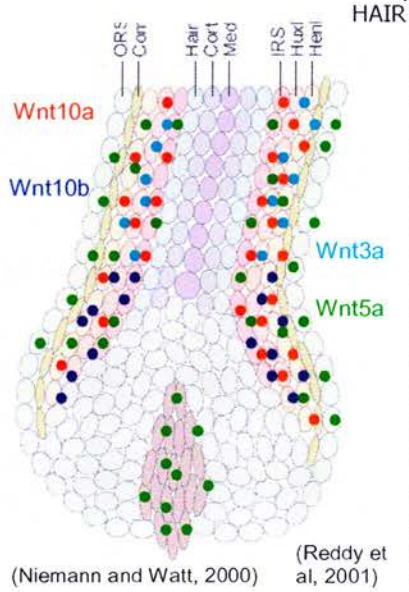

[B] Both WT and *dep* Dhhc21 are expressed in the IRS, which is consists of 3 distinct cell lineages surrounding the matrix cells, the substrate that is affected must also reside in the IRS. It is speculated that Wnts are involved because 4 members of the Wnt family are known to express in the IRS (Reddy et al., 2001). Moreover, Wnt3a requires palmitoylation to be bioactive and to obtain the concentration required for the signal. So it maybe the case that *dep* affects palmitoylation of a Wnt proteins, causing a loss of canonical Wnt signaling in the nearby matrix cells, resulting in a lack of TCF/Lef1 differentiation of matrix cells which bind to and drive the promoter of hair-specific keratins to form a functional hair shaft which can break through the skin to form a nice even coat. If there is no differentiating hair shaft cells, melanin transfer will become abnormal and uneven. The hyperplasia phenotype maybe caused by ongoing Shh/Ihh signaling which is normal and cause cells to enter the other lineages when Wnt signaling is compromised.

Figure 6.2. *dep* has reduced number of HF progenitors at onset of anagen
Lef1 immunohistochemistry on wild type (A) and *dep* (B,C,D) dorsal hair follicles at 4-week.Immunostaining of Lef1shows a very specific pattern in the wild-type matrix, as well as the cortex of the hair shaft (A). Whereas in *dep*, the expression pattern in the matrix is aberrant, and there is a lack of signal further up the hair shaft (B,C,D). While the melanosomes are clearly visible in wild-type as black granules, *dep* follicles lack such appearance possibly due to an absence of hair shaft progenitor cells that import the melanosomes. (E) At 5 week, *dep* follicles resumes Lef1 expression in the hair shaft cortex, and the medulla is now visible with appearance of melanosomes in appropriate compartments. However, the outer root sheath appears thickened (white bars) even though the HS development becomes normal again. (F) Staining with the secondary antibody (biotin-conjugated anti-rabbit) alone does not give any specific signal, indicating that the specific nuclear staining is not due to non-specificity of the secondary antibody. Scale bars, 50_m.
_-Lef1 (matrix, pre-cortex, cortex, dermal papillae)

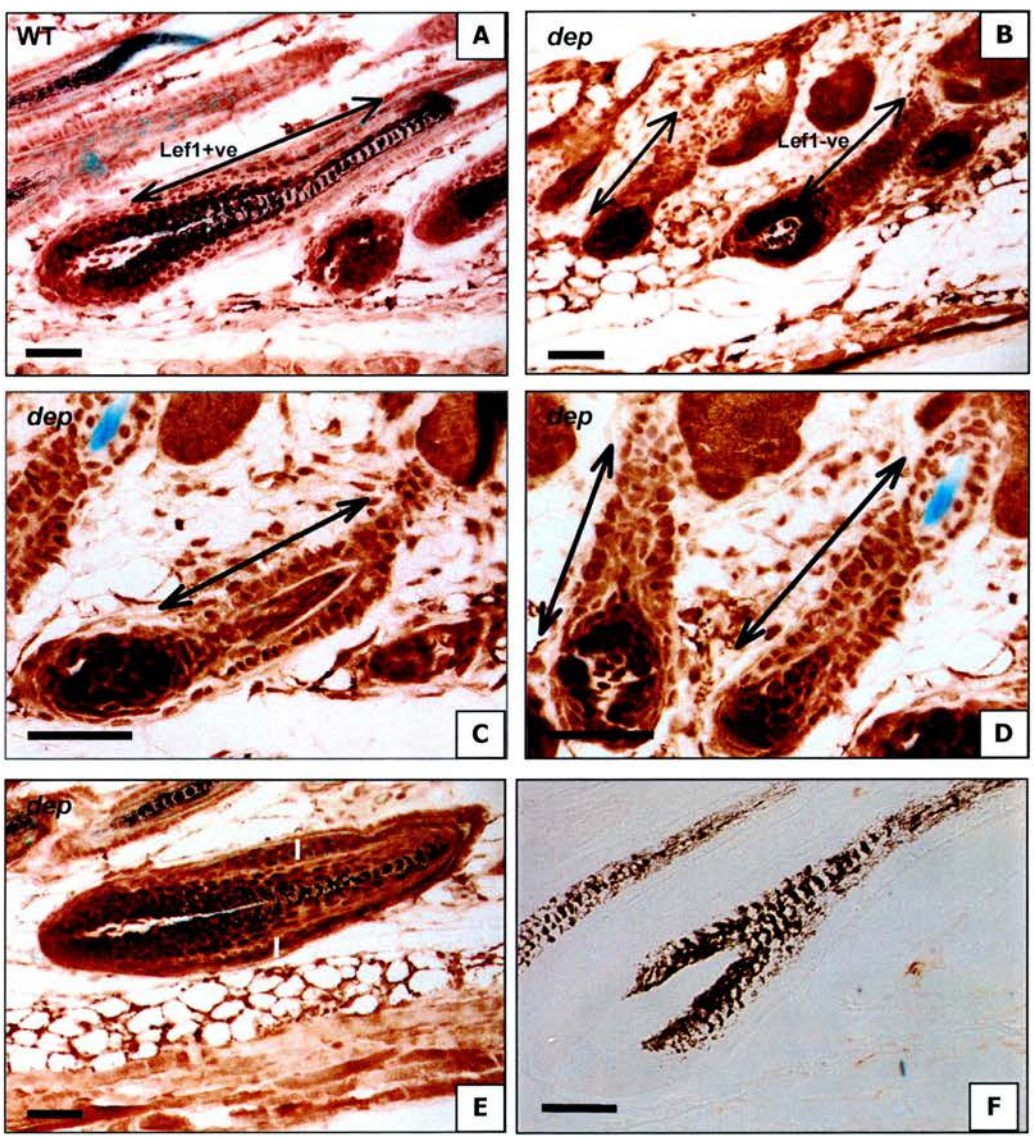

Figure 6.3. Lack of Wnt response in *dep* follicles at early anagen
Representative images of β-catenin immunostaining at 4-wk [A] and 5-wk [B] dorsal skin of wild-type and *dep*. Nuclear β-catenin is clearly observed in the hair shaft progenitors of wild-type matrix and hair shaft cortex at 4-wk. Whereas β-catenin expression in *dep* matrix appears to be non-nuclear and possibly cytoplasmic and at cell-cell junctions at this stage. [B] At 5-wk, nuclear expression of β-catenin can be seen in hair cortex of *dep*, and is comparable to wild-type. The same pattern was observed in 4.5-wk skin (data not shown). Scale bars, 50μm.
β-catenin (nuclear expression in Wnt responsive cells)
α-K5 (IFE, ORS, basal layer)

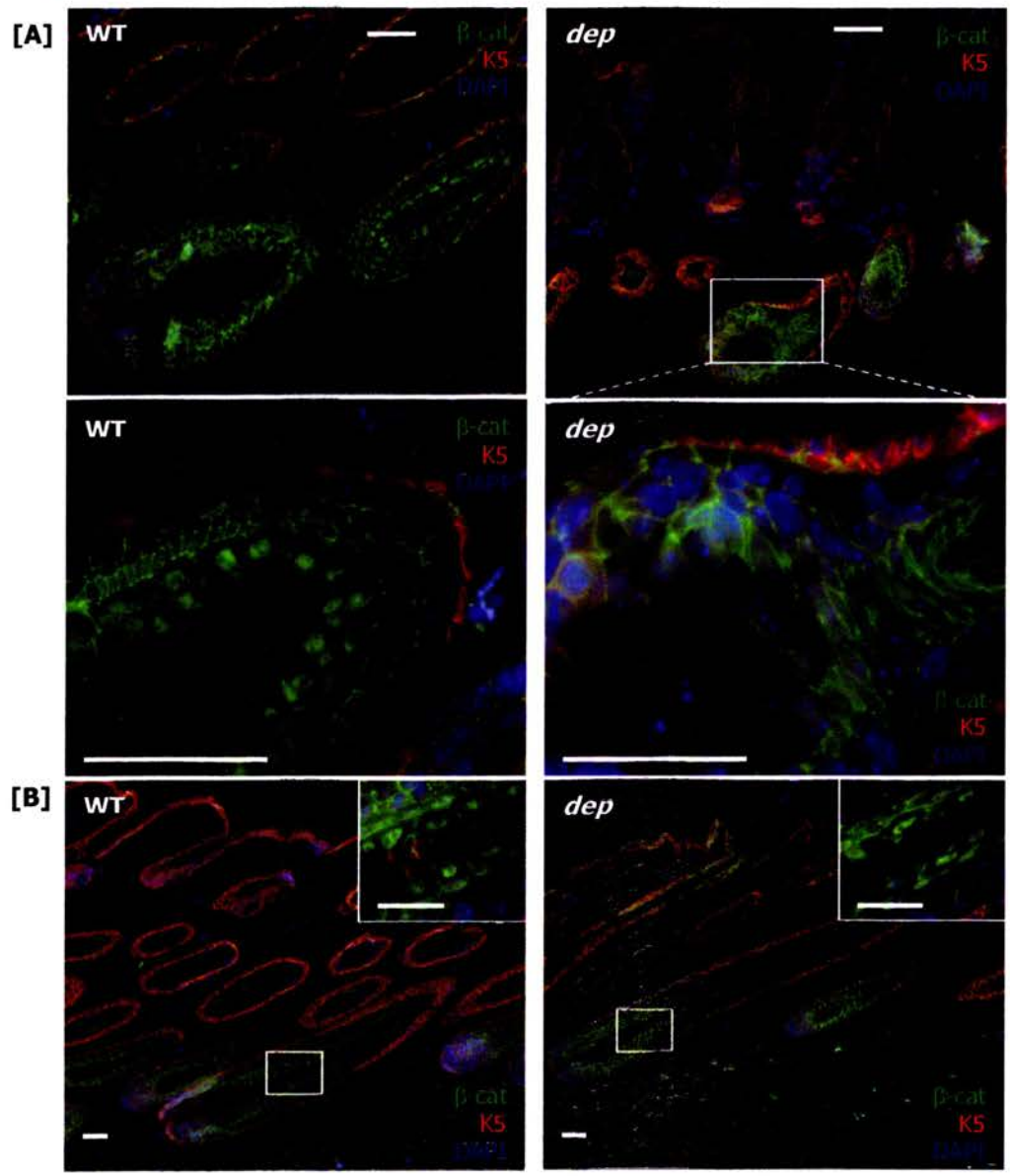

6.4. Discussion

6.4.1. Testing Wnt response *in vivo* and *in vitro*

In addition to looking at the expression of Lef1 and β-catenin, the Wnt response may be assayed by using the β-catenin-activated transgene driving expression of nuclear galactosidase (BAT-gal) transgenic mice that expresses the lacZ gene under the control of β-catenin/ Tcell factor responsive elements (Maretto et al., 2003).

The advantage of BAT-gal reporter mice over the existing β-catenin staining data is that the former provides a more specific signal in the nuclei of Wnt-responding cells. Excess or non-stablised β-catenin normally accumulates at cell-cell junctions, making it difficult to look for nuclear signal against cytoplasmic expression because the background signal may obscure interpretation of nuclear signal against noise.

Previous literatures have demonstrated that the BAT-gal transgenic mice are reliable reporter of Wnt/ β-catenin activity (Barolo, 2006). Normally, BAT-gal activity can be detected during anagen (P4) in the hair shaft precortex, dermal papillae and matrix cells, even though individual hairs display differences in expression pattern (Maretto et al., 2003). Based on the expression data of Lef1 and β-catenin, we expect that the LacZ activity in *dep* may be reduced. Using the BAT-gal transgenic reporter mouse, it may be possible to determine the effect of *dep* mutation on canonical Wnt activity, and support the expression data of β-catenin and Lef1.

The Wnt response may also be reported in cell culture assay using the *TOPFlash/ FOPFlash*-luciferase reporters of Lef1/β-catenin signaling. TOP (Tcf-optimal promotor) is an artificial promoter that contains multimerized Lef1/Tcf binding sites, whereas *FOPFlash* is a negative control plasmid that contains mutant binding sites (DasGupta and Fuchs, 1999). The assay has been used in conjunction with various reporter genes to identify Wnt-responsive cells (Kobielak et al., 2007). Cultured wild-type and *dep* keratinocytes may be subjected to assays with the *TOPFlash* reporter gene, which is active when β-catenin and Lef1 are stabilized. It is predicted that without nuclear β-catenin expression, there will be a reduced level of Lef1-dependent transactivation of *TOPFlash* in the *dep* assay.

6.4.2. Melanin Transfer in hair shaft progenitor cells of *dep*

As *dep* exhibits a remarkable depigmentation phenotype in early stage epidermis and in hair coat, we hypothesize that there is inadequate differentiation of hair shaft keratinocytes for normal transfer of melanin granules (melanosomes). Skin sections of early anagen have shown a lack of melanosomes in *dep* HFs, however, it is unclear whether this is due to a hair shaft defect or a disrupted programme in melanocyte differentiation.

To study the nature of the depigmentation phenotype, the Dct-lacZ reporter may be used to trace differentiating cells of the melanoblast lineage. The Dct-lacZ transgenic mouse carries the lacZ reporter under the control of the Dct promotor (Mackenzie et al., 1997), and has been used to show that the receptor tyrosine kinase, KIT, is involved in guiding melanoblast distribution in developing hair follicles (Jordan and Jackson, 2000). The Dct-lacZ reporter mouse has also enabled the identification of melanocyte stem cells in the bulge region of hair follicles throughout the hair cycle (Nishimura et al., 2002).

By crossing the Dct-lacZ transgenic mouse to the *dep* mutant and tracing the expression of the lacZ reporter gene using a β-gal assay, we may trace migration of differentiating cells of the melanoblast lineage before they produce visible melanin pigment. This will provide clues to whether the abnormal transfer of melanosome in *dep* is due to a lack of differentiating HF progenitor at the onset of anagen, as predicted by our hypothesis, or a misregulation in melanoblast migration.

6.4.3. The rate of cell proliferation in *dep* epidermis

The hyperplasia phenotype in the SG, HF and ORS observed in *dep* maybe due to an increased rate of proliferation, as judged by the elevated number of P63 cells that have proliferative potential and an expansion of the K5+ compartment. To determine whether the rate of cell proliferation is increased in *dep* skin, the BrdU pulse-chase labelling protocol may be applied in which all newly synthesized DNA are in S-phase cells are labelled with Brdu. The cells that divide infrequently, such as the bulge stem cells, and the stem cells of the IFE, SG and HF, will retain the BrdU label into adulthood, and can then be visualized as DNA label-retaining cells (LRC) (Braun et al., 2003). The development of whole-mount labeling techniques in human

and mouse epidermis have greatly facilitated the evaluation of SC number and location (Braun et al., 2003).

While the LRC reservoirs are not significantly depleted by successive hair growth cycle, the expression of ΔNLef1 to block β-catenin signaling induces transdifferentiation of HFs into IFE and sebocytes, and causes depletion of LRC primarily through proliferation (Braun et al., 2003). It was concluded that LRCs are sensitive only to certain proliferative stimuli, and that changes in lineage can occur with or without the recruitment of LRC into the cycle.

Assuming that the number of stem cells in wild type and *dep* were equal at the time of Brdu injection (However, we must be cautious with the possibility that this may not be the case), an increase of BrdU+ cells in the IFE, SG or HF after the chase period would indicate an increase in proliferation rate in those compartments. This maybe coupled with a depletion of LRC by successive hair growth cycle, which indicates an elevated rate of proliferation and/or transdifferentation into the hyperplastic compartments.

6.4.4. The *dep* mutation may affect the Wnt signaling pathway

To date, 19 Wnt members have been identified in mouse, each of which contains at least one site for N-glycosylation, and has up to 23 to 26 conserved cysteines (Coudreuse and Korswagen, 2007). In the postnatal HF alone, 7 members of the Wnt family are reported to express independently with overlapping but unique patterns in keratinocytes of different lineage and differentiated state (Reddy et al., 2001). This suggests that the Wnt family is involved in maintaining a normal HF, and that individual Wnt members are likely to have a highly specific role. Furthermore, different Wnt members are recruited at different stages of development. The specificity of spatial and temporal expression of individual Wnt members allows the establishment of local signaling centers in specific niches that are required for correct terminal differentiation of keratinocytes of specific lineages.

The specificity in Wnt expression may partially explain why *dep* does not display a macroscopic phenotype until a certain stage, why the mutation does not result in a more severe phenotype and why the mutation predominantly affects the epidermis but not other tissues despite the overall significance of Wnt signaling.

The sparse HFs in *dep* in Fig 5.5B may be explained by a disruption of Wnt signaling in placode formation, since a loss of function mutation of Lef1 causes absence of vibrissae and greatly reduces number of hair follicles throughout the body (van Genderen et al., 1994). However, histological sections do not show a difference in HF density between wild-type and *dep* at the same stage. If *dep* has a normal HF density despite partial loss of Wnt function, it may be the case that postnatal initiation of anagen requires long-range Wnt signaling events between the Henle's layer and the matrix, i.e. between Wnt-secreting and Wnt-responsive cells. Whereas during placode formation, the epithelial- mesenchymal distance would be relatively short and so signaling events may act in a more paracrine manner.

Another possibility that is not mutually exclusive to the above notion, is that the Wnt members may be redundant for other functions such as the progression of hair cycling (since the growth of HS catches up in late anagen), but not for maintaining epidermal homeostasis, as judged by the hyperplasia phenotype that persists into telogen.

On the other hand, the Dhhc family may also be redundant for palmitoylating certain substrates of Dhhc21 including those required for hair follicle development and hair cycle progression through a Dhhc21-independent mechanism. However, it is conceivable that in the hair follicle, the PAT activity of Zdhhc21 is indispensable for maintaining certain aspects of epidermal homeostasis as evident in the apparent disruption in the system.

In addition to differential expression of Wnt members, there may also be distinct difference in the way HF and IFE cells respond to increasing β-cat expression. The SC progeny migrating from the bulge may change in chemistry as they migrate along and the response to Wnt may change. This is demonstrated in (DasGupta et al., 2002), which shows that stabilized β-cat acts in epidermis to promote hair fates and in hair cells to promote epidermal fate.

6.4.4.1. Experiments for testing dep effect on Wnt palmitoylation

To test whether the *dep* mutation has an effect on Wnt palmitoylation, and whether Wnt is a direct palmitoylated substrate of *dep*, the [^{3}H] palmitate labeling protocol may be used as described in Chapter 4. However, this protocol is notorious for requiring extensive exposure time, often up to one month. Due to this limitation, alternative protocols have been developed, for example, cells may be co-transfected with the PAT (Dhhc21-*dep*) and candidate substrate (Wnt) DNA constructs, and treated with 1M hydroxylamine (pH7) for 20 hours, followed by an

assay for a band shift. As hydroxylamine removes palmitate groups attached to cysteines via thioester linkage, the loss of palmitate may be detected by a change in protein migration on SDS-PAGE.

The efficiency of the bandshift method is dependent on the number of palmitate groups the substrate incorporate. Using this method, a number of DHHC clones have been shown to increase palmitoylation of CSP (Cysteine String Protein) in HEK culture, since CSP palmitoylation adds up to 14 palmitates and thus the extent of it can be successfully detected by a 8kDa bandshift on blots of transfected cells (Greaves and Chamberlain, 2006).

Members of the Wnt family are cysteine-rich with over 5% of the protein sequences being cysteines (Coudreuse and Korswagen, 2007). Although the Wnt family is known to be palmitoylated (Willert et al., 2003), it is not known how many palmitate groups the Wnt proteins incorporate. But despite the abundance in cysteine residues, only one cysteine (C77) that locates at the N-terminal of Wnt3a has been reported to associate with a palmitate group. Since the incorporation of one palmitate group is unlikely to be detected by a band shift, the conventional [^{3}H] labeling protocol can be used, however, the exposure time may take up to one month.

6.4.4.2. Loss of PAT activity in dep is likely to have an indirect effect on Wnt signaling

The key but still largely unanswered question is how Zdhhc21 can affect the Wnt signaling pathway. Despite previous findings that Wnt3a requires palmitoylation for bioactivity (Willert et al., 2003) and that Zdhhc21 is a PAT (Fernandez-Hernando et al., 2006), members of the Wnt family are unlikely to be direct substrates of Zdhhc21 for palmitoylation.

Based on the proposed topology of most DHHC proteins, the Dhhc putative catalytic motif is predicted to be intracellular rather than in the lumen of the cis-Golgi (Fukata et al., 2006; Keller et al., 2004). And if the Dhhc motif is cytosolic, Wnts are unlikely to be palmitoylated by Dhhc21.

Dhhc21localizes to the cis-Golgi, whereas Wnt palmitoylation is believed to take place in the ER, possibly by porcupine (Coudreuse and Korswagen, 2007). As Wnts are secreted proteins

that require active translocation via its signal peptide to cross the membrane and reach the lumen, Wnt palmitoylation would require to occur prior to translocation into the lumen.

Proteins that are shown to be specific palmitoylation substrates of Zdhhc21 are intracellular such as eNOS (Fernandez-Hernando et al., 2006) and Lck (Fukata, unpublished data). This implies that the active site of Dhhc21 faces the cytosol, and so the substrates for DHHC PATs are likely to be cytosolic, non-secreted proteins.

In a more recent study, however, it was proposed that the palmitoylation of Wnt3a may take place in the Golgi (Komekado et al., 2007). When cells are treated with Brefeldin A, an inhibitor of vesicle transport from ER to Golgi, Wnt3a was not palmitoylated although glycosylation is unaffected, indicating that palmitoylation of Wnt3a may take place in the Golgi, where Zdhhc21 resides.

It may be possible that Wnts can undergo other lipid modification such as isoprenylation which tethers Wnts to the cis-Golgi membrane, where they can access the catalytic motif of Dhhc21.

6.4.5. Potential palmitoylated substrates of Dhhc21

6.4.5.1. Candidate substrates for the skin and hair phenotype

Having shown that *dep* HFs displays a Wnt-related phenotype as judged by the lack of nuclear staining of Lef1 and β-catenin, the substrate of Dhhc21 is likely to be a player in the canonical Wnt signaling pathway. Since the mutant protein is shown to have a loss of PAT activity in cell culture, the substrate is likely to be a palmitoylated protein that is expressed in the Henle's layer of the IRS. In addition, based on the predicted topology of the Dhhc motif and the identification of intracellular substrates for Dhhc21, the substrates targeted in the hair loss phenotype must also be an intracellular, cytosolic protein.

Given the loss of nuclear expression of β-catenin and Lef1 in *dep* follicles at early anagen, we can speculate that the loss of Dhhc21 PAT activity may affect translocation of β-catenin into the nuclei of Wnt-responding cells. Alternatively, the unpalmitoylated substrate may affect other mechanisms upstream of β-catenin translocation that may potentially reduce responsiveness to Wnt signaling (e.g. Frizzled). On the other hand, based on the differential

expression of different Wnt members in the hair follicles, there is a possibility that the problem exists in the Wnt-secreting cells, possibly during the process of post-translational modification, sorting or secretion.

Another category of proteins that partially fulfill the above criteria are the extracellular matrix receptors of the integrin family. Integrins do not only play a role in adhesion and signal transduction between cells, their roles in regulation of stratification and the initiation of terminal differentiation are also well-documented (Watt, 2002). Normally, keratinocytes of the basal layer and ORS express several integrins including α2β1-, α3β1-, α5β1-, α9β1-, αvβ5- and α6β4-integrins (Watt, 2002). Ectopic expression of integrin β1 in the suprabasl layer can lead to perturbed keratinocyte differentiation (Carroll et al., 1995).

It was also shown that the ligation or mutation of the β1 integrin subunits can negatively regulate the initiation of terminal differentiation in primary human keratinocyte culture (Levy et al., 2000), probably via its ability to directly bind and control the activity of focal adhesion kinase (FAK), which negatively regulates cellular tension (Fuchs, 2007). Furthermore, the α3, α6 and β4 subunits are known to be palmitoylated (Yang et al., 2004), making this category of proteins a possible candidate of Zdhhc21 PAT target.

On the other hand, in a recent study, targeted deletion of integrin-linked kinase (ILK) in epidermal keratinocytes was shown to cause epidermal defects and hair loss phenotype (Lorenz et al., 2007) which is similar to *dep* in terms of the premature HF appearance and hyperplasia of the suprabasal layer and ORS. However, this phenotype was revealed to be caused by the inability of keratinocytes to firmly stabilize lamellipodia (cytoskeleton actin projections), leading to an impaired downward migration of ORS cells to replenish the matrix and an accumulation of progenitor cells in the ORS. It is however, not a result of abnormal β-catenin stability, matrix differentiation or stem cell maintenance (Lorenz et al., 2007).

In addition, the deletion of integrin α3 in the epidermis (Conti et al., 2003) also shows some degree of similarities to *dep* such as defective differentiation of HF keratinocytes and stunt follicles. These abnormalities are reported to result from a combination of factors including F-actin disorganization and a defect in lamina densa integrity. To test the possibility that integrins may be involved in the HF phenotype of *dep*, we may investigate the expression of individual integrin subunits to look for any abnormal pattern which may lead to the observed phenotype.

In addition to the HF phenotype, interactions between cells and the extracellular matrix is known to regulate melanocyte behaviour (Li et al., 2004). So the loss of integrin function in keratinocytes may potentially disturb melanocyte distribution (Lopez-Rovira et al., 2005), which may potentially lead to pigmentation phenotype as seen in *dep*.

The insulin-like growth factor (IGF-I) also plays a role in epidermal homeostasis in which it predominantly enhances cell proliferation, survival and migration. Disturbance in the IGF signaling pathway has been implicated in the pathophysiology of several skin perturbations, particularly those exhibiting epidermal hyperplasia (Edmondson et al., 2003).

6.4.5.2. Loss of PAT activity may affect substrates that cause other phenotypes

Given the widespread expression pattern of *Zdhhc21* based on RT-PCR, there is the possibility that *dep* may affect palmitoylation of substrates other than that involved in the hair loss phenotype. The effects on the loss of Zdhhc21 PAT activity on other tissues are unclear. However, both our RNA *in-situ* and immunohistochemistry data show a specific expression in the hair follicle; and the effect of the *dep* mutation on hair-related phenotype was discussed in Chapter 5.

Although the major phenotype of *dep* appears to be hair-related, it is apparent that *dep* also exhibit other phenotype during development as well as in adulthood. During early development (first few weeks postnatal), homozygotes often appear smaller in body size and body mass, even though the difference becomes insignificant as the mutant enters adulthood. It may be possible that the loss of PAT activity has an effect on certain growth-related factors that are required for the early development stage. It is unclear of whether the molecular causes behind this observation have any effects on the adult mutants.

In several occasions, the mouth region of *dep* appears to be expanded (personal observation). Histological sections show a severe epidermal hyperplasia of the lips. In addition to the epithelial phenotype, there also seems to be a subtle craniofacial/ maxillo-mandibular difference between wild-type and *dep*, in that the jaw of *dep* seems to be broader comparing to wild-type.

6.4.5.3. Identification of palmitoylation targets of Zdhhc21

To identify genuine substrate that are underpalmitoylated in *dep*, the ABE chemistry protocol could be applied. Primary cell culture can be set up from wild-type and *dep* epidermal keratinocytes or embryonic fibroblasts. The culture may then be subjected to ABE chemistry in which all the palmitoylated proteins are labeled with biotin. The biotinylated proteins are then pulled down by streptavidin beads and visualized by 2D-PAGE. The protein spot pattern of wild-type and *dep* can be compared and in theory, any loss of band in *dep* would represent a protein that is under-palmitoylated. The corresponding spots in wild-type can then be extracted and subjected to sequence analysis by mass spectrometry (MS). This approach provides the potential to identify novel substrates that without the need of any assumption and knowledge of the pathways.

Another approach that may be applicable is by using an MS-based technique called the stable isotope labeling with amino acids in cell culture (SILAC) developed in the group of Matthias Mann (Ong and Mann, 2006). SILAC is a simple and accurate approach that involves growing 2 populations of cells (e.g. wild-type and *dep* keratinocytes) in culture media that are identical except that one media contains amino acids labeled with stable isotopes, and the other one with unlabeled amino acids.

After adequate number of cell divisions, the 2 populations of cells can then be harvested and mixed together to allow identical subsequent treatments. The palmitoylated proteins can then be pulled down by the ABE chemistry, and subjected to MS analysis, which compares the abundance of palmitoylated proteins between the wild-type and *dep*. This method allows subtle difference in degree of palmitoylation to be detected in a standardized way.

Chapter 7 - Concluding Remarks

The initial effort to identify novel genes following germ cell mutagenesis half a century ago has allowed the spontaneous *dep* mutation to be mapped to the *b-del* interval on chromosome 4. The advent of increasingly abundant genomic data and DNA-based molecular markers has allowed the del-233F mutation to be readily identified in *Zdhhc21*.

In this project, the subsequent verification of characterization of the mutant allele has opened up an unexpected area of focus, which is the PAT activity *in vivo*. The combination of BAC transgenic rescue and cell culture assay has identified *dep* to be the first example that demonstrates a role of PAT enzymatic activity *in vivo*.

Currently, large-scale production of targeted mutations in C57BL/6N ES cells in the EUCOMM project is underway. Zdhhc21 was among the first set of constructs to be made in the recombineering pipeline. Once the Zdhhc21 knockout (floxed) mutant ES cell line is made into mice, the mutation may be activated by crossing with the desired Cre recombinase driver strain, such as the K5-Cre, which targets the epidermal stem and transit-amplifying cells, or other keratin promoters such as K1, K6, K14 and involucrin, to investigate the role of Zdhhc21 in specific epidermal compartment.

Using the ABE proteomic screen for Zdhhc21 substrates, we may identify the causative component of *dep* that is affected by PAT-deficiency. Based on existing knowledge on Wnt signaling pathway and its involvement in epidermal homeostasis, the proteomic approach may potentially identify a novel member of the Wnt pathway.

Once the specific substrate is identified, it may also be conditionally targeted in hair follicles to see if it produces any *dep*-related phenotype. If it is a protein-coding gene that has previously been characterized, a knockout and conditional ES cell line may be available from the EUCOMM ES cell mutagenesis archive. Furthermore, the mutation may be activated by crossing with a specialized K14-Cre strain (Benitah et al., 2005; Silva-Vargas et al., 2005), in which the Cre recombinase can be induced by 4-hydroxy-tamoxifen (4OHT) in a temporally controlled manner. This will allow us to inactivate the target gene at specific stages of the hair

cycle. According to our observations, the predominant *dep* phenotype occurs during early anagen when matrix progenitors are differentiating. Using the tamoxifen-induced knockout strain, we may verify this finding.

Currently, several members of the DHHC family have been associated with human conditions such as mental retardation and schizophrenia. In addition, out of all the PATs in mouse, there is increasing evidence that supports a role in palmitoyation (Section 4.1.3.). However, none of these literatures has reported an identified substrate associated with a mammalian condition. The conditional targeting approach, in combination with the proteomic screen, will prove the link between the PAT-deficient Zdhhc21 and the *dep* phenotype. This will not only facilitate our understanding on the role of palmitoylation, it will potentially add insight to our current understanding of epidermal homeostasis and hair cycle regulation.

Chapter 8 – Materials and Methods

8.1. Nuclei Acid Manipulation

8.1.1. Solutions used in molecular biology

The following solutions were prepared by HGU technical staff and autoclaved and stored at room temperature: 1M Tris (tris [hydroxymethyl] aminomethane) ph7.5 and ph8.0, TE buffer, EDTA (ethyldiaminetetra-acetic acid di-sodium salt), 20xTBE (Tris-Borate-EDTA[20]), 20%SDS (sodium dodecyl sulfate), 20x SSC (sodium chloride/ sodium citrate buffer[21]), 5M NaCl (Sodium Chloride), 5M NaOH (Sodium Hydroxide). Adjustment to any pH is accomplished by adding either HCl or NaOH, and monitored using a pH meter (Fisherbrand Hydrus 400) calibrated over a range of standard buffer.

8.1.2. Gel electrophoresis

The loading buffer used in most agarose gel electrophoresis was 6x bromophenol blue loading buffer (30% glycerol and 0.025% bromophenol blue in dH_2O). To make an agarose gel for electrophoresis, required amount of agarose powder (Hi-Pure, Biogene) was dissolved in 1xTBE by heat. Different concentrations of agarose gel (w/v) were used to resolve DNA fragments of different size. Molten agarose was cooled before the addition of Ethidium Bromide, which stains nucleic acid, to a final concentration of 0.5μg/100ml. The DNA marker used were 100bp marker (Promega) and 1kb marker (Invitrogen) depending on the expected size of fragments and strength of gel. The gel was then placed in a gel tank with 1xTBE, which acts as a buffer and provide ions for conductivity, and a current is applied. After adequate migration as indicated by the loading buffer, the gel is placed on a UV-transilluminator.

8.1.3. Determining concentrations of nucleic acids

The intensity of DNA maybe visualized and estimated against DNA of a known concentration on agarose gel by electrophoresis, or by measuring the absorbance (optical density, OD) in a spectrophotometer (GeneQuant) at a wavelength of 260nm (A_{260}). A 260/280 ratio of 1.8-2.0 indicates DNA purity.

8.1.4. Digestion by restriction enzymes

Most restriction enzymes (restriction endonuclease) used were from Roche. To cut double-stranded DNA, enzyme was added to a concentration of 5-10u/μg DNA in 1x Roche buffer. For fragments that were subjected to further DNA manipulation, DNA was digested for 3-4 hours.

---

[20] 20xTBE: [216.0g Tris Base + 110.0g Boric acid + 80ml 0.5M EDTA (pH8.0)] in 1 litre H_2O.
[21] 20xSCC: (175.3g Sodium Chloride + 88.2g Sodium Citrate) in 1 litre H_2O.

DNA digested for genotyping purpose was typically digested overnight. The digested fragments were then visualized by electrophoresis. For DNA manipulation, desired fragment of expected size was excised from the gel and purified by the QIAquick® Gel Extraction Kit.

8.1.5. Ligations

The vector and insert to be ligated were purified with QIAquick® Gel Extraction Kit or QIAquick® PCR purification kit. Alternatively, the DNA may be precipitated by EtOH in 10% v/v 3M NaOAc (Sodium Acetate) and 3 volumes of chilled 100%EtOH, incubated at -70°c for 20mins. The tubes were spun at 13k rpm for 10mins to pellet DNA, and washed with 70% EtOH before resuspending in TE buffer. The fragments used for ligation were often treated with SAP (shrimp alkaline phosphatase) at 37°c for 1 hour to remove phosphate group so that the ends do not re-anneal.

To join the 5'phosphate and 3'hydroxyl groups of double stranded DNA, the following reaction was typically used: 1µl 10xT4 ligase buffer, 6:1 molar ratio of insert to vector[22] and 0.5µl T4 ligase (Roche) up to 10µl ddH_2O. Larger ligation mixes were often used especially when the concentration of insert is low, and the volume needs to be compromised. A control reaction with no insert is included. The reactions were incubated at 16°c overnight, before bacterial transformation.

8.1.6. Polymerase Chain Reaction (PCR)

The Invitrogen DNA polymerase was used for most PCR reactions. For PCR that requires high fidelity, Pfu[23] (Stratagene) was added to the PCR reaction. For difficult GC-rich and repetitive sequences, Bio-x-act[24] (Bioline) was used according to manufacturer's specifications.

Working stocks of dNTPs (deoxyribonucleotide triphosphate) were made into 10mM from dATPs, dCTPs, dGTPs, dTTP, and a final concentration of 0.2mM is used for each reaction. Primers were designed using the Primer3[25] software and purchased as lyophilized desalted compounds (from Sigma Genosys, Invitrogen or Eurogentec). On arrival, stocks were resuspended in ddH_2O into 1mg/ml and stored at -20°c. Working stocks of 50ng/µl were made and about 2.5ng/µl of each primer was used in each PCR reaction.

---

[22] 6:1 molar ratio of insert to vector: Insert mass (ng) = 6x [insert length (bp)/ vector length (bp)] x vector mass (ng)
[23] Pfu: isolated from the hyperthermophilic marine archaebacterium, *Pyrococcus furiosus*, possess both 5'-to 3'-DNA polymerase as well as 3'- to 5'- exonuclease activities which prevent mis-incorporation of nucleotides.
[24] Bio-X-act is a formulation of several enzymes which delivers high specificity for long or difficult reactions. It also posses the proofreading 3'- to 5'- activity as does Pfu.
[25] Primer3: https://sourceforge.net/projects/primer3

Routine PCRs were carried out in Abgene thin-walled thermo tubes on the Hybaid Omnigene 96-well thermocycler. A typical PCR reaction using the Invitrogen Taq is as follows, unless otherwise stated:

10x buffer	1.5µl
50mM Mg^{2+}	0.5µl [1.67mM], 0.6µl [2.0mM]
10mM dNTPs	0.3µl
50ng/µl F primer	0.5µl
50ng/µl R primer	0.5µl
10µg/µl DNA	1.0µl
Invitrogen Taq	0.1µl
ddH_2O	up to 15µl.

The cycling conditions are as follows unless otherwise stated:

5'@94°c
[30"@94°c => 30"@Tann[26] => 1'@72°c] x 30cycles
10'@72°c
10'@4°c
END (may store at -20°c)

8.1.7. Reverse Transcription (RT)-PCR

(a) RNA extraction

BALB/c mice were sacrificed and tissues were collected and immediately placed into blue RNAse-free mortar tubes that are used with the hand-held electric homogeniser on dry ice. Total RNA for the selected tissues were extracted with TRI Reagent® (Sigma) according to the manufacturer's specifications. Briefly, tissues were disrupted in the phenol-based reagent which contains denaturants and RNase inhibitors. Chloroform was then mixed with the lysate and centrifuged to separate mixture into 3 phases. RNA was then precipitated from the aqueous phase with propan-2-ol.

(b) RT-PCR expression profile

Gene-specific RT primers were designed to amplify across the last 2 or 3 exons of the gene to ensure clear distinction of cDNA from any genomic contaminants. Sequences of RT primers

[26] 'Tann': the annealing temperature, which is about 5°C below the Tm, where $T_m=[4x(G+C)+2x(A+T)]°C$.

are available on request. RT-PCR reactions were carried out using the Promega Access RT-PCR system according to the company instructions except that quarter reactions were used.

8.1.8. DNA sequencing

In many cases, PCR primers used for amplifying a region of interest were used for sequencing. But in some cases, additional sequencing primers internal to the region of interest were used. Sequencing primers were diluted to a concentration of 50µg/µl or 20µM and submitted to the HGU Technical service together with the PCR products or purified plasmids.

The dye terminators used was BigDye (Perkin-Elmer), which consists of DNA polymerase, dNTPs, and ddNTPs-Dye terminators. Successive rounds of amplification results in incorporation of one of the 4 ddNTPs, each tagged with a different fluorescent dye in each extension product.

The sequencing reaction was as follows:

Sequencing primer	5 pmol
DNA template	10ng
Mg^{2+}	0.4mM
BigDye Terminator	0. 5µl
ddH_2O	up to 20µl

The sequencing program was as follows: [30"at 96°c => 15"@55°c => 4'@60°c] x 25cycles Sequencing products were EtOH precipitated and separated with an ABI3100 by the HGU Technical service to discriminate ssDNA fragments of different length. Sequencing traces were analyzed using Sequencher software.

8.2. Microbiology

DNA plasmids (usually carry an antibiotic-resistance gene e.g. Ampr) may be transformed into Subcloning Efficiency® Dh5α Chemically Competent cells (Invitrogen) according to manufacturer's specifications. Briefly, plasmids were transformed into bacterial cells by heat shock at 37°c for 20secs, during which the uptake of plasmid DNA take place. The plasmid-containing cells were then selected by streaking the transformant onto an L-agar plate[27] containing the antibiotics (e.g. ampicillin at a concentration of 10µg/ml).

[27] L-agar: (10.0g Tryptone + 5.0g Yeast extract + 10.0 NaCl + 15.0g Agar) in 1litre H_2O.

Individual colonies maybe tested by PCRs for identity, before being inoculated into appropriate volume of L-Broth[28] containing the antibiotics, and grown at 37°c overnight at 250rpm for large scale cultures. The plasmid DNA were then isolated and purified from the culture using QiaPREP® Spin miniprep kit or EndoFree® Plasmid Maxi kit according to manufacturer's specifications.

Briefly, cell pellets were suspended with an alkaline solution with detergent (NaOH/SDS) and RNaseA. The alkaline conditions denature DNA and proteins; and the detergent lyses cells and denature proteins. The mixture was then neutralized and adjusted to a high salt condition which is necessary for binding of DNA onto column. The plasmid DNA remains in solution whereas the cell debris and protein precipitates and are removed. The plasmid was further purified using a column containing silica gel that binds DNA at high salt conditions, and elutes DNA in low salt conditions.

[L-Broth and L-agar were prepared by HGU technical staff and autoclaved and stored at 4°c until use.]

8.3. Cell culture and Protein assay

8.3.1. Protein manipulation

Maintenance of cells

The cell lines used in this thesis includes: NIH3T3 (mouse embryonic fibroblast cell line), HEK293 (human embryonic kidney cell line) and COS7 (African green monkey kidney cell line). Cells were maintained in conical flasks in Dulbecco's Modified Eagle's Medium (DMEM, Gibco Life Technologies) supplemented with 10% foetal calf serum (FCS, Sigma), 2% L-glutamine (30mg/ml), Penicillin and Streptomycin at 37°c in a well-ventilated and sterile tissue culture incubator with 5% CO_2. 1x Phosphate Buffered Saline (Dulbecco's PBS, Life Technologies), an isotonic saline solution was used for washing cells.

[28] L-Broth: (10.0g Tryptone + 5.0g Yeast extract + 10.0 NaCl + 1.0g Glucose) in 1litre H_2O.

Passaging cells

The cell density was monitored daily and passaged when the culture reached ~80% confluence. To passage cells, the growth medium was removed by aspiration and the cells were washed briefly with 1xPBS. The cells were then trypsinized for no longer than 4 mins in 5ml trypsin[29] - versene[30] solution at 37°c, followed by inactivation of trypsin was then inactivated by diluting in growth media. (For COS7 cells, cells were rinsed with versene prior to trypsinization.) The cell suspension was then diluted into desired amount in tissue culture flasks.

Preparation of frozen stock

To prepare frozen stock for long-term storage, cells were trypsinized and counted under a coverslip on a conventional hemacytometer viewed under the microscope. Cells were washed in 1xPBS, and resuspended to $1x10^6$ cells per ml of freezing medium[31]. Appropriate amount of cell suspension were then dispensed into 2ml cryovials and stored at -80°c overnight, before transferring to liquid nitrogen for long-term storage.

Protein extraction from tissue culture cells

200µl 1xPLB (passive lysis buffer) from Promega was added to 6-well plates, incubated at RT with shaking and scraping. The cell suspension was then centrifuged at 13000 rpm, for 10mins at 4°c. The supernatant was used for protein assay or stored at –80°c.

Transfection of DNA plasmids into cells

DNA plasmids were transfected into cells using Lipofectamine 2000 (Invitrogen) *as per* manufacturer's specifications. For a 6-well plate, 2µg of DNA plasmids (in no more than 4µl) was mixed with 100µl OPTIMEM (Gibco Life Technologies), and 6µl Lipofectamine was diluted in 100µl OPTIMEM and incubated at RT for 5mins. The 100µl DNA mixture and 100µl Lipofectamine were then mixed and incubated at RT for 20mins. At the end of the incubation, 800µl OPTIMEM was added to the mixture, before dispensing into the well containing cells of 80-95% confluence. The cells were incubated in the mixture for 4-5hrs before replacing with fresh growth medium.

---

[29] Trypsin (pH7.8): (1:250 Trypsin + 5.0ml Phenol Red + 0.06g Penicillin + 0.13g Streptomycin) in 1litre PBS.
[30] Versene: (10 Dulbeccos tablets + 0.4g sodium EDTA + 0.2% Phenol Red) in 1 litre H_2O.
[31] Freezing medium: 10% dimethyl sulfoxide (DMSO) in FCS.

For immunofluorescence, a coverslip was added in each 6-cell well prior to cell plating. The coverslips may be treated with 0.1% polylysine for 1hour to improve adhesion of cells to the coverslip.

Protein concentration measured using the Bio-Rad Bradford total protein assay

The bovine serum albumin (BSA) standard curve was set up at concentrations: 0, 5, 10, 20, 30, 40 and 50μg per ml of 20% Biorad assay solution. 5μl of protein extract was added to 1ml assay solution. The assay was run on GeneQuant, which uses the standard curve to determine the concentration according to the OD value. The concentration of the protein extract was then worked out (x200).

8.3.2. Western Blotting

Preparation of protein extracts

Protein extracts were diluted into 2μg/μl and 10μl of which was mixed with 10μl 2xSDS-PAGE (sodium dodecyl sulfate- polyacrylamide gel electrophoresis) loading buffer[32] that disrupts the disulfide bonds. The SDS disrupts the 2°, 3° and 4° structures and coats protein with negative charge. Sometimes, the protein was further denatured at 95°c for 2mins, and loaded onto the protein gel, alongside with 10μl Precision Plus protein Kaleidoscope size standard (Bio-rad) to determine the molecular weight of the protein in question.

Preparation for SDS-PAGE (sodium dodecyl sulfate- polyacrylamide gel electrophoresis)

The apparatus to hold gel was set up ready for the gel to be poured. The separating gel and stacking gel were prepared as follows. In both cases, Temed (TetraMethylenediamine) was only added immediately before pouring the gel because it activates the acrylamide monomers, causing them to begin the polymer chain reaction and crosslink randomly with the elongating polymer. This polymerisation takes place as soon as Temed is added. The protein is first sieved through the larger-pore stacking gel which tightening the protein band, followed by the separating gel which resolves negatively charged proteins by size.

---

[32] 2xSDS loading buffer: 1ml 1.5MTris (pH6.8) +600μl 20%SDS +3ml glycerol +1.5ml β-mercaptoethanol +0.2% bromophenol blue + up to 10ml H_2O. Stock and working solutions stored at –20°c and 4°c respectively.

12% Separating gel (10ml)	Stacking gel (5ml)
3ml Acrylamide (29:1)	0.5ml Acrylamide (29:1)
2.5ml 4xSeparating buffer[33]	1.25ml 4xStacking buffer[34]
4.4ml dH_2O	3.2ml dH_2O
100µl 10%APS (Ammonium Persulfate)	50µl 10%APS (Ammonium Persulfate)
18µl Temed	5µl Temed

Once the gel was set, it was placed in the tank in 1x Tris-glycine running buffer[35] (25mM Tris, 250mM Glycine, 0.1% SDS). After the samples and size standard were loaded on gel, it was run at 200V for about 40mins until the loading buffer is near the bottom of the gel.

Transfer and detection of protein

The resolved proteins were then transferred onto a polyvinylidene difluoride membrane (Hybond-P, Amersham Pharmacia Biotech) in a semi-dry blotter with minimal amount of cathode buffer (0.025M Tris pH9.4, 20% MeOH, 0.04M glycine)[36] for transferring protein.

Non-specific binding sites were blocked by incubating in 5% non-fat dry milk in 1xTBST [20mMTris-pH7.6, 150mM NaCl and 0.1% Tween20 (v/v)] for 30mins before probing with appropriate primary antibody in diluted in 5% non-fat dry milk in TBST for 1hr. After stringent wash in 1xTBST, the filter was incubated with the secondary antibody conjugated to horseradish peroxidase (HRP, Amersham) and detected using enhanced chemiluminescence substrate (ECL plus) Western blot detection system (Amersham Pharmacia Biotech). See Table 8.2. for primary and secondary antibody details.

Total proteins may also be visualised by staining with non-permanent Ponceau S solution (Sigma).

8.4. Animal Husbandry

All mice were maintained in the MRC Transgenic Unit in a specific pathogen free (SPF) environment and experiments were carried out under Home Office license. The *dep* mutants were maintained by either (het x het) or (hom x hom) cross. The morning of vaginal plug detection counted as embryonic day 0.5 (E0.5).

---

[33] 4x Separating buffer (1.5M Tris/HCl pH8.8): (18.2g Tris Base + 4ml 10% SDS) in 100ml H_2O adjusted to pH8.8.
[34] 4x Stacking buffer (0.5M Tris/HCl pH6.8): (6.1g Tris Base + 4ml 10% SDS) in 100ml H_2O adjusted to pH6.8.
[35] 5xTris-glycine buffer: (15.1g Tris Base +94g Glycine +50ml 10%SDS) up to 1 litre deionised H_2O.
[36] Cathode buffer: (6.25ml 1MTris pH9.4 + 50ml MeOH + 0.75g glycine) up to 250ml H_2O.

Crosses between *dep* heterozygotes were set up and skin samples were collected at weekly interval of up to 12 weeks. Earclips from all mice were collected for genotyping on weaning so that a set of wild-type, heterozygote and homozygote was collected for each timepoint. Comparison between *dep* and a control littermate is necessary due to the complicated breeding background of *dep* and the possible discrepancy in morphology as a result of strain difference. This also ensures that the animals are age-matched at every stage. For timepoints prior to 3 weeks of age, the whole litters were sacrificed to comply with the Home Office regulations regarding to live tissue collection.

8.5. Generation of Transgenic BAC Rescue line

8.5.1. Preparation of BAC transgenic constructs

(i) BAC clone

The BAC clone used in this study was supplied by BAC PAC Resources Center (BPRC) at the Children's Hospital Oakland Research Institute, CA. The clone is from the RP23 mouse BAC library, with clone number RP23-76J17, and is hosted by the *E.coli* DH10B strain. The plasmid contains a chloramphenicol resistant (Cm^R) gene, which can be selected for by growing cells in medium containing Cm. RP23-76J17 contains genomic region of mouse chr.4 of approximately 228kb. The candidate gene, *Zdhhc21*, and both ends of the BAC were sequenced to confirm the physical position of the clone. The clone includes an intact copy of *Zdhhc21*, and *Cer1*, which lies ~40kb upstream to *Zdhhc21*.

(ii) Generation of ΔCer1 BAC construct

In the first step, the targeted region of *Cer1* in RP23-76J17 was replaced with the zeocin resistant (zeoR) gene. In the second step, the zeoR gene was removed by treatment with FLP recombinase, leaving only 85bp of foreign DNA in the modified BAC (Figure 8.1.).

Bacterial strain: EL250 has an integrated λ prophage inserted in the bacterial genome. The prophage encodes the heat inducible recombination enzymes control of the λcl857 heat inducible promoter. The prophage also encodes FLP recombinase on the arabinose inducible pBAD promoter. Throughout the experiment, EL250 was maintained at 30°c because the prophage encodes toxic sequences that can be induced by heat in 40'. In EL250 the FLP is in the part of the prophage occupied by Tetracycline resistant (TetR) in DY380. This means there is no antibiotic selection for strain EL250.

Amplification primers for targeting *Cer1*: The *FRT-ZeoR-FRT* cassette used for targeting *Cer1* was amplified from plasmid pBSKGFPFRTzeoFRT with the following primers (698bp):

5'-cgactgtagccgtgCAGAGGGAGCCTCTCTTTTAGGCCCGTCCATCTGTGATCTTATCATGTCTGGATCAGATCC- 3'
5'-GCATCACCATCTTGACCACGGGGGTTGGGCTGGTGCAGTTCAGCATCAAGTGCCCAGCGCCCTCTGATCA- 3'.

These primers contain the 5' regions (the 50bp in gray) homologous to the flanking regions of the targeted *Cer1* sequence, and the 3' regions (20-25bp in blue) homologous to sequences in pBSKGFPFRTzeoFRT flanking the *FRT-ZeoR-FRT* cassette.

The PCR conditions used were as followed: 1.0mM Mg^{2+}, 0.4μM dNTPs, 0.2mM each primer, 150ng DNA in a 25μl reaction. Touchdown PCR was optimized to start from 64°c to 60°c for 15 cycles to minimize PCR-induced errors.

pBSKSGFPFRTzeoFRT was linearized with *Apa*I and *Sac*I, and cleaned up on Qiagen prior the PCR. The PCR products were further digested with *Not*I, *Sal*I and *Dpn*I to remove trace of intact plasmid. This step ensures that all zeoR colonies are the EL250 cells that contain BAC, but not the host bacteria of pBSKGFPFRTzeoFRT. Digested and amplified products were then purified using Qiaquick, and finally drop dialysed before being transfected into the EL250 cells.

Induction of λ recombination: Overnight EL250 culture containing the target BAC was grown from a single colony, diluted 40-fold in LB with Cm, and grown to an $OD_{600} = 0.4$ at 32°c (3-4hrs). The culture was then transferred into a 42°c shaking water bath at 200rpm (by hand) for 15'. This temperature induced production of the RED enzymes for recombination. After the 15-min induction, the culture was immediately placed on ice slurry to cool down.

Preparation of electroporation-competent cells: The culture was centrifuged at 3500rpm in Sorvall RT6000 (4°c for 15'); the cell pellet was then resuspended in ice-cold sterile water. This process was repeated twice before transferring into a 1.5ml Eppendorf tube and further centrifuged at 13k rpm for 2'. This preparation applies to (1) unmodified BAC transformation into EL250 cells [electro-competent EL250 cells provided by Peter Budd]. (2) PCR product of donor DNA containing *FRT-zeoR-FRT* cassette into BAC-containing EL250 cells.

Cell transformation: About 100ng in 1μl purified linear donor DNA (drop dialysed) is transferred into 50μl competent cells in a precooled electroporation cuvette using a Bio-Rad

gene pulser set at 2.5kV, 25μFD with a pulse controller set at 200 Ohms. The electroporated cells are immediately diluted with 1ml of LB medium and incubated at 32°c for 30' with shaking. The transformation is then plated on low salt LB with zeocin and chloramphenicol respectively. Six colonies from the Zeo plate are then transferred to 200ml low-salt LB (Zeo/Cm) from which maxipreps are made and subsequently amplified with primers flanking the targeted region to be deleted, or digested with several restriction enzymes and compare pattern with parent DNA to ensure that the right clones are selected and that rearrangement had not occurred.

The PCR primers flanking the target *Cer1* region were:

5'-tatgtgatgccccgactgta-3' (Cer1_KO_20mer-F)
5'-CGTCTTCACCATGCACTGAC-3' (Cer1_KO_20mer-R)

Arabinose Induction of FLP recombinase: Overnight EL250 culture containing the intermediate modified BAC [Figure 8.1(iv)] is grown from a fresh colony, diluted 50-fold with a concentration of 1% Arabinose and grown in LB (Cm) for 3 hrs with shaking. The culture is then spread in different dilutions on plate with Cm and grown overnight at 30°c. Ten colonies are selected and grid on both Chloramphenicol and low salt Zeocin plates. This method should identify colonies which have lost the zeoR gene, following induction of the FLP by arabinose (i.e. the colony should grow on Cm but not Zeo). The validated colony is then re-spread to single colony and maxiprep is prepared for further validation by sequencing.

8.5.2. Injection into mouse fertilised eggs[37]

The BAC was then linearised to minimise the amount of foreign DNA[38]. After linearization, the modified BAC transgene was microinjected individually into hundreds of male pronuclei in fertilised eggs. To detect BAC transgene integration, Southern blot analysis using a FRT probe or PCR using BAC-specific primers and primers flanking the *dep* deletion may be performed.

Female mice were superovulated with 2 gonadotrophins: PMS (Pregnant Mare's Serum) and hCG (human chorionic gonadotrophin) and mated to males. Zygotes were then dissected out of the oviduct a day after intravaginal plug is observed (i.e. 1-cell stage), at which point fertilised eggs are visible as a bulge in the oviduct. The cumulus was digested with hylauronidase and

[37] Microinjection/ transfer of embryos: all procedures performed by Margaret Keighren, HGU, MRC.
[38] Linearising BAC before microinjection: Abe and colleagues (Abe et al., 2004)reported a 3-fold reduction of transgene integration rate and fewer intact transgene integration when circular BAC DNA was injected.

removed. After dissection, the zygotes were recovered in the KSOM culture medium with CO2 supply at 37°c for 30mins. Embryos were then concentrated in droplets of injection medium FHM in oil, for ease of handling.

The microinjection apparatus were set up. Embryos were held by Vacutips (Eppendorf) with minimal suction and about 3μl of 2ng/μl constructs were injected into each pronucleus with the Femotips needles (Eppendorf). The injected embryos were cultured in KSOM medium to 2-cell stage and transferred to oviducts of pseudopregnant recipients.

Figure 8.1: Strategy for deleting *Cer1* in a BAC using prophage/ recombination
Step1 - The *FRT-zeoR-FRT* cassette (ii) is generated by PCR from plasmid pBSKGFPFRTzeoFRT (i) using recombination oligonucleotides which contains 50bp homology with the target BAC (iii).
Step2 – The target BAC clones are transfected into EL250 cells which are then induced for λ recombinase function at 42°c. These cells are made electroporation-competent and transfected with the amplified *FRT-zeoR-FRT* cassette (ii) by electorporation. Recombination occurs between the linear cassette and the target BAC, resulting an intermediate modified BAC (iv).
Step3 – The FLP recombinase is induced by arabinose to remove part of the *FRT-ZeoR-FRT* cassette, leaving about 85bp of foreign DNA (replacing the 2-kb *Cer1* sequence) in the final modified BAC (v).

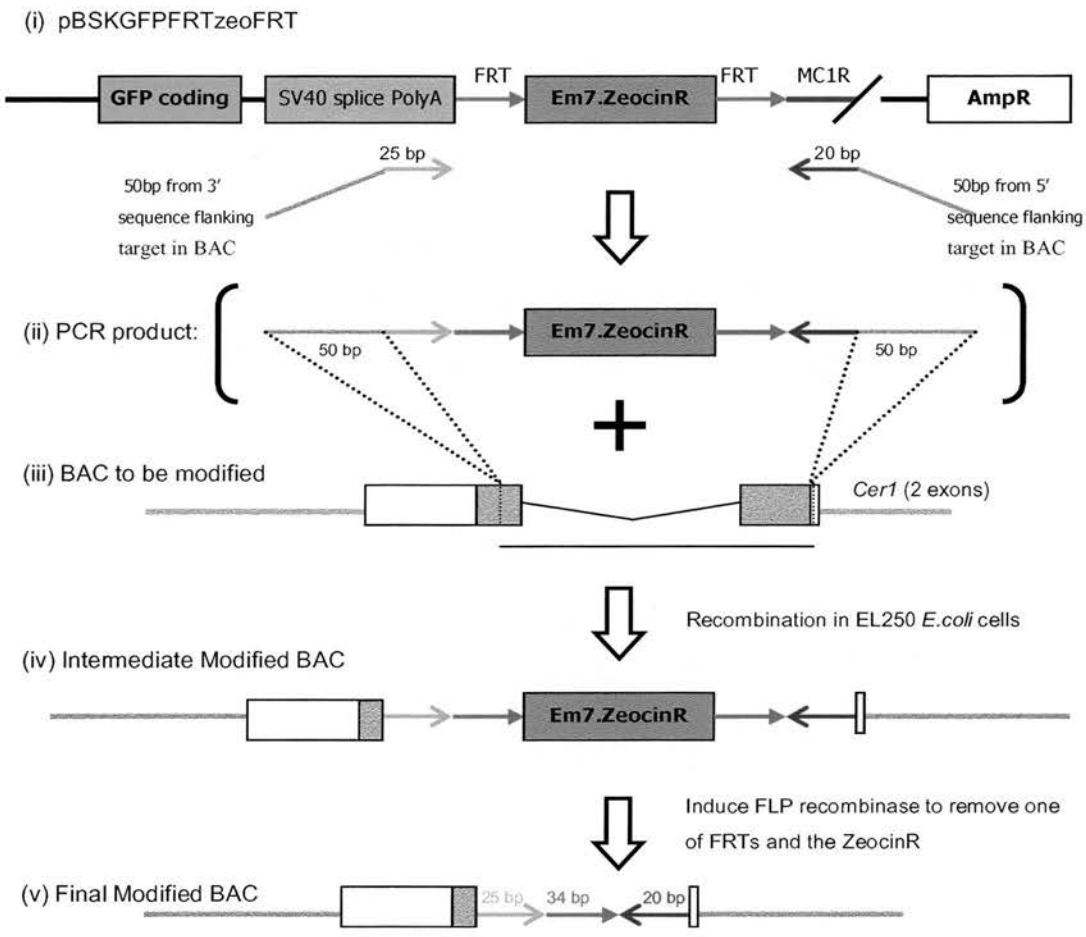

8.6. Screening ENU-DNA archive for Zdhhc21 mutations.

8.6.1. Screening for *Zdhhc21* alleles in the Harwell archive:

DNA source

DNA samples analysed in this screen include the original GSK-Harwell archive, which consists of twenty-four 96-well plates, and the "ethiologics" archive of better DNA quality that consists of 32 plates. In total, approximately 5300 F_1 ENU DNA samples were screened for possible substitution within *Zdhhc21* Exon3 and 4. DNA from F1 mice of C3H/HeH x BALB/c hybrids with the BALB/c male parent treated with ENU. All samples were obtained from Harwell MRC.

Primer design and exon choice

The 7 exons in *Zdhhc21* were sequenced in BALBc/C3H DNA to check for polymorphism. Exon 3 and exon 4 were selected on the basis of their size and predicted functional importance which may be more likely to impact the integrity and function of the protein (Figure 3.1C). Exon 3 contains the Znf_dhhc domain which is highly conserved across species; the domain extends to exon 4 which encodes for the third transmembrane domain.

PCR products for exon 3 and 4 are 257bp and 312bp in length; in which 112bp and 139bp are coding sequences respectively. In total, approximately 1.33Mb of coding sequence was screened. Primer sequences for exon3 and 4 are as follow:

```
5'FAM-GTCTGAGCATCCCTCGCT-3' (Zdhhc21-ex3F),
5'-GCTGACAGGTTCTCACTGTCTT-3' (Zdhhc21-ex3R);
5'FAM-TGATCCTGATGTGAGCATCTT-3' (Zdhhc21-ex4F),
5'-CCCGTAAAGCTCACTGGTGT- 3' (Zdhhc21-ex4R).
```

Conformation Sensitive Capillary Electrophoresis (CSCE)

According to a protocol previously optimized by Joanne Morgan (HGU, MRC). Mutation detection was performed on an ABI 3100 automated capillary DNA Sequencer that utilizes conformation sensitive capillary Electrophoresis (CSCE). DNA samples from 4 individuals were pooled (2.5µl of 5ng/µl DNA) giving a total of 50ng in the PCR reaction. Conditions for PCR were as followed: 200µM dNTPs, 1.5 mM MgCl2, 0.2µM forward and reverse primer, 1x Invitrogen buffer and 0.5 unit Taq (Invitrogen). PCR was carried out using the following

cycling conditions: 94°c for 15', 40cycles of [94°c for 30", annealing temperature at 55°c for 45", 72°c for 1']. The final extension at 72°c for 10'.

Heteroduplex formation

Following amplification, heteroduplexes were formed using the conditions: 96°c for 10', 72 cycles of [96°c for 20", decreasing temperature by 0.5°c per cycle], followed by 60°c for 30'. FAM used on ABI310 with Tamra350 size standard.

Re-derivation of mutant allele

Frozen sperm stocks were obtained from Harwell, and the mutation was re-derived by Brendan Doe (MRC Transgenic Unit, Edinburgh). The mutation was successfully rederived by intracytoplasmic sperm injection (ICSI), which involves direct injection of a single sperm into an oocyte to increase the chance of fertilization.

8.6.2. Optimizing PCR conditions for screening the RIKEN archive

The RIKEN archive consists for 10 000 DNA samples from F1-ENU mutagenised mice from a cross between C57BL/6 and DBA/2. Any polymorphism between the 2 strains was checked by sequencing, and avoided by re-designing PCR primers where possible.

The PCRs were optimized as 10µl reaction with Takara EX Taq® as follows:
10x buffer, 1.0µl; 50mM Mg^{2+}, 0.0µl[1.5mM], 0.1µl[2.0mM], 0.2µl[2.5mM], 0.3µl[3.0mM]; 2.5mM dNTPs, 0.8µl; 5µM F primer, 0.4µl; 5µM R primer, 0.4µl; 0.01µg/µl DNA, 1.0µl; Takara EX Taq, 0.05µl; and H_2O up to 10µl.

The PCR cycling conditions for each exon have been optimized as below; the annealing temperature for each primer pair is indicated in the below table.
5'@94°c => [30"@94°c, 30"@Tann, 1'@72°c] x 30cycles => 10'@72°c => 10'@4°c => END

Table 8.1. Optimised conditions for PCRs of *Zdhhc21* exons

Exon	Primers	Mg2+ (mM)	Tann (°c)	Coding (bp)	Product size	Polymorphism
1	TTCTCCCCAGGATTGTCTTG CTTCACAGAAGGTAATAATAC	2.5 - 3.0	50-55	154	239	Checked and avoided.
2	CCTGATAGATGTTGACTAAAATGC GAGTGCTTGCAACTGAAAACGG	2.0 - 2.5	55	99	335	Checked
3	GTCTGAGCATCCCTCGCT GCTGACAGGTTCTCACTGTCTT	1.5 - 2.5	55-58	112	257	Checked
4	TGATCCTGATGTGAGCATCTT CCCGTAAAGCTCACTGGTGT	1.5 - 2.5	55-58	139	312	Checked
5		N/a	N/a	117	N/a	1 coding SNP
6		N/a	N/a	44	N/a	Too many
7	AGCTGACTGAAGGGCACC AAAACCTGTAACGCATTTCCA	1.5 - 2.0	55-58	134	249	Checked

8.7. Zdhhc21 knockdown experiment using siRNA technology

Preparation of pDECAP-Zdhhc21expression vector

The vector was designed and constructed by Ian Smyth and Peter Budd in summer 2004, when the experiment was carried out for the first time. Single colonies were grown from frozen glycerol stock in SURE cells and purified using Quiagen DNA maxiprep DNA.

Generation of transgenic mice

The 2-kb fragment of pDECAP-Zdhhc21 was released from the background sequences by digesting the vector with *Bgl*II and *Bam*HI and cleaned up on Quiagen Quiaquick gel purification columns, re-run on LMP and concentrated on a PCR purification column. The fragment was further purified on Microcon and SpinX and microinjected into fertilised mouse oocytes and transferred into oviduct at one-cell stage.

Genotyping

The embryos or mice at appropriate stage were then typed by PCR amplified to detect the expression of both the forward and the reverse sequence as dsRNA, assuming that a hairpin structure is formed. The primers used are as follow (Figure 3.17):

(1) 5′-AAGAATTCAAACATCAGTGCATAGCAAG- 3′
(2) 5′-AATCTAGAAAGGTACCATGGGTCTTCGGATTCATTTG-3′
(3) 5′-AAGGTACCACATGGATGGGTCTTCGGATTCATT-3′
(4) 5′-AATCTAGAAAACATCAGTGCATAGCAAG-3′

If an embryo is positive for both fragments, dsRNA may have successfully expressed.

8.8. Genotyping Embryos and Mice

8.8.1. DNA extraction

Tail tip or ear clip samples were digested in 1.5 microfuge tubes at 55°c overnight in 500µl lysis buffer (50mM Tris, 100mM EDTA, 0.5%SDS)[39] with 0.2mg/ml proteinaseK (sigma). The following day, tubes were vortexed and centrifuged at full speed for 10mins, genomic DNA was then precipitated with 500µl isopropanol, washed with 70% EtOH and resuspended in appropriate amount of TE buffer.

8.8.2. Genotyping *dep* mutation

Breeding animals were genotyped by PCR amplification of Exon7 fragments from genomic DNA extracted from tail biopsies or ear clips. The exon7 of *Zdhhc21* is amplified by standard PCR (Tann 58°c, 1.5mM Mg^{2+}) using the following primers, one of which is labeled with a fluorescent tag: 5'FAM-AGCTGACTGAAGGGCACC3' (Exon7F) and 5'AAAACCTGTAACGCATTTCCA 3' (Exon7R), which yields a 249bp fragment.

The 3-bp deletion in *dep* was then detected on the ABI 310 genetic analyzer. The PCR fragments were first denatured in 70% formamide solution[40] at 95°c for 5mins to separate dsDNA into single strands, and were cooled immediate to 4°c to prevent re-annealing of unwound DNA. The samples were then run on the ABI 310 genetic analyzer which reads out the size difference of denatured fragment robustly.

8.8.3. Genotyping the Harwell L91F mutation

Standard PCR was performed using the following primer pair: 5'GTCTGAGCATCCCTCGCT-3' (Zdhhc21-ex3F), 5'-GCTGACAGGTTCTCACTGTCTT-3' (Zdhhc21-ex3R) which yields a fragment of 257bp. The 479C->T mutation disrupts a *Sac*I restriction site, which normally cut once at GAGCT^C and divide the 257bp PCR fragment into about 174bp and 83bp with 3' overhang. The mutant PCR fragment contains a mutation at the *Sac*I site and therefore remains uncut. This method allows rapid genotyping between wild-type, heterozygote and homozygote mice for the Harwell allele. 15µl of PCR product was cut in 2µl buffer with 10U(1µl) *Sac*I restriction endonuclease (Roche) in a 20µl reaction at 37°c, and visualized by electrophoresis.

---

[39] Tissue lysis buffer: (5ml 1MTris.HCl pH8 + 20ml 0.5MEDTA + 5M 10%SDS) up to 100ml ddH_2O.
[40] 70% formamide solution: 13.5µl deionised formamide (Sigma), 0.5µl Size standard (GeneScan–350 TAMRA); 4.0µl ddH_2O; 1µl diluted PCR product.

8.8.4. Genotyping of BAC transgenic litters

(i) Distinguishing between homozygotes and heterozygotes

In the case where the BAC construct was microinjected into heterozygous embryos between *dep* and F1 (C57/CBA), the homozygotes and heterozygotes of the resulting progeny were genotyped by the proximal and distal sputnik markers immediately flanking the BAC region. Sputnik markers from genomic DNA were developed using the Sputnik program[41] to spot tandem repeat motifs.

The proximal sputnik marker (274bp) was amplified by:

```
5'CTGCTTCTCAAAAGCCAAGG-3'  (prox138F)
5'CCTGGAAAGCAGTAGCCATC-3'  (prox138R)
```

The distal sputnik marker (389bp) was amplified by:

```
5'GGCTTGAACTGGTGGAGAAA-3'  (dis145F)
5'GCCCAGCTTTAGGCTGTAGA-3'  (dis145R)
```

(ii) Genotyping the BAC transgene

The presence of the BAC transgene in the genome was genotyped by 3 markers, including the CmR marker which is specific to the plasmid, and two markers at both ends of the BAC region, amplifying the borders between the BAC carrier plasmid and the BAC genomic region.

The primers used for amplifying the CmR gene from the BAC-containing plasmid were:

```
5'TCCATGAGCAAACTGAAACG-3'  (CmR-F)
5'CATGATGAACCTGAATCGCC-3'  (CmR-R)
```

The primers used for amplifying the proximal end of the BAC clone was:

```
5'TAATACGACTCACTATAGGG-3'(T7-L348)
5'GAGCTTCATGTATGTCCTT-3'  (76J17-3'Rii)
```

The primers used for amplifying the distal end of the BAC clone was:

```
5'TATTTAGGTGACACTATAG-3'  (SP6)
5'GCAACTTGTAACTTGGGTAT-3'  (76J17-5'Ri)
```

Out of the 3 markers, the BAC end markers were more reliable at typing incorporation of the BAC transgene. The CmR marker often resulted in false positives.

[41] Sputnik program: http://espressosoftware.com/pages/sputnik.jsp

8.9. Detailed phenotypic analysis of dep

8.9.1. Preparation of samples

(a) Processing and Sectioning

After dissection, skin samples were fixed in 4% PFA for several hours depending on the age of sample. Samples for cryostat sectioning were fixed for a minimal of 1 hour and cryo-protected in 30% sucrose overnight before embedded in optimal cutting temperature (OCT, Raymond A Lamb) compound on dry ice. Samples for paraffin embedding were fixed for longer and dehydrated through a graded EtOH series of 30%(1hr), 50%(1hr), 70%(1hr), 95%(2hr x3) and 100%EtOH (1hr x2).

The samples were placed in a cassette and flanked by biopsy pads then processed as follows:
50%EtOH +50%Xylene (15')
Xylene (40' x2)
50%xylene +50%Wax (30', @60°c)
Wax (45' x2, 120' x1, @60°c).
After processing, the skin samples were embedded in wax at stored at 4°c until sectioning. Sections of 5-6μm were cut on a microtome and collected on SuperFrost® Plus silanized slides.

For cryosections, frozen samples were stored at -80°c until sectioning on a cryostat microtome. The cryosections were allowed to come to RT and post-fixed in -20°c acetone for 10' before subsequent experiments.

(b) Tail epidermis preparation

Whole tail was cut off from the mouse, and the skin is subsequently peeled off from the bone and connective tissue. The skin was then put in 5mM EDTA in 1xPBS and incubated at 37°c for 4 hours, after which the epidermis can be easily separated from dermis using watchman forceps to expose the follicles underneath the epidermal layer. The epidermis/ follicles were then fixed in 4% PFA for a few hours, dehydrated through EtOH series, and stored at 4°c until required.

(c) Preparation of whole-mount hair slide

Hairs were plucked from the upper back of the mouse, and use glycerol as a mounting medium with a refractive index similar to that of glass will be used so as to maximize the microscopic lighting.

8.9.2. Hematoxylin and Eosin (H & E) staining

Sections of 6μm were stained with haematoxylin and eosin (H&E) stain for initial analysis. Hematocylin stains cytoplasm and acidophilic structure red. Eosin stains nuclei and other basophilic structure blue.

Paraffin sections were dewaxed with xylene (2x5'), then washed in 100%EtOH (2x5') and hydrated in decreasing EtOH series of 90%, 70%, 50% and 30% (2' each), followed by a final wash in dH_2O.

Slides were stained in haematoxylin for 4-5mins, and differentiated in acid/ alcohol (1%HCl in 70%MeOH) for a few seconds. The sections were then blued up in saturated Lithium Carbonate ($LiCO_3$) for a few seconds. For eosin staining, sections were incubated in eosin stain[42] for 1-5mins depending on the thickness of sections. Each step described is followed by thorough wash under tap water.

After stringent wash in water, the sections were then washed in 100%EtOH (2x2'), and hydrated through an increasing series of EtOH (2'each). Slides were then cleared in xylene (3x5') and mounted in DePex mounting medium (BDH).

8.9.3. Immunohistochemistry (IHC) and Immunocytochemistry (ICC)

All steps were performed at room temperature (RT) unless otherwise stated.
Paraffin sections were dewaxed in xylene twice for 30' and 15', and subsequently hydrated through EtOH series: 100% x2, 90%, 70%, 50% and 30%, followed by washes in 1 X TBST[43] (15'x3).

---

[42] Eosin stain: (3parts 1% aqueous Eosin + 1part 1% EtOH). Acetic acid added to a final concentration of 0.05%.
[43] 1xTBST (0.01% Triton-X) - 1ml 10% Triton-X and 100ml 10xTBS into 900ml Ultrapure water.
10xTBS - 385ml 1M Tris.HCl, 13.9g Tris Base (Trizma), 87.66g NaCl into 1L in ultrapure H_2O, adjusted to pH7.6-7.8, autoclaved. 10% Triton-X - 5g Triton in 50ml Ultrapure H_2O. Heat at 65°c to dissolve if necessary. Sterilize by filtering through 0.22μm filter using a 60ml syringe.

For sections that will be labelled with Horseradish Peroxidase (HRP), endogenous peroxidase was quenched to avoid background staining: sections were incubated in a hydrogen peroxide solution (3% H_2O_2/ 10% MeOH/ 1xTBST) for 30mins, followed by washes in 1xTBST (15'x3).

For successful immunostaining, *antigen retrieval* was carried out to denature any protein folding or other cellular component around the antigen. This technique was especially applicable for paraffin-embedded sections. Cryostat sections were exempted from this step because of their fragility that makes them easily destroyed by heat. Sections were heated in 1mM EDTA solution adjusted to ph7.5-8.0[44], or in citrate buffer (1.8mM citrate acid and 8.2mM sodium citrate solution)[45] for about 30mins depending on the antigen, during which the power was monitored and adjusted intermittently to avoid sections being boiled off from the slides. The slides were then cooled for at least 30mins before washing in 1x TBST for 15mins (x3).

Slides were then blocked in 10% donkey serum[46] (Sigma) (or against host of secondary antibody) in 1 x TBST for 1 hour, followed by washes in 1xTBST (5'x3). Primary antibodies (1° Ab) diluted in 5% donkey serum were then added onto slides and incubated overnight at 4°c in humidified chamber.

After washes in 1xTBST (15'x3), secondary antibodies (2° Ab) diluted in 5% donkey serum was added and incubated for 1 hour, followed by stringent washes in 1xTBST (3x15'). [Biotinylated 2° Ab was used for colormetric reaction.]

[Following 2°Ab incubation, ABC substrate [HRP-streptavidin, Vectorstain Elite avidin-biotinylated protein complex (ABC) kit] was added to slides and incubated for 30min in humidified chamber. After brief washes (2x5'), appropriate color substrate was added (Nova-red, Vector Lab, which produces a red precipitate). The reaction was closely monitored under light microscope and stopped in water when the signal to noise ratio is optimal.]
For fluorescent labeled staining, samples were co-stained with DAPI (4'6-Diamidino-2-phenyl-indole) which counterstains DNA in the nuclei. For colourmetric reactions, 0.01% light green was used for counterstain.

---

[44] 1mM EDTA solution (1ml 0.5M EDTA in 500ml ddH_2O).
[45] Citrate Buffer (9ml 0.1M citric acid solution + 41ml 0.1M sodium citrate solution + 450ml ddH_2O, adjusted to pH6)
[46] Donkey serum (from Sigma) – heat inactivated at 65°c for 30mins before use.

After brief washes, fluorescent slides were mounted in Vectashield (H-1000) mounting medium, and the edges were sealed with clear nail polish. [The colormetrically sections were then dehydrated through EtOH series and then into Xylene, which allows slides to be mounted in the xylene-soluble, non-aqueous DePex mounting medium (BDH), and have a longer-lasting conserving effect on the stain.]

The advantage of using the ABC kit is that it enhances response to signal, and that it allows sections to be permanent mounted in a non-aqueous mounting media. Furthermore, it enables control over the intensity of signal by close observation. The drawback is that double labeling (counter-staining) with another antibody may be difficult and that it limits the possibility of improving image presentation using graphics editor.

8.9.4. Antibodies used for analysis

Table 8.2. List of antibodies used for *dep* analysis

Antigen	Clone Name	Host Species	Dilution
AE13	T.T.Sun lab	Mouse	IHC 1:10 (serum)
AE15	T.T.Sun lab	Mouse Ig	IHC 1:2 (serum)
Brdu	BUI/75 (Abcam)	Rat	IHC 1:100
Brdu	B44 (BD)	Mouse IgG1	IHC 1:50
Brdu	BU-33 (Sigma)	Mouse IgG1	IHC 1:400 (not work)
β-catenin	15B8 (Sigma)	Mouse IgG1	IHC 1:500
β-catenin	(Sigma C2206)	Rabbit	IHC 1:2000
β-galactosidase			IHC
Cleaved Caspase3 (Asp175)	(Cell Signaling)	Rabbit IgG	IHC
c-myc	9E10 (Sigma)	Mouse	IHC 1:200 (not work)
GATA3	HG3-31	Mouse	IHC 1:75
Gm130	35 (BD)	Mouse IgG1	ICC 1:200
Grp78	(Stressgen)	Rabbit	IHC 1:500
HA	(Upstate)	Mouse IgG3	WB 1:400 IF 1:200
HA	(Sigma)	Rabbit	IF 1:25
K5	(Covance)	Rabbit	IHC1:1000
Mouse keratin 6 (MK6)	(Covance)	Rabbit	1:500
Mouse keratin 10 (MK10)	(Covance)	Rabbit	IHC
Ki67	TEC-3 (DakoCyto)	Rat	IHC 1:50
Lef1[47]	Grosschedl lab	Rabbit	IHC 1:500
P63	BC4A4	Mouse	IHC 1:50
Phosphohistone H3 (Ser10)	P04H3	Rabbit	IHC 1:50
Lck	3A5 (Chemicon)	Mouse IgG2bk	WB 1:600
N-dhhc21- custom made by Eurogentec	GRLPENPKIPHAE RE	Rabbit	WB 1:500, ICC, IHC[48] 1:100

[47] Lef1 antibody was provided by Prof. Rudolf Grosschedl, Max-Planck Institute of Immunobiology.
[48] IHC using the purified N-Dhhc21 antibody requires citrate buffer treatment for antigen retrieval.

The 2° Abs used for Western blotting were:
ECL α-Mouse IgG, Horseradish Peroxidase-conjugated (sheep), 1:10000 (GE Healthcare UK Limited).
ECL α-Rabbit IgG, Horseradish Peroxidase-conjugated (sheep), 1:10000 (GE Healthcare UK Limited).

The 2° Abs used for IHC and ICC were:
Rhodamine (TRITC)-conjugated (donkey) α-Rabbit IgG (Jackson Immunoresearch Lab)
FITC-conjugated (donkey) α-Mouse IgG 1:250 (Jackson Immunoresearch Lab)
Alexa 488 (donkey) α-Mouse IgG 1:500 (Invitrogen – Molecular Probes)
Alexa 594 (donkey) α-Rabbit IgG 1:2000 (Invitrogen – Molecular Probes)
Alexa 488 (donkey) α-Rat IgG 1:500 (Invitrogen – Molecular Probes)
Biotin-conjugated (donkey) α-Rabbit IgG 1:400 (Jackson Immunoresearch Lab)

8.9.5. Alkaline Phosphatase (AP) Staining

Vector® Red Alkaline Phosphatase substrate kit (Vector Labs) was used according to manufacturer's instructions. Two drops of Reagent 1 was added to 5ml AP substrate buffer (100mM Tris.HCl pH8.2-8.5) and mixed well. Two drops of Reagent 2 and 3 were subsequently added to the buffer respectively and mixed in between. The sections were incubated with AP substrate solution at RT and monitored under a light microscope. The substrate also produce a highly fluorescent, bright red precipitate when viewed with rhodamine excitation and emission filter system. When suitable staining develops, the reaction was stopped by washing sections in buffer for 5mins, followed by brief wash in water. The sections were then dehydrated with increasing series of EtOH concentrations, cleared in xylene and mounted in DePex mounting media (BDH).

8.9.6. RNA *in-situ* hybridisation

*All solutions used for hybridization or prior to hybridisation were treated with (or made from solutions treated with) diethyl pyrocarbonate (DEPC[49], Sigma), which is a strong inhibitor of RNases.
*RNaseZap® (Ambion) was also used to remove RNase contamination on work surface and equipment.

Making Zdhhc21 RNA probes for in-situ *hybridisation*

The *Zdhhc21* cDNA transcript was generated by RT-PCR from E12.5 RNA using the Promega Access RT-PCR kit. The cDNA product (747-bp) was then cloned into pGEM-T and grown on L-Amp plate. A single colony was grown into an overnight culture of 200ml LB + Amp at 37°c and purified by the Qiagen® maxiprep kit. The RT-PCR primers used are as follows: `5'-CATGGGCTTGATTGTCTTTGT-3'(F)` and `5' -ACGTGATTGGCAAAGTGGTAG-3'(R)`. The insert is orientated by direct sequencing using T7 and Sp6 primers.

[49] Depc treatment: depc was added to solutions (0.1% depc), left in fume hood overnight and autoclaved by heat.

Preparing RNA probes from existing plasmids

RNA probes were made from the following plasmids. The restriction endonuclease used for linearising and the RNA polymerase used for probe labeling are also indicated:

Plasmid	Probe	Linearising enzyme	RNA polymerase
pBSKS(+)-Zd21	*Zdhhc21* (α-S)	*Spe*I	T7
pBSKS(+)-Zd21	*Zdhhc21* (sense)	*Hind*III	T3
PBluescriptII KS_M_shh_16.1	*Shh* (α-S)	*Hind*III	T3
pBluescriptII KS.Gli1.#58	*Gli1* (α-S)	*Not*I	T3
pBluescriptII KS_ptch1	*Ptc1* (α-S)	*Bam*HI	T3
'HK15'	*HK15* (α-S)	*Spe*I	T7
pBS-HK17-3'UTR	*HK17* (α-S)	*Eco*RI	T3

Plasmids for the following probes: *Shh*, *Gli1*, *Ptc1*, *HK15*, and *HK17* were provided by Dr. Pleasantine Mill (Mill et al., 2003).

The following labeling reactions were set up to label riboprobes with digoxygenin (DIG) and incubated at 37°c for 2hrs:

2µl 10x transcription buffer
2µl 10x Dig RNA labeling mix (Roche)
1µl RNase inhibitor (Promega)
2µl RNA polymerase (T7 or T3)
1µl linearized template DNA (1µg/µl)
10.5µl ddH_2O (depc-treated)

2µl RNase-free DNaseI was added and incubated at 37°c for 2hrs to remove template DNA. The reaction was stopped by added 2µl 0.2M EDTA (pH8).

RNA was precipitated with 2.5µl 4MLiCl and 75µl -20°c chilled 100%EtOH, incubated at -80°c for at least 30mins. It was then centrifuged at full speed for 15' at 4°c, and washed with 70%EtOH. The pellet was resuspended in 110µl depc-treated H_2O and stored in aliquots at -80°c.

Preparation of slides for RNA in-situ hybridisation

Prior to hybridization, the sections were deparaffined in xylene, rehydrated in decreasing series of EtOH concentrations, treated for 30mins with 20µg/ml proteinaseK prewarmed to 37°c, acetylated for 10mins in 0.1M triethanolamine (TEA)/ 0.25% acetic anhydride solution[50], dehydrated in increasing series of EtOH concentration and air dried.

[50] 0.1M TEA/0.25% acetic anhydride: (1ml 5M NaOH +10ml 100%TEA +1.5ml acetic anhydride) up to 500ml ddH_2O.

RNA in-situ hybridisation

About 5-8µl labeled probes in 200µl hybridization buffer[51] were denatured at 85°c for 10mins, and applied to each slide and incubated in humidified chamber[52] at 55°c overnight.

Post-hybridisation

The slides were washed at 60°c in decreasing concentrations of SSC buffer (5x, 2x, 0.2x, each for 15' x2). Slides were then blocked in 1xblocking reagent (Roche) in 1xTBST for 1hour, and the hybridised probes were detected with sheep α-digoxigenin antibody (Roche), conjugated to AP (1hour). Unreacted conjugate was removed by washing in 2mM Levamisole in 1xTBST (2x15') with agitation. Sections were equilibrated in APB buffer[53] for 15' before addition of the BM Purple colour substrate (Boehringer Mannheim), which contains BCIP that is oxidized by AP to indigo, and NBT that is reduced, as a result forms a dark blue precipitate.

Stop colour reaction and mounting

The slides were closely monitored under light microscope and the color development was stopped in ddH_2O when sufficient signal has developed (i.e. optimal ratio of signal:noise). The slides were then dehydrated with increasing concentration of EtOH, cleared in xylene and mounted with Depex mounting media (BDH).

8.10. Palmitoylation Assay

8.10.1. [^{3}H] palmitate labelling

Metabolic labeling with [^{3}H] palmitate was carried out by Masaki Fukata as a collaboration; and the protocol was described in Methods (Fukata et al., 2006). Very briefly, NIH3T3 cells were labeled with [^{3}H] palmitate by a 4hr-incubation with 0.25-0.5mCi [^{3}H] palmitate diluted in DMEM supplemented with BSA. Total proteins were then extracted and resolved by SDS-PAGE. The gel was fixed in isopropanol: H_2O: acetic acid (25:65:10) and subjected to fluorography for at least 24hr.

---

[51] Hybridisation buffer: 50% distilled formamide, 5xSSCpH4.5, 1%SDS, 50µg/ml yeast tRNA and 100µg/ml heparin.
[52] Chamber buffer (5xSSC pH4.5/ 50% formamide).
[53] APB buffer: (20ml $MgCl_2$ +20ml 2MTris pH9.5 +8ml 5MNaCl +4ml 10%Tween20 +600µl 2M levamisole) up to 400ml with ddH_2O.

8.10.2. Acyl-Biotinyl Exchange (ABE) chemistry

(i) Preparation of expression plasmids

The mammalian expression plasmid pcDNA3-Lck was provided by Masaki Fukata (originated from Dr. Arthur Weiss, UCSF), based on GenBank Accession no. M12056.
The mammalian expression vector of wild-type Zdhhc21, pEFBos-HA-Zdhhc-21 (with EF1-alpha promoter), was provided by Masaki Fukata. It was then modified by using the QuikChange® Site-Directed Mutagenesis Kit (Stratagene), to introduce single nucleotide changes for the following *Zdhhc21* alleles: L91F, C95S and C106S. The *dep* mutation, del-233F, was modified from pEFBos-HA-Zdhhc-21 by subcloning *dep* cDNA (by RT-PCR) into the *Bam*HI sites flanking the insert (by Peter Budd).
The primers used for sequencing the insert were:

```
5'CTCAgACAgTggTTCAAAgT-3' (pEF-Bos-5')
5'TgggAgACCTgATACTCTCA-3' (pEF-Bos-3')
```

(ii) ABE protocol

All buffers were added with the serine protease inhibitor, phenylmethylsulphonyl fluoride (PMSF) to a final concentration of 50µg/µl.

Harvesting proteins and NEM treatment
NIH3T3 cells were co-transfected with 2µg of PAT (Dhhc21) and substrate (Lck) expression vectors as described in Section 8.3.1. Transfected cells were washed twice in 1xPBS/ 10mM NEM, briefly resuspended in 100µl 1% SDS/ 10mM NEM/ LB[54] (RT, 5'), and solubilized with addition of 900µl 2% Triton/ 10mM NEM/ LB. The mixture was then rotated for at 4°c for 1hr, and centrifuged at 13000rpm (4°c, 10'). Protein was precipitated from the supernatant by the chloroform-methanol (CM) method[55] (Wessel and Flugge, 1984). Precipitated protein was resolubilized and denatured with 200µl of 10mM NEM/ SB[56] (37°c, 10'), and diluted with 800µl 0.2% Triton/ 1mM NEM/ LB. The supernatant was transferred into 1.5ml tube and rotated at 4°c overnight.

[54] LB (lysis buffer): 50mM Tris/HCl pH7.5, 5mM EDTA, 50mM NaCl.
[55] CM precipitation: samples were transferred into 15ml Corning centrifuge tubes before each precipitation. All other steps were performed in 1.5ml centrifuge tubes.
[56] SB (solubilization buffer): 4%SDS, 50mM Tris/HCl pH7.5, 5mM EDTA.

Hydroxylamine treatment and biotin labeling

The next day, NEM was removed by three sequential CM precipitations, after each precipitation the protein was resolubilized in 200µl (37°C, 10'), and divided into 2 portions to be treated with or without hydroxylamine with rotation (RT, 1hr):
800µl of 1M Hydroxylamine pH7.4/150mM NaCl/ 0.2% Triton/ 1mM Biotin-HPDP (Pierce).
800µl of 1M Tris pH7.4/ 150mM NaCl/ 0.2% Triton/ 1mM Biotin-HPDP.

Both samples were then CM precipitated, dissolved in 100µl TB[57], diluted in 900µl 0.2% Triton/ 0.2% SDS/ LB, and rotated at 4°c for 30mins. Following full-speed centrifugation (4°c, 3') to remove particulates, samples were incubated 30µl streptavidin-agarose (Pierce) with rotation (4°c, overnight).

Unbound proteins were removed from the beads by 3 washes with 1ml 0.1% SDS/ 0.2% Triton/ LB; and the bound proteins were eluted through cleavage of the cysteine-biotin disulfide linkage with 200µl of 1xSDS/ 10mM DTT (37°c, 15mins).

[57] TB: 2% SDS, 50mM Tris/HCl pH7.5, 5mM EDTA.

Chapter 9 – References

1. **Abe,K., Hazama,M., Katoh,H., Yamamura,K., and Suzuki,M.** (2004). Establishment of an efficient BAC transgenesis protocol and its application to functional characterization of the mouse Brachyury locus. *Exp. Anim* **53,** 311-320.

2. **Acconcia,F., Ascenzi,P., Bocedi,A., Spisni,E., Tomasi,V., Trentalance,A., Visca,P., and Marino,M.** (2005). Palmitoylation-dependent Estrogen Receptor {alpha} Membrane Localization: Regulation by 17{beta}-Estradiol. *Mol. Biol. Cell* **16,** 231-237.

3. **Allen,T. and Potten,C.** (1974) Fine-structural identification and organization of epidermal proliferative unit. Journal of Cell Science 15[2], 291-319.

4. **Andl,T., Reddy,S.T., Gaddapara,T., and Millar,S.E.** (2002). WNT signals are required for the initiation of hair follicle development. *Dev. Cell* **2,** 643-653.

5. **Arnold,I. and Watt,F.M.** (2001). c-Myc activation in transgenic mouse epidermis results in mobilization of stem cells and differentiation of their progeny. *Curr. Biol* **11,** 558-568.

6. **Ashurst,J.L., Chen,C.K., Gilbert,J.G., Jekosch,K., Keenan,S., Meidl,P., Searle,S.M., Stalker,J., Storey,R., Trevanion,S. et al.** (2005). The Vertebrate Genome Annotation (Vega) database. *Nucleic Acids Res.* **33,** D459-D465.

7. **Barolo,S.** (2006). Transgenic Wnt/TCF pathway reporters: all you need is Lef? *Oncogene* **25,** 7505-7511.

8. **Bell,J.A., Rinchik,E.M., Raymond,S., Suffolk,R., and Jackson,I.J.** (1995). A high-resolution map of the brown (b, Tyrp1) deletion complex of mouse chromosome 4. *Mamm. Genome* **6,** 389-395.

9. **Benitah,S.A., Frye,M., Glogauer,M., and Watt,F.M.** (2005). Stem cell depletion through epidermal deletion of Rac1. *Science* **309,** 933-935.

10. **Bennett,D.C., Huszar,D., Laipis,P.J., Jaenisch,R., and Jackson,I.J.** (1990). Phenotypic rescue of mutant brown melanocytes by a retrovirus carrying a wild-type tyrosinase-related protein gene. *Development* **110,** 471-475.

11. **Blanpain,C. and Fuchs,E.** (2007). p63: revving up epithelial stem-cell potential. *Nat Cell Biol* **9,** 731-733.

12. **Botchkarev,V.A., Botchkareva,N.V., Nakamura,M., Huber,O., Funa,K., Lauster,R. et al.** (2001) Noggin is required for induction of the hair follicle growth phase in postnatal skin. The FASEB Journal 15[12], 2205-2214.

13. **Braun,K.M., Niemann,C., Jensen,U.B., Sundberg,J.P., Silva-Vargas,V., and Watt,F.M.** (2003). Manipulation of stem cell proliferation and lineage commitment: visualisation of label-retaining cells in wholemounts of mouse epidermis. *Development* **130,** 5241-5255.

14. **Brown,S.D., Chambon,P., and de Angelis,M.H.** (2005). EMPReSS: standardized phenotype screens for functional annotation of the mouse genome. *Nat Genet.* **37,** 1155.

15. **Bull,J.J., Pelengaris,S., Hendrix,S., Chronnell,C.M., Khan,M., and Philpott,M.P.** (2005). Ectopic expression of c-Myc in the skin affects the hair growth cycle and causes an enlargement of the sebaceous gland. *Br. J. Dermatol.* **152,** 1125-1133.

16. **Cadinanos,J. and Bradley,A.** (2007). Generation of an inducible and optimized piggyBac transposon system. *Nucleic Acids Res.* **35,** e87.

17. **Carroll,J.M., Romero,M.R., and Watt,F.M.** (1995). Suprabasal integrin expression in the epidermis of transgenic mice results in developmental defects and a phenotype resembling psoriasis. *Cell* **83,** 957-968.

18. **Clayton,E., Doupe,D.P., Klein,A.M., Winton,D.J., Simons,B.D., and Jones,P.H.** (2007). A single type of progenitor cell maintains normal epidermis. *Nature* **446,** 185-189.

19. **Clevers,H.** (2006). Wnt/beta-catenin signaling in development and disease. *Cell* **127,** 469-480.

20. **Coghill,E.L., Hugill,A., Parkinson,N., Davison,C., Glenister,P., Clements,S., Hunter,J., Cox,R.D., and Brown,S.D.** (2002). A gene-driven approach to the identification of ENU mutants in the mouse. *Nat Genet.* **30,** 255-256.

21. **Conti,F.J., Rudling,R.J., Robson,A., and Hodivala-Dilke,K.M.** (2003). alpha3beta1-integrin regulates hair follicle but not interfollicular morphogenesis in adult epidermis. *J. Cell Sci.* **116,** 2737-2747.

22. **Copeland,N.G., Jenkins,N.A., and Court DL** (2001). Recombineering: a powerful new tool for mouse functional genomics. *Nat Rev Genet.* **2,** 769-779.

23. **Coudreuse,D. and Korswagen,H.C.** (2007). The making of Wnt: new insights into Wnt maturation, sorting and secretion. *Development* **134,** 3-12.

24. **DasGupta,R. and Fuchs,E.** (1999). Multiple roles for activated LEF/TCF transcription complexes during hair follicle development and differentiation. *Development* **126,** 4557-4568.

25. **DasGupta,R., Rhee,H., and Fuchs,E.** (2002). A developmental conundrum: a stabilized form of beta-catenin lacking the transcriptional activation domain triggers features of hair cell fate in epidermal cells and epidermal cell fate in hair follicle cells. *J. Cell Biol.* **158,** 331-344.

26. **Davis,A.P. and Justice,M.J.** (1998). An Oak Ridge legacy: the specific locus test and its role in mouse mutagenesis. *Genetics* **148,** 7-12.

27. **Denning,G.M., Anderson,M.P., Amara,J.F., Marshall,J., Smith,A.E., and Welsh,M.J.** (1992). Processing of mutant cystic fibrosis transmembrane conductance regulator is temperature-sensitive. *Nature* **358,** 761-764.

28. **Di-Poi,N., Michalik,L., Desvergne,B., and Wahli,W.** (2004). Functions of peroxisome proliferator-activated receptors (PPAR) in skin homeostasis. *Lipids* **39,** 1093-1099.

29. **Drisdel,R.C. and Green,W.N.** (2004). Labeling and quantifying sites of protein palmitoylation. *Biotechniques* **36,** 276-285.

30. **Dupuy,A.J., Jenkins,N.A., and Copeland,N.G.** (2006). Sleeping beauty: a novel cancer gene discovery tool. *Hum. Mol. Genet.* **15 Spec No 1,** R75-R79.

31. **Edmondson,S.R., Thumiger,S.P., Werther,G.A., and Wraight,C.J.** (2003). Epidermal homeostasis: the role of the growth hormone and insulin-like growth factor systems. *Endocr. Rev* **24,** 737-764.

32. **Fernandez-Hernando,C., Fukata,M., Bernatchez,P.N., Fukata,Y., Lin,M.I., Bredt,D.S., and Sessa,W.C.** (2006). Identification of Golgi-localized acyl transferases that palmitoylate and regulate endothelial nitric oxide synthase. *J. Cell Biol.* **174,** 369-377.

33. **Fleming,J., Rogers,M.J., Brown,S.D., and Steel,K.P.** (1994). Linkage analysis of the whirler deafness gene on mouse chromosome 4. *Genomics* **21,** 42-48.

34. **Friedel,R.H., Seisenberger,C., Kaloff,C., and Wurst,W.** (2007). EUCOMM the European Conditional Mouse Mutagenesis Program. *Brief. Funct. Genomic. Proteomic.* **6,** 180-185.

35. **Frye,M., Gardner,C., Li,E.R., Arnold,I., and Watt,F.M.** (2003). Evidence that Myc activation depletes the epidermal stem cell compartment by modulating adhesive interactions with the local microenvironment. *Development* **130,** 2793-2808.

36. **Fuchs,E.** (2007). Scratching the surface of skin development. *Nature* **445,** 834-842.

37. **Fuchs,E., Merrill,B.J., Jamora,C., and DasGupta,R.** (2001). At the roots of a never-ending cycle. *Dev. Cell* **1,** 13-25.

38. **Fuchs,E. and Raghavan,S.** (2002). Getting under the skin of epidermal morphogenesis. *Nat. Rev. Genet.* **3,** 199-209.

39. **Fukata,M., Fukata,Y., Adesnik,H., Nicoll,R.A., and Bredt,D.S.** (2004). Identification of PSD-95 palmitoylating enzymes. *Neuron* **44,** 987-996.

40. **Fukata,Y., Iwanaga,T., and Fukata,M.** (2006). Systematic screening for palmitoyl transferase activity of the DHHC protein family in mammalian cells. *Methods* **40,** 177-182.

41. **Gat,U., DasGupta,R., Degenstein,L., and Fuchs,E.** (1998). De Novo hair follicle morphogenesis and hair tumors in mice expressing a truncated beta-catenin in skin. *Cell* **95,** 605-614.

42. **Greaves,J. and Chamberlain,L.H.** (2006). Dual role of the cysteine-string domain in membrane binding and palmitoylation-dependent sorting of the molecular chaperone cysteine-string protein. *Mol Biol Cell* **17,** 4748-4759.

43. **Greaves,J. and Chamberlain,L.H.** (2007). Palmitoylation-dependent protein sorting. *J. Cell Biol* **176,** 249-254.

44. **Green,M.C.** (1970) New mutant: a new recessive mutation, depilated (dep), arose in our T tf/+ tf stock in 1966. Mouse News Letter 31, 43.

45. **Grunder,A., Ebel,T.T., Mallo,M., Schwarzkopf,G., Shimizu,T., Sippel,A.E., and Schrewe,H.** (2002). Nuclear factor I-B (Nfib) deficient mice have severe lung hypoplasia. *Mech. Dev.* **112,** 69-77.

46. **Gu,L.H. and Coulombe,P.A.** (2007). Keratin expression provides novel insight into the morphogenesis and function of the companion layer in hair follicles. *J. Invest Dermatol.* **127,** 1061-1073.

47. **Hanahan,D., Wagner,E.F., and Palmiter,R.D.** (2007). The origins of oncomice: a history of the first transgenic mice genetically engineered to develop cancer. *Genes Dev.* **21,** 2258-2270.

48. **Hannon,G.J.** (2002). RNA interference. *Nature* **418,** 244-251.

49. **Hayashi,S. and McMahon,A.P.** (2002). Efficient recombination in diverse tissues by a tamoxifen-inducible form of Cre: a tool for temporally regulated gene activation/inactivation in the mouse. *Dev. Biol* **244,** 305-318.

50. **Hayashi,T., Rumbaugh,G., and Huganir,R.L.** (2005). Differential regulation of AMPA receptor subunit trafficking by palmitoylation of two distinct sites. *Neuron* **47,** 709-723.

51. **Horsley,V., O'Carroll,D., Tooze,R., Ohinata,Y., Saitou,M., Obukhanych,T., Nussenzweig,M., Tarakhovsky,A., and Fuchs,E.** (2006). Blimp1 defines a progenitor population that governs cellular input to the sebaceous gland. *Cell* **126,** 597-609.

52. **Huang,K., Yanai,A., Kang,R., Arstikaitis,P., Singaraja,R.R., Metzler,M., Mullard,A., Haigh,B., Gauthier-Campbell,C., Gutekunst,C.A. et al.** (2004). Huntingtin-interacting protein HIP14 is a palmitoyl transferase involved in palmitoylation and trafficking of multiple neuronal proteins. *Neuron* **44,** 977-986.

53. **Huelsken,J., Vogel,R., Erdmann,B., Cotsarelis,G., and Birchmeier,W.** (2001). beta-Catenin controls hair follicle morphogenesis and stem cell differentiation in the skin. *Cell* **105,** 533-545.

54. **Ito,M., Yang,Z., Andl,T., Cui,C., Kim,N., Millar,S.E., and Cotsarelis,G.** (2007). Wnt-dependent de novo hair follicle regeneration in adult mouse skin after wounding. *Nature* **447,** 316-320.

55. **Jahoda,C.A., Horne,K.A., and Oliver,R.F.** (1984) Induction of hair growth by implantation of cultured dermal papilla cells. 311, 560-562.

56. **Javerzat,S. and Jackson,I.J.** (1998). White-based brown (Tyrp1B-w) is a dominant mutation causing reduced hair pigmentation owing to a chromosomal inversion. *Mamm. Genome* **9,** 469-471.

57. **Jensen,K.B. and Watt,F.M.** (2006). Single-cell expression profiling of human epidermal stem and transit-amplifying cells: Lrig1 is a regulator of stem cell quiescence. *Proc. Natl. Acad. Sci. U. S. A* **103,** 11958-11963.

58. **Jensen,U.B., Lowell,S., and Watt,F.M.** (1999). The spatial relationship between stem cells and their progeny in the basal layer of human epidermis: a new view based on whole-mount labelling and lineage analysis. *Development* **126,** 2409-2418.

59. **Jones,P.H. and Watt,F.M.** (1993). Separation of human epidermal stem cells from transit amplifying cells on the basis of differences in integrin function and expression. *Cell* **73,** 713-724.

60. **Jordan,S.A. and Jackson,I.J.** (2000). A late wave of melanoblast differentiation and rostrocaudal migration revealed in patch and rump-white embryos. *Mech. Dev.* **92,** 135-143.

61. **Justice,M.J., Noveroske,J., Weber,J., Zheng,B., and Bradley,A.** (1999). Mouse ENU Mutagenesis. *Hum. Mol. Genet.* **8,** 1955-1963.

62. **Kaufman,C.K., Zhou,P., Pasolli,H.A., Rendl,M., Bolotin,D., Lim,K.C., Dai,X., Alegre,M.L., and Fuchs,E.** (2003). GATA-3: an unexpected regulator of cell lineage determination in skin. *Genes Dev.* **17,** 2108-2122.

63. **Kaur,P.** (2006). Interfollicular epidermal stem cells: identification, challenges, potential. *J Invest Dermatol.* **126,** 1450-1458.

64. **Keller,C.A., Yuan,X., Panzanelli,P., Martin,M.L., Alldred,M., Sassoe-Pognetto,M., and Luscher,B.** (2004). The {gamma}2 Subunit of GABAA Receptors Is a Substrate for Palmitoylation by GODZ. *J. Neurosci.* **24,** 5881-5891.

65. **Kleinjan,D.A. and van Heyningen,V.** (2005). Long-range control of gene expression: emerging mechanisms and disruption in disease. *Am. J Hum. Genet.* **76,** 8-32.

66. **Kobielak,K., Pasolli,H.A., Alonso,L., Polak,L., and Fuchs,E.** (2003). Defining BMP functions in the hair follicle by conditional ablation of BMP receptor IA. *J. Cell Biol* **163,** 609-623.

67. **Kobielak,K., Stokes,N., de la,C.J., Polak,L., and Fuchs,E.** (2007). Loss of a quiescent niche but not follicle stem cells in the absence of bone morphogenetic protein signaling. *Proc. Natl. Acad. Sci. U. S. A* **104,** 10063-10068.

68. **Komekado,H., Yamamoto,H., Chiba,T., and Kikuchi,A.** (2007). Glycosylation and palmitoylation of Wnt-3a are coupled to produce an active form of Wnt-3a. *Genes Cells* **12,** 521-534.

69. **Kopan,R., Lee,J., Lin,M.H., Syder,A.J., Kesterson,J., Crutchfield,N., Li,C.R., Wu,W., Books,J., and Gordon,J.I.** (2002). Genetic mosaic analysis indicates that the bulb region of coat hair follicles contains a resident population of several active multipotent epithelial lineage progenitors. *Dev. Biol* **242,** 44-57.

70. **Koster,M.I., Dai,D., Marinari,B., Sano,Y., Costanzo,A., Karin,M., and Roop,D.R.** (2007). p63 induces key target genes required for epidermal morphogenesis. *Proc. Natl. Acad. Sci. U. S. A* **104,** 3255-3260.

71. **Koster,M.I., Kim,S., Mills,A.A., DeMayo,F.J., and Roop,D.R.** (2004). p63 is the molecular switch for initiation of an epithelial stratification program. *Genes Dev.* **18,** 126-131.

72. **Kulessa,H., Turk,G., and Hogan,B.L.** (2000). Inhibition of Bmp signaling affects growth and differentiation in the anagen hair follicle. *EMBO J.* **19,** 6664-6674.

73. **Lane,P.** (1963) Whirler mice: a recessive behavior mutation in linkage group VIII. J.Hered. 54, 263-266.

74. **Legue,E. and Nicolas,J.F.** (2005). Hair follicle renewal: organization of stem cells in the matrix and the role of stereotyped lineages and behaviors. *Development* **132,** 4143-4154.

75. **Levy,L., Broad,S., Diekmann,D., Evans,R.D., and Watt,F.M.** (2000). beta1 integrins regulate keratinocyte adhesion and differentiation by distinct mechanisms. *Mol. Biol. Cell* **11,** 453-466.

76. **Li,G., Fukunaga,M., and Herlyn,M.** (2004). Reversal of melanocytic malignancy by keratinocytes is an E-cadherin-mediated process overriding beta-catenin signaling. *Exp. Cell Res.* **297,** 142-151.

77. **Limat,A., Hunziker,T., Waelti,E., Inaebrit,S., Wiesmann,U., and Braethen,L.R.** (1993) Soluble factors from human hair papilla cells and dermal fibroblasts dramatically increase the clonal growth of outer root sheath cells. Arch.Dermatol.Res. 285, 205-210.

78. **Linder,M.E. and Deschenes,R.J.** (2004). Model organisms lead the way to protein palmitoyltransferases. *J. Cell Sci.* **117,** 521-526.

79. **Linder,M.E. and Deschenes,R.J.** (2007). Palmitoylation: policing protein stability and traffic. *Nat Rev Mol Cell Biol* **8,** 74-84.

80. **Liu,Y., Lyle,S., Yang,Z., and Cotsarelis,G.** (2003). Keratin 15 promoter targets putative epithelial stem cells in the hair follicle bulge. *J. Invest Dermatol.* **121,** 963-968.

81. **Lobo,S., Greentree,W.K., Linder,M.E., and Deschenes,R.J.** (2002). Identification of a Ras palmitoyltransferase in Saccharomyces cerevisiae. *J. Biol. Chem.* **277,** 41268-41273.

82. **Logan,C.Y. and Nusse,R.** (2004). The Wnt signaling pathway in development and disease. *Annu. Rev. Cell Dev. Biol.* **20,** 781-810.

83. **Lopez-Rovira,T., Silva-Vargas,V., and Watt,F.M.** (2005). Different consequences of beta1 integrin deletion in neonatal and adult mouse epidermis reveal a context-dependent role of integrins in regulating proliferation, differentiation, and intercellular communication. *J. Invest Dermatol.* **125,** 1215-1227.

84. **Lorenz,K., Grashoff,C., Torka,R., Sakai,T., Langbein,L., Bloch,W., Aumailley,M., and Fassler,R.** (2007). Integrin-linked kinase is required for epidermal and hair follicle morphogenesis. *J. Cell Biol* **177,** 501-513.

85. **Loveland,J.** (2005). VEGA, the genome browser with a difference. *Brief. Bioinform.* **6,** 189-193.

86. **Mackenzie,M.A., Jordan,S.A., Budd,P.S., and Jackson,I.J.** (1997). Activation of the receptor tyrosine kinase Kit is required for the proliferation of melanoblasts in the mouse embryo. *Dev. Biol.* **192,** 99-107.

87. **Mansouri,M.R., Marklund,L., Gustavsson,P., Davey,E., Carlsson,B., Larsson,C., White,I., Gustavson,K.H., and Dahl,N.** (2005). Loss of ZDHHC15 expression in a woman with a balanced translocation t(X;15)(q13.3;cen) and severe mental retardation. *Eur. J. Hum. Genet.* **13,** 970-977.

88. **Maretto,S., Cordenonsi,M., Dupont,S., Braghetta,P., Broccoli,V., Hassan,A.B., Volpin,D., Bressan,G.M., and Piccolo,S.** (2003). Mapping Wnt/beta-catenin signaling during mouse development and in colorectal tumors. *Proc. Natl. Acad. Sci. U. S. A* **100,** 3299-3304.

89. **Mayer,T.C., Kleiman,N.J., and Green,M.C.** (1976). Depilated (dep), a mutant gene that affects the coat of the mouse and acts in the epidermis. *Genetics* **84,** 59-65.

90. **Mecklenburg,L., Nakamura,M., Sundberg,J.P., and Paus,R.** (2001). The nude mouse skin phenotype: the role of Foxn1 in hair follicle development and cycling. *Exp. Mol Pathol.* **71,** 171-178.

91. **Merrill,B.J., Gat,U., DasGupta,R., and Fuchs,E.** (2001). Tcf3 and Lef1 regulate lineage differentiation of multipotent stem cells in skin. *Genes Dev.* **15,** 1688-1705.

92. **Mesilaty-Gross,S., Reich,A., Motro,B., and Wides,R.** (1999). The Drosophila STAM gene homolog is in a tight gene cluster, and its expression correlates to that of the adjacent gene ial. *Gene* **231,** 173-186.

93. **Mill,P., Mo,R., Fu,H., Grachtchouk,M., Kim,P.C., Dlugosz,A.A., and Hui,C.C.** (2003). Sonic hedgehog-dependent activation of Gli2 is essential for embryonic hair follicle development. *Genes Dev.* **17,** 282-294.

94. **Millar,S.E., Willert,K., Salinas,P.C., Roelink,H., Nusse,R., Sussman,D.J., and Barsh,G.S.** (1999). WNT signaling in the control of hair growth and structure. *Dev. Biol.* **207,** 133-149.

95. **Mitchell,D.A., Vasudevan,A., Linder,M.E., and Deschenes,R.J.** (2006). Protein palmitoylation by a family of DHHC protein S-acyltransferases. *J. Lipid Res.* **47,** 1118-1127.

96. **Molina,T.J., Kishihara,K., Siderovskid,D.P., van Ewijk,W., Narendran,A., Timms,E., Wakeham,A., Paige,C.J., Hartmann,K.U., Veillette,A. et al.** (1992). Profound block in thymocyte development in mice lacking p56lck. *Nature* **357,** 161-164.

97. **Morris,R.J., Liu,Y., Marles,L., Yang,Z., Trempus,C., Li,S., Lin,J.S., Sawicki,J.A., and Cotsarelis,G.** (2004). Capturing and profiling adult hair follicle stem cells. *Nat Biotechnol.* **22,** 411-417.

98. **Mou,C., Jackson,B., Schneider,P., Overbeek,P.A., and Headon,D.J.** (2006). Generation of the primary hair follicle pattern. *PNAS* **103,** 9075-9080.

99. **Mukai,J., Liu,H., Burt,R.A., Swor,D.E., Lai,W.S., Karayiorgou,M., and Gogos,J.A.** (2004). Evidence that the gene encoding ZDHHC8 contributes to the risk of schizophrenia. *Nat. Genet.* **36,** 725-731.

100. **Muller,U.** (1999). Ten years of gene targeting: targeted mouse mutants, from vector design to phenotype analysis. *Mech. Dev.* **82,** 3-21.

101. **Muller-Rover,S., Handjiski,B., van,d., V, Eichmuller,S., Foitzik,K., McKay,I.A., Stenn,K.S., and Paus,R.** (2001). A comprehensive guide for the accurate classification of murine hair follicles in distinct hair cycle stages. *J. Invest Dermatol.* **117,** 3-15.

102. **Nagy,A.** (2000). Cre recombinase: the universal reagent for genome tailoring. *Genesis.* **26,** 99-109.

103. **Nakamura,M., Sundberg,J.P., and Paus,R.** (2001). Mutant laboratory mice with abnormalities in hair follicle morphogenesis, cycling, and/or structure: annotated tables. *Exp. Dermatol.* **10,** 369-390.

104. **Nguyen,H., Rendl,M., and Fuchs,E.** (2006). Tcf3 governs stem cell features and represses cell fate determination in skin. *Cell* **127,** 171-183.

105. **Niemann,C. and Watt,F.M.** (2002). Designer skin: lineage commitment in postnatal epidermis. *Trends Cell Biol* **12,** 185-192.

106. **Nieuwenhuis,E., Barnfield,P.C., Makino,S., and Hui,C.C.** (2007). Epidermal hyperplasia and expansion of the interfollicular stem cell compartment in mutant mice with a C-terminal truncation of Patched1. *Dev. Biol.*

107. **Nishimura,E.K., Jordan,S.A., Oshima,H., Yoshida,H., Osawa,M., Moriyama,M., Jackson,I.J., Barrandon,Y., Miyachi,Y., and Nishikawa,S.** (2002). Dominant role of the niche in melanocyte stem-cell fate determination. *Nature* **416,** 854-860.

108. **Nord,A.S., Chang,P.J., Conklin,B.R., Cox,A.V., Harper,C.A., Hicks,G.G., Huang,C.C., Johns,S.J., Kawamoto,M., Liu,S. et al.** (2006). The International Gene Trap Consortium Website: a portal to all publicly available gene trap cell lines in mouse. *Nucleic Acids Res.* **34,** D642-D648.

109. **O'Neal,K.R. and Agah,R.** (2007). Conditional targeting: inducible deletion by Cre recombinase. *Methods Mol. Biol* **366,** 309-320.

110. **Okuyama,R., Tagami,H., and Aiba,S.** (2007). Notch signaling: Its role in epidermal homeostasis and in the pathogenesis of skin diseases. *J. Dermatol. Sci.*

111. **Ong,S.E. and Mann,M.** (2006). A practical recipe for stable isotope labeling by amino acids in cell culture (SILAC). *Nat. Protoc.* **1,** 2650-2660.

112. **Oro,A.E., Higgins,K.M., Hu,Z., Bonifas,J.M., Epstein,E.H., Jr., and Scott,M.P.** (1997). Basal Cell Carcinomas in Mice Overexpressing Sonic Hedgehog. *Science* **276,** 817-821.

113. **Oshima,H., Rochat,A., Kedzia,C., Kobayashi,K., and Barrandon,Y.** (2001). Morphogenesis and renewal of hair follicles from adult multipotent stem cells. *Cell* **104,** 233-245.

114. **Ovcharenko,I., Loots,G.G., Nobrega,M.A., Hardison,R.C., Miller,W., and Stubbs,L.** (2005). Evolution and functional classification of vertebrate gene deserts. *Genome Res.* **15,** 137-145.

115. **Pan,Y., Lin,M.H., Tian,X., Cheng,H.T., Gridley,T., Shen,J., and Kopan,R.** (2004). gamma-secretase functions through Notch signaling to maintain skin appendages but is not required for their patterning or initial morphogenesis. *Dev. Cell* **7,** 731-743.

116. **Panteleyev,A.A., Jahoda,C.A., and Christiano,A.M.** (2001). Hair follicle predetermination. *J. Cell Sci.* **114,** 3419-3431.

117. **Paus,R. and Cotsarelis,G.** (1999). The biology of hair follicles. *N. Engl. J. Med.* **341,** 491-497.

118. **Peters,L.L., Robledo,R.F., Bult,C.J., Churchill,G.A., Paigen,B.J., and Svenson,K.L.** (2007). The mouse as a model for human biology: a resource guide for complex trait analysis. *Nat Rev Genet* **8,** 58-69.

119. **Peterson,R.L., Tkatchenko,T.V., Pruett,N.D., Potter,C.S., Jacobs,D.F., and Awgulewitsch,A.** (2005). Epididymal cysteine-rich secretory protein 1 encoding gene is expressed in murine hair follicles and downregulated in mice overexpressing Hoxc13. *J. Investig. Dermatol. Symp. Proc.* **10,** 238-242.

120. **Porter,R.M.** (2003). Mouse models for human hair loss disorders. *J. Anat.* **202,** 125-131.

121. **Potter,C.S., Peterson,R.L., Barth,J.L., Pruett,N.D., Jacobs,D.F., Kern,M.J., Argraves,W.S., Sundberg,J.P., and Awgulewitsch,A.** (2006). Evidence that the satin hair mutant gene Foxq1 is among multiple and functionally diverse regulatory targets for Hoxc13 during hair follicle differentiation. *J. Biol Chem.* **281,** 29245-29255.

122. **Qiao,W., Li,A.G., Owens,P., Xu,X., Wang,X.J., and Deng,C.X.** (2006). Hair follicle defects and squamous cell carcinoma formation in Smad4 conditional knockout mouse skin. *Oncogene* **25,** 207-217.

123. **Quwailid,M.M., Hugill,A., Dear,N., Vizor,L., Wells,S., Horner,E., Fuller,S., Weedon,J., McMath,H., Woodman,P. et al.** (2004). A gene-driven ENU-based approach to generating an allelic series in any gene. *Mamm. Genome* **15,** 585-591.

124. **Randall,V.A., Sundberg,J.P., and Philpott,M.P.** (2003). Animal and in vitro models for the study of hair follicles. *J. Investig. Dermatol. Symp. Proc.* **8,** 39-45.

125. **Raymond,F.L., Tarpey,P.S., Edkins,S., Tofts,C., O'Meara,S., Teague,J., Butler,A., Stevens,C., Barthorpe,S., Buck,G. et al.** (2007). Mutations in ZDHHC9, which encodes a palmitoyltransferase of NRAS and HRAS, cause X-linked mental retardation associated with a Marfanoid habitus. *Am. J. Hum. Genet.* **80,** 982-987.

126. **Reddy,S., Andl,T., Bagasra,A., Lu,M.M., Epstein,D.J., Morrisey,E.E., and Millar,S.E.** (2001). Characterization of Wnt gene expression in developing and postnatal hair follicles and identification of Wnt5a as a target of Sonic hedgehog in hair follicle morphogenesis. *Mech. Dev.* **107,** 69-82.

127. **Reynolds,A.J., Lawrence,C., Cserhalmi-Friedman,P.B., Christiano,A.M., and Jahoda,C.A.** (1999). Trans-gender induction of hair follicles. *Nature* **402,** 33-34.

128. **Rhee,H., Polak,L., and Fuchs,E.** (2006). Lhx2 Maintains Stem Cell Character in Hair Follicles. *Science* **312,** 1946-1949.

129. **Rinchik,E.M.** (1994). Molecular genetics of the brown (b)-locus region of mouse chromosome 4. II. Complementation analyses of lethal brown deletions. *Genetics* **137,** 855-865.

130. **Rinchik,E.M., Bangham,J.W., Hunsicker,P.R., Cacheiro,N.L., Kwon,B.S., Jackson,I.J., and Russell,L.B.** (1990). Genetic and molecular analysis of chlorambucil-induced germ-line mutations in the mouse. *Proc. Natl. Acad. Sci. U. S. A* **87,** 1416-1420.

131. **Rinchik,E.M., Bell,J.A., Hunsicker,P.R., Friedman,J.M., Jackson,I.J., and Russell,L.B.** (1994). Molecular genetics of the brown (b)-locus region of mouse chromosome 4. I. Origin and molecular mapping of radiation- and chemical-induced lethal brown deletions. *Genetics* **137,** 845-854.

132. **Rosenthal,N. and Brown,S.** (2007). The mouse ascending: perspectives for human-disease models. *Nat Cell Biol* **9,** 993-999.

133. **Roth,A.F., Feng,Y., Chen,L., and Davis,N.G.** (2002). The yeast DHHC cysteine-rich domain protein Akr1p is a palmitoyl transferase. *J. Cell Biol.* **159,** 23-28.

134. **Roth,A.F., Wan,J., Bailey,A.O., Sun,B., Kuchar,J.A., Green,W.N., Phinney,B.S., Yates,J.R., III, and Davis,N.G.** (2006). Global analysis of protein palmitoylation in yeast. *Cell* **125,** 1003-1013.

135. **Sakuraba,Y., Sezutsu,H., Takahasi,K.R., Tsuchihashi,K., Ichikawa,R., Fujimoto,N., Kaneko,S., Nakai,Y., Uchiyama,M., Goda,N. et al.** (2005). Molecular characterization of ENU mouse mutagenesis and archives. *Biochem. Biophys. Res. Commun.* **336,** 609-616.

136. **Shawlot,W., Min,D.J., Wakamiya,M., and Behringer,R.R.** (2000). The cerberus-related gene, Cerr1, is not essential for mouse head formation. *Genesis.* **26,** 253-258.

137. **Shesely,E.G., Maeda,N., Kim,H.S., Desai,K.M., Krege,J.H., Laubach,V.E., Sherman,P.A., Sessa,W.C., and Smithies,O.** (1996). Elevated blood pressures in mice lacking endothelial nitric oxide synthase. *Proc. Natl. Acad. Sci. U. S. A* **93,** 13176-13181.

138. **Shinagawa,T. and Ishii,S.** (2003). Generation of Ski-knockdown mice by expressing a long double-strand RNA from an RNA polymerase II promoter. *Genes Dev.* **17,** 1340-1345.

139. **Silva-Vargas,V., Lo,C.C., Giangreco,A., Ofstad,T., Prowse,D.M., Braun,K.M., and Watt,F.M.** (2005). Beta-catenin and Hedgehog signal strength can specify number and location of hair follicles in adult epidermis without recruitment of bulge stem cells. *Dev. Cell* **9,** 121-131.

140. **Simpson,E.H., Johnson,D.K., Hunsicker,P., Suffolk,R., Jordan,S.A., and Jackson,I.J.** (1999a). The mouse Cer1 (Cerberus related or homologue) gene is not required for anterior pattern formation. *Dev. Biol* **213,** 202-206.

141. **Simpson,E.H., Suffolk,R., Bell,J.A., Jordan,S.A., Johnson,D.K., Hunsicker,P.R., Weber,J.S., Justice,M.J., and Jackson,I.J.** (2000). A comparative transcript map and candidates for mutant phenotypes in the Tyrp1 (brown) deletion complex homologous to human 9p21-23. *Mamm. Genome* **11,** 58-63.

142. **Simpson,E.H., Suffolk,R., and Jackson,I.J.** (1999b). Identification, sequence, and mapping of the mouse multiple PDZ domain protein gene, Mpdz. *Genomics* **59,** 102-104.

143. **Smithies,O., Gregg,R.G., Boggs,S.S., Koralewski,M.A., and Kucherlapati,R.S.** (1985). Insertion of DNA sequences into the human chromosomal beta-globin locus by homologous recombination. *Nature* **317,** 230-234.

144. **Smotrys,J.E. and Linder,M.E.** (2004). Palmitoylation of intracellular signaling proteins: regulation and function. *Annu. Rev Biochem.* **73,** 559-587.

145. **Smotrys,J.E., Schoenfish,M.J., Stutz,M.A., and Linder,M.E.** (2005). The vacuolar DHHC-CRD protein Pfa3p is a protein acyltransferase for Vac8p. *J. Cell Biol* **170,** 1091-1099.

146. **Smyth,I., Du,X., Taylor,M.S., Justice,M.J., Beutler,B., and Jackson,I.J.** (2004). The extracellular matrix gene Frem1 is essential for the normal adhesion of the embryonic epidermis. *Proc. Natl. Acad. Sci. U. S. A* **101,** 13560-13565.

147. **Smyth,I.M., Wilming,L., Lee,A.W., Taylor,M.S., Gautier,P., Barlow,K., Wallis,J., Martin,S., Glithero,R., Phillimore,B. et al.** (2006). Genomic anatomy of the Tyrp1 (brown) deletion complex. *Proc. Natl. Acad. Sci. U. S. A* **103,** 3704-3709.

148. **Sowden,H.M., Naseem,K.M., and Tobin,D.J.** (2005). Differential expression of nitric oxide synthases in human scalp epidermal and hair follicle pigmentary units: implications for regulation of melanogenesis. *Br. J. Dermatol.* **153,** 301-309.

149. **Sparwasser,T. and Eberl,G.** (2007). BAC to immunology - bacterial artificial chromosome-mediated transgenesis for targeting of immune cells. *Immunology* **121,** 308-313.

150. **St-Jacques,B., Dassule,H.R., Karavanova,I., Botchkarev,V.A., Li,J., Danielian,P.S., McMahon,J.A., Lewis,P.M., Paus,R., and McMahon,A.P.** (1998). Sonic hedgehog signaling is essential for hair development. *Curr. Biol.* **8,** 1058-1068.

151. **Stenn,K.S. and Paus,R.** (2001). Controls of hair follicle cycling. *Physiol Rev* **81,** 449-494.

152. **Sutherland,H.G., Newton,K., Brownstein,D.G., Holmes,M.C., Kress,C., Semple,C.A., and Bickmore,W.A.** (2006). Disruption of Ledgf/Psip1 results in perinatal mortality and homeotic skeletal transformations. *Mol. Cell Biol.* **26,** 7201-7210.

153. **Swarthout,J.T., Lobo,S., Farh,L., Croke,M.R., Greentree,W.K., Deschenes,R.J., and Linder,M.E.** (2005). DHHC9 and GCP16 constitute a human protein fatty acyltransferase with specificity for H- and N-Ras. *J. Biol. Chem.* **280,** 31141-31148.

154. **Takeda,H., Lyle,S., Lazar,A.J., Zouboulis,C.C., Smyth,I., and Watt,F.M.** (2006). Human sebaceous tumors harbor inactivating mutations in LEF1. *Nat Med.* **12,** 395-397.

155. **Thaung,C., West,K., Clark,B.J., McKie,L., Morgan,J.E., Arnold,K., Nolan,P.M., Peters,J., Hunter,A.J., Brown,S.D. et al.** (2002). Novel ENU-induced eye mutations in the mouse: models for human eye disease. *Hum. Mol. Genet.* **11,** 755-767.

156. **Uetani,N., Kato,K., Ogura,H., Mizuno,K., Kawano,K., Mikoshiba,K., Yakura,H., Asano,M., and Iwakura,Y.** (2000). Impaired learning with enhanced hippocampal long-term potentiation in PTPdelta-deficient mice. *EMBO J.* **19,** 2775-2785.

157. **Valdez-Taubas,J. and Pelham,H.** (2005). Swf1-dependent palmitoylation of the SNARE Tlg1 prevents its ubiquitination and degradation. *EMBO J.* **24,** 2524-2532.

158. **van Genderen,C., Okamura,R.M., Farinas,I., Quo,R.G., Parslow,T.G., Bruhn,L., and Grosschedl,R.** (1994). Development of several organs that require inductive epithelial-mesenchymal interactions is impaired in LEF-1-deficient mice. *Genes Dev.* **8,** 2691-2703.

159. **Warming,S., Costantino,N., Court DL, Jenkins,N.A., and Copeland,N.G.** (2005). Simple and highly efficient BAC recombineering using galK selection. *Nucleic Acids Res.* **33,** e36.

160. **Watt,F.M.** (2002). Role of integrins in regulating epidermal adhesion, growth and differentiation. *EMBO J.*

161. **Watt,F.M., Lo,C.C., and Silva-Vargas,V.** (2006). Epidermal stem cells: an update. *Curr. Opin. Genet. Dev.* **16,** 518-524.

162. **Wessel,D. and Flugge,U.I.** (1984). A method for the quantitative recovery of protein in dilute solution in the presence of detergents and lipids. *Anal. Biochem.* **138,** 141-143.

163. **Willert,K., Brown,J.D., Danenberg,E., Duncan,A.W., Weissman,I.L., Reya,T., Yates,J.R., III, and Nusse,R.** (2003). Wnt proteins are lipid-modified and can act as stem cell growth factors. *Nature* **423,** 448-452.

164. **Wojcik,S.M., Bundman,D.S., and Roop,D.R.** (2000). Delayed wound healing in keratin 6a knockout mice. *Mol. Cell Biol* **20,** 5248-5255.

165. **Wu,X., Quondamatteo,F., Lefever,T., Czuchra,A., Meyer,H., Chrostek,A., Paus,R., Langbein,L., and Brakebusch,C.** (2006). Cdc42 controls progenitor cell differentiation and beta-catenin turnover in skin. *Genes Dev.* **20,** 571-585.

166. **Yanai,A., Huang,K., Kang,R., Singaraja,R.R., Arstikaitis,P., Gan,L., Orban,P.C., Mullard,A., Cowan,C.M., Raymond,L.A. et al.** (2006). Palmitoylation of huntingtin by HIP14 is essential for its trafficking and function. *Nat. Neurosci.* **9,** 824-831.

167. **Yang,X., Kovalenko,O.V., Tang,W., Claas,C., Stipp,C.S., and Hemler,M.E.** (2004). Palmitoylation supports assembly and function of integrin-tetraspanin complexes. *J. Cell Biol.* **167,** 1231-1240.

Appendix IA: Mapping data across the *brown* deletion complex.

deletion/ marker	12N13	Rgs3	RgNov	RgNov	Rg	LOC	D4mit87	257P7	20K13	D4mit82	D4Nds9	151D13	D4mit25	D4Mit7	s65.16	D4mit178	435B11	C2a	78N10	313C24	434E13
	T7	(ex7)-3'	lastex	3'	-61	230237		SP6	SP6			SP6			T/C		SP6		T7	SP6	T7
11R30M	R	R	R	R	R?	L	L	L		L	L		L	L		L			L		L
49HATh							R		?	L	L		L	L		L			L		
37Pub							R	R	R	R	L	L	R	L		L					L
9Pu							R			R	R	?	R	L		L			L		
3YPSc							R			R			R	R		R	L	L	L		
13R75M							R	R	R	R		R	R	R		R	R	L	L		L
5CHLe							R	R	R	R		R	R	R		R			R		
12Pu							R			R			R	R		R			R		
33G							R	R	R	R		R	R	R		R			R		
11Pu							R			R			R	R		R					
9R75VH							R			R			R	R		R					
8Pub							R	R	R	R		R	R	R		R			R		
1OZ							R			R			R	R		R			R		
46UTHc							R			R				R		R					
Relative Location*	60.6	61.03	61.03	61.03	61.1	61.2	61.42	61.45		62.85	63.67	63.73	63.88		65.16	65.5	66.5	66.7		67.98	68.61
33IK							R			R	L		L			L					
13DT							R			R	R		R	?	?	L					
37DTD							R			R	ND		R			R	?	?	?	?	?
173G							R			R	ND		R			R	?	?	?	?	?
ITHIO-IV							R			R	ND		R			R	?	?	?	?	?
1DF1OD							R			R	ND		R			R	?	?	?	?	?
47DthWb							R			R	ND		R			R					
51DthWb							R			R	ND		R			R					
55Cos							R			R	ND		R			R					
26R60L							R			R	ND		R			R					
3YPSH							R			R	ND		R			R					

marker	data from Bell et. al. (1995)
marker	markers designed by me
marker	published/ BAC end markers
marker	The remaining markers are most likely designed by Ian Smyth
R	Genomic region retained
L	genomic region loss/ deleted
?	undecided
*	The relative location of the marker is determined by searching the primer sequence against the *Mus Musculus* genome using Blastn.

402H11 SP6	D4mit132	D4mit83	140B18 T7	D4mit85	222P16 T7	237E18 T7	D4Rck4	D4mit142	Jmjd2c-ex1	Jmjd2c-ex11	Jmjd2c-ex18	Jmjd2c-3'	Jmjd2c ex22	D4mit141	274a7 SP6	D4Mit86	D4Rck122	471C18 T7	Ptprd ex18	247N05 T7	8Pub 74.9	8Pub 75.1
	L	L		L			L	L						L		L	L					
L	L	L		L			L	L						L		L	L					
	L	L		L			L	L						L		L	L					
L	L	L		L			L	L					L	L		L	L					
L	L	L		L			L	L						L		L	L					
L	L	L	L	L	L	L	L	L						L	L	L	L					
R	R	R	?	L	L	L	L	L						L	L	L	L					
R	R	R		R		L	L	L						L		L	L					
	R	R	R	R	R	R	R	L						L	L	L	L		L			
	R	R		R			R	R	R	R	R/L endpoint			L		L	L	L				
	R	R		R			R	R						R	R	R	R			R	R	R
R	R	R		R			R	R					R	R	R	R	R	R		R	R	L
	R	R	R	R			R	R						R		R	R					
	R	R		R			R	R						R		R	R					
68.63	69	69.29	70.2	70.71	71.3		71.5	72.49	72.52	72.61	72.65	72.68	72.68	72.79	72.89		73.41	73.55	74.3	74.66	74.9	75.1
	L	L		L			L	L						L		L	L					
	L	L		L			L	L						L		L	L					
?	L	L		L			L	L						L		L	L		L			
?	L	L		L			L	L						L		L	L					
?	L	L		L			L	L						L		L	L					
?	L	R		L			L	L						L		L	L					
	R	L		L			L	L						L		L	L					
	R	R	?	L			L	L						L		L	L					
	R	R	?	L			L	L						L		L	L					
	R	R		R	?	?	L	L						L		L	L					
	R	R		R			R	L						L		L	L					

Ptprd

8Pub	D4mit84	245P22	r	r	r	221I18	r	r	129L11	r	r	D4mit114	D4mit81	~~TYRP1~~	Ty-5'	Ty-3'	TyBg	TyBg	TyBg	TyBg	TyBg	Big1	Big1	395J04	**395J04**	s79.48	s79.49	s79.50
		T7				SP6			T7								10	20	30	40	50	ex1	ex2	SP6	**10k**			
75.4	75.5	76.31	76.5	76.7	76.9	76.96	77.1	77.3	77.49	77.8	78	78.25	78.98	79.1	79.1	79.1								79.3				
	L											L	L	L														
	L											L	L	L														
	L											L	L	L														
	L											L	L	L														
	L											L	L	L														
	L	L				L			L			L	L	L														
	L					L			L			L	L	L														
	L											L	L	L														
	L	L				L			L			L	L	L	L		R	R		R	?	R	R	R				
	L											L	L	L														
L	L											L	L	L														
L?	L	R?Ambiguous				L			L			L	L	L														
	R	?	R	R	R	?	R	R	L	L	L	L	L	L														
	R	?	R	R	R	?	R	R	L	L	L	L	L	L														
	L											L	L	L	?	?						L	R	R				
	L											L	L	L	?	?								?	L	L	L	L
	L											L	L	L	?	?								?	L			
	L											L	L	L	?	?		L		L	L			?	L	R	R	R
	L											L	L	L	L	?		L		L	L	L	L	L	R	R	R	R
	L											L	L	L														
	L											L	L	L	?	?								?	R	R	R	R
	L											L	L	L	?	?								?	L			
	L											L	L	L														
	L											L	L	L														
	L											L	L	L														

Tyrp1

Big1

s79.51	s79.53	s79.54	Mpdz ex47-3'	Mpdz39	338C16 T7	s79.57 G/A	s79.74 G/A	286H15 T7	D4Rck140	435P05 SP6	299I21 SP6	s80.23 a/a	459G06 T7	228D06 SP6	D4mit289	D4Rck9	Nfib3'	NfiBex4lge
					L			L	R	R	?		R		R		R	
		L	L		L	L	L	L	L	L	L			R	R	R	R	
									L						R			
					L			L	R	R	R		R	R	ND	R		
		L	L						L						ND	R		
									L						L	L		
									L						R (X)	L		
									L						L	L		
				R	R	R	R	R	R	R	?	R	R	R	ND			
									L						L	L		
									L	L	L			L	R(X)	L	L	L
									L						L	L		
									L	L			L	L	L	L	L	
									L						L	L	L	
				79.56	79.56 (!)	79.6	79.7	79.77	79.88	79.89	79.91	80.23	80.27		80.42	80.57	80.57	80.63
		L	R	?	R	?	R	?	R	?	?							
		L	L	?	L	?	R	?	R	?	?							
				R	R	?	R	R	R	R	?	R	R	R				
		R	R	?	R	R	R	R	R	?	?							
		R	R	R	R	R	R	R	R	R	?	R	R	R				
									L			?	?	?	?	?	?	?
		R	R	?	R	R	R	R	R	?	?							
		L	L	?	L	?	R	?	R	?	?							
		L	L						L			?	?	?	?	?	?	?
		L	L						L			?	?	?	?	?	?	?
									L									

Mpdz

								x														
Nfib5'	95F05l	NfibRealex1	D4MIT115	469/c16354	s81.07	95F05m	cer	D4MIT298	33N20	Depc5th	Frem1	Frem1	Frem1	DEPC2-	Frem1	Frem1	Frem1	depc2-	Frem1	469c16/357	Frem1	Frem1
	SP6			SP6	(A/G)	T7			SP6	lastex	iii-ex4	ii-ex5	ii-ex3	823	ii-ex2	ii-ex1	ex7	67	ex6	T7	ex4	ex2
R			R					R														
			R					R														
			L					R														
			R					ND														
			R					ND														
			L					L														
			L					R (X)			L			L		L	L	L	L	L		
			L					L														
			R					ND														
			L					L	?	?	L			L		L	L	L	L	L		
	R	R	R	R		R	R	R	R											R		
	?		L	?	?	?	L	R (X)	L	L	L			L		L	L	L	L	L		
L	L		L	L	?	R	R	R	R					R						R		
L	L		L	L		L	L	L	L		L	?	?	R	?	R	R	R	R	R	?	?
80.78	80.93	80.98		81.04	81.07	81.1	81.16	81.16	81.18	81.18	81.188	81.19	81.2	81.2	81.21	81.21	81.23	81.23	81.23	81.23	81.24	81.24
			R																			
			R																			
			R																			
			R																			
			R																			
?		?	R																			
			R																			
			R																			
?		?	R																			
?		?	R																			
	?		L	?	?	?	?	?	?	?				?						?		

x																	
D4mit79	410K19	bM39	17021	Nov81.5 3'	Nov81.5 5'	354A04 T7	311B24 T7	LEDGF	Snap c50	psip1 lastex	nov-trans psip1	493047 A06Rik(prox)	Novel1	s82.38 T/C	Novel2 (Bnc2)	D4Jkn1	bo247I15 SP6
R																R	
R																R	
R																R	
R																R	
R																R	
L							L	L	L	?	?	R	R/ R	?	R	R	R
R (x)	L	L	?	L	?	L	L		L	?	?	R	R	?	R	R	R
L						L	L	?	R?			R	R	?	R	R	
R																R	R
R																R	
R																R	
R(X)	L	L	?	L	?	L	L	?	L			L	L	?	L	R	R
R																R	R
R																R	
81.27						81.66	81.69	81.73	81.73			81.88	82.14	82.38	82.55	82.95	
																R	
																R	
																R	
																R	
																R	
																R	
																R	
																R	
																R	
																R	
?						?	?	?	?			?	?	?	?	R	

Appendix IB: Primer sequences of markers used for mapped the *b-del* chromosomes.

Marker	Forward	Reverse
12N13-T7	TTTGTCTTTGGTAGCTCATCTG	TTCCTGCTTCCCAACTCTC
'Rgs3(ex7)'	TGTGAACCTCAGAAGCCTGTC	AGGGCGTTAAGGACCTGATG
RgNov-lastex	ACCATGTCCCTCTGCGACT	CTTGGTGCGAACGCTGAG
RgNov-3'	CCTGATGCCCACACATACAG	TTGATACCAAAGGGGTCTCG
Rg(61.1)	TACCACAGGTGTGGAGGACA	TCCTGCTTCTGTGTGTTTCG
LOC230237	GCTCCTCCATTCTTCCATACTG	ATTCCAGACATTCTGTTTGCAC
D4mit87(Bell)	ACAGGTAGGAATGGAGCCCT	TCATCCCTTTGCCAAAGC
257P7-SP6	TCAAGGGATCAGAAATCAGGG	ATATGCTCACACACATACCAAG
20K13-SP6	AGCAGGCAGGGAAAAGAG	AGCACGAAGCATACAGGAC
D4mit82 (Bell)	ATGTGTGCCATTTTGCATGT	AGTATTGCTTGATAAATTTGCATG
D4Nds9 (Bell)	(Bell et al, 1995)	
151D13-SP6	TGCCACCCTGCTTAGTGTTC	CATTTCCCCTCTCGCCTTTC
D4mit25(bell)	(Bell et al, 1995)	
D4mit7	N/A	
s65.16(T/C)	ATTGGTCCAGGGGCTTAGAT	TTTAGCATGGTGAGCCTGA
D4mit178 (Bell)	GCCCTGAAGGTAAATCAGTAACT	GCTCAGGAGGTACATTGCCT
435B11-SP6	TCAATGTGCCCATACATCAAG	TGTCTATGGCATTGTTAGTAGC
C2a	TGAGCCACTGTTTTTACTCTGG	TGAAGTAGATGGTAAGGGTGGC
~~78n10-T7~~	BAC location	
313C24-SP6	CACAACATGTCCTTCACACC	CTAGCTCAGTAGCACCACTC
434E13-T7	GTCCTCCCCTAAAATAAAGCC	TCCTCCATTCCCACTTTCTATC
402H11-SP6	CCTACAAAAGCCCAGCAAC	CCCATGATCTGAATGACACAC
D4mit132 (Bell)	ACAATATTGACAGGTTCAATCAATT	TCCACCTCCATATGTGTCACA
D4mit83 (Bell)	TTCCTGACACTTGTATTTGTCTGA	AGACCCAGGGTTTAGTCTTTAATG
140B18-T7	CAATTCCCAGTGGTTGACTG	GATAGGAAAGACAGCCCAAAG
D4mit85 (Bell)	CAGGGAAGGTGTTTGCAAAT	TCTCCCCTCCTGGTAGGG
222P16-T7	GAGCAATACCAAGCCAGAAAC	TCCAGTGGAGTTCAGCACAC
237E18-T7	TTTCCTCCTTCGTTGTTTTTG	ACAATCCCCAACCCTTTCTC
D4Rck4(Bell)	CATCAGATAAGTTAATTTGC	CAAAACAGTAACACAATGGG
D4mit142 (Bell)	TGCTTGCTCAATGGAACTTG	CAGAATGCACACATTCACTGC
jmjex1	TTAAGTGCATGAGGCAGACC	TCACACCCTCAGTTCCATGA
jmjex11	TGCAGTGCAATACTTACTATGAGTT	TCAATGAACACAGCAGAATTACAA
jmjex18	CTGATAAGGCCCCAGAATCA	ACCACGTAAGGCCAGTCATC
jmjd2c-3'	AATCCAAGGGGAGAGGAAGA	GTCCCAATGTGTACCCCAAG
jmjex22	TAGGTTCCTTCGACCCTGTG	TGGGGTCAAACAAATGACTG
D4mit141(Bell)	TTCAGTGGCATATTTCAGTTGG	TGGGCAAGGAAGGTAGGAC
274A7-SP6	GGGATTAAAAGTGTCCTGGC	CCTCGCTGTACTAAACTAGC
D4Mit86 (Bell)	(Bell et al, 1995)	
D4Rck122 (Bell)	TGATCTGACATTTGACTG	TGATAGAATATCTTTACC
471C18-T7	CATGTTTGAGACCGAGCATC	ACATATGCTGTGTTGTCATTCC
Ptprd -ex18 (Fehr, 20	GGAGTCCAGAAAGAGCAGC	GGTGTTTGAAAGTTAAGGCG
247N05-T7	TGAATCCAGGGCTTGTCAG	CACAACACCCCCAAATACAC
8pub74.9	TGCAAATGATGGTGAAGAGG	CCATAATGCAAGACCCCACT
8Pub75.1	GCACAAGAGACCTGGGAGAC	TTTCCTCAGGATCCTCTCCA
8Pub75.4	CACAAGCCATAAAACCAGGA	TTGTGAACTGGGAAGCACAC
D4mit84	GTTGGGTCTTTTTTGTTTGTATTG	TTCATCTGACAAAATTAATGCCC
245P22-T7	TCATGTCAGCTCAGGCTTTG	TGGCTCTCACCTGTATGAGTG
r76.5	GCTACTGGATATGTGAGCGAAT	TTGTCAGCCAGCTCCAATTA
r76.7	GGACCCTCGTACTTGTAGTCCA	AGACTTTCGGCTTTTTGAATC
r76.9	CCACTAACTGCCCATCTGCT	CGAGAGCTATCTGTAAGGGCTTT
221I18-SP6	TCAGTGAACCTGTGGAGGTG	TCCTTTCTCAGCCCAGGTTG
r77.1	CAGCCACCCCTTATCACTGT	GCAGCTATGGCTCACCTCAG
r77.3	TGCACACAATAAAGTTGAAAGG	TGTGGAGACTCTCAGGAAAACA
129L11-T7	GGGCCTTTTACTCTGGTGAC	ATTTGTTTCCCCTGCAAACC
r77.8	TCTTGTATGCAAAGGAAGTTGAGA	TGACTCTTTGAGTCCTCAGTGG
r78.0	GAAACAACTATAACAACTAATGCCAGA	AAGGACTTCTACCTGTTTGGTTG
D4mit114	CTAACAGTTAATGACTTTCCAACACA	TGAACAGAACCTAAAAAGGACTAGG
D4mit81	GACCTGAGTCTTTCTTAAGATGGA	GCTTGCTTTTTTGGCTTCTG

~~TYRP1~~	N/A	
Tyrp1-5'	CAGCAGAGAAACCTTCCAGG	GTGCTCAGATGAAAATACAGC
Tyrp1-3'(5SNPs)	GGGAAGCAACCTGATTGAAA	TCCATAAGAATGGGCACTCA
TyBg10	AGCGTTTCAACAGCCCCTA	TGTTTTGCTCTGAGTGGCATT
TyBg20	AGTGCCAACCAGACATAGGG	CCTGACATTCAGGACATGGA
TyBg30	TGTGGTGCACCTCTAACTGC	AAAATTGGGTTCCTAAGTGTTCC
TyBg40	CAATAATACCGCTCTTCCTTGG	CTCGACACATCCATCAGGTG
TyBg50	AAATGGGTCTCTGCATCTCTG	GAGTGCATAAAGGCCAAATCA
Big1-ex1	GCCCTCTGCCTTTACTGTCA	GCCTCTGACGCATCACACT
Big1-ex2	TGGACTGCAGTGATATGAGCA	ACACCAGTCCCATGCAAAA
395J04-SP6	GGGTTGTGGGTTCTCAGTG	CTAGCTAGCGTTTCGTGCAG
395J04-10k	GGAATGGCGAGAGAAATGAA	GTCTCAGCAAGCCTGACCTC
395J04-20k	AGGAGCACTCTTGGCTTCTG	CCAGCCTCCTTTGACCATAA
s79.48	GTGAGTGTGTGGGGGACTTT	TCCCTGCTCCTATTGCATCT
s79.49	TGGCATTGTGATTTTGATGC	CCACCAGAGAAATTGGAGGA
s79.50	TGGGATCACAAGCTGGTACA	CACCTCTGACTGTGGGAATG
s79.51	TGCTCTGAGTTCTGCTTCCA	AGGTAAGGGCGGAAACTCTC
s79.53	AACAAATGAGCCCCACACAT	GTGTTTGAGGGAAGCCACAT
s79.54	ATGCGATTGGTGCATACAGA	CCATCTGCAGGAAATTGTGA
Mpdz -ex47-3'	ATGCAGAGCAATTTGCATTC	TCTCCGACCAACACAGCATA
Mpdz -ex39 (Fehr, 200	GGAGACTGATGCAAGGGGAC	ACTTTAGCAGGGCAGCGAC
338C16-T7	TCAACTCAACTACTCTCCAGTCG	GGGGGAGTGAAAGATGACAG
s79.57(g/a)	AGGCCTGAGCACAGATCAT	AAAATGGCACAGCTGACTC
s79.74(g/a)	TGCTTTGGGGTGTCACCTA	CACACAATTGCCCAACTCA
286H15-T7	AGTCAGCTGAGACCACAGGAG	GAATTGACGGGAAGTCACAG
D4Rck140(bell)	CATGATCTGGCTGCTGCG	GAATTCACTTCACAGCTA
435P05-SP6	TTTGGGAAAGCTGGATCAAC	GCAGTTACCCCTGCAATGTT
299I21-SP6	CCTCCCACTCTGAGAAGCAA	TGGGTCATGGAGAGAAAAGC
s80.23(a/a)	AAAGGGCACTATGGCAGAC	TGGCATAGAACCCAGGAAA
459G06-T7	CTTGTGTGCCCCTGAGAAAC	CTTGGGCCTCCAGACTCTCT
228D06-SP6	CCATCTCTTCACCACCCAAC	TTGGTCATTTCCCATAAGTGG
D4mit289	ATTTTCACCTGAGAAAAGAAGCC	CAAGTCTCTATTTCTTTAATTGTTGGG
D4Rck9	N/A	
Nfib3'	AGGAAAGAGGAAGACTGG	GTGCTTATAAAATGGCTGG
nfibex4lage	AGATGCATTCAGAGCGTGTC	TGAGCGTTACAGAACACAAGG
Nfib5'	GCTCGCAGCAAAGTTTCG	AGATGCCCAAGAAAATCTTCC
95F05(I)-SP6	GCACTCACAGAGAGCAGGTG	ATGGGAAGACCCAAACACAG
Nfibrealex1	GCCCACTTGCAAGCTACTTC	CACCCTGCCTTTTCAGAGAG
D4mit115	(Bell et al, 1995)	
469C16-SP6 (354)	CTCTGTCCGTCCTGCGTACT	CAAGCCATGATGCAGAGGTA
s81.07(a/g)	CGTGGCAACACAGGTACAA	GGGGGCTAGGAAGGTAGAC
95F05(m)-T7	GTCTGCTGCCTCATCCTTAC	AGCAGAGCAATGCCACTAAG
cer1	CTCAACAGAAAGCAAAACCTCA	TGAGGCCAGCTGAGAATACA
D4mit298	TTAGTCTTTCATTTCCTTTCTGTTTG	CTCAACCCCACATGTTGAGG
33N20-SP6	TGACATCACCAATGTAAAATGC	ATCGCAAGCCTTCAAAATCA
Depc5th last exon	TTGTTTTTGTTTGCTGTTTTCC	AACTTGGGGTCCATTTTGTG
Frem1iii-ex4	AACGGAAGGCCAAAATATCC	TTGGGGTCCATTTTGTGAAT
Frem1ii-ex5	CTGAACTCCCCTGTGAATGC	CCAGGACTGCTCCTGATTTC
Frem1ii-ex3	CAGCTTGGACTTGAGATGGTC	CAATTTGCAGTTTAGAGTTGTTACC
DEPC2-823	AGGCGCAACATTAAGTTCTATC	TGGGTCCTAATGATGTCCTTTC
Frem1ii-ex2	GAATTCATCCACGAGCGATT	GCAGAGCCAGTGAATAATGGA
Frem1ii-ex1	CCCGTATCACACACTTGCAC	CGTACAATGGGCCTCGTAAA
Frem1-ex7	AAATTTCCTTGCCACACAGG	TGCTATGTCCATTTGGCTGA
depc2-67	CATTCATGCAAAACCACTCG	GGGGCACACTGACCTCACTC
Frem1-ex6	TTCAGATAGGGAGGGACTGG	GTTGTCCTCATCCCAGAGGT
469c16/357	TGTGGAAGGCTGGTAGGAAG	GGCCCTCCTGAGGTTGATAC
Frem1-ex4	TTCCAGGAATGAAGCTGGTC	tcacTTGCTTAGCGTTGGTG
Frem1-ex2	TCCCTGGGAAGTGCTCTTTA	GCAAGGTCAGGAGCTTCATC
D4mit79	TTGTCTTTCCACTTTTAAGGGG	GATCTTTTTTTGAACACCCACC
410K19	AAGGAAGCTGGGAAGAAAGC	GCGGGAAGCAGGTACTTACA
bM391m19	TTGAAGTCACCCAACCTTTG	TTTCCTGGGGAGATGTGAAG
17021	AAGGTCATCCCAGAGCTGAA	AGGTGGAAGTGTGGGAGTTG
nov81.5-3'	AGAAACCTTCCACGGACTGA	ACTCCGATGACAGGAAGTGG

nov81.5-5'	GGGCATTAGCCTGGCATC	ACACCCACAGGGAACTCAGA
354A04-T7	TAAAGCAGAGGCCATTAGGG	CCAGTGAATGGGGATACTGC
311B24-T7	AAAGCAACCTTTTCACGAGTG	GGAGAGAGCCGAATGTGATT
LEDGF	GGCCATGCTTTGACTTTTTAAG	CTTTAACTCTGGGCCTGCTC
SNAPC50	CCACGGTATTTGGGAAAGATT	GCCAGACCTAGACTGCTTCCTA
psip1-lastex	TTTAATGCCCTGTTTGCTCA	CTGAAGTCTGCCGACCTAGT
novtrans-psip1	AGAAGGTTGGGAAAGCACCT	TCTGTGCTTGTGCCTTCAAC
493047A06Rik(prox)	AATGCCGATGTTAATGAGTTTG	AGAAAACCACACAAGTGGTGCATG
Novel1	GTTCCAGTTTTTCCTCCATTGTC	AGACATATCCCTGCACACATTG
s82.38(t/c)	GGGCAGTCTCTGTGGAAAAG	TCTACAGCTTGGGTCCATCC
Novel2 (Bnc2)	TTTGGTCAACAGTTTTACGATGC	TGCACCAGGAACAGTTTATTTG
D4Jkn1(bell)	GGACCGGGCTACATAGAGAAG	CTATATCTCTTACTAATTTCTTAAGTG
bo247l15-SP6	GTGGAATCCTTGCCTGAG	CCACAGTGTTTGGGGAAAAC

N/A' - published markers, or markers that are described on www.informatics.jax.org

Genomic anatomy of the Tyrp1 (brown) deletion complex

Ian M. Smyth*, Laurens Wilming†, Angela W. Lee*, Martin S. Taylor*, Phillipe Gautier*, Karen Barlow†, Justine Wallis†, Sancha Martin†, Rebecca Glithero†, Ben Phillimore†, Sarah Pelan†, Rob Andrew†, Karen Holt†, Ruth Taylor†, Stuart McLaren†, John Burton†, Jonathon Bailey†, Sarah Sims†, Jan Squares†, Bob Plumb†, Ann Joy†, Richard Gibson†, James Gilbert†, Elizabeth Hart†, Gavin Laird†, Jane Loveland†, Jonathan Mudge†, Charlie Steward†, David Swarbreck†, Jennifer Harrow†, Philip North‡, Nicholas Leaves‡, John Greystrong‡, Maria Coppola‡, Shilpa Manjunath‡, Mark Campbell‡, Mark Smith‡, Gregory Strachan‡, Calli Tofts‡, Esther Boal‡, Victoria Cobley‡, Giselle Hunter‡, Christopher Kimberley‡, Daniel Thomas‡, Lee Cave-Berry‡, Paul Weston‡, Marc R. M. Botcherby‡, Sharon White*, Ruth Edgar*, Sally H. Cross*, Marjan Irvani¶, Holger Hummerich¶, Eleanor H. Simpson*, Dabney Johnson§, Patricia R. Hunsicker§, Peter F. R. Little¶, Tim Hubbard†, R. Duncan Campbell‡, Jane Rogers†, and Ian J. Jackson*||

*Medical Research Council Human Genetics Unit, Edinburgh EH4 2XU, United Kingdom; †Wellcome Trust Sanger Institute, and ‡Medical Research Council Rosalind Franklin Centre for Genome Research, Hinxton CB10 1SA, United Kingdom; §Life Sciences Division, Oak Ridge National Laboratory, Oak Ridge, TN 37831; and ¶Department of Biochemistry, Imperial College, London SW7 2AZ, United Kingdom

Communicated by Liane B. Russell, Oak Ridge National Laboratory, Oak Ridge, TN, January 9, 2006 (received for review September 15, 2005)

Chromosome deletions in the mouse have proven invaluable in the dissection of gene function. The *brown* deletion complex comprises >28 independent genome rearrangements, which have been used to identify several functional loci on chromosome 4 required for normal embryonic and postnatal development. We have constructed a 172-bacterial artificial chromosome contig that spans this 22-megabase (Mb) interval and have produced a contiguous, finished, and manually annotated sequence from these clones. The deletion complex is strikingly gene-poor, containing only 52 protein-coding genes (of which only 39 are supported by human homologues) and has several further notable genomic features, including several segments of >1 Mb, apparently devoid of a coding sequence. We have used sequence polymorphisms to finely map the deletion breakpoints and identify strong candidate genes for the known phenotypes that map to this region, including three lethal loci (*l4Rn1*, *l4Rn2*, and *l4Rn3*) and the fitness mutant *brown-associated fitness* (*baf*). We have also characterized misexpression of the basonuclin homologue, *Bnc2*, associated with the inversion-mediated coat color mutant *white-based brown* (B^w). This study provides a molecular insight into the basis of several characterized mouse mutants, which will allow further dissection of this region by targeted or chemical mutagenesis.

brown locus | chromosome deletion | mouse genome sequence

The mouse *brown* (*b*) mutation is one of the oldest known loci and was one of the first to be cloned. The mutation is in the *tyrosinase-related protein 1* (*Tyrp1*) gene, encoding a melanocyte enzyme required for the production of dark eumelanin (1). Homozygous loss of *Tyrp1* results in a brown coat; because it was a simply scored phenotype, *brown* was used as part the mouse-specific locus test carried out at the Oak Ridge National Laboratories and elsewhere (reviewed in ref. 2). Wild-type mice were exposed to chemical or radiological mutagens and crossed with a tester stock homozygous for seven recessive visible mutations. The efficacy of the mutagenic treatments is assessed in the resulting F_1 progeny. These experiments generated many chromosomal deletions that inactivated *Tyrp1*, particularly in the progeny of animals exposed to radiation or clastogenic chemical mutagens such as chlorambucil or melphalan.

Deletions around the seven specific loci have provided a unique opportunity to study gene function within these intervals. Individual deletions are hemizygous viable but when homozygous or in combination with others give lethal or visible phenotypes, which indicate the presence of essential genes neighboring the specific loci. Intercrossing deletions of different extents provided an avenue to map the resulting phenotypes. The deletions also provided the means to produce physical maps of genetic markers. Studies of this kind have been published for several loci, including *albino* (*Tyr*), *piebald* (*Ednrb*), *pink-eyed dilution* (*p*), and the *brown* deletion complex (2–6).

Studies of the *brown* deletions established genetic and physical maps of the interval by using a panel of 25 deletions spanning ≈8.5 cM of chromosome 4 (6–8). Complementation analyses defined phenotypic loci in the region, including three lethals and a phenotype, termed *brown-associated fitness* (*baf*), which results in postnatal runting and increased preweaning mortality. Previous studies have also described a chromosomal inversion, *white-based brown* (B^w), that was hypothesized to cause inappropriate expression of an unknown gene, resulting in melanocyte death and loss of hair pigmentation (9).

We have generated a finished and manually annotated sequence from a bacterial artificial chromosome (BAC) contig spanning the *brown* deletion complex. The region is very gene-poor and includes several large segments devoid of any protein-coding genes. We identified single-nucleotide polymorphisms that permit refinement of the deletion breakpoints that delineate known phenotypes. The sparse gene content means that we have identified one or a few candidate genes for each of the five phenotypes.

Results and Discussion

Sequence and Annotation of the *Tyrp1* Deletion Complex. The finished sequence of each of 172 BACs from a clone contig encompassing the *Tyrp1* deletion complex was individually annotated to identify genes, transcripts, and pseudogenes (Fig. 1; for a complete version of this figure, see Fig. 5, which is published as supporting information on the PNAS web site). The annotations can be viewed in the Vertebrate Genome Annotation (VEGA) browser (http://vega.sanger.ac.uk/index.html). The extent of the deletion complex was determined by locating the endpoints of those deletions extending furthest proximally ($Tyrp1^{11R30M}$) and distally ($Tyrp1^{8Pub}$). These deletions define an unusually gene-poor genomic segment of ≈21 megabases (Mb) from a point just distal to *Rgs3* as far as, and including, *Bnc2*. This

Conflict of interest statement: No conflicts declared.

Abbreviations: BAC, bacterial artificial chromosome; Mb, megabase.

Data deposition: The sequences reported in this paper have been deposited in the EMBL/GenBank database. For a complete list of accession nos., see Table 4, which is published as supporting information on the PNAS web site.

||To whom correspondence should be addressed. E-mail: ian.jackson@hgu.mrc.ac.uk.

www.pnas.org/cgi/doi/10.1073/pnas.0600199103

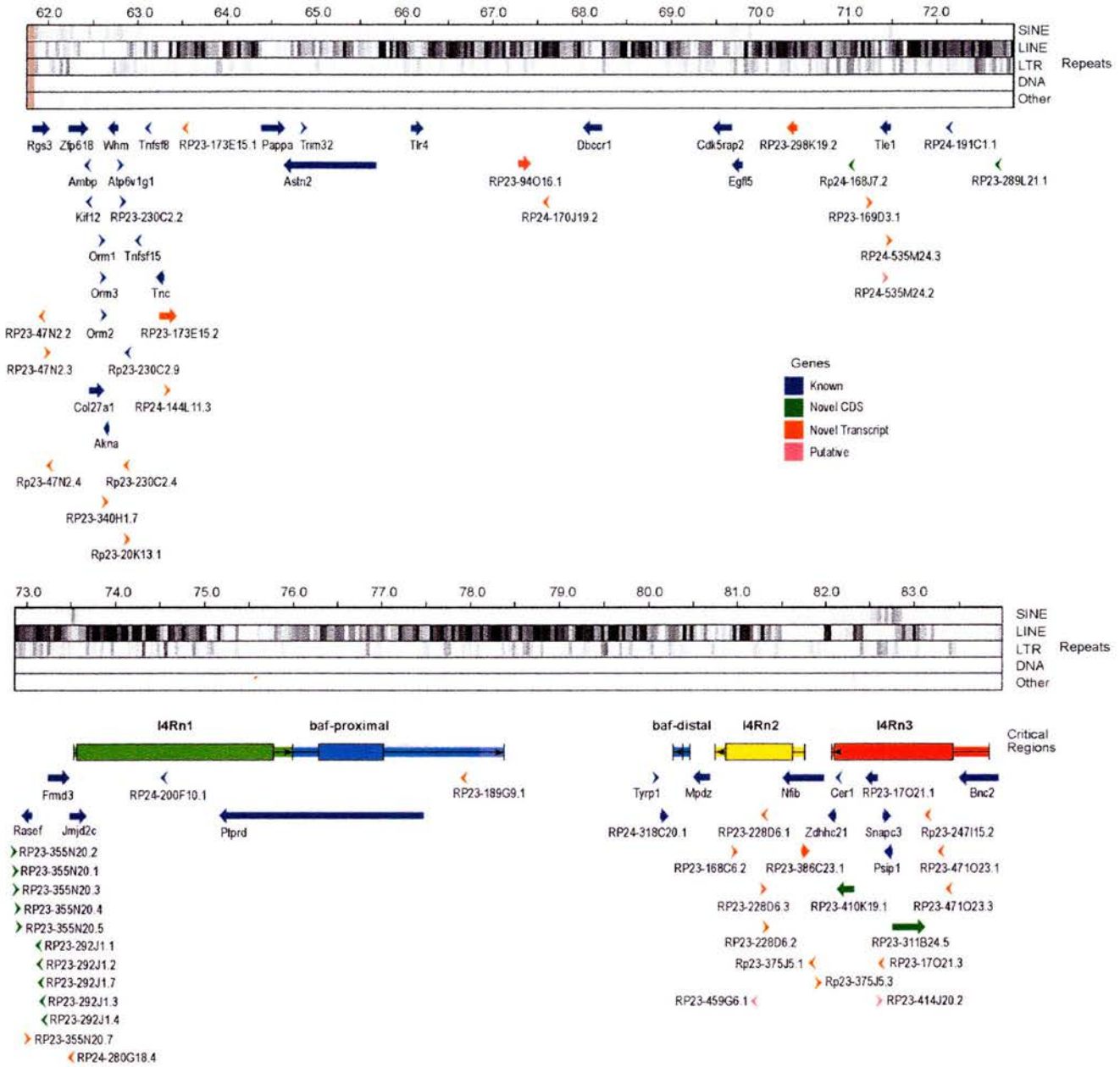

Fig. 1. Schematic representation of the annotation of the *Tyrp1* deletion region. The deletion interval extends as far as, but not including, *Rgs3* at the proximal end and includes *Bnc2* at the distal end. Yellow blocks represent finished sequences, marked with accession numbers (available at http://vega.sanger.ac.uk/index.html), of individual BAC clones forming the tiling path across the region. A black block on the end of the clone represents an overlapping, redundant sequence. The five gray-black tracks show the distribution of different types of repeats, as defined by REPEATMASKER. The red line indicates a fraction of G and C nucleotides. Arrows show the position and orientation of annotated genes and pseudogenes, with the color of the arrows indicating the type as shown in the key. The five colored boxes are the extents of the critical regions for the deletion phenotypes as indicated. The wider box is the minimal critical region, the narrow box is the maximum, and the boxes are delineated by the deletions and markers listed in Tables 2 and 3. The ends of the boxes are the positions of the markers. The arrows in the boxes reflect the intact chromosomal ends, pointing into the deletion.

segment contains only 53 protein-coding genes (see Table 1, which is published as supporting information on the PNAS web site). We can be confident that 39 of these genes are true genes because they have orthologous protein-coding transcripts in other species. The remaining 14 genes are all identified by the existence of mouse cDNAs, which contain ORFs distributed across multiple exons and are predicted to encode peptides containing between 110- and 354-aa residues. One of them is derived from the 3′ end of the adjacent *Frmd3* gene. None of the remaining thirteen, however, shows significant homology to transcripts from any other species nor do their predicted protein products have any recognizable motifs. Ten of these predicted genes arise from a 10-fold local amplification of a 15-kb genomic segment. Although there are EST matches to these amplified arrays, none of them are perfect, and it is not clear which of the repeated segments are transcribed. Furthermore, the human

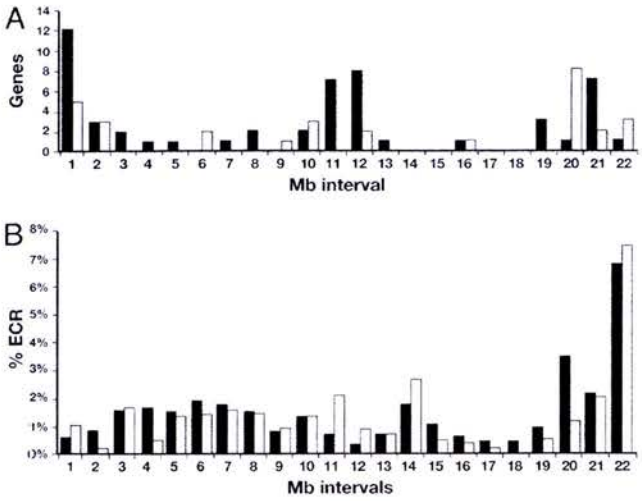

Fig. 2. Distribution of genes and evolutionary-conserved regions (ECRs). (*A*) The number of protein-coding genes (black bars) and noncoding RNAs (white bars) in each 1-Mb interval across the region, beginning at the 3′ end of *Rgs3*. Where a gene or transcript spans more than one interval, it is placed in the one containing the 5′ end of the 5′ most transcript. (*B*) The percentage of ECR content in each 1-Mb interval, as in *A*. The fraction is calculated as the total length of sequence, after masking repeats and exons, that reaches the threshold. Black bars are mouse–human ECRs at 80% identity over >200 bp, and white bars are mouse–chicken ECRs at 70% identity over >100 bp.

genome sequence contains a recognizable homologue neither to the transcript nor to the 15-kb amplified segment from which it derives. The rat genome does contain a single orthologous genomic segment, but this segment is located on rat chromosome 15 not on the rat homologue of mouse chromosome 4, which is chromosome 5.

The deletion complex also gives rise to 28 spliced transcripts, identified by mouse cDNAs, which are derived from between two and five exons but contain neither any significant ORF nor show homology to transcripts from other species. In addition, there are 74 recognizable pseudogenes, almost all of them processed.

The overall gene density across this region is just >2 genes per Mb compared with the genome average of ≈10 genes per Mb. Furthermore, the genes are not evenly spaced (Fig. 2*A*). More than half are located in the megabases at each end of the complex and in a 2-Mb region in the center, leaving only 20 genes spaced across the remaining 18 Mb. There are seven stretches of >1 Mb, including one of 2.5 Mb, that are totally devoid of any protein-coding transcript. Another large segment of 1.9 Mb is solely occupied by 10 exons encoding isoforms of the 5′ UTR of the *Ptprd* gene. Furthermore, the 29 spliced noncoding transcripts are also not evenly distributed across the region; rather, they appear to be clustered in those regions that are enriched for genes (Fig. 2*A*).

The function, if any, of these noncoding RNA is unknown. Their localization near to established genes may indicate that the transcripts are hitherto unidentified parts of transcripts of the known protein-coding genes, or their expression may be a nonfunctional by-product of local transcriptional activity. Alternatively, it is possible that their transcription has a function in opening up the chromatin, or maintaining it in an open state, to facilitate expression of protein-coding genes.

Repeat content is correlated with gene density in the mammalian genome (10). Fig. 1 illustrates this correlation across the deletion region. Gene-poor segments are rich in LINE elements, whereas SINEs are more abundant in the gene-rich areas. The

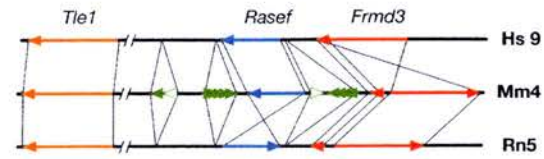

Fig. 3. Schematic representation of a region of striking evolutionary rearrangement. The orthologous regions of human chromosome 9 (Hs9), mouse chromosome 4 (Mm4), and rat chromosome 5 (Rn5) are shown. The orientations of the genes are indicated by the following colored arrows: *Tle1* in orange, *Rasef* in blue, and *Frmd3* in red. Lines connect the 3′ and 5′ ends of each. The second, short red arrow in mouse and rat genome represents the RP23-292J1.4 transcript, which apparently derives from a 3′ end duplication and inversion of *Frmd3*. The 10 green arrowheads in the mouse line represent the 9-fold amplification encoding the transcripts related to RP23-289L21.1, which are absent from the rat and human lines. Open green arrowheads are the two pseudogenes of the same gene.

gene and transcript "deserts," however, still contain substantial numbers of nontranscribed conserved sequences. Fig. 2*B* shows the distribution of nontrancribed segments that are conserved between the mouse sequence and the orthologous human and chicken sequences. Surprisingly, the locations of the conserved segments do not appear to correlate with transcript locations. The gene-rich first megabase of the region has a lower concentration of noncoding conserved segments, and the central part, which is also relatively enriched for genes, has a low level of noncoding conservation.

The function of most of the conserved segments in the genome is unknown, and they may indeed have a diversity of roles. The conserved sequences located close to genes are candidates for regulatory elements. Even those elements very distant from the 5′ end of a gene may still play a role; there is increasing evidence that sequences at several megabases distant can be essential for correct gene expression (11). Recently, Ovcharenko *et al.* (12) have examined gene deserts in the human, which they define as intergenic intervals of >640 kb, the longest 3% of all intergenic intervals. They find that the human–chicken sequence conservation in these deserts range from none to 12% and suggest that those with 2% or more conservation may be more likely to house long-range regulatory elements. Using the same criteria for conservation, we find that most intervals in this deletion region have <2% conservation.

A Site of Striking Evolutionary Rearrangement. The entire region is homologous to human chromosome 9 but is not contiguous in humans. There is a striking correlation between gene density and human chromosome G-banding patterns. The deserts lie within dark G bands, and the gene-rich segments are in light bands (10). The proximal end of the region is homologous to 9q32-33, the distal end to 9p22-24, and an ≈3.5-Mb segment in the middle is homologous to 9q21.32. The distal end of this central segment has undergone considerable rearrangements over evolution. The protein-coding gene, RP23-289L21.1, is ≈600 kb from where the homology changes to 9p22-24. As mentioned, this gene is locally amplified ≈200 kb upstream, and in the opposite orientation are five tandemly arranged, almost identical, 15-kb segments that derive from the genomic segment encoding the gene. A further four copies of the segment are found another 100 kb further along the chromosome, between *Rasef* and *Frmd3*. Two pseudogenes derived from these genes are also presenting this region (Fig. 3). Characterization of this array of highly similar sequences required that the sequence produced for the region was high-quality and hand-finished. Earlier drafts of the region had only a single copy of the amplified array, which illustrates the value of hand-finished sequence.

The chromosomal orthology breakpoint is immediately adja-

cent to the 3′ end of *Frmd3*, and this gene also seems to have undergone considerable evolutionary rearrangement. In mice, *Rasef* and *Frmd3* are divergently transcribed from opposite strands, whereas the human orthologues are transcribed from the same strand (Fig. 3). The 3′ portions of both human and mouse *Frmd3* are transcribed from within an intron by using an alternative, conserved exon. In mouse, a homologue of this shorter transcript is present in a second copy (RP23-292J1.4), in reverse orientation (the same orientation as the human transcript). There appears to have been a duplication accompanying the inversion (Fig. 3), and the human gene orientation is ancestral. Examination of the rat genome sequence reveals that *Frmd3* in this species has the same orientation as in mouse and also has the duplicated 3′ transcript, indicating that the rearrangement occurred before the mouse and rat lineages diverged. In rat, however, the *Rasef* gene is reversed compared with the mouse, apparently a result of another gene inversion in the rat lineage (Fig. 3). The genomic arrangement in zebrafish is different yet again; in this case, *Rasef* and *Frmd3* are transcribed from opposite strands, as in mouse, but are divergent not convergent (data not shown).

Alignment of the entire 22 Mb *Tyrp1* deletion region reveals at least two other small inversions in the mouse genome with respect to the human genome of 80 and 100 kb, but nether of these inversions include any genes or transcripts.

Identification of Deletion Phenotypes. To accurately identify candidate genes for loci previously mapped to the deletion complex, we mapped the ends of deletion breakpoints using SNPs between the strains of origin of the deletion chromosomes and *Mus spretus* in deletion/*spretus* heterozygotes. We focused on those deletions that had been used to define mutant loci. The minimal and maximal extents of key deletion intervals are illustrated in Fig. 1. Tables 2 and 3, which are published as supporting information on the PNAS web site, list the deletions and markers used to define the endpoints. The relevant markers from Table 3 map on Fig. 1 as the maximum and minimum extents of each deletion.

Embryonic Lethal Phenotypes. Combinations of deletions identify three embryonic or neonatal lethal phenotypes (7, 8, 13), and their endpoints define the locations of essential genes deleted or mutated by them.

l4Rn1 is a deletion phenotype resulting in *in utero* death before E14.5 (13). The physical map of Bell *et al.* (8) indicates that it lies between the proximal end points of the $Tyrp1^{8Pub}$ and $Tyrp1^{11Pu}$ deletions. $Tyrp1^{8Pub}$ breaks within the *Ptprd* gene and is the most proximal viable deletion, whereas $Tyrp1^{11Pu}$ breaks within the *Jmjd2c* gene and is the most distal lethal deletion. *l4Rn1*, therefore, lies in the 2.45-Mb interval defined by these endpoints (Fig. 1). Despite the length of this segment, only three genes are within the interval. We can exclude *Ptprd* as a candidate because $Tyrp1^{8Pub}$ disrupts *Ptprd* yet does not delete *l4Rn1*. The remaining two candidates are *Jmjd2c* and an uncharacterized gene, RP24-200F10.1, defined by the Institute of Physical and Chemical Research (Japan) (RIKEN) clone no. 3110001D03, which is the mouse orthologue of human *C9orf123*. *Jmjd2c* is the orthologue of a characterized human gene, *GASC1*, which is amplified in esophageal cancer cell lines (14). The encoded protein contains two jumonji domains, jmjC and jmjD, which are found together in numerous mouse proteins and may indicate function as a transcription factor. Any potential function of the product of the *C9Orf123* orthologue is difficult to predict; the protein is only 111 aa in length but has two potential transmembrane domains that are conserved in humans.

Mice homozygous for *l4Rn2* deletions die neonatally, and the locus is defined by the distal end of deletion $Tyrp1^{11R30M}$ and the distal end of deletion $Tyrp1^{9R75VH}$ (6). Our deletion mapping indicates that this interval contains only part of only one gene, *nuclear factor I-B* (*Nfib*), encoding a transcription factor expressed at high levels in the embryonic lung (15) (Fig. 1). *Nfib* mutant pups die shortly after birth as a result of severe pulmonary hypoplasia (16), and this phenotype is entirely consistent with that of mice bearing homozygous deletions of *l4Rn2*. We suggest deletion of *Nfib* is responsible for the *l4Rn2* phenotype.

The final early embryonic lethal deletion locus, *l4Rn3*, lies between the distal ends of the $Tyrp1^{46UThc}$ deletion and $Tyrp1^{8Pub}$ (Fig. 1). This interval contains six genes: RP23-410K19.1, which is the *Frem1* gene (17); the PC4 and SFRS1 interacting protein 1, *Psip1*; the small nuclear activating complex protein 3 (*Snapc3*); basonuclin 2 (*Bnc2*); and two uncharacterized genes, RP23-17O21.2, encoding the cDNA *1810054D07Rik*, and RP23-311B24.5, encoding *A330015D16Rik*, which are the mouse orthologues of human *C9Orf52* and *C9Orf93*, respectively. We can exclude *Frem1* as a candidate as loss-of-function mutations of this gene result in the *head blebs* (*heb*) phenotype (17). The SNAPC3 protein forms part of the small nuclear RNA-activating protein complex and reduction of protein *in vitro* leads to inhibition of RNA polymerase II- and III-mediated small nuclear RNA gene transcription (18). PSIP is a nuclear protein important for cellular protection against stress-induced apoptosis in which activity is regulated by caspase-mediated cleavage (19, 20). Neither protein has been knocked out but, given their cellular functions, either would make a good candidate for *l4Rn3*. Of the two unknown function transcripts, only the *C9Orf93* orthologue has any recognizable protein domain, including coiled coils and tropomyosin motifs. Very few of the *brown* deletions were mapped relative to *l4Rn3*; we were unable to further reduce this locus, and all five genes remain candidates.

***Brown-Associated Fitness* (*baf*).** Previous studies of the deletion complex showed that appropriate combinations of chromosomal deletions complement the embryonic lethal phenotypes. All complementing deletions reported result in mice with poor growth rates, alterations in behavior, and compromised survival (6, 7). This phenotype, termed *brown-associated fitness* (*baf*), must result from the loss of a gene or genes very close to *Tyrp1*. However, certain deletion combinations, namely $Tyrp1^{1OZ}$ with $Tyrp1^{37DTD}$ and $Tyrp1^{47UTHc}$ with $Tyrp1^{37DTD}$, $Tyrp1^{33G}$, or $Tyrp1^{1THO\text{-}IV}$ result in phenotypically normal mice, indicating that the gene(s) in which deletion results in *baf* must lie outside these deletions (E. M. Rinchik, unpublished data). Paradoxically, each of these deletions, in combination with others, can produce *baf* mice. We must conclude that there are two genetic elements, one on each side of *Tyrp1*, the deletion of either of which gives rise to the *baf* phenotype (Fig. 1).

The maximum deletion interval on the proximal side that defines *baf* contains a part of only one gene, *Ptprd*. This gene has been mutated by gene targeting and results in mice with neurological defects that fail to thrive without ground feeding (21). This phenotype is consistent with *baf*, and we conclude that the phenotype caused by deletions proximal to *Tyrp1* is due to loss of *Ptprd*. It is worth noting that these deletions remove a 2.5-Mb gene desert in addition to *Ptprd*, yet the mice have a phenotype no more severe than a targeted mutation of *Ptprd* alone. The cause of the distal *baf* phenotype is less clear. Seventy kilobases distal of *Tyrp1* is an uncharacterized gene RP24-318C20.1, the orthologue of human *C9Orf150*. However, deletion of all or part of this gene, from $Tyrp1^{1THO\text{-}IV}$ and $Tyrp1^{37DTD}$, does not result in the *baf* phenotype. Rather, the distal *baf* is defined by the endpoints of $Tyrp1^{1THO\text{-}IV}$ $Tyrp1^{173G}$ (Fig. 1), which encompass a 180-kb segment between the *C9Orf150* orthologue and *Mpdz*, containing no predicted genes or transcripts. Comparison of this sequence with other mammalian species reveals numerous segments with a high level of sequence identity consistent with evolutionary conservation of regulatory element(s). It is possible that these are long-range control element(s) necessary for the

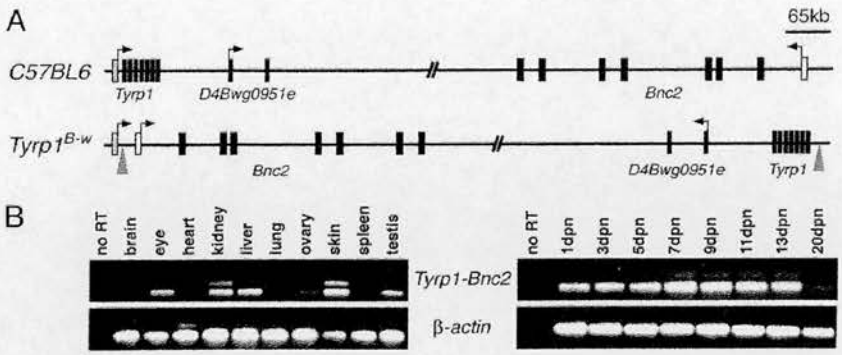

Fig. 4. *White-based brown* inversion. (*A*) Schematics of the C57BL/6J and *Tyrp1*$^{B\text{-}w}$ chromosomes showing the regions around the *Tyrp1* and *Bnc2* genes, and the intervening *D4Bwg0951e* gene for orientation. Arrows indicate transcriptional start sites. The gray arrowheads mark the breakpoints of the inversion. (*B*) RT-PCR showing transcription of the *Tyrp1-Bnc2* fusion transcript in a range of adult tissues and in the skin of mice between 1 and 20 days postnatal (dpn).

expression of *Ptprd*, for which the 5′ end is some 3 Mb away, and this finding would account for the consistency of phenotype between distal and proximal *baf* deletions.

Characterization of *White-Based Brown* (*Tyrp1*$^{B\text{-}w}$). *White-based brown* (*Tyrp1*$^{B\text{-}w}$) is a mutation of the *brown* locus that arose spontaneously during a radiation mutagenesis experiment (22). The *Tyrp1*$^{B\text{-}w}$ chromosome carries a dominant mutation that results in the absence or reduction in pigment at the base of the hair follicle but which is also a recessive loss-of-function allele of *Tyrp1*. This curious phenotype has been partially explained by preliminary molecular characterization showing that it results from an inversion that inactivates *Tyrp1* by interrupting the gene in the first intron (9, 23). It has been proposed that the dominant pigmentation loss in the mice results from ectopic expression of a second gene from the *Tyrp1* promoter, which either abrogates pigment production or leads to melanocyte death during the latter stages of the hair growth cycle. Short sequences bordering the inversion breakpoints have been cloned (9), and the genome sequence of the interval allowed us to determine the exact nature of the rearrangement.

The proximal end of the inversion is 105 bp from the exon-2 splice acceptor site in *Tyrp1* intron 1 (Fig. 4*A*). The other breakpoint lies distal of the *brown* deletion complex, ≈15-kb upstream of the recently characterized *Basonuclin 2* (*Bnc2*) gene (24). RT-PCR analysis demonstrated the expression of a *Tyrp1-Bnc2* fusion transcript in several *Tyrp1*$^{B\text{-}w}$ tissues (Fig. 4*B*). Normal *Tyrp1* expression is restricted to melanocytes; however, we detect expression of the fusion transcript in several other tissues such as the kidney, liver, ovary, and testis. This finding indicates that enhancer elements associated with *Bnc2* are driving ectopic expression of *Tyrp1* in these tissues or that *Tyrp1* expression is normally repressed by elements subsequently separated from the locus by the inversion. To determine whether melanocyte death occurred during the hair follicle cycle, we examined expression of the fusion transcript during the first hair cycle. *Tyrp1* is normally activated shortly after birth when melanocytes begin to produce pigment during anagen, and this expression stops by 13 days postnatal. However, we observed persistent expression of the fusion transcript in the skin both at birth and after 13 days postnatal, presumably as a consequence of the ectopic expression.

We sequenced multiple RT-PCR products of the *Tyrp1-Bnc2* fusion transcript. Normal splicing of *Tyrp1* exons 1 and 2 uses three different donor sites (25), which were all detected in the fusion transcripts spliced to *Bnc2*. We identified promiscuous splicing of *Tyrp1* to splice acceptor sites in *Bnc2* exons 1a and 2 (Fig. 4*A*) of which products of splicing to 1a would produce normal protein products. Because expression of the coding region of *Tyrp1* at the proximal end of the inversion is not detected (23), we propose that overexpression of *Bnc2* underlies the dominant loss of pigment in *Tyrp1*$^{B\text{-}w}$ animals.

Other Deletion Complexes. The surprisingly low gene density of this deletion complex may account for the viability of large deletions encompassing *Tyrp1*. Certain other specific locus regions, such as *Tyr* and *Ednrb*, also have large, viable deletions and appear to be gene-poor. By contrast, the *agouti* region is relatively gene rich, but relatively few deletions have been recovered from the region. Once other regions of the mouse genome are annotated at high quality, it will be interesting to correlate gene content with the presence or absence of large deletions that have been identified at many other chromosomal sites following radiation mutagenesis.

Materials and Methods

BAC Contig Construction, Sequencing, and Annotation. A BAC contig spanning the entire *brown* deletion complex was constructed by using clones from RCPI-23 and -24 C57BL/6J strain mouse libraries (26). Clones containing genes known to map to the interval were identified by hybridization to gridded libraries, and contigs were extended by using probes produced by overlapping oligonucleotides (overgos) designed to the ends of these BACs. The contig was also extended by using BAC fingerprint data (27). Contiguous BAC clones were sequenced by the Rosalind Franklin Centre for Genome Research and the Sanger Institute, as described in ref. 28. Manual annotation was performed by using established criteria and methodologies (www.sanger.ac.uk/HGP/havana/havana.shtml). Detailed annotation of the complete *brown* deletion sequence is available at the Vega web site (http://vega.sanger.ac.uk/index.html). Details of phenotypes defined in the region are in the Mouse Genome Database (www.informatics.jax.org).

Deletion Mapping. Deletion endpoints were mapped by using a panel of deletion/*Spretus* DNAs (7). Primer pairs were predominantly designed to amplify nonrepetitive BAC end sequences, although in some cases were designed specifically to map genes against deletions. Primers used for mapping key endpoints are listed in Table 3. Additional primer sequences and their amplification conditions are available on request.

Analysis of the *B*^{w} Inversion. The proximal end of the B^{w} inversion was identified by using the short sequence known to border the inversion (12). The genomic structure and sequence of mouse *Basonuclin 2* (*Bnc2*) was determined by assembling ESTs and comparing these with both the *Basonuclin 1* (*Bnc1*) sequence and expanding the gene structure in the human, fugu, and zebrafish genome assemblies by using GENEWISE (29). RT-PCR analysis of

splicing between *Tyrp1* and *Bnc2* was performed by using a forward primer in *Tyrp1* exon 1 (TCA GGG GAA AAG CAG ACA TC) and a reverse primer in exon 3 of *Bnc2* (GGT GCA GTT TAC CAA TGT GC). RNA was extracted from homogenized mouse tissues by using the Total RNA Isolation System kit (Promega) and cDNA and PCR were undertaken by using the Access RT-PCR Kit (Promega) following the manufacturers protocols.

The following people contributed at the Wellcome Trust Sanger Institute by finishing the sequence of between one and five BAC clones: Lucy Matthews, Harminder Sehra, Matthew Ellwood, Karen Oliver, Matthew Dunn, Neil Sycamore, Alan Tracey, Jeff Almeida, Jamieson Lovell, Ben Hopkins, Mike Kay, Rebekah Hall, Anthony Tromans, Sarah McGuire, Elliot Harrison, Michelle Smith, Debbie Wright, Phil Howden, Nicholas Matthews, Heena Lad, Siobhan Whitehead, David Lloyd, Paul Heath, Giselle Kerry, Joanna Chapman, Andrew Ellington, and Sophie Williams. This work was supported by the Medical Research Council (MRC) U.K. Mouse Genome Sequencing Program, the Wellcome Trust, and the U.S. Department of Energy. I.M.S. was a Wellcome Trust Fellow. Collaboration between the MRC Human Genetics Unit and the Oak Ridge National Laboratories has been aided by North Atlantic Treaty Organization Collaborative Research Grant CRG910945.

1. Bennett, D. C., Huszar, D., Laipis, P. J., Jaenisch, R. & Jackson, I. J. (1990) *Development (Cambridge, U.K.)* **110,** 471–475.
2. Davis, A. P. & Justice, M. J. (1998) *Genetics* **148,** 7–12.
3. Kelsey, G. & Schutz, G. (1993) *Curr. Opin. Genet. Dev.* **3,** 259–264.
4. Peterson, K. A., King, B. L., Hagge-Greenberg, A., Roix, J. J., Bult, C. J. & O'Brien, T. P. (2002) *Genomics* **80,** 172–184.
5. Rinchik, E. M., Bultman, S. J., Horsthemke, B., Lee, S. T., Strunk, K. M., Spritz, R. A., Avidano, K. M., Jong, M. T. & Nicholls, R. D. (1993) *Nature* **361,** 72–76.
6. Rinchik, E. M., Bell, J. A., Hunsicker, P. R., Friedman, J. M., Jackson, I. J. & Russell, L. B. (1994) *Genetics* **137,** 845–854.
7. Simpson, E. H., Suffolk, R., Bell, J. A., Jordan, S. A., Johnson, D. K., Hunsicker, P. R., Weber, J. S., Justice, M. J. & Jackson, I. J. (2000) *Mamm. Genome* **11,** 58–63.
8. Bell, J. A., Rinchik, E. M., Raymond, S., Suffolk, R. & Jackson, I. J. (1995) *Mamm. Genome* **6,** 389–395.
9. Javerzat, S. & Jackson, I. J. (1998) *Mamm. Genome* **9,** 469–471.
10. Craig J.M. & Bickmore W.A. (1993) *Bioessays* **15,** 349–354.
11. Kleinjan, D. A. & van Heyningen, V. (2005) *Am. J. Hum. Genet.* **76,** 8–32.
12. Ovcharenko, I., Loots, G. G., Nobrega, M. A., Hardison, R. C., Miller, W. & Stubbs, L. (2005) *Genome Res.* **15,** 137–145.
13. Rinchik, E. M. (1994) *Genetics* **137,** 855–865.
14. Yang, Z. Q., Imoto, I., Fukuda, Y., Pimkhaokham, A., Shimada, Y., Imamura, M., Sugano, S., Nakamura, Y. & Inazawa, J. (2000) *Cancer Res.* **60,** 4735–4739.
15. Chaudhry, A. Z., Lyons, G. E. & Gronostajski, R. M. (1997) *Dev. Dyn.* **208,** 313–325.
16. Grunder, A., Ebel, T. T., Mallo, M., Schwarzkopf, G., Shimizu, T., Sippel, A. E. & Schrewe, H. (2002) *Mech. Dev.* **112,** 69–77.
17. Smyth, I. M., Du, X., Taylor, M. S., Justice, M. J., Beutler, B. and Jackson, I. J. (2004) *Proc. Natl. Acad. Sci. USA* **101,** 13560–13565.
18. Henry, R. W., Ma, B., Sadowski, C. L., Kobayashi, R. & Hernandez, N. (1996) *EMBO J.* **15,** 7129–7136.
19. Sharma, P., Singh, D. P., Fatma, N., Chylack, L. T., Jr., & Shinohara, T. (2000) *Biochem. Biophys. Res. Commun.* **276,** 1320–1324.
20. Wu, X., Daniels, T., Molinaro, C., Lilly, M. B. & Casiano, C. A. (2002) *Cell Death Differ.* **9,** 915–925.
21. Uetani, N., Kato, K., Ogura, H., Mizuno, K., Kawano, K., Mikoshiba, K., Yakura, H., Asano, M. & Iwakura, Y. (2000) *EMBO J.* **19,** 2775–2785.
22. Hunsicker, P. R. (1969) *Mouse News Lett.* **40,** 41.
23. Jackson, I. J., Chambers, D., Rinchik, E. M. & Bennett, D. C. (1990) *Genetics* **126,** 451–459.
24. Vanhoutteghem, A. & Djian, P. (2004) *Proc. Natl. Acad. Sci. USA* **101,** 3468–3473.
25. Jackson, I. J., Chambers, D. M., Budd, P. S. & Johnson, R. (1991) *Nucleic Acids Res.* **19,** 3799–3804.
26. Osoegawa, K., Tateno, M., Woon, P. Y., Frengen, E., Mammoser, A. G., Catanese, J. J., Hayashizaki, Y. & de Jong, P. J. (2000) *Genome Res.* **10,** 116–128.
27. Marra, M. A., Kucaba, T. A., Dietrich, N. L., Green, E. D., Brownstein, B., Wilson, R. K., McDonald, K. M., Hillier, L. W., McPherson, J. D. & Waterston, R. H. (1997) *Genome Res.* **7,** 1072–1084.
28. Mallon, A. M., Wilming, L., Weekes, J., Gilbert, J. G., Ashurst, J., Peyrefitte, S., Matthews, L., Cadman, M., McKeone, R., Sellick, C. A., *et al.* (2004) *Genome Res.* **14,** 1888–18901.
29. Birney, E. & Durbin, R. (2000) *Genome Res.* **10,** 547–548.